

Ph.D. Thesis

**Tetraparametric Assembly Method for the
simulation and optimization of bolt tightening
sequences in ASME ring type joints**

Presented by:

Ibai Coria Martínez

Belonging to the:

**Mechanical Engineering Department
Faculty of Engineering in Bilbao
University of the Basque Country (UPV/EHU)
Spain**

To obtain the degree of:

Doctor of Philosophy in Mechanical Engineering

Thesis Advisors:

**Dr. Mikel Abasolo Bilbao
Dr. Josu Aguirrebeitia Celaya**

February 2018

Acknowledgements

Cuando se finaliza un trabajo tan extenso y tan duro como el desarrollo de una Tesis Doctoral, es imposible no mirar atrás y darse cuenta de que no hubiera sido posible sin el apoyo de un gran número de personas. Por ello, es un verdadero placer dedicar estas líneas a todas aquellas personas que me han apoyado durante este tiempo.

En primer lugar, mi infinita gratitud a mis directores de tesis Mikel y Josu. Me quedo con la honestidad y sinceridad que os caracteriza. Desde el primer día que os conocí, me hicisteis sentir uno más del grupo, formando parte de todos vuestros proyectos y valorando siempre mi opinión. De aquello hace ya casi cinco años y os puedo asegurar que os sigo admirando como el primer día. Gracias por vuestra disponibilidad, vuestra paciencia y la amabilidad con la que me habéis tratado siempre que lo he necesitado, a pesar de vuestros múltiples compromisos. Por último, destacar vuestra brillantez y geniales ideas, las cuales forman la mayor parte de esta Tesis Doctoral. Gracias de corazón a los dos.

También me gustaría dar las gracias a Igor. No sólo por los conocimientos de mecánica que has compartido conmigo, sino por todo lo que me has aportado en otros ámbitos como la electrónica y la informática que me han sido de gran utilidad. No puedo olvidar todas las veces que me he reído oyéndote contar con mucha gracia diferentes historias y anécdotas.

I also would like to express my gratitude to Hakim, the person who receives me in his university and believes in me without knowing me. I can only say good words about you; you have always been kind and positive with me, you are clever and bright, and your passion in every type of research activity is

admirable. My stay in Canada was unforgettable; I will be always in debt with you.

Deseo agradecer también a las empresas ULMA y MATZ-ERREKA por su manifiesto interés en los resultados de esta Tesis Doctoral, y su colaboración en el suministro de todo el equipamiento de los ensayos experimentales, así como por su participación en dichos ensayos.

Ha sido un placer y un orgullo compartir aula de doctorandos con mis compañeros y compañeras. La energía positiva que se respiraba era inmejorable y envidiable, haciéndote ir a trabajar con una buena sensación en el cuerpo. Siempre había alguien dispuesto a ayudarte o alegrarte el día de mil formas diferentes, lo que hacía que el trabajo nunca fuera monótono. Hemos compartido muchos cafés y comidas, en las que hemos reído día tras día, donde he aprendido con cada uno de los debates que han surgido y con todas vuestras opiniones. Gracias a todos.

Por último, me gustaría dedicar esta Tesis Doctoral a mi ama, a mi aita, a mi hermano, a mi amama, a mi aitite, a mi yaya y a mi yayo. Desde el inicio de mis estudios habrían sido muy pocas las personas que hubieran confiado en mí pero no fue así en vuestro caso. Es por ello que estoy orgulloso de dedicaros el resultado final de mi esfuerzo como estudiante. Gracias por todo el cariño, la paciencia, la humildad y los valores que defendéis y que tan bien me habéis transmitido. Ha sido este conjunto de cosas las que me han definido como la persona que soy hoy en día. Estoy muy orgulloso de haberos tenido siempre a mi lado.

Ibai

Abstract

In the Oil & Gas sector, due to the large length of most oil and gas pipelines, every pipeline must be manufactured in small sections which must be subsequently joined in situ. This also makes it possible to reduce manufacturing costs, because this way it is possible to manufacture general purpose components (straight pipeline sections, pipe elbows, valves, etcetera). Among the different types of joint, bolted joints are particularly used given how easy it is to disassemble them, making it possible to perform maintenance tasks or connect new devices to the pipeline in a simple manner. Nevertheless, for this type of joint uniform stress distribution must be achieved on the gasket in order to avoid, or at least minimize, the leakages as much as possible. To this end, a uniform load distribution is obviously required on every bolt of the joint. This is not an easy task because when a bolt is tightened during the tightening sequence, the joint gets compressed and therefore the load of the previously tightened bolts decreases. This phenomenon is known as elastic interaction; due to the loss of load of the bolts during the tightening sequence, the level of load of the bolts at the end of the tightening sequence is different to the tightening load applied to each bolt. Moreover, the magnitude of these load variations depends on a large number of parameters whose influence is difficult to predict, such as geometry and material of the joint components, load magnitude, bolt spacing, assembly pattern, amongst others factors. To this regard, it is difficult to foresee the load level of the bolts at the end of the tightening sequence, and therefore it is also difficult to obtain uniform stress distribution on the gasket at the end of the tightening sequence.

In order to solve this problem, various standards were developed (ASME, NORSOK, API, amongst others) with several assembly procedures that provide the target uniform final load on the bolts. Accordingly, uniform

stress distribution is obtained on the gasket, and the leakages in the joint are reduced as much as possible. However, the tightening sequences provided by the standard are extremely costly as more passes are required; and the more passes, the more time that is required for the joint assembly. Also, excluding the last passes, the tightening sequence usually follows a star assembly pattern, which complicates the assembly even more. As a consequence, taking into account that the number of joints in Oil & Gas pipelines is usually very high, the assembly cost of the pipeline is usually highly relevant. Regarding the tightening sequences provided by the standards, it must be pointed out that the standards indicate that they only serve as indications, and therefore, they suggest that each assembler should develop a specific tightening sequence for each product and working condition. In short, in order to become reliable and competitive the creation of a specific assembly procedure that applies to each particular product is indispensable.

In order to obtain different tightening sequences for each particular joint, and thus obtain more efficient sequences, over the last few years, different methods have been developed which define the sequences known as optimized tightening sequences. Amongst these, the most popular methods in specialist literature are the “Elastic Interaction Coefficients Methods” (EICM) and the “Inverse Sequence Method” (ISM). These methods examine the behaviour of the joint during the tightening sequence in order to predict the loss of load of every bolt. Thus, it is possible to calculate the tightening load of each bolt related with the target final load, and obtain a uniform final load in just one or two passes. However, these optimization methods have the disadvantage that obtaining the optimized tightening sequence is very costly because a large number of tightening operations and measurements must be performed beforehand. As a consequence, the optimization procedures only are profitable when many joints are to be assembled or when a critical application is involved.

The overall objective of this Doctoral Thesis is to study the optimization process of bolt tightening sequences for Ring Type Joints (RTJ) with an ASME metal gasket. These joints are widely used in the Oil & Gas sector due to their capacity to provide high integrity seals at very high temperature and internal pressures. Their efficient sealing is obtained by inserting the metallic gasket in a groove which is machined on each sealing surface. To define the optimization process, the first goal is to study the previously mentioned two optimization methods in this type of joint and thus obtain their advantages

and disadvantages. The second goal, and also the main objective of the Doctoral Thesis, is to develop a new method for the optimization of bolt tightening sequences in RTJs. To conclude this Doctoral Thesis, the final goal is to program the newly developed methodology in “Visual Basic for Applications” in Microsoft Excel, to create an application which is extremely applicable and user friendly.

To this end, the Doctoral Thesis has been divided in several chapters and has been structured as explained below.

Firstly, in **Chapter 1** the introduction, the background and the objectives are explained. It starts by explaining the necessity of bolted joints in Oil & Gas pipelines, and the complexity that is involved for the correct assembly of these joints due to several phenomena that complicate obtaining a uniform bolt load distribution. The various alternatives that are used nowadays for the correct assembly of bolted joints are also explained. This Chapter also presents the type of bolted joint that has been studied in this Doctoral Thesis.

In **Chapter 2**, the analysis tools that are used throughout the Doctoral Thesis are presented. On the one hand, a multiparametric Finite Element model developed in ANSYS® Workbench is presented, which has automated results extraction. On the other hand, a test bench of the bolted joint is presented which was manufactured and assembled in cooperation with the companies ULMA and MATZ-ERREKA. Moreover, state-of-the-art technology was implemented for the test bench in order to obtain extremely precise results. Finally, in this Chapter the Finite Element model is also validated, comparing its results under different load cases with the results that the test bench provides.

Chapter 3 provides a detailed explanation of the previously mentioned two optimization methods to define optimized tightening sequences: the EICM and the ISM. Next, both methods are carefully studied and validated with the Finite Element model for the type of joint that is studied throughout the Doctoral Thesis, because, in specialist literature, there is no research relating to the optimization of bolt tightening sequences on RTJs.

In **Chapter 4** the new method for the optimization of the RTJ tightening sequences is explored, which was called the “Tetraparametric Assembly Method” (TAM). In this Chapter, the method is only developed for one-pass tightening sequences and it is only validated for the specific geometry of the

test bench. With this method, it is possible to define the behaviour of the joint during the tightening sequence with just four coefficients, which can be obtained from a simple analysis procedure. It is also shown how this method is much more efficient than the previous methods when an RTJ is studied. The validations are carried out via the Finite Element method and with the test bench.

In order to develop a completely applicable method in different situations, in **Chapter 5** the new method is generalized for multiple-pass tightening sequences. The generalization is particularly useful because, in some cases, in order to avoid possible damages on the joint, it is necessary to reduce the tightening loads, and for that purpose, multiple-pass tightening sequences must be applied (two passes is usually enough). The validation is again carried out via the Finite Element method, and experimentally. On the other hand, in this Chapter, the range of application of the new method is also studied among the RTJs of ASME standard. A library is also then generated with the four coefficients of every joint inside the range of application. Thus, previous analyses are avoided to define optimal tightening sequences, increasing yet more the efficiency of the method.

In **Chapter 6** an application is presented which was programmed in “Visual Basic for Applications” in Microsoft Excel. In the application, the generalized TAM is implemented and the library with every coefficient is entered. As a result, a very useful and powerful application is obtained, which is very easy to implement in an Oil & Gas company given its simplicity. For a better understanding, an illustrative example is also presented, step-by-step, where its full potential can be appreciated.

In **Chapter 7**, another optimization method is developed, but in this case to study optimal tightening sequences in other types of joints, which are therefore outside the range of application established in Chapter 5. This method, which is also much more efficient than the optimization methods explained in Chapter 3, is based on the superelements technique. Compared with a conventional Finite Element model, a much more efficient model is obtained because the computational cost is considerably less with no loss of precision. To this end, through the superelements technique, a condensed stiffness matrix is built based on the correct selection of the master nodes of the model. Thus, the dimensions and the cost of the problem are reduced considerably.

Chapter 8, on the one hand, presents the main conclusions obtained throughout the Doctoral Thesis. On the other hand, it also presents several research lines that have been left open as a consequence of the research work studied during the Doctoral Thesis. To conclude the Chapter, all the publications derived from the Doctoral Thesis are listed.

Finally, all the cited bibliography throughout the Doctoral Thesis is listed in the reference section.

Resumen

En el sector del Oil&Gas, debido a la gran longitud que suelen tener las tuberías de los oleoductos y gasoductos submarinos, se hace necesario fabricar las tuberías en pequeños tramos para posteriormente unirlos mediante uniones in situ. Además, esto permite abaratar los costes de fabricación ya que hace posible fabricar piezas de carácter general (tramos rectos de tubería, codos, válvulas, etcétera). Entre los diferentes tipos de uniones, las uniones atornilladas son muy utilizadas debido a su fácil desmontaje, ya que hace posible realizar tareas de mantenimiento o acoplar nuevos dispositivos a las tuberías de una manera muy sencilla. No obstante, en este tipo de uniones es necesario obtener una distribución de presiones uniforme en la junta para así evitar o al menos reducir al máximo sus fugas. Para ello, obviamente, es preciso obtener una carga uniforme en todos los tornillos de la unión. Esto no es una tarea sencilla ya que cuando un tornillo es precargado durante la secuencia de atornillado, la unión se comprime y por lo tanto la carga de los tornillos que han sido previamente precargados se reduce. Este fenómeno es conocido como interacción elástica. Debido a la pérdida de carga de los tornillos durante la secuencia de atornillado, la carga que tienen los tornillos al final de la secuencia de atornillado es diferente de la carga de apriete que se ha aplicado a los tornillos. Además, la magnitud de estas variaciones de carga depende de un gran número de parámetros cuya influencia es muy difícil de prever, como por ejemplo la geometría y el material de los componentes de la unión, el orden de apriete, el espaciado entre tornillos, etcétera. En este sentido, se hace difícil prever las cargas finales en los tornillos, y por lo tanto, también es complicado obtener una distribución de cargas uniforme en la junta al final de la secuencia de atornillado.

A fin de resolver esta problemática, existen diferentes normas (ASME, NORSOK, API, entre otras) que contienen procedimientos de ensamblado

para obtener la carga final uniforme deseada en los tornillos. De este modo, se obtiene una distribución uniforme de presiones en la junta, y así se consiguen reducir al máximo las fugas en la unión. Sin embargo, las secuencias propuestas en las normas son muy costosas debido a que requieren un gran número de pasadas, y cuantas más pasadas, mayor es el tiempo de ensamblado de cada unión. Además, exceptuando las últimas pasadas, la secuencia de atornillado suele seguir un orden de apriete en estrella, lo cual complica aún más el ensamblado. En consecuencia, teniendo en cuenta que el número de uniones suele ser muy elevado, el coste económico del ensamblado acaba adquiriendo una gran importancia. Respecto a las secuencias de atornillado que proponen las normas, también cabe destacar que ellas mismas advierten que solo son orientativas y por lo tanto recomiendan que cada ensamblador desarrolle sus propias secuencias de atornillado para sus productos y condiciones de trabajo en particular. Resumiendo, para ser fiables y competitivos es indispensable crear procedimientos de ensamblado propios que se adapten a los productos propios.

A fin de obtener diferentes secuencias para cada unión en particular y así obtener secuencias más eficientes, en los últimos años se han desarrollado métodos que definen las llamadas secuencias optimizadas. Entre ellos, los más populares en la literatura especializada son el “Método de los Coeficientes de la Interacción Elástica” (MCIE) y el “Método de la Secuencia Inversa” (MSI). Estos métodos estudian el comportamiento de la unión durante la secuencia de atornillado para así predecir las pérdidas de carga de todos los tornillos. De este modo, se pueden calcular las cargas de apriete de cada tornillo para una carga final deseada, y obtener una carga uniforme en tan solo una o dos pasadas. Sin embargo, estos métodos de optimización tienen la desventaja de que obtener la secuencia optimizada es bastante costoso porque hay que realizar un gran número de aprietes y mediciones previas. Es por ello, que estos procesos de optimización solo resultan rentables cuando el número de uniones a ensamblar es muy elevado o cuando se trata de una aplicación bastante crítica.

Esta Tesis Doctoral tiene como objetivo global estudiar el proceso de optimización de secuencias de atornillado en las uniones Ring Type Joint (RTJ) de ASME con junta metálica. Estas uniones son ampliamente utilizadas en el sector del Oil&Gas por su capacidad de proporcionar un buen sellado a temperaturas y presiones internas muy elevadas, gracias a la junta metálica que va introducida en el surco que tiene mecanizado cada una de las superficies de

sellado. Para definir su proceso de optimización, el primer objetivo es estudiar los dos métodos anteriormente mencionados en este tipo de uniones y así obtener sus ventajas y sus desventajas. El segundo objetivo, y también el objetivo principal de esta Tesis Doctoral, es desarrollar una nueva metodología para la optimización de secuencias de atornillado en uniones RTJ. Para finalizar con la Tesis Doctoral, el último objetivo es programar la nueva metodología desarrollada en “Visual Basic for Applications” de Microsoft Excel, para dar lugar a una aplicación de gran aplicabilidad y muy sencilla de utilizar.

Para ello, la tesis Doctoral se ha dividido en varios capítulos y se ha estructurado como se expone a continuación.

En primer lugar, en el **Capítulo 1** se describen los antecedentes y se presentan los objetivos. Se comienza explicando la necesidad de utilizar uniones atornilladas en las líneas de tuberías destinadas al Oil&Gas, y la dificultad que supone ensamblar correctamente estas uniones debido a fenómenos muy diversos que complican obtener una distribución de cargas uniforme en los tornillos. Además, se explican las diferentes alternativas que existen hoy en día para tratar de ensamblar correctamente una unión. En este Capítulo también se presenta el tipo de unión atornillada a estudiar a lo largo de esta Tesis Doctoral.

En el **Capítulo 2** se presentan las herramientas de análisis utilizadas a lo largo de la Tesis Doctoral. Por un lado, se presenta un modelo multiparamétrico de Elementos Finitos desarrollado en ANSYS® Workbench, el cual tiene automatizada toda la extracción de resultados. Por otro lado, se presenta un banco experimental de la unión atornillada que ha sido fabricado y ensamblado con la ayuda de las empresas ULMA y MATZ-ERREKA. Además, se le ha implementado tecnología muy avanzada con el fin de obtener resultados muy precisos. Por último, en este Capítulo también se valida el modelo de Elementos Finitos comparando bajo diferentes situaciones de carga sus resultados con los resultados que proporciona el banco experimental.

El **Capítulo 3** explica en profundidad los dos métodos mencionados anteriormente para definir secuencias de atornillado óptimas: el MCIE y el MSI. Seguidamente, ambos métodos son detenidamente estudiados y validados mediante Elementos Finitos para el tipo de unión estudiado a lo largo de esta Tesis Doctoral, ya que en la literatura especializada no se

encuentran estudios acerca de la optimización de secuencias de atornillado en uniones RTJ.

En el **Capítulo 4** se desarrolla la nueva metodología para la optimización de secuencias de atornillado en uniones RTJ, la cual se ha llamado el “Método Tetreparamétrico de Ensamblado” (TAM). En este Capítulo la metodología se desarrolla únicamente para secuencias de atornillado de una sola pasada y se valida únicamente para la geometría de unión del banco experimental. Con dicha metodología se consigue definir el comportamiento de una unión mediante tan solo cuatro coeficientes que se obtienen de un sencillo análisis; además, se demuestra que es más eficiente que los métodos anteriormente expuestos. Las validaciones se realizan tanto por Elementos Finitos como por el banco experimental.

Con el fin de generar una metodología completamente aplicable en diferentes situaciones, en el **Capítulo 5** se generaliza la metodología para secuencias de atornillado de múltiples pasadas. Esta generalización es de gran utilidad ya que en ocasiones, con el fin de no dañar la unión, es imprescindible reducir las cargas de apriete, lo que conlleva secuencias de atornillado de múltiples pasadas. La validación se hace nuevamente mediante Elementos Finitos y mediante el banco experimental. Por otro lado, en este mismo Capítulo también se estudia y se define el rango de aplicación de la metodología dentro de las uniones RTJ. Además, a continuación se genera una librería con los cuatro coeficientes de todas las uniones que se encuentran dentro del rango de aplicación.

En el **Capítulo 6** se desarrolla una aplicación programada en “Visual Basic for Applications” de Microsoft Excel, en la que se implementa el MTE generalizado y la librería con todos los coeficientes. Da lugar a una aplicación de gran interés y muy sencilla de utilizar para los usuarios, y por lo tanto fácil de implementar en una compañía del área del Oil&Gas. Para su mejor entendimiento, también se presenta un ejemplo ilustrativo paso a paso en el que se puede apreciar en detalle todo su potencial.

En el **Capítulo 7** se desarrolla otra metodología de optimización, pero en este caso para el estudio de secuencias optimizadas en otro tipo de uniones, que por lo tanto están fuera del rango de aplicación establecido en el Capítulo 5. Esta metodología, la cual también es mucho más eficiente que los métodos explicados en el capítulo 3, está basada en la técnica de los superelementos. En comparación con un modelo de Elementos Finitos convencional, se

consigue un modelo mucho más eficiente ya que reduce el coste computacional sin tener ninguna pérdida de precisión. Para ello, mediante la técnica de los superelementos se construye una matriz de rigidez condensada a partir de una selección apropiada de los nodos principales del modelo. Así se reducen significativamente las dimensiones y el coste del problema.

En el **Capítulo 8**, se presenta por un lado todas las conclusiones principales obtenidas a lo largo de toda la Tesis Doctoral. Por el otro lado, también se presentan las líneas de investigación que han quedado abiertas como consecuencia del trabajo de investigación realizado. Además, para concluir con el Capítulo, se listan todas las publicaciones derivadas de esta Tesis Doctoral.

Por último, el apartado bibliográfico recoge las referencias citadas a lo largo de toda la Tesis Doctoral.

General Index

Acknowledgements	I
Abstract	III
Resumen	IX
General Index	XV
List of Figures	XXI
List of Tables	XXIX

Chapter 1: Introduction, Background and Objectives	1
1. Overview	3
2. Preload in Bolted Joints	12
2.1. Preloaded Bolted Joints Performance.....	12
2.2. Preload in Pipelines Bolted Joints	19
3. Uncertainty Factors in Bolt Preload	21
3.1. Bolt Initial Load Uncertainty Factors	21
3.1.1. Torque Wrench	22
3.1.2. Bolt Tensioner.....	28
3.2. Uncertainty Factors in Bolt Final Load.....	30
3.2.1. Short Term Relaxation.....	30
3.2.2. Elastic Interaction	33
3.2.3. Rigid Body Motion.....	35

4. Standards for the Correct Assembly of Bolted Joints.....	36
5. Tools for the Simulation of Tightening Sequences	42
5.1. Experimental Methods.....	42
5.2. Finite Element Method.....	43
5.3. Metamodel.....	45
5.4. Analytical Models.....	45
5.5. Models Using Substructuring.....	46
6. Motivation and Objectives of the Doctoral Thesis	46

Chapter 2: Tools Used for the Simulation of Tightening Sequences 49

1. Introduction.....	51
2. Test Bench	51
3. Parametric Finite Element Model.....	55
3.1. Material.....	56
3.2. Geometry	56
3.3. Contacts.....	59
3.4. Mesh	59
3.5. Loads and Boundary Conditions	62
3.6. Results Extraction.....	63
3.7. Possible Sources of Error.....	64
4. Finite Element Model Validation.....	65

Chapter 3: Existing Methods for the Optimization of Bolt Tightening Sequences 69

1. Introduction.....	71
2. Inverse Sequence Method	71
3. Elastic Interaction Coefficients Method	76

3.1. General Description.....	77
3.2. Calculation Algorithm for the Matrix [A].....	78
3.3. Discussion of the Method.....	80
3.4. Validation of the EICM for One-Pass Tightening Sequence on RTJs.....	81
3.4.1. First Validation Analysis	82
3.4.2. Second Validation Analysis	84
3.5. Generalization of the EICM for Two-Pass Tightening Sequences on RTJs	85
3.6. Validation of the EICM for Two-Pass Tightening Sequences on RTJs.....	87
4. Comparison of Both Methods: EICM and ISM.....	88

Chapter 4: Tetraparametric Assembly Method	91
1. Introduction.....	93
2. Study of the Elements of Matrix [A]	93
3. Development of the Tetraparametric Assembly Method	99
4. Results and Validation of the Tetraparametric Assembly Method.....	108
4.1. Comparison Between TAM and EICM.....	108
4.2. Validation of the Tetraparametric Assembly Method with the Finite Element Model.....	110
4.3. Validation of the Tetraparametric Assembly Method with the Test Bench.....	113
5. Concluding Remarks	114

Chapter 5: Generalization of the Tetraparametric Assembly Method	117
1. Introduction.....	119

2. Multiple-Pass Tightening Sequences with the Tetraparametric Assembly Method	120
2.1. General Description.....	120
2.2. Validation.....	123
3. One and a Half Pass Tightening Sequences	126
3.1. General Description.....	127
3.2. Illustrative Example and Validation.....	130
4. Range of Application of the Tetraparametric Assembly Method	134
5. RTJ Coefficients Library	140

Chapter 6: Application in Excel VBA of the Tetraparametric Assembly Method 153

1. Introduction	155
2. Optimization Section of the Application	155
3. Simulation Section of the Application	164
4. Illustrative Example	169

Chapter 7: Alternative Optimization Methodology for Other Types of Joints 177

1. Introduction	179
2. Basics of the Superelements Technique	179
3. Model Developed Based on the Superelement Technique	182
4. Test Benches	186
4.1. ROT Machine.....	186
4.2. Experimental Set Up of the Joint.....	187
5. Validation of the Model	188
5.1. Mechanical Properties of the Gasket.....	189

5.2. Validation with Linear Gasket.....	191
5.3. Validation with Non-Linear Gasket.....	192
6. Concluding Remarks.....	193

Chapter 8: Conclusions and Further Research	195
1. Conclusions.....	197
2. Further Research.....	198
3. Publications Obtained During the Doctoral Thesis.....	198

References	201
-------------------	------------

List of Figures

Figure 1.1.	Oil pipeline	3
Figure 1.2.	Measurement of a leakage with two flowmeters.....	4
Figure 1.3.	Bolted joint.....	5
Figure 1.4.	Production system of the forged steel flanges.....	6
Figure 1.5.	Flanges forging production system	7
Figure 1.6.	Machining process for flanges (in red the machined surfaces of that step)	7
Figure 1.7.	Standardized flanges in standard ASME B16.5 [Asm´13(1)] a) Welding Neck (WN) b) Slip On (SO) c) Socket Weld (SW) d) Lap (LJ) e) Threaded (TH) f) Blind (BL)	8
Figure 1.8.	Type of flange faces [Asm´11]: a) Flat face (FF) b) Raised face (RF) c) Male & Female (MF) d) Ring Type Joints (RTJ)	9
Figure 1.9.	Transversal profile of ring gaskets [Asm´12(2)].....	10
Figure 1.10.	Pull/tow method for the assembly of offshore pipelines.....	10
Figure 1.11.	Methods for the assembly of offshore pipelines: a) S-lay method b) J-lay method c) Reel-lay method	11
Figure 1.12.	Preloaded joint	13
Figure 1.13.	Joint diagram of the Figure 1.12 [Aba´12].....	14
Figure 1.14.	Preloaded joint under external axial load [Aba´12].....	14
Figure 1.15.	Joint diagram of the Figure 1.14 [Aba´12].....	16
Figure 1.16.	Preloaded joint under external axial load which is applied on an intermediate plane [Aba´12]	16

Figure 1.17.	Behaviour of one bolt when it is not preloaded (1) and when it is preloaded (2)	18
Figure 1.18.	Methods to prevent screw-loosening [Bic'95].....	19
Figure 1.19.	Acting forces on a bolted joint [Vei'03]	20
Figure 1.20.	Parameters which affect the ratio between the torque and the initial load [Aba'12]	22
Figure 1.21.	Typical values for the nut coefficient K [Bic'95].....	24
Figure 1.22.	Relation between the initial load and the rotation of the nut during the bolt tightening process [Aba'12].....	26
Figure 1.23.	Relation between bolt initial load and nut rotation for different friction coefficients [Aba'12].....	27
Figure 1.24.	Tools for the bolt load measurement: a) micrometer b) washer with a load indicator c) bolt with a load indicator [Bic'95].....	28
Figure 1.25.	Bolt tensioner [Ith'www].....	29
Figure 1.26.	Working procedure of a bolt tensioner a) the threaded element is attached b) the bolt is tensed c) the nut is tightened d) the bolt tensioner is removed [Bic'95]	30
Figure 1.27.	Shape of the contact surfaces using a microscope [Bic'95]	31
Figure 1.28.	Joint with poor thread engagement [Bic'95].....	31
Figure 1.29.	Joint with oversized fillets or undersized holes [Bic'95].....	32
Figure 1.30.	Oversized hole [Bic'95].....	33
Figure 1.31.	Elastic interaction phenomenon during the assembly process of a joint a) tighten bolt number 2 b) tighten bolt number 1 c) tighten bolt number 3 [Aba'12].....	34
Figure 1.32.	Rigid body motion phenomenon on a bolted joint [Aba'12]	35
Figure 1.33.	NFC5 joint under the design loads [Nor'13].....	37
Figure 1.34.	Imperfections on joints and gaskets [Nor'13].....	38
Figure 1.35.	Flange misalignment [Nor'13]	38
Figure 1.36.	Tightening sequences with 2 and 4 tightening tools [Nor'13]	39
Figure 1.37.	Tightening sequence called Legacy Pattern and suggested by ASME [Asm'13(2)]	40

Figure 1.38.	Experimental set-up to study tightening sequences [Nas'06]	43
Figure 1.39.	Finite Element model of a bolted joint (flange, gasket and bolt) [Kha'15]	44
Figure 1.40.	Gasket with a highly non-linear behaviour [Fuk'12].....	44
Figure 1.41.	Biparametric metamodel of the bolted joint of a wind turbine tower [Aba'12]	45
Figure 2.1.	Test Bench.....	51
Figure 2.2.	Joint type of the test bench: a) RTJ of NPS 24", Class 150 and SCHD 40 [Asm'13(1)] b) metal ring gasket with octagonal profile R76 [Asm'12(2)]	52
Figure 2.3.	Torque wrench of the test bench.....	52
Figure 2.4.	Portable pump of the test bench.....	53
Figure 2.5.	Ultrasound measuring device [Bic'95]	54
Figure 2.6.	Time variation due to: bolt length variation (line A), sound wave speed variation (line B) and a variation of both (line C).....	54
Figure 2.7.	Bolt equipped with i-bolt ® technology [Loa'www]	55
Figure 2.8.	Measurement of bolt preload during the load process.....	55
Figure 2.9.	Joints geometric characteristics	57
Figure 2.10.	Components of the sector a) flange and pipe section b) gasket c) bolt.....	58
Figure 2.11.	Complete model of the joint	58
Figure 2.12.	Lower order hexahedron (Solid185 in Ansys ®).....	59
Figure 2.13.	Higher order tetrahedron (Solid187 in Ansys ®).....	60
Figure 2.14.	Target and contact two-dimensional elements (Conta174 and Targe170 in Ansys ®).....	61
Figure 2.15.	Mesh of the Finite Element model	61
Figure 2.16.	Finite Element model's boundary conditions.....	62
Figure 2.17.	Pretension section of one bolt.....	63
Figure 2.18.	Studied assembly patterns a) assembly pattern 1: 1-11-6-16 → 3-13-8-18 → 5-15-10-20 → 2-12-7-17 → 4-14-9-19 b) assembly pattern 2: 1-11-6-16 → 2-12-7-17 → 3-13-8-18 → 4-14-9-19 → 5-15-10-20.....	65

Figure 2.19.	Experimental vs Finite Element in the obtained final load of the bolts a) tightening load 350 kN and assembly pattern 1 b) tightening load 200 kN and assembly pattern 2	67
Figure 3.1.	An example of a joint with five bolts.....	72
Figure 3.2.	Obtained tightening loads (in the table) and final loads (in the polar diagram) with the ISM for assembly pattern 1, target load 250 kN and friction coefficient 0.25	75
Figure 3.3.	Relation between the applied tightening load on the bolts and their vertical displacement during loading and unloading.....	76
Figure 3.4.	Illustrative example of a joint with three bolts.....	78
Figure 3.5.	Load level of bolts during the tightening sequence of the first validation analysis (horizontal axis load step, vertical axis level of load on the bolts).....	83
Figure 3.6.	Obtained initial loads (in the table) and final loads (in the polar diagram) with the EICM using assembly pattern1, target load 350 kN and friction coefficient 0.2.....	83
Figure 3.7.	Load level of the bolts during the tightening sequence of the second validation analysis (horizontal axis load step, vertical axis level of load on the bolts)	84
Figure 3.8.	Obtained initial loads (in the table) and final loads (in the polar diagram) with the EICM using assembly pattern2, target load 200 kN and friction coefficient 0.3.....	85
Figure 3.9.	Obtained final load distribution with an optimized two-pass tightening sequence obtained with the EICM.....	88
Figure 4.1.	Obtained matrix [A] with the assembly pattern 1 and with a) $\mu=0.3$ - $F=200\text{kN}$ b) $\mu=0.2$ - $F=200\text{kN}$ c) $\mu=0.3$ - $F=350\text{kN}$ d) $\mu=0.2$ - $F=350\text{kN}$	95
Figure 4.2.	Obtained matrix [A] with the assembly pattern 2 and with a) $\mu=0.3$ - $F=200\text{kN}$ b) $\mu=0.2$ - $F=200\text{kN}$ c) $\mu=0.3$ - $F=350\text{kN}$ d) $\mu=0.2$ - $F=350\text{kN}$	98
Figure 4.3.	Matrix [A] for the reviewed joint and a) assembly pattern 1 b) assembly pattern 2.....	100

Figure 4.4.	Explanation of the two load steps of the TAM to obtain matrix [A] in a joint with 20 bolts.....	103
Figure 4.5.	Illustrative example of the TAM on a joint with 20 bolts a) first load step b) second load step	105
Figure 4.6.	Two load step analysis of the TAM on joints with a) 12 bolts b) 16 bolts c) 24 bolts.....	107
Figure 4.7.	Comparison of the ratio between the initial and the final load on the bolts using the EICM and the TAM a) assembly pattern 1 b) assembly pattern 2.....	110
Figure 4.8.	Finite Element results obtained with the TAM in analysis 1	112
Figure 4.9.	Finite Element results obtained with the TAM in analysis 2.....	112
Figure 4.10.	Obtained experimental results with the TAM (target load 200 kN and assembly pattern 1).....	113
Figure 4.11.	Obtained experimental results with the TAM (target load 200 kN and star-circular pattern).....	114
Figure 5.1.	Matrix [B] for a joint with 20 bolts and assembly pattern 1 ...	121
Figure 5.2.	Final load distribution obtained experimentally for analysis 1 with the multiple-pass TAM	125
Figure 5.3.	Final load distribution obtained experimentally for analysis 2 with the multiple-pass TAM	126
Figure 5.4.	Matrix [M] when the first 8 bolts exceed the yielding load and when assembly pattern 1 is used.....	128
Figure 5.5.	Final results in the illustrative example	134
Figure 5.6.	Studied range of application	135
Figure 5.7.	Results obtained with the TAM for different joints a) NPS10 Class150 b) NPS10 Class1500 SCHD160 c) NPS24 Class150 SCHD10 d) NPS24 Class1500 SCHD160..	138
Figure 6.1.	Input data of the optimization section.....	156
Figure 6.2.	Pop-up Windows for the type of joint and number of passes.....	157
Figure 6.3.	Pop-up window of the assembly patterns.....	157

Figure 6.4.	Assembly patterns on a joint with 20 bolts a) star assembly pattern 1: 1-11-6-16→3-13-8-18→5-15-10-20→2-12-7-17→4-14-9-19 b) star assembly pattern 2: 1-11-6-16→2-12-7-17→3-13-8-18→4-14-9-19→5-15-10-20 c) circular pattern: 1-2-3-4-5-6-7-8-9-10-11-12-13-14-15-16-17-18-19-20 d) star-circular pattern: 1-11-6-16→2-3-4-5-7-8-9-10-12-13-14-15-17-18-19-29 e) enter assembly pattern.....	159
Figure 6.5.	Update of the input data when several parameters are altered	160
Figure 6.6.	Results obtained in the optimization section introducing the input data of Figure 6.1	161
Figure 6.7.	Report_O1 of the application	162
Figure 6.8.	Report_O2 of the application	163
Figure 6.9.	Input data of the simulation section	165
Figure 6.10.	Results obtained in the simulation section with the input data of Figure 6.9	166
Figure 6.11.	Report_S1 of the application.....	167
Figure 6.12.	Report_S2 of the application.....	168
Figure 6.13.	Warning message when the tightening loads exceed bolt yielding load.....	169
Figure 6.14.	The results obtained in the illustrative example for the one-pass tightening sequence in the optimization section	171
Figure 6.15.	The results obtained in the illustrative example for the two-pass tightening sequence in the optimization section	172
Figure 6.16.	Input data in the simulation section of the illustrative example	174
Figure 6.17.	The results obtained in the simulation section of the illustrative example.....	175
Figure 6.18.	Report_S2 with the obtained final results in the illustrative example	176
Figure 7.1.	Conventional Finite Element model of the plane	180
Figure 7.2.	Finite Element model of the plane based on the superelements technique	181
Figure 7.3.	Conventional Finite Element model.....	183

Figure 7.4.	Modelled bolts in the a) conventional model b) simplified model.....	183
Figure 7.5.	Superelement of the flange	184
Figure 7.6.	Superelement master nodes (thicker nodes 6 DOF, thinner nodes 1 DOF).....	185
Figure 7.7.	Finite Element model based on the superelement technique	185
Figure 7.8.	ROTT machine	186
Figure 7.9.	Experimental set up of the joint.....	187
Figure 7.10.	Torque multiplier.....	188
Figure 7.11.	Solid metal with facing gasket.....	188
Figure 7.12.	Behaviour of the half of the gasket under a compression load.....	189
Figure 7.13.	Common behaviour of a gasket under a compression load ...	190
Figure 7.14.	Behaviour of a previously compressed gasket (black line) and linear simplification (grey line)	191
Figure 7.15.	Tightening loads obtained with the superelement-based model, and the final load distribution obtained in the test bench using the linear gasket.....	192
Figure 7.16.	Tightening loads obtained with the superelement-based model, and the obtained final load distribution applying those loads on the test bench using the non-linear gasket.....	193

List of Tables

Table 1.1	Tightening torque to apply on bolts and the corresponding preload according to the tool type used for a preload of 70% [Nor'13]	41
Table 3.1.	Schematic representation of the ISM.....	73
Table 3.2.	Load level of every bolt in every load step during the inverse sequence.....	74
Table 3.3.	Load level on the bolts during the tightening sequence	79
Table 3.4.	Obtained tightening loads with the EICM for an optimized two pass tightening sequence.....	87
Table 4.1.	The four different load cases of matrix [A] elements. The equations were deduced from equation (3.5)	101
Table 4.2.	Values of matrix [A] coefficients using the EICM	102
Table 4.3.	Coefficients value of matrix [A] according to the TAM.....	108
Table 4.4.	Obtained initial loads with the Finite Element validation analyses	111
Table 5.1.	Experimental analyses performed for the validation of the multiple-pass TAM	124
Table 5.2.	Initial loads corresponding to the analyses of the Table 5.1	125
Table 5.3.	Obtained tightening loads with equation (3.4) for the illustrative example, and modification to avoid yielding load...	131
Table 5.4.	Additional loads and the new tightening loads obtained for the illustrative example	132
Table 5.5.	Obtained initial loads for the first pass with three iterations ...	133
Table 5.6.	Obtained initial loads for the second pass using the initial loads of the Table 5.5	133

Table 5.7.	Coefficients obtained with the TAM.....	136
Table 5.8.	Assembly patterns for the different joints	136
Table 5.9.	Relative errors obtained in each analysis.....	139
Table 5.10.	Obtained maximum errors in the four RTJs	139
Table 5.11.	Coefficients obtained with the TAM for the RTJs of class 150 a) coefficient α b) coefficient β c) coefficient γ d) coefficient δ	142
Table 5.12.	Coefficients obtained with the TAM for the RTJs of class 300 a) coefficient α b) coefficient β c) coefficient γ d) coefficient δ	144
Table 5.13.	Coefficients obtained with the TAM for the RTJs of class 400 a) coefficient α b) coefficient β c) coefficient γ d) coefficient δ	146
Table 5.14.	Coefficients obtained with the TAM for the RTJs of class 600 a) coefficient α b) coefficient β c) coefficient γ d) coefficient δ	148
Table 5.15.	Coefficients obtained with the TAM for the RTJs of class 900 a) coefficient α b) coefficient β c) coefficient γ d) coefficient δ	150
Table 5.16.	Coefficients obtained with the TAM for the RTJs of class 1500 a) coefficient α b) coefficient β c) coefficient γ d) coefficient δ	152
Table 7.1.	Geometrical dimensions of the gasket prior to the compression test.....	189
Table 7.2.	Geometrical dimensions of the gasket after the compression test.....	191

CHAPTER 1. INTRODUCTION, BACKGROUND AND OBJECTIVES

1. OVERVIEW

Oil pipelines are generally used for the transportation of petroleum, its derivatives and biobutanol right up to refineries or seaports (see Figure 1.1). Likewise, natural gas is transported via gas pipelines. The underlying idea of these systems is based on the aqueducts designed by the Romans for water transportation. The material used for Oil & Gas pipelines is plastic or metal, and the pipes can be built over ground, underground and also underwater [Zhi'16].



Figure 1.1. Oil pipeline

Pipelines for the Oil & Gas sector may run lengths of up to hundreds of kilometres to transport the product from one country to another. Aside from this, Oil & Gas pipeline designs are always different. Therefore, for the manufacturing of pipelines, general purpose pieces are manufactured (straight pipeline sections, pipe elbows, valves, etcetera), and subsequently they are assembled using joints [Tir'13]. Transportation is also simplified by reducing pipeline length. However, joints usually have leakages, whereby they have to be studied so as to increase their efficiency.

There are different criteria and measuring methods to determine if a joint is leaking or not [Sch'99]. In some applications, maximum loss rate can be a

drop of water per second and can be quantified with two flowmeters as in Figure 1.2, while in others, it is quantified as the number of soap bubbles under certain pressure conditions; in the most severe operating conditions, mass spectrometers can be necessary. As an illustrative example, in industrial applications zero leakage is usually defined as a helium leakage range between $1e-4$ and $1e-8$ cm^3/s ; however, in the Johnson Space Center (NASA), in Houston (Texas), a Nitrogen leakage value of $1.4e-3$ cm^3/s at 20.68 bars and room temperature is established as zero leakage. Accordingly, the admissible leakage rate is a relative concept and it must be carefully established for each application, taking the following features into account [Vei'03]:

- Fluid to be sealed.
- Environmental impact if the fluid leaks to the atmosphere.
- Risk of fire or explosion.
- Leakage limit rate.
- Other relevant factors to be considered in each situation.

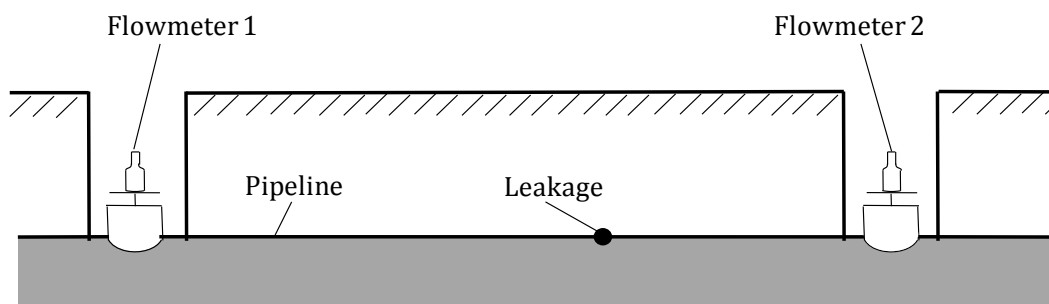


Figure 1.2. Measurement of a leakage with two flowmeters

The type of joint also has an important influence on the amount of leakages, as the seal is different for each joint. Nowadays, the most common joints are screwed joints, welded joints (with submerged arc welding or high frequency welding) and bolted joints.

The use of screwed joints is one of the oldest methods to connect two pipelines. It is cheap and also easy to assemble but, due to low mechanical strength, fluid sealing cannot be guaranteed. Therefore, they are generally used for pipelines with a diameter of less than 4", such as in low pressure secondary installations (condensers or water and air pipelines) or household pipelines (water and gas). Standard ASME B 31.3 [Asm'12(1)] requires conical

screws and an additional sealing weld is recommended when flammable, toxic or other dangerous fluids are transported via the pipeline.

Regarding welded joints, submerged arc welding and high frequency welding are the most commonly used methods. This method provides excellent mechanical strength (usually equivalent to pipeline strength), perfect and permanent sealing, good thermal insulation and requires little maintenance. On the other hand, the main disadvantages are disassembly difficulties and the need for skilled labour.

Finally, bolted joints are used to join two or more components and achieve a non-destructive disassembly point. As Figure 1.3 shows, it is composed by two flanges that have to be welded to the pipelines, a gasket to maximize sealing performance, and various bolts that pass through the holes of both flanges in order to keep them together. Bolted joints are especially used to join pipelines to valves, nozzles and other equipment. They are also used when, by using two flanges, a point that enables the disassembly of any element of the pipeline is required.

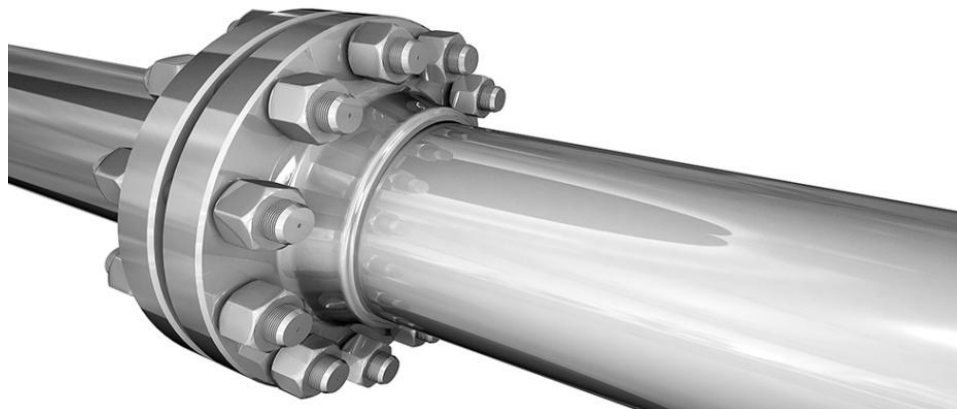


Figure 1.3. Bolted joint

Therefore, the main advantage of bolted joints is the ease of disassembly, which is also very useful for maintenance work. With these joints it is also very easy to join components of different materials, manufacturing processes or heat treatments. Furthermore, in contrast to welded joints, they do not add any form of residual stress or warping in the pipeline. However, these joints are not totally leakage-free. Besides, due to dynamics loads, temperature variations and other phenomena that will be later explained, bolts can lose part of their load, thus increasing leakages. This involves maintenance

operations, with studies on minimizing leakages to increase the efficiency of the pipeline usually performed, which entails a very high cost.

Bolted joint flanges are made with materials such as stainless steel, cast steel, aluminium, brass, bronze, plastic, etcetera, but most commonly with forged steel (with the subsequent machining process). Figure 1.4 shows the production system of forged steel flanges. It starts with heating and cutting the raw material in small blocks intended for each flange; then the block is forged to obtain the shape of the flange. Later, a heat treatment process is employed to improve the mechanical properties, and finally the flange is machined in order to obtain the desired surface finish.

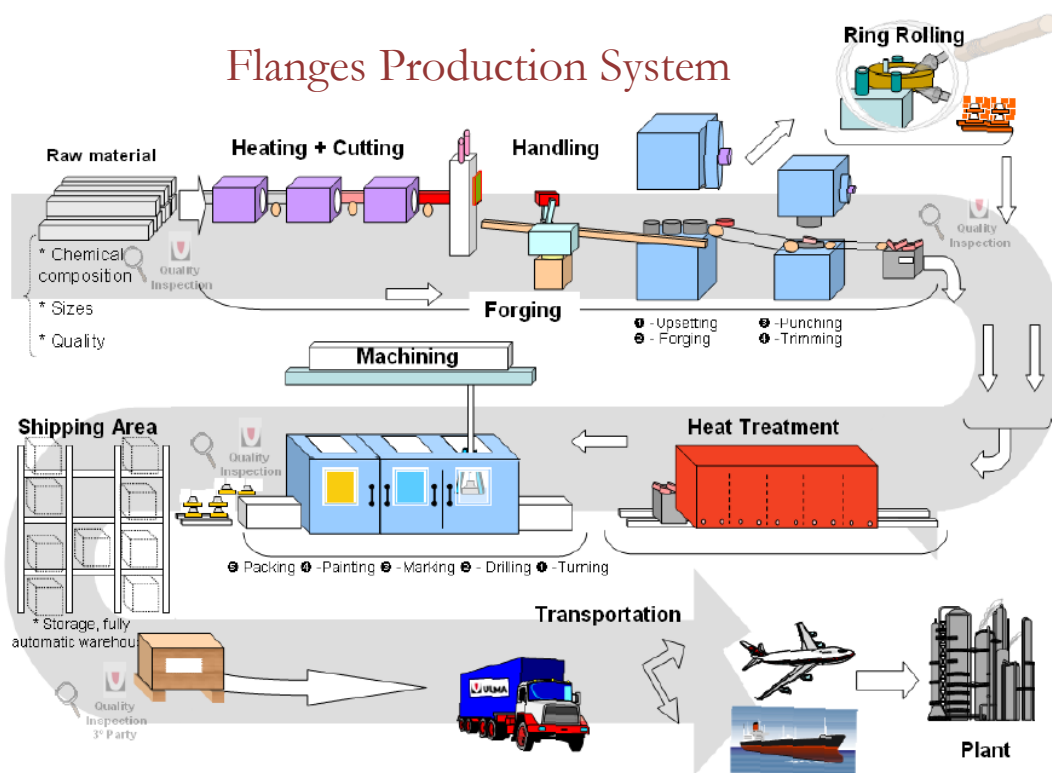


Figure 1.4. Production system of the forged steel flanges

Hot forging used in this process allows for the creation of objects with large dimensions and complex geometries. Excellent mechanical properties are also achieved. Homogenization and ductility are also improved, and chemical impurities are eliminated. The forging process starts with the block obtained from the raw material; then the pre-form is shaped out of the block which is subsequently forged, thus almost obtaining the final shape of the flange; finally, punching and clipping is applied to obtain the final shape. Figure 1.5 shows this forging process.

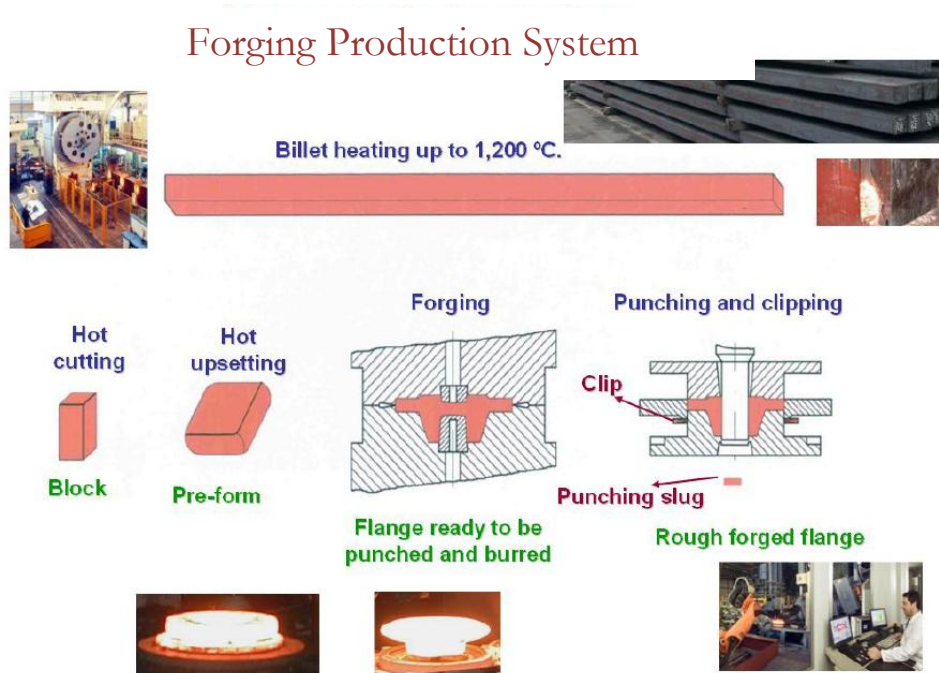


Figure 1.5. Flanges forging production system

In the machining process, the desired surface finish is obtained and bolts holes are created. Figure 1.6 shows the machining process for flanges. As can be seen, flange geometry is different for different flange types, and therefore the machining process is also different (flange types will be explained below).

Machining Production System

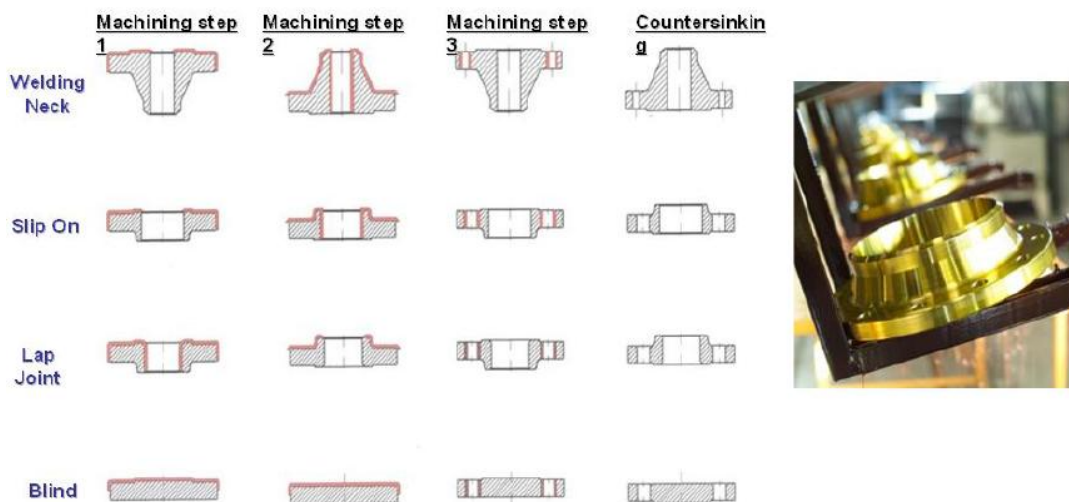


Figure 1.6. Machining process for flanges (in red the machined surfaces of that step)

In the Oil & Gas sector, the most common joints are Welding Neck (WN), Slip On (SO), Socket Weld (SW), Lap (LJ), Threaded (TH) and Blind (BL) flanges (see Figure 1.7). These flanges are standardized for unification, serial production and storage purposes. One additional reason is that, due to this standardization, these flanges do not have to be calculated but rather selected for the working conditions where they are to be applied. One of the most used standards is ASME B16.5 [Asm'13(1)], which establishes different flange classes depending on the working pressure-temperature ranges.

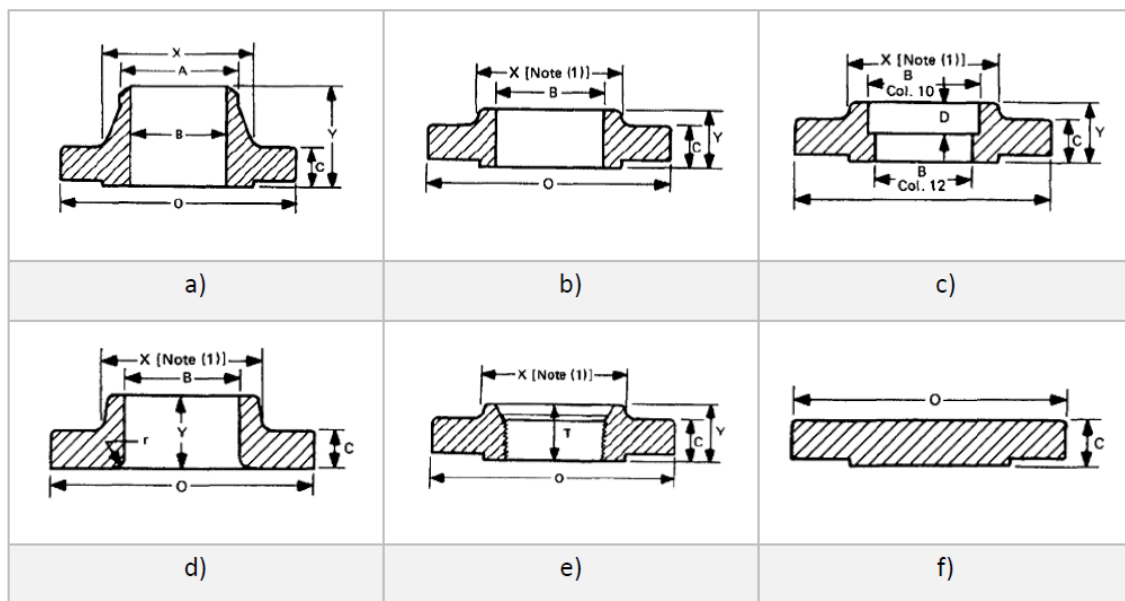


Figure 1.7. Standardized flanges in standard ASME B16.5 [Asm'13(1)] a) Welding Neck (WN) b) Slip On (SO) c) Socket Weld (SW) d) Lap (LJ) e) Threaded (TH) f) Blind (BL)

When pressure, temperature and size requirements fall outside the Standard range, special flanges must be used. These flanges are designed and calculated according to ASME BPVC Section VIII Division 1 Appendix 2 and S [Asm'11].

In addition to the aforementioned type of flanges, depending on the pressure and temperature requirements and on the nature of the fluid to be transported, the different flange faces shown in Figure 1.8 can be used: Flat face (FF), Raised face (RF), Male & Female (MF) and Ring Type Joints (RTJ) [Asm'11; Vei'03].

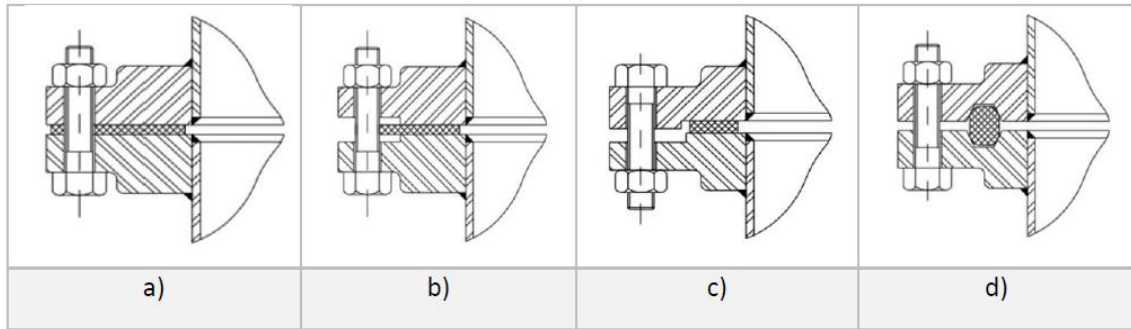


Figure 1.8. Type of flange faces [Asm´11]: a) Flat face (FF) b) Raised face (RF)
c) Male & Female (MF) d) Ring Type Joints (RTJ)

WN flanges (Figure 1.7a) with RTJ faces (Figure 1.8d) are very commonly used for Oil & Gas offshore pipelines, and they are selected according to three parameters [Asm´12(2); Asm´13(1)]: Nominal Pipe Size (NPS), Schedule (SCHD) and Class. NPS is the outer diameter of the flange (dimension A in Figure 1.7a); SCHD is the thickness of the pipe, and therefore, it establishes the inner diameter of the flange (dimension B in Figure 1.7a); finally, Class depends on the working pressure and temperature values. As the pressure and/or temperature increases the class is higher, and therefore, the joint will be larger.

WN flanges are butt-welded to the pipe. They are extremely resistant due to their reinforced neck and therefore they are used for high pressure conditions. On the other hand, flanges with an RTJ face have a groove in the sealing surface where a steel ring gasket is mounted. The gasket transversal profile can be oval or octagonal as shown in Figure 1.9. These joints can prevent leakages even when the internal pressure is extremely high. Also, if the internal pressure increases, the sealing pressure increases, because flange-gasket contact pressure is increased (see Figure 1.8d).

Therefore, a WN flange with an RTJ face (and with its metallic ring gasket), provides excellent performance even for extremely demanding pressures and/or temperatures. As mentioned before, these properties make them suitable for offshore applications, both top-side and sub-sea. This market is related mainly with oil platforms and vessels in the energy sector for oil and gas extraction. The strong isolation and reliability requirements in these transportation lines make these types of flange an optimal solution.

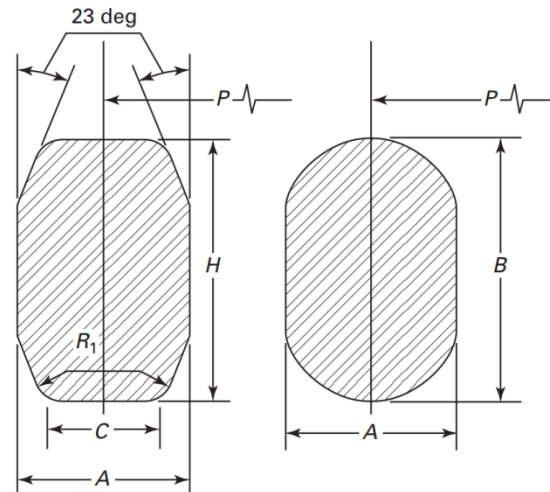


Figure 1.9. Transversal profile of ring gaskets [Asm'12(2)]

The main disadvantage of offshore applications is the pipeline construction due to the complexity of the process and the high cost they involve. There are various methods by which to perform this process depending on the following parameters: environmental conditions (for instance, ocean currents or the water regime), equipment availability and cost, water depth, pipeline diameter and length, and restrictions caused by the presence of other offshore structures [Ger'07]. The most popular methods are pull/tow, S-lay, J-lay and Reel-lay.

The pull/tow method joins offshore pipeline segments onshore, and the pipeline is then placed in the desired location as shown in Figure 1.10. The main advantage of this method is that the first inspections are carried out onshore [Fer'81; Pal'04].

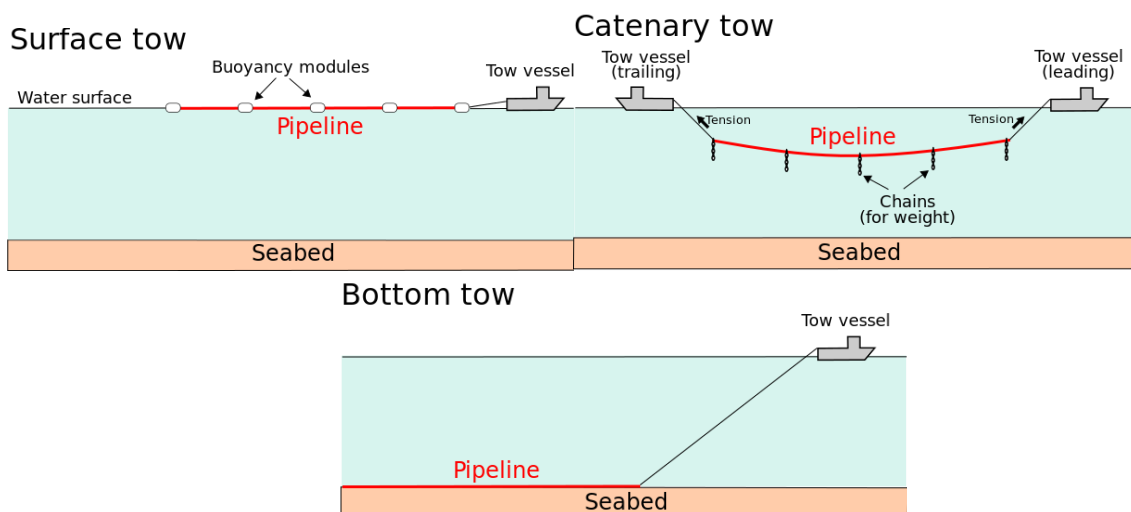


Figure 1.10. Pull/tow method for the assembly of offshore pipelines

The S-lay method is illustrated in Figure 1.11a. This method consists of joining pipeline segments in-situ, over a vessel which has all the necessary equipment. Then, it is positioned on the seabed using a stinger attached at the end of the vessel and a tensioning system (see Figure 1.11a). This creates the S-shape as the pipeline is positioned on the seabed. Nevertheless, this method is not adequate for extreme depths because the pipeline requires longer stinger and higher tension resulting in more risk. In this situation, the J-lay method is used because the pipeline is virtually vertical between the vessel and the seabed, so less tension is required (see Figure 1.11b). Besides, the stinger is not required. Comparing this method with the previous one, the main disadvantage is that only one pipe segment can be assembled at a time, so it is slower. Finally, in Figure 1.11c the Reel-lay method is shown. This is similar to the previous two methods but, in this case, the pipeline is assembled onshore and is later rolled in a reel of large dimensions (these dimensions depend on the flexibility of the pipeline). The disadvantage of this method is that it can only be used for pipelines with diameters of under 400 mm [Alk'08; Guo'94].

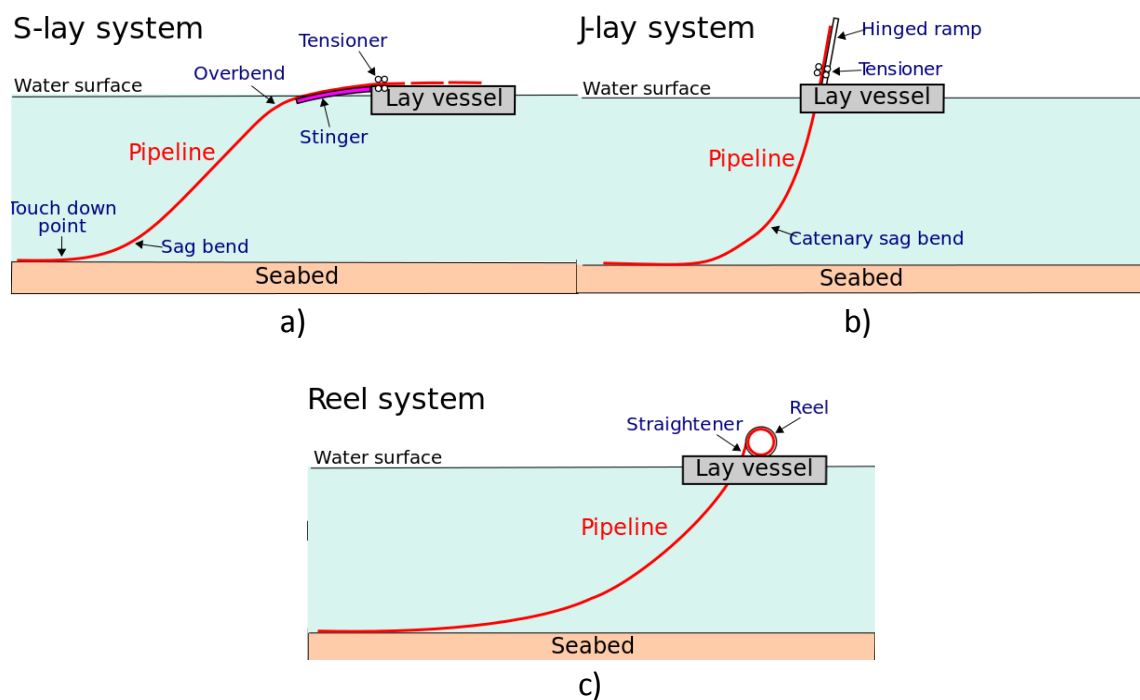


Figure 1.11. Methods for the assembly of offshore pipelines: a) S-lay method b) J-lay method c) Reel-lay method

Finally, it must be mentioned that the bolts of bolted joints in these pipelines must be tightened to a uniform load in order to ensure uniform stress distribution on the gasket so as to guarantee a good sealing. Minimizing

leakages is critical because fluid losses can be dangerous (environmental impact or personal injuries); besides, the efficiency of the pipeline decreases and the maintenance work increases, causing significant financial loss.

Even though obtaining a uniform bolt load may seem a simple task, it is not straightforward and it requires many work hours. The reasons for this complexity are the phenomena known as elastic interaction, solid rigid motion and short-term relaxation (explained in section 3 of this Chapter). Besides, as it can be read in specialized literature, sealing load is not obtained just with high quality elements or with a good flange design. Sealing load is generally obtained with the tools and procedures that have been provided in the assembly line and under the particular working conditions. To this end, it is very important to understand the assembly process [Bic'95]. In next sections this process and all the difficulties to obtain a uniform bolt load will be explained with the purpose of finding a solution to this problem.

2. PRELOAD IN BOLTED JOINTS

Bolted joints need to be preloaded to a uniform bolt load to adequately fulfil their structural role. This uniform bolt load is known as the preload of the joint [Deu'75; Juv'00; Nor'06; Shi'77]. Thus, continuity of the structure is obtained, and the structure's performance against external loads can be improved. Additionally, in pipelines, preloading is necessary to avoid leakage of the fluid or gas being transported.

In this section, the performance of preloaded joints is reviewed together with bolt load variations when external loads are applied. Accordingly, it will be possible to understand the benefits of preloading and take advantage of them hereinafter. Furthermore, the influence of preloading is studied more specifically in pipeline bolted joints.

2.1. PRELOADED BOLTED JOINTS PERFORMANCE

In the last fifty years, significant improvements have been obtained in bolts design and reliability. Nevertheless, even a well-designed bolt does not make the joint safer. For that purpose it is necessary to understand the joints mechanical performance. Bolt preloading is very important because, among other things, with this it is possible to improve joint performance against

external loads. In order to study preload advantages, first the mechanical balance of a preloaded joint with a single bolt is studied as shown in Figure 1.12.

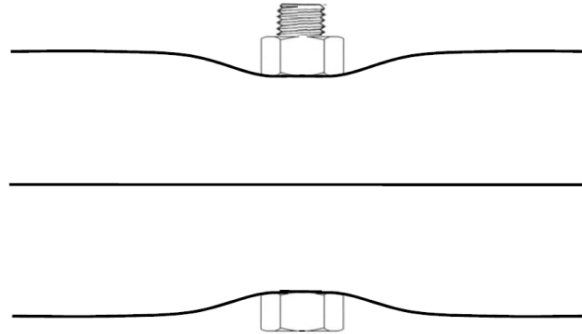


Figure 1.12. Preloaded joint

In this case, the bolt is under a tension load while the elements to be joined are withstanding a compression load. As the joint is in static balance, the tension load and the compression load module have the same value. In order to simplify the complexity of the system, it is possible to replace the system with two springs working in parallel and located between the bolt head and the nut, one of them working under tension (the bolt), and the other one compression (elements to join). The static balance equation of the system can be formulated as follows [Aba'12]:

$$F_p = F_e = F_t = K_e \cdot \delta_e = K_t \cdot \delta_t \quad (1.1)$$

Where:

F_p = preload

F_e = compression load of the elements to join

F_t = tension load of the bolt

K_e = compression stiffness of the elements to join

K_t = axial stiffness of the bolt

δ_e = deformation of the elements to join

δ_t = deformation of the bolt

The state of balance of joints is usually represented with the joint diagram, which can be seen in Figure 1.13. On the left of the diagram is the load and deformation that the bolt is withstanding, and on the right, the load and deformation that the elements to join are withstanding. Thus, the resulting slope of the lines is the stiffness of both elements, or if the simplified model is used, of both springs.

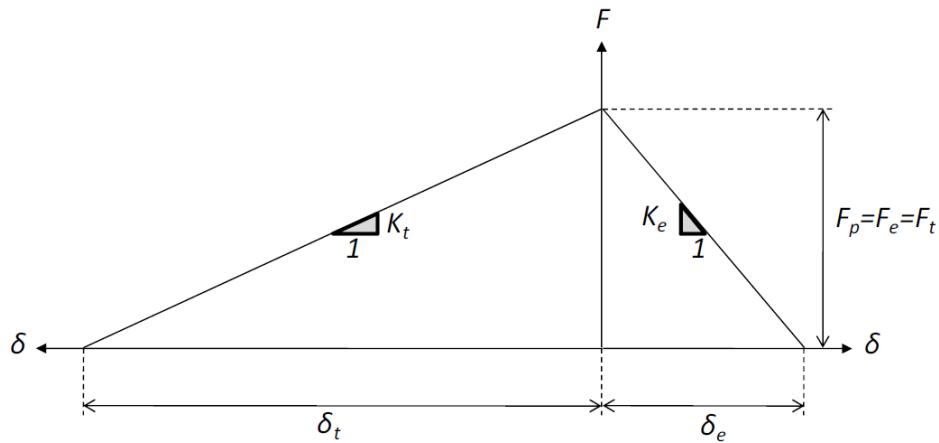


Figure 1.13. Joint diagram of the Figure 1.12 [Aba '12]

Assuming that the joint is in the state of balance of Figure 1.12, an external axial load P will be applied as shown in Figure 1.14. Usually, this simplified load case does not take place in practice; however, it is a good way to understand joints performance and its representation on the joint diagram.

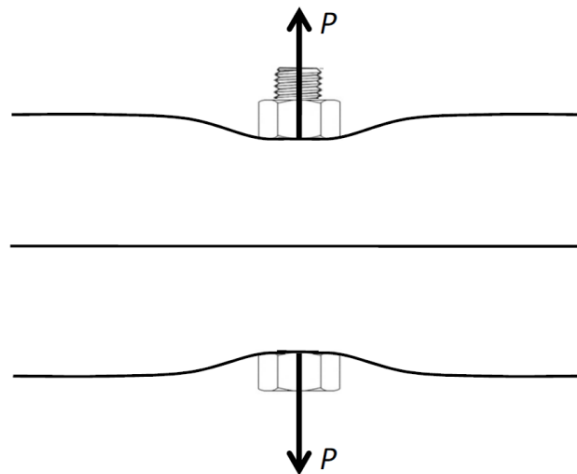


Figure 1.14. Preloaded joint under external axial load [Aba '12]

After applying the external load P , the new load on the bolt and on the elements to join are [Aba'12]:

$$F_e = F_p - K_e \cdot \Delta\delta \quad (1.2)$$

$$F_t = F_p + K_t \cdot \Delta\delta$$

Where the applied external load is P :

$$P = (K_t + K_e) \cdot \Delta\delta \quad (1.3)$$

At this point, the load factor of the joint is defined [Jun'74]:

$$C = \frac{K_t}{K_t + K_e} \quad (1.4)$$

Replacing (1.3) and (1.4) in (1.2), the load of the bolt and of elements to be joined can be obtained according to the load factor.

$$F_e = F_p - (1 - C) \cdot P \quad (1.5)$$

$$F_t = F_p + C \cdot P$$

Prior to applying the external load (Figure 1.12), the bolt was under a tension load F_p and the elements to join under a compression load F_e . The applied external load helps the elements to withstand the load applied by the bolt, i.e., the elements to join are relieved when the external load is applied. As the deformation and the stress are proportional, reducing the load of the elements to join results in partial recovery of their initial thickness. In the same way, the bolt tension load is increased because its displacement increases. It should be noted that the length increase of the bolt is equal to the thickness increase of the elements to join. This will help to understand the joint diagram of the Figure 1.15.

Usually, bolt stiffness is much less than the stiffness of the elements to join. This means that the same deformation implies a higher load variation in the elements to join than in the bolt. On the other hand, the applied external load P must be the sum of the load variation of the bolt and of the elements to join (see Figure 1.15). In this sense, bolt load increase is much lower than the applied external load; the rest of the external load is absorbed by the elements to join.

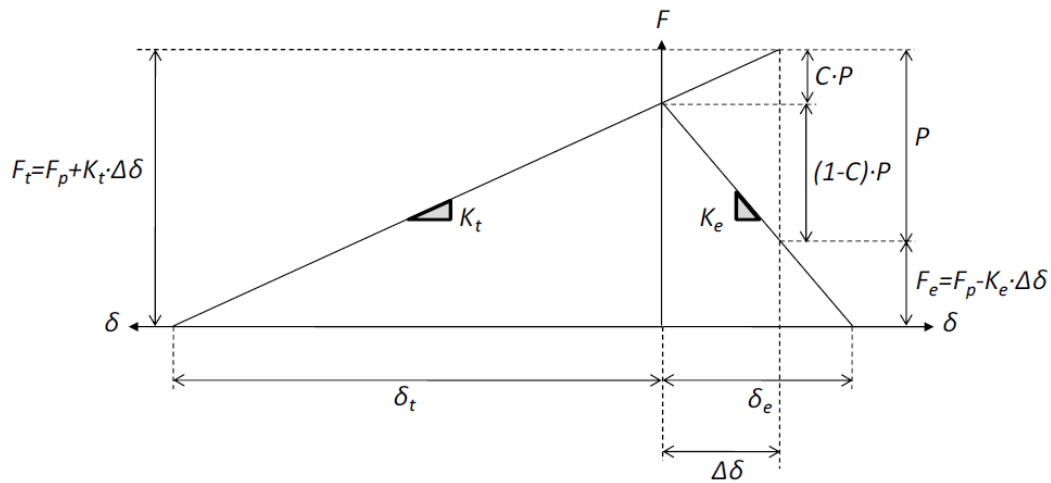


Figure 1.15. Joint diagram of the Figure 1.14 [Aba '12]

Once understood the performance of joints under external loads which are applied on bolt heads and the nut (see Figure 1.14), the influence of external loads applied on an intermediate plane of the joint will be studied (see Figure 1.16). This case can be considered more realistic than the previous one when a bolted joint is withstanding an axial load. Now the equation (1.5) cannot be directly used because the elements to join are not completely decompressed, only the part of the elements located between the two load planes is decompressed; the compression load of the elements remaining part increases.

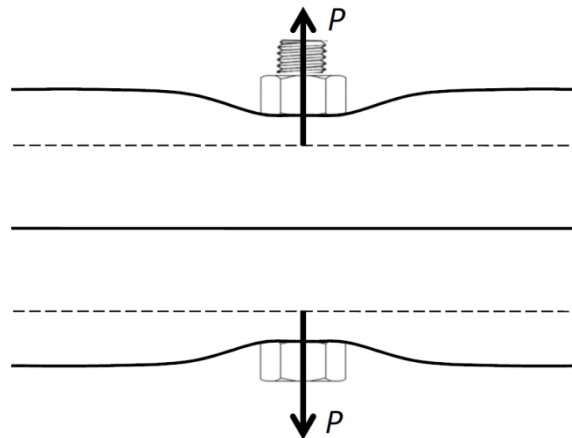


Figure 1.16. Preloaded joint under external axial load which is applied on an intermediate plane [Aba '12]

In this case, in order for the equation (1.5) to be valid, the load factor has to be multiplied by a coefficient n called loading plane factor, which varies between zero and one [Bic'95]. More precisely, the loading plane factor is equal to the ratio between the distance between load planes and the distance between bolt head and nut. Thus, the lower the distance between load planes,

the lower the load that will be absorbed by the bolt. Therefore, modifying equation (1.5) for external loads on intermediate planes:

$$F_e = F_p - (1 - n \cdot C) \cdot P \quad (1.6)$$

$$F_t = F_p + n \cdot C \cdot P$$

The extreme situation takes place when the external loads are applied on the contact plane of the elements to join. In this case the loading plane factor is null ($n=0$), and therefore, bolt load does not increase when an external load is applied. The last hypothesis is only valid while the external load is lower than the preload, because on reaching this point the contact between the elements to join will be lost. The same happens with the previously obtained equations: they are only valid while the elements to join are in contact.

Based on the mathematical reasoning presented it may appear that studying a joint under external axial loads is quite simple. However, estimating joint stiffness and loading plane factor is very complicated. Different ways can be used to calculate joint stiffness, where the volume under compression load between the bolt head and the nut is considered as a barrel [Mot'76], cylinder [Mey'72] or truncated cone [Osg'72] shape. On the other hand, to calculate the loading plane factor the location of the loading planes needs to be known. Nevertheless, the loading plane is a theoretical concept as point loads. Regardless, estimates and assumptions can be made by performing the Finite Element analyses.

With these examples, it has been proven that a preloaded joint's performance improves considerably against axial external loads. This is because the elements to join absorb the majority of the external load due to their higher level of stiffness. Therefore, it will be more difficult to reach bolt yielding load and, as a consequence, joint failure. Likewise, if the axial load is variable over time, the bolt will only absorb part of that load. In this situation, the bolt has a mean and an alternating load: the preload F_p of the bolt generates a mean load, while the external load P generates a mean and/or alternating load, depending on its behaviour. Thus, the mean and the alternating load in the bolt, F_{tm} and F_{ta} , are:

$$F_{tm} = F_p + C \cdot P_m \quad (1.7)$$

$$F_{ta} = C \cdot P_a$$

Where P_m and P_a are the mean and the alternating components of the external load P . As a consequence, bolt fatigue failure will be less likely. As an illustrative example, Figure 1.17 shows the behaviour of one bolt when it is not preloaded (1) and when it is preloaded (2), and as it can be seen, in the first situation it exceeded the fatigue limit while in the second one it does not exceed the limit.

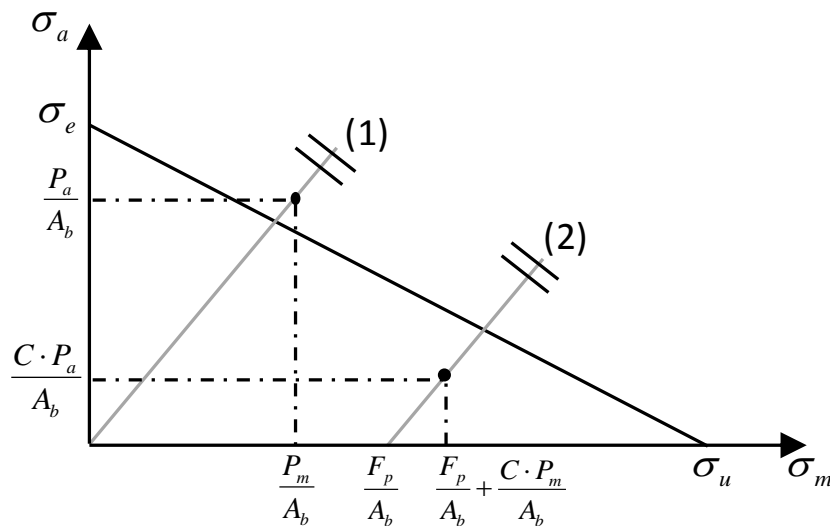


Figure 1.17. Behaviour of one bolt when it is not preloaded (1) and when it is preloaded (2)

On the other hand, preload is also advantageous when the joint is withstanding shear loads. Due to preload, the normal force that arises on the contact surfaces is higher, so the friction force will also be higher. Friction load applies resistance against bolt shearing load, and against crushing and tearing of the elements to be joined. Accordingly, performance against shear external loads is improved.

Finally, preload also avoids screw-loosening over time due to different phenomena such as vibrations, thermal cycles or impacts, amongst others [Bau'66; Daa'90; Esn'79; Jun'69; Sak'78]. All works agree that screw-loosening is caused by the reduction or elimination of friction load between bolt threads and between the nut and the element. However, they disagree on the mechanism which generates friction load loosening. Nevertheless, it is clear that the higher the preload of the joint, the greater the normal force between bolt head and element and between nut and element. To this regard, due to preload friction the load will increase, and therefore, the screw-loosening phenomenon will decrease.

If screw-loosening does occur, there are other methods to avoid this phenomenon [Aba'12]: increasing the friction coefficient between contact surfaces [Mck'80], preventing sliding contact between surfaces designing the elements for that purpose [Bon'80], reducing the tilt angle of the screw thread, using bolts or nuts with insertions [Ifi'82; Ifi'87; Ifi'93], using geometrical distortions on the bolt or nut in order to generate an interference on the contact surface [Spi'80; Dur'80], using locking pins and wires, or applying an adhesive [Loc'79] or even welding. It is also common to use special washers, which serve to maintain bolt preload (Belleville nut) or generate an interference on the nut element contact surface (serrated lock washers) or both things at the same time (spring lock washers) [Cha'91]. Figure 1.18 shows several of these methods and mechanisms.

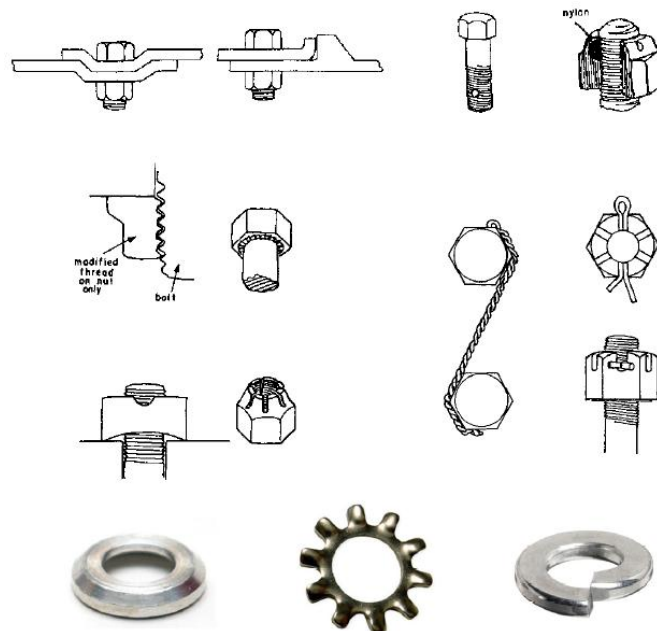


Figure 1.18. Methods to prevent screw-loosening [Bic'95]

2.2. PRELOAD IN PIPELINES BOLTED JOINTS

To discover the advantages the preload provides to the pipelines bolted joints, the loads that the joint is withstanding must first be known. Figure 1.19 shows the main loads that appear in this type of bolted joints [Vei'03]:

- Radial load: Is caused by the internal pressure and tends to expel the gasket.
- Separating load or hydrostatic load: Is also caused by the internal pressure, but in this case it tends to separate the flanges.

- Preload on the bolts: Is the total load provided by the tightening of the bolts.
- Load of the flanges: Is the load that compresses the flanges against the gasket. Initially, this load is equal to the preload of the bolts, but once the system is pressurized, this load is equal to the preload of the bolts minus the separating load.

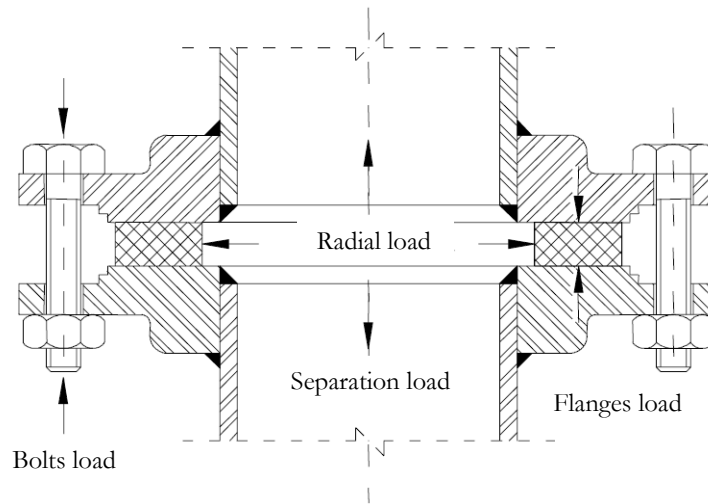


Figure 1.19. Acting forces on a bolted joint [Vei '03]

The preload of the bolts, in addition to compensating the separating load caused by the internal pressure, must compress the gasket to avoid leakage of the fluid to be transported. Additionally, recalling the advantages that the preload generally provides for the performance of bolted joints, the requirement of preloads in the pipelines bolted joints is demonstrated.

In the bolted joints of pressurized pipelines, to calculate bolt optimum load it is necessary to use the standard ASME BPVC Section VIII Division 1 Appendix 2 section 2-5 [Asm'11]. This standard explains that in the design of a bolted joint, the calculations must be performed for two different design conditions: operational conditions and assessment of the gasket.

The operational conditions are those required to support the hydrostatic load caused by the design pressure and keep enough compression load on the gasket contact surface to ensure a hermetic joint (everything at the design temperature). The minimum load is in accordance with the design pressure, gasket material and the effective contact area.

The gasket assessment is a loss of load on the bolts after they have been preloaded due to small plastic deformations that occur on the joint. The

assessment level depends on the microscopic imperfections on the contact surfaces, the material of the elements in contact and in the effective contact area between threads. This phenomenon will be explained in more detail in the next section.

3. UNCERTAINTY FACTORS IN BOLT PRELOAD

With the requirement of preloading bolted joints explained, the way in which this preload is obtained will be explained. Assembly of pressurized pipeline bolted joints is a very complex process that, as mentioned before, aims to ensure the integrity of the joint between two pipe sections, in order to obtain a successful seal so as to avoid leakage of the fluid to be transported. Most failures on bolted joints are due to an inadequate preload on the bolts rather than due to design flaws of the flanges or bolts. To this regard, calculations have shown that 75% of joint failures can be avoided if correct bolt preloading is achieved [Loa'www]. However, obtaining a uniform preload on the bolts (and with that a uniform pressure distribution on the gasket) is a difficult task. This is the result of several uncertainty factors that affect bolt preloads. The most significant uncertainty factors are reviewed in this section.

Before explaining the uncertainty factors, two important terms used throughout this Doctoral Thesis must be explained: initial load and final load on the bolts. On the one hand, the term initial load relates to the load the bolts are tightened to during the tightening sequence, i.e. the tightening load. On the other hand, the term final load relates to the load of bolts once the tightening sequence has been completed. Generally, there is a significant difference between the initial and final load on the bolts due to bolt final load uncertainty factors. Moreover, as will be explained next, it is also very difficult to obtain a precise value of the desired initial load due to bolt initial load uncertainty factors.

3.1. BOLT INITIAL LOAD UNCERTAINTY FACTORS

Bolt initial load can be obtained with a torque wrench or with a bolt tensioner. However, the uncertainty each method generates in the initial load is different. Accordingly, the uncertainties arising from the use of each method are explained in this section.

3.1.1. TORQUE WRENCH

Nowadays, the most common method for applying bolts initial load is a torque wrench. It is used because it is a cheap method and because the accuracy it provides is sufficient for most applications. It consists of increasing the torque value until the bolt is preloaded to the desired initial load. Experience and theoretical analysis indicates that, as a general rule, there is a linear relation between both factors.

In order to study this phenomenon theoretically, it can be assumed that the ratio between the torque and the obtained initial load behaves as a block over an inclined plane (see Figure 1.20) [Shi'77; Nor'06; Juv'00; Deu'75]. Thus, the block represents a nut thread that tries to climb along the bolt thread when a tightening load F_a is applied with the torque wrench. Therefore, the angle of the inclined plane is equal to the thread angle (λ), and the block weight is equal to the bolt load (F), as explained in [Aba'12].

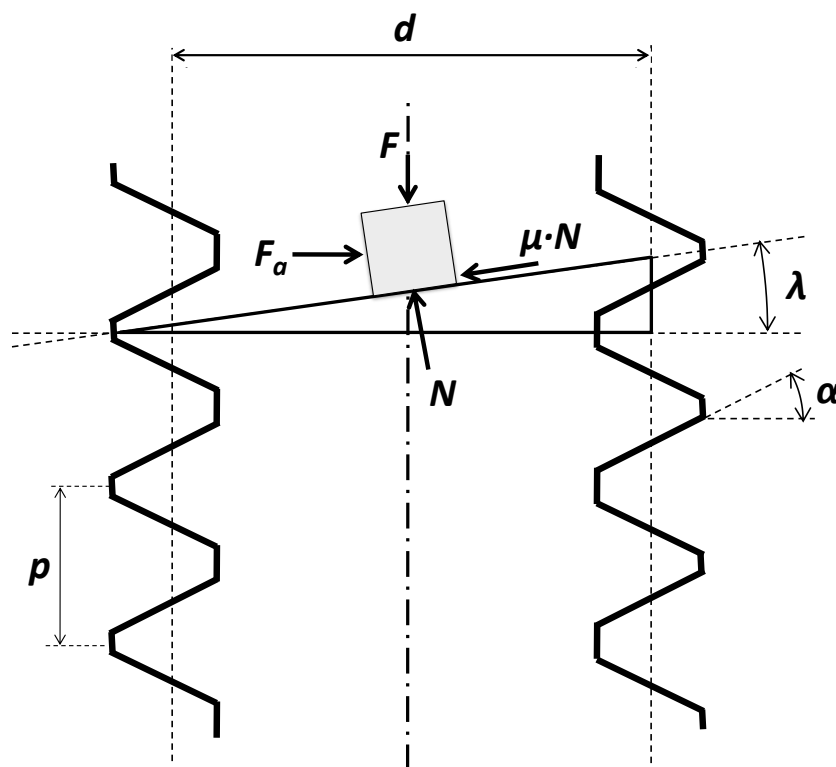


Figure 1.20. Parameters which affect the ratio between the torque and the initial load [Aba'12]

As can be seen in Figure 1.20, to raise the block along the inclined plane it is necessary to overcome bolt load multiplied by the sine of the thread angle, and the generated friction load between the threads. It is also necessary to

overcome the generated friction load between the nut and one of the elements to be joined. Thus, it is possible to devise the equation (1.8) which relates the applied torque T (F_a if it is considered as a force) in the bolt with the obtained bolts initial load F [Juv'00]:

$$T = F_a \cdot \frac{d}{2} = F \cdot \frac{(\mu + tg\lambda \cdot \cos\alpha)}{(\cos\alpha - \mu \cdot tg\lambda)} \cdot \frac{d}{2} + \mu' \cdot F \cdot \frac{d_t}{2} \quad (1.8)$$

Where:

λ = angle of the threads

α = angle of the threads section

μ = friction coefficient between the threads of the bolt and the nut

μ' = friction coefficient between the nut and the element to be joined

d = diameter of the bolt (metric)

d_t = average diameter of the nut, the value of which usually is taken as $1.5 \cdot d$

Instead of using the equation (1.8), it is possible to use the equation (1.9) which was devised by Motosh and simplify the equation assuming that $\cos\alpha \gg \mu \cdot tg\lambda$. The main advantage of this equation is that is possible to clearly differentiate between the three resistances that the torque has to overcome: the part of the bolt load (first term of the equation), the friction between threads (second term of the equation) and the friction between the nut and the elements to join (third term of the equation).

$$T = F_a \cdot \frac{d}{2} = F \cdot tg\lambda \cdot \frac{d}{2} + F \cdot \frac{\mu}{\cos\alpha} \cdot \frac{d}{2} + \mu' \cdot F \cdot \frac{d_t}{2} \quad (1.9)$$

In this equation, the load F_a has a horizontal direction like the other loads that take place in the equation. Having said this, a more simplified equation is typically used:

$$T \cong K \cdot F \cdot d \quad (1.10)$$

Where the coefficient K is called nut factor, and has the following value:

$$K = 0.5 \cdot \frac{(\mu + tg\lambda \cdot \cos\alpha)}{(\cos\alpha - \mu tg\lambda)} + 0.625 \cdot \mu' \quad (1.11)$$

However, experience has shown that the coefficient K can only be obtained experimentally, and besides this, it has to be recalculated for each application. Accordingly, it is possible to take into account everything that affects the ratio between the torque and the initial load of the bolt, including friction, torsional deformation, bending, plastic deformation on the threads and any other factor that may have influence.

Nevertheless, for a general purpose study, specialist literature shows that K has an approximate value of 0.2, with a standard deviation of 0.05 (see Figure 1.21) [Bic'95]. The main reason for this scatter is the friction coefficient dispersion, since its value depends on the lubrication used, thread maintenance, the materials and many other factors that are widely known. The scatter is also caused due to phenomena such as geometric imperfections on the joint elements (perpendicularity, thread tolerance), misalignment between bolt and hole, accuracy of the torque wrench, operator skills, amongst others [Ste'73; Cle'89]. As a consequence of these dispersions, when a bolt is torque tightened, the result has a typical approximate error of 30% in the bolt initial load.

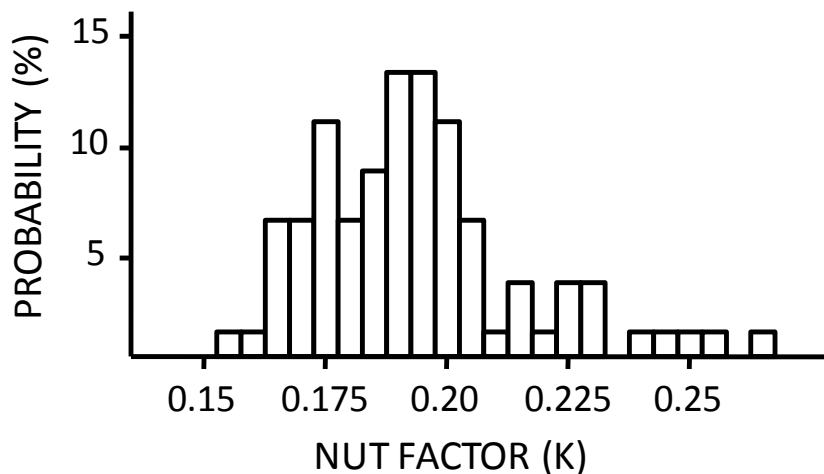


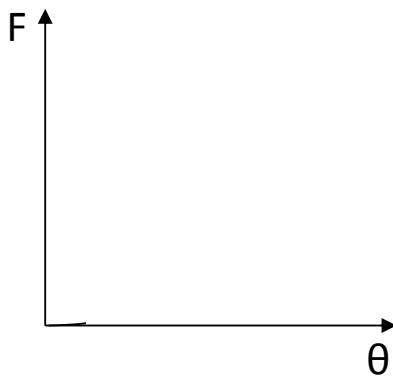
Figure 1.21. Typical values for the nut coefficient K [Bic'95]

Another method to control the bolt initial load is to control the rotation of the nut. After all, torque is applied in order to rotate the nut and obtain a linear displacement that compresses the elements to be joined. And it is simple to obtain the linear displacement of the nut because it is directly related

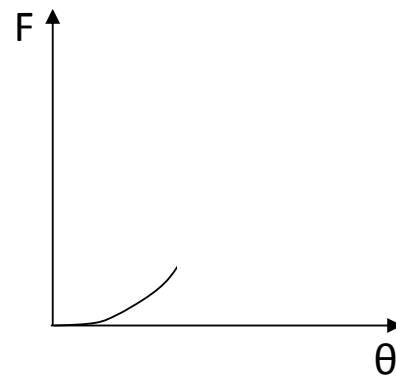
to the rotation of the nut by the pitch. However, obtaining the initial load is not as easy as it appears. It will be assumed that a joint is being preloaded. In the first turns, the nut does not generate any initial load because the nut and the elements to join are not in contact yet, so the nut rotates without increasing the preload of the bolt. This is illustrated in Figure 1.22a. Once the nut is in contact, the elements to join start to get compressed while the bolt starts to be tensed. However, the elements to join are not completely flat due to geometric imperfections, and the same is the case with the washer. As a consequence of these imperfections, the bolt load will start to increase but most of the nut rotation will be absorbed by the joint in order to correct these defects. Therefore, as illustrated in Figure 1.22b, the bolt load will increase slightly. Once all the imperfections have disappeared, bolt tension begins to increase and the elements to join start to get compressed in relation to their stiffness (see Figure 1.22c). At this point, the initial load starts to increase rapidly, in a linear fashion, with the following slope:

$$\text{Slope} = \frac{\Delta F}{\Delta \theta} = \frac{K_t \cdot K_e}{K_t + K_e} \cdot \frac{p}{360} \quad (1.12)$$

Where ΔF is the bolt initial load variation, $\Delta \theta$ variation of the nuts rotation (in degrees), K_t and K_e the stiffness of the bolt and of the elements to join and p is the bolt pitch. If it were possible to measure the moment at which this phase starts, it would be possible to obtain an precise measure of the preload. However, it is very difficult to measure this moment, and aside from that, it is also very different for different joints. Finally, if the rotation of the nut continues, some parts of the joint will start to plasticize. This phase corresponds to Figure 1.22d.



a)



b)

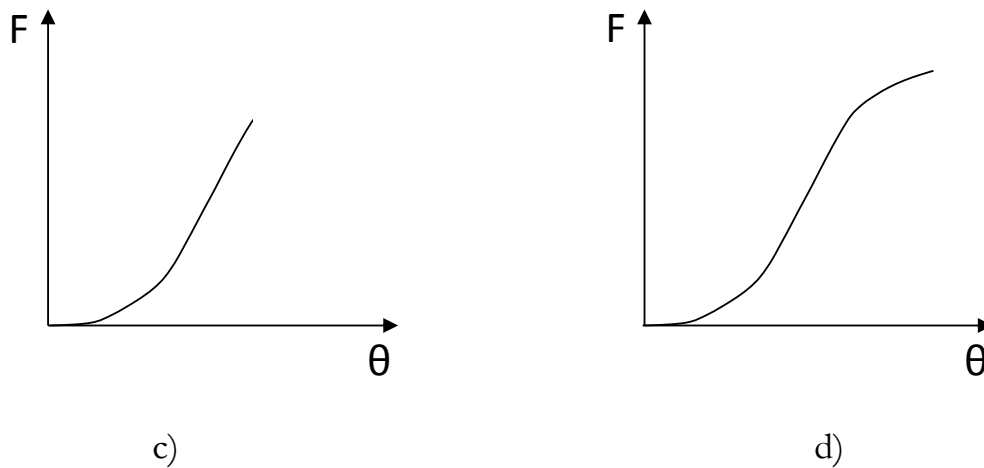


Figure 1.22. Relation between the initial load and the rotation of the nut during the bolt tightening process [Aba '12]

This method may appear simpler than the previous one which relates torque with the bolt initial load, because until this moment the friction coefficient did not bear any influence. However, friction coefficient can only be avoided if relative rotation between the nut and bolt head is measured, and not the absolute rotation, as is usually measured. Excluding laboratories, nut rotation is always measured against a machine, the floor or other fixed reference point. In this case, the nut may start rotating without increasing the initial load, due to an elevated friction load on the threads that the tightening load has not been able to overcome. On the other hand, the bolt may be well lubricated and therefore the relative rotation is equal to the absolute rotation due to a null friction load. However, on a real joint, an intermediate case takes place where the initial bolt load increases but not entirely, as is the case due to the friction coefficient, because, as mentioned before, it produces a scatter between the absolute rotation and the relative rotation.

Consequently, as in the method that relates torque with the bolt initial load, in this method, the friction coefficient also has a significant influence. Figure 1.23 shows the relation between bolt initial load and the rotation of the nut for different friction coefficients. As can be seen, the friction coefficient has a considerable influence.

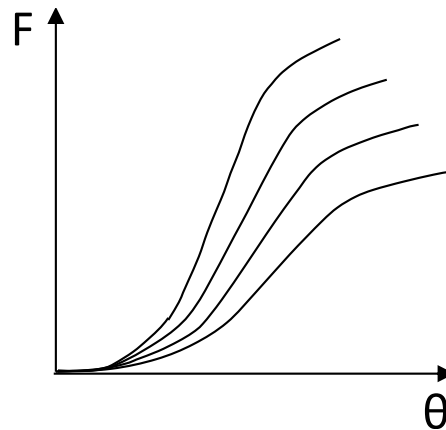


Figure 1.23. Relation between bolt initial load and nut rotation for different friction coefficients [Aba '12]

Another way to measure bolt initial load is to control bolt length variation and accordingly directly obtain the load that the bolt is withstanding. With these procedures it is possible to obtain more accurate results, but it is generally more expensive. The various tools that can be used for this procedure are strain gauges, micrometers, washers or cells with a load indicator, bolts with a load indicator or the ultrasonic measurement tools, amongst others (see Figure 1.24).

The most common method to measure length variation is by putting strain gages in the bolts [Bib'92; Bib'96; Kum'03; Lej'11; Nas'05]. In each bolt, two strain gages are located with a 180° separation between them, in the non-threaded zone and in a longitudinal direction. The deformation of the strain gages is obtained with an acquisition system which is connected to a computer. The reason for applying two strain gages on each bolt is to control the bending deformation. To obtain the final result, the computer obtains the average deformation of the two strain gages and, with the average deformation, obtains the bolt preload. The main advantage of this method is that it provides accurate results and is not overly expensive. However, it has the disadvantage that test bench assembly is more laborious than with other methods.

Furthermore, ultrasound measuring equipment is more expensive than strain gages but it is easier to assemble and provide very precise measurements [Bic'95; Jha'06]. This method has been used for the test bench designed and used in this Doctoral Thesis. To this regard, a more detailed explanation is provided in Chapter 2.

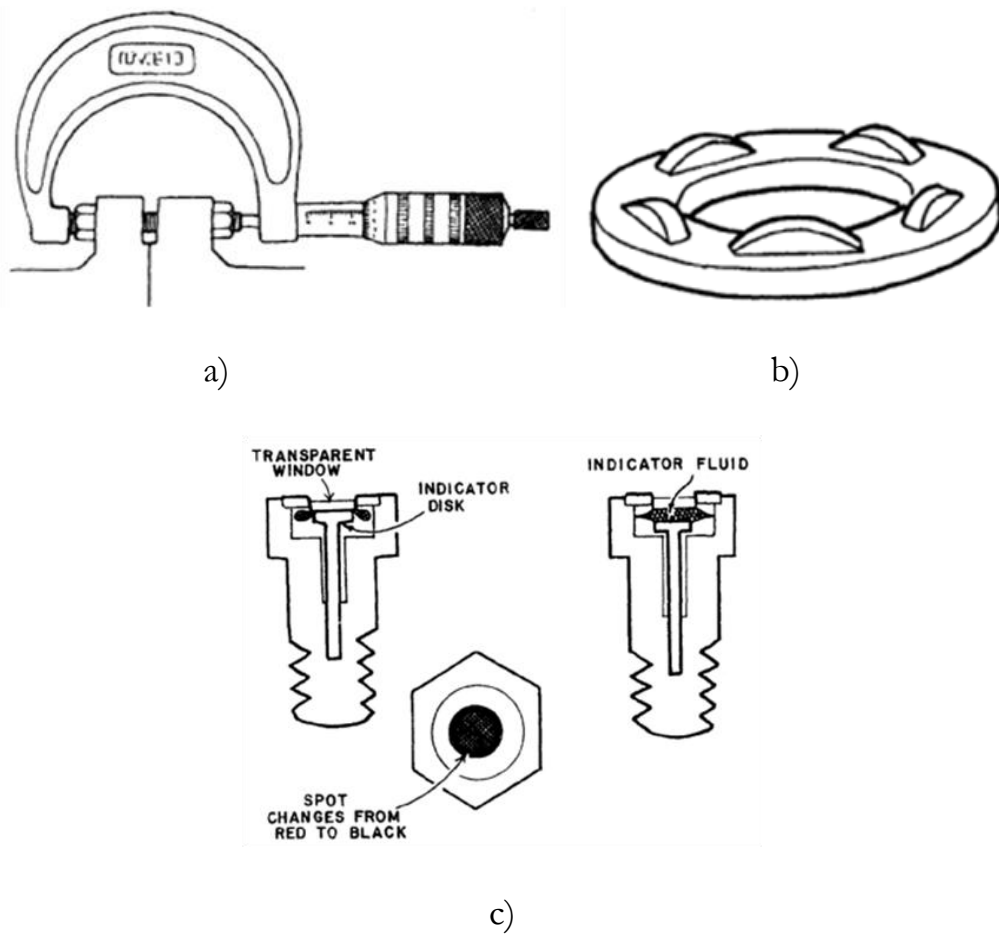


Figure 1.24. Tools for the bolt load measurement: a) micrometer b) washer with a load indicator c) bolt with a load indicator [Bic '95]

3.1.2. BOLT TENSIONER

In all the methods presented thus far, the load in the bolt was applied with a torque wrench. However, there is another tool that applies and measures the bolt load at the same time: this is called a bolt tensioner (see Figure 1.25). This tool applies tension directly on the bolt and therefore simultaneously controls the initial load of the bolt. As will be explained next, this procedure has very significant advantages, but just as the previous procedures, its precision is far from perfect.

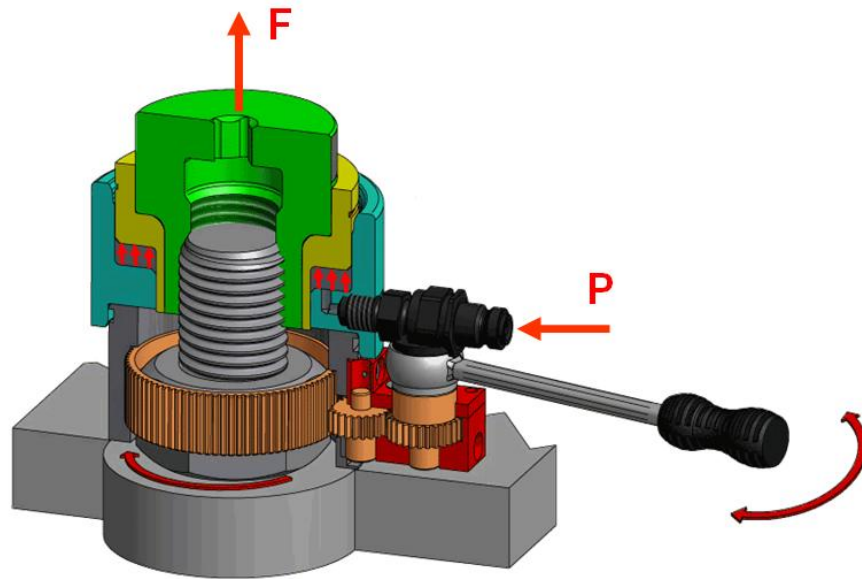
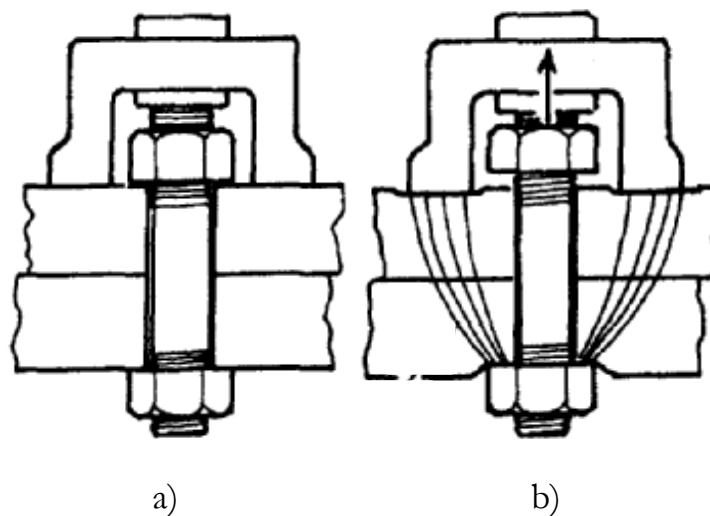


Figure 1.25. Bolt tensioner [Ith 'www]

The working procedure of the bolt tensioner can be understood with Figure 1.26. To start tensing the bolt, a threaded element is applied on the last part of the bolt (beyond the nut). This element will later apply the tension load on the bolt. This first step is shown in Figure 1.26a. Once the bolt and the threaded element are attached, a pressurized fluid (usually oil) is added and, as a consequence, the threaded element moves up, tensioning the bolt, as shown in Figure 1.26b. At this point of the process, the bolt load is accurately monitored. In the next step, the nut is tightened with a torque wrench until it comes into contact with the elements to join as shown in Figure 1.26c. Finally, the bolt tensioner is depressurized and removed so the nut starts to withstand the bolt load (see Figure 1.26d).



a)

b)

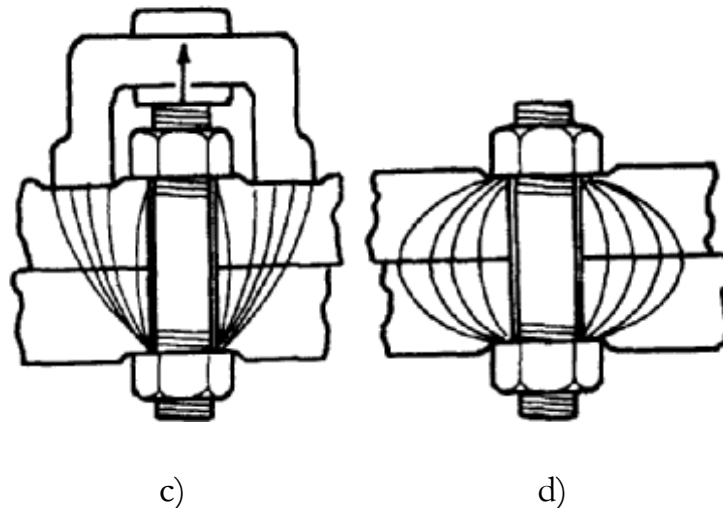


Figure 1.26. Working procedure of a bolt tensioner a) the threaded element is attached b) the bolt is tensed c) the nut is tightened d) the bolt tensioner is removed [Bic'95]

The main advantage of this method is that the involved error is much smaller than applying the initial load with a torque wrench, especially because the friction coefficient is not involved in the process; nevertheless, the error is still not null [Bic'95]. The error is due to the fact that the stress transmission lines are different before and after removing the bolt tensioner, and therefore, the compressed volume is different; this phenomenon can be seen in Figures 1.24c and 1.24d.

3.2. UNCERTAINTY FACTORS IN BOLT FINAL LOAD

As has been discussed in the previous section, obtaining the desired bolt initial load is not straightforward and this considerably complicates the assembly process for the bolted joints. Moreover, there are further factors that complicate obtaining a correctly preloaded joint. In spite of the fact the error in initial load would be null, the effects of the uncertainty factors in the bolt final load should still be minimized. As a consequence of these factors, the value of the final load is different from the value of the initial load, with the final load usually lower. The phenomena which most affected this uncertainty will next be explained in detail [Bic'95].

3.2.1. SHORT TERM RELAXATION

Short term relaxation is a phenomenon that produces a loss of load on the bolts due to the relaxation of the joint over time. This relaxation is the

consequence of small plastic deformations caused for various different reasons:

Surface finish: Bolt and nut threads are not completely flat like the contact surfaces of the joint. Using a microscope, it is possible to see that the surface finish consists of small peaks and valleys as shown in Figure 1.27. At the beginning, when the joint is preloaded, there are small contact areas which are unable to withstand the contact pressure with elastic behaviour. To this regard, plastic deformation takes place until the contact surface is large enough. This process usually lasts a few minutes. Generally, this phenomenon has a greater effect with new components. Accordingly, in order to reduce short term relaxation, the joint can be loaded and unloaded several times. However, due to the cost that this process implies, it is only performed with extremely critical applications [Bic'95].

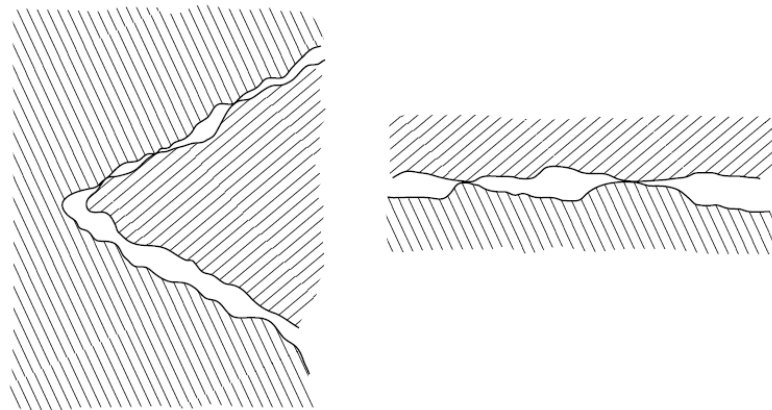


Figure 1.27. Shape of the contact surfaces using a microscope [Bic'95]

Poor thread engagement: If bolt dimensions are smaller than those required or if the nut is oversized, contact areas will be smaller than areas expected by the designer (see Figure 1.28). As a consequence, the plastic deformation will be higher [Fri'77].

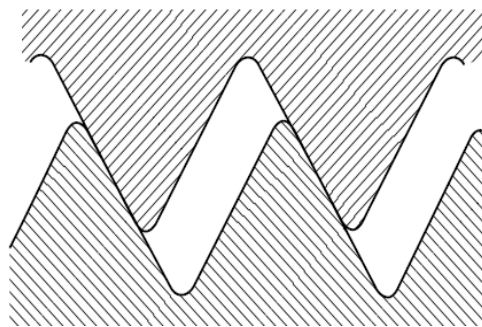


Figure 1.28. Joint with poor thread engagement [Bic'95]

Short thread engagement: Thread engagement in steel bolts has to be at least 0.8 times the nominal diameter of the bolt. If the engagement is shorter, there will be fewer threads in contact and, as a consequence, the plastic deformation will be higher.

Bolts bending: If the bolt is under a bending moment after applying the initial load, the farthest areas from the neutral line will be under higher stress. As a consequence, it is more likely that the yield stress will be exceeded and therefore there will be a higher loss of load.

Oversized fillets or undersized holes: In this situation, the contact is in the fillet instead of in the bolt head as shown in Figure 1.29. Therefore, there will be an elevated stress concentration and the contour of the bolt hole will suffer extreme plastic deformation. This phenomenon generally results in a very significant loss of load, whereby producing a big difference between the initial and final load.

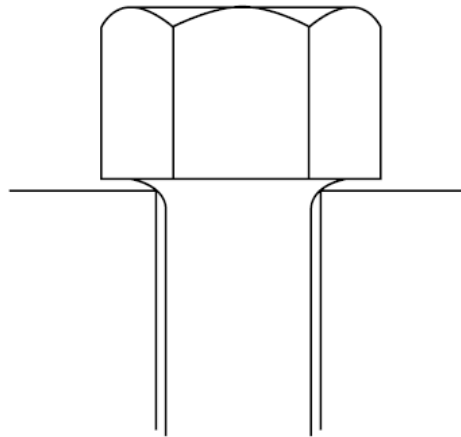


Figure 1.29. Joint with oversized fillets or undersized holes [Bic´95]

Oversized holes: This is also a problem because the contact area between nut or bolt head and the elements to join is very small (unless a washer is used). Due to the high pressure that occurs on the contact surface, it may be deformed as shown in Figure 1.30 [Fri´77].

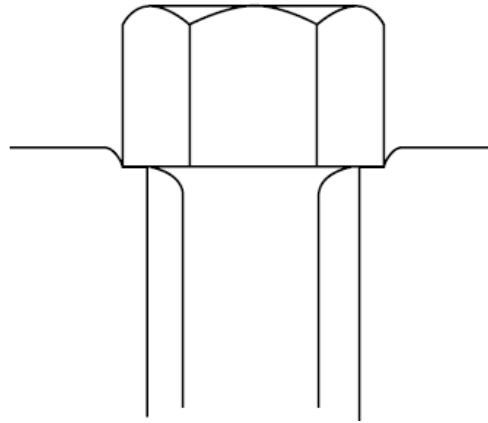


Figure 1.30. Oversized hole [Bic '95]

3.2.2. ELASTIC INTERACTION

As explained above, the short term relaxation phenomenon is based on the “relaxation” of the bolt over a short period of time due to small plastic deformations on contact surfaces. In the elastic interaction, bolt load variation occurs when another bolt of the same joint is tightened. This phenomenon is the consequence of the deformation of the elements to join and of the gasket, so the stiffness of these components is of utmost importance [Bic '98]. Elastic interaction will now be explained with an illustrative example.

Imagine that there is a joint with three bolts in which target load is a uniform bolt load of 10 kN. To achieve the target load, firstly bolt number 2 is tightened to 10 kN, as shown in Figure 1.31a. Secondly, bolt number 1 is tightened to 10 kN and, as a consequence of joint deformation, there is a load loss on bolt number 2 (see Figure 1.31b). Therefore, in this moment, bolt number 1 has a load of 10 kN, bolt number 2 has a load smaller than 10 kN and bolt number 3 is not tightened. Finally, bolt number 3 is tightened to 10 kN and therefore the load of bolts 1 and 2 decrease as shown in Figure 1.31c. In this sense, it is appreciated that when every bolt is tightened to the same load, only the last bolt will maintain this load, so only the last bolt will be tightened to the target load.

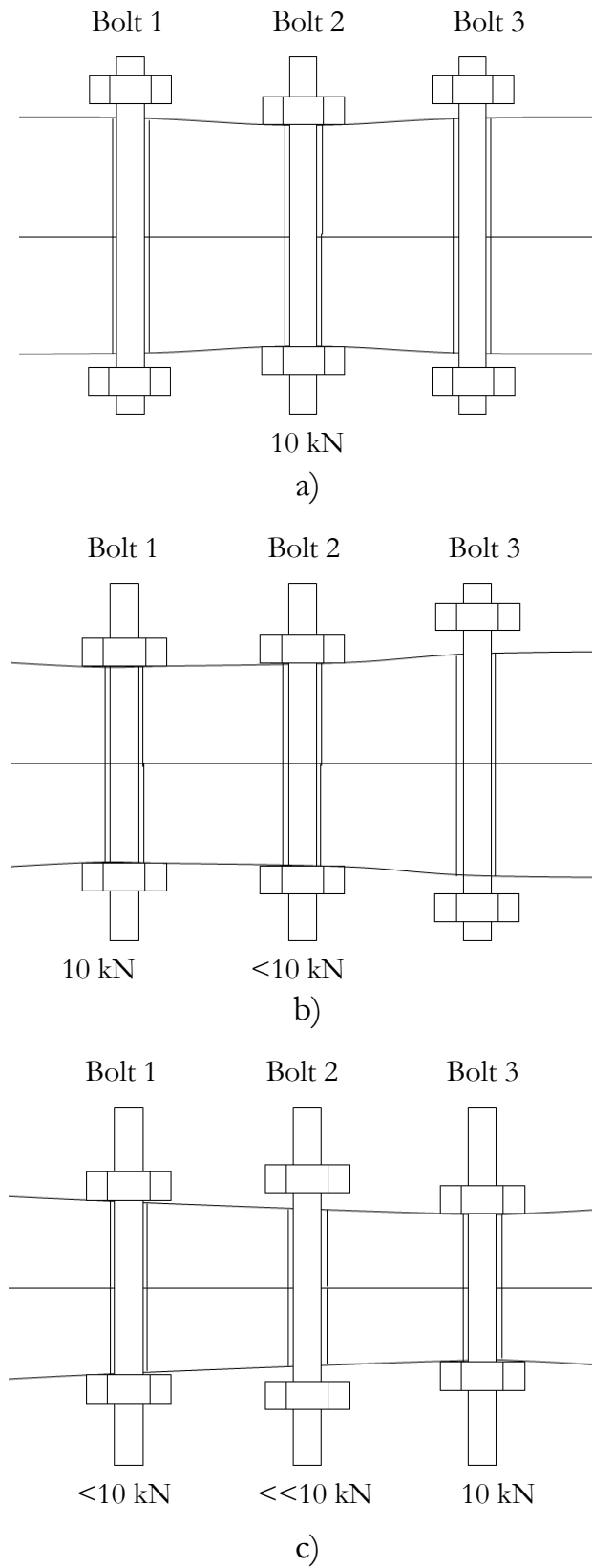


Figure 1.31. Elastic interaction phenomenon during the assembly process of a joint

a) tighten bolt number 2 b) tighten bolt number 1 c) tighten bolt number 3

[Aba '12]

In pipelines this phenomenon is usually the main reason for the difference between the initial and final load. Moreover, this phenomenon is dependent on a large number of parameters whose influence is difficult to predict, such as geometry and the material of joint components, load level, bolt spacing, and assembly pattern, amongst others [Nas'05; Tak'02]. On the other hand, the short term relaxation phenomenon is easier to control and quantify, and it can be compensated performing another pass after several minutes.

One solution to avoid the elastic interaction phenomenon is to preload every bolt at the same time. Nevertheless, this process is very costly as it requires a bolt tensioner or a torque wrench for each bolt and they must be programmed in order to apply bolt load simultaneously. Moreover, pipeline assembly is performed in situ, which usually implies limited tools and equipment.

3.2.3. RIGID BODY MOTION

This phenomenon is similar to the elastic interaction because bolt load variation occurs when another bolt of the joint is tightened. In this case, bolt load variation is due to rigid body motion of the flanges, and not due to deformation as is the case with elastic interaction. Figure 1.32 provides an illustrative example where a bolt is tightened and, due to the rigid body motion, the load of the bolt located on the opposite side increases (the opposite of elastic interaction which results in a load loss).

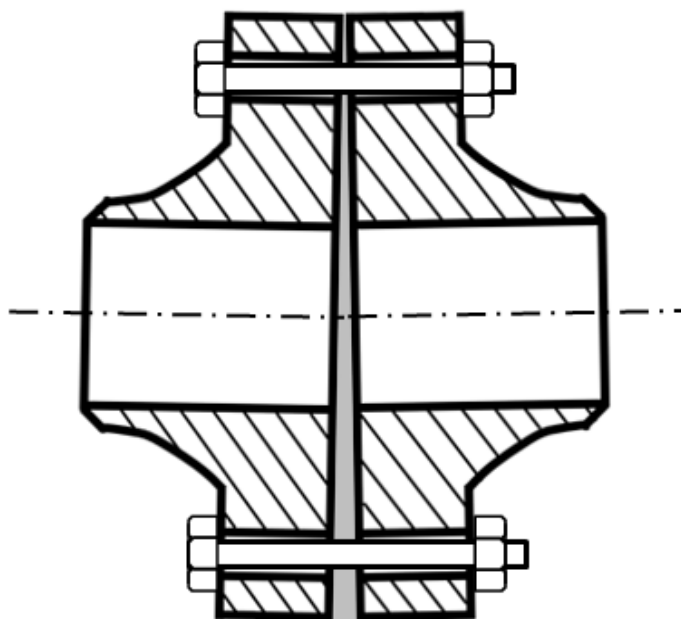


Figure 1.32. Rigid body motion phenomenon on a bolted joint [Aba'12]

4. STANDARDS FOR THE CORRECT ASSEMBLY OF BOLTED JOINTS

As explained in previous sections, obtaining a uniform final load is no easy task due to the uncertainty factors that affect the initial and final loads of bolts. However, in order to perform the assembly process as efficiently as possible, several standards provide various recommendations that improve the final result. Among these standards there is one developed by the American Society of Mechanical Engineers ASME [Asm'13(2)], another by the American Petroleum Institute API [Api'11] and another by the Norwegian petroleum industry Norsok [Nor'13]. These standards are primarily intended for pressure vessels and pipelines, which transport gas or fluid, and therefore they are preloaded in order to compress the gasket and thus avoid leakage. The three standards provide similar general and informational recommendations, which will be briefly outlined in the following paragraphs.

As an example, one of the standards includes a study of joint NCF5, which can be seen in Figure 1.33. These flanges have conical faces on the contact surface in order to obtain high pressure on the heel of the flanges. A ring joint is also placed between both flanges to ensure joint sealing during operation. This design, which is very similar to the ASME RTJ explained in the first section of this Chapter, also prevents corrosion on the contact surface, on the bolts, and on the gasket. Nevertheless, the purpose of every standard is to improve sealing efficiency and for that purpose they specify that the joint must possess at least the strength of the pipe, and must be designed to avoid failure as a result of plastic deformation, leakage or fatigue.

Focusing on handling, installation and assembly of bolted joints, standards first explain how to protect flanges and gaskets to avoid damages. To this regard, they warn that flange contact surfaces should be protected at all times with a wooden board or plastic cover. Also, the gasket (on RTJ), the metal ring), must be in its original packaging until final installation. Usually, in the handling process, defects are generated on the components, so qualified employees are recommended so as to avoid these problems. To this end, it is recommended that they be instructed with short theory courses and even in the field with all the equipment.

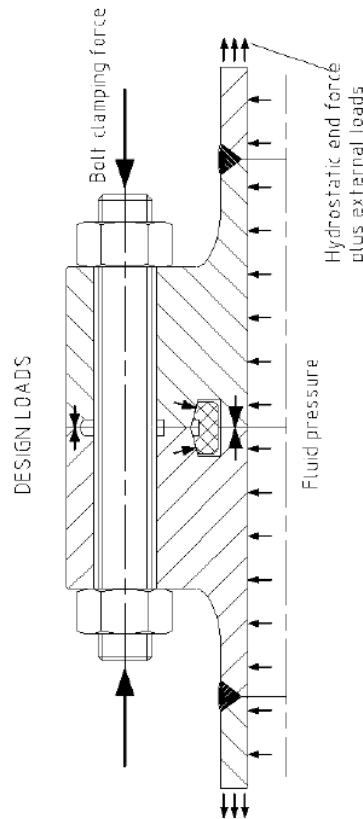
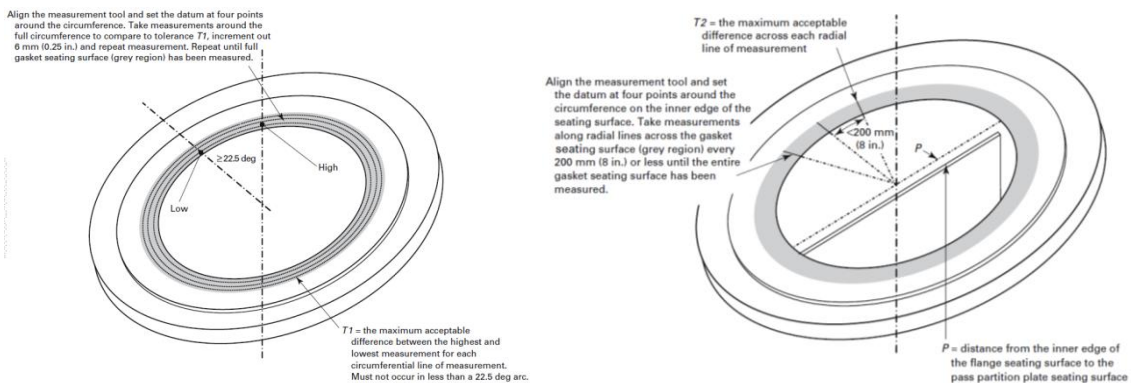


Figure 1.33. NFC5 joint under the design loads [Nor´13]

Before commencing the tightening process, contact surfaces must be cleaned with a soft tissue, and not abrasive, to remove any kind of dirt. An inspection must also be performed to ensure there is no damage or rust. After all, joint sealing depends on a good surface finish, so there can be no scratches, irregularities or marks (see Figure 1.34). Gaskets and bolts must be also inspected, and replaced if they are damaged. Bolt threads must be lubricated in order to obtain the target load, applying the minimum tightening torque.



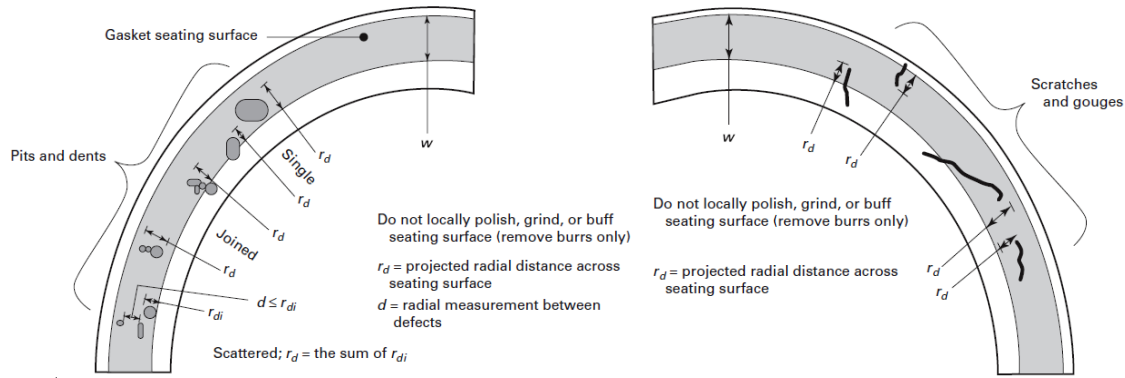


Figure 1.34. Imperfections on joints and gaskets [Nor´13]

Flanges must be also parallel aligned in such a way that the misalignment is less than the established value in the standards, as shown in Figure 1.35. Bolt holes must also be properly aligned to ensure that the bolts are applied easily.

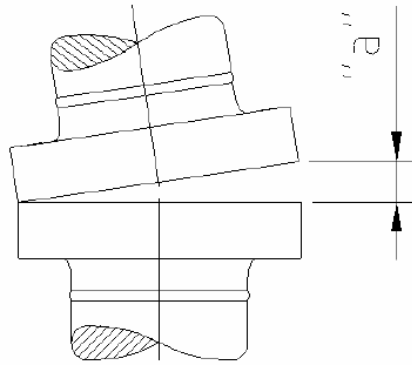


Figure 1.35. Flange misalignment [Nor´13]

Once correct flange alignment has been verified, the joint tightening sequence is performed. Standards suggest several tightening sequences, but all of them are performed in several passes, with the load gradually increased in each pass. Thus, local overload on the gasket is avoided during the tightening sequence. With the same purpose of avoiding overloads on the gasket, tightening sequences are always performed with a star pattern, or at least alternating bolts, and if a circular pattern is performed, this is always in final passes of the tightening sequence.

A tightening sequence of a standard will now be presented where the bolts are first tightened following a star pattern until the tips of the flanges are in contact (for the NFC5 flange presented above); the tightening torque to complete this operation must not exceed 10% of the final torque. After completing this step, one of the tightening sequences in Figure 1.36 is

performed. The assembly pattern is repeated several times gradually increasing bolt load in the different passes until reaching the target load. It is stressed that the first pass must not exceed 30% of the target load, and that the tightening sequence must start at the point where there the gap between flanges is the biggest. These tightening sequences have the inconvenience that 2 or 4 tightening tools are necessary to preload the bolts simultaneously during the assembly procedure, and sometimes only one tightening tool is available.

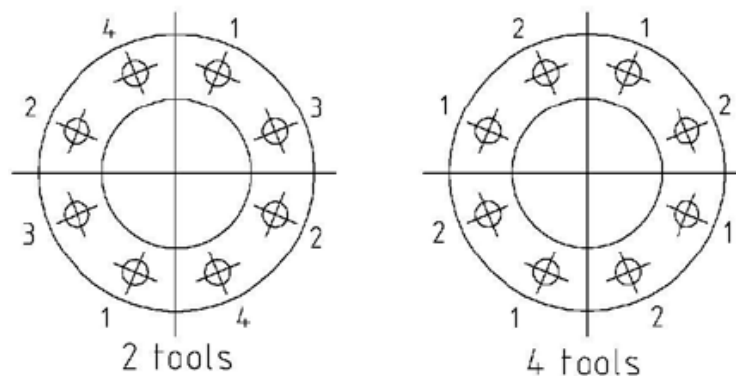
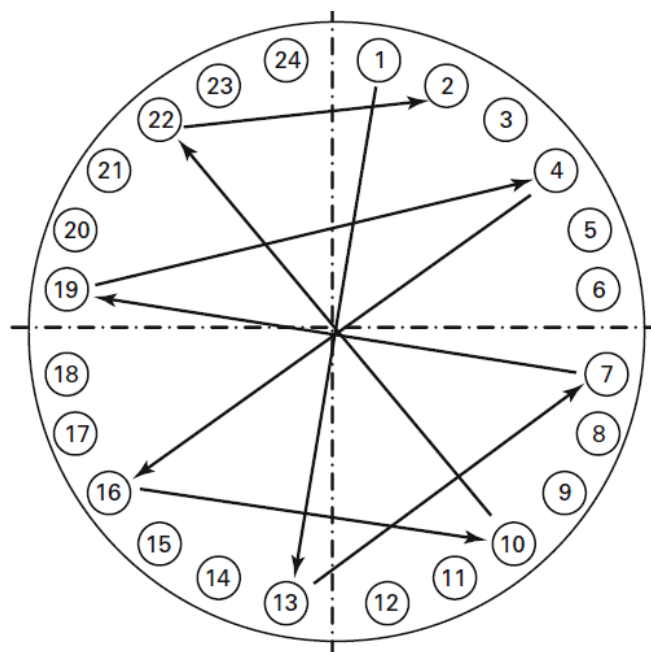


Figure 1.36. Tightening sequences with 2 and 4 tightening tools [Nor '13]

If only one tightening tool is available to perform the tightening sequence, the tightening sequence of Figure 1.37 can be performed which is popularly known as the Legacy Pattern [Asm'13(2)]. This tightening sequence is performed in 5 passes increasing the load gradually in each pass in order to avoid joint overloading.



GENERAL NOTES:

- (a) Pass 1 – 20% to 30% of Target Torque
1,13,7,19 – 4,16,10,22 – 2,14,8,20 – 5,17,11,23 –
3,15,9,21 – 6,18,12,24
- (b) Pass 2 – 50% to 70% of Target Torque
Same pattern as Pass 1.
- (c) Pass 3 – 100% of Target Torque
Same pattern as Pass 1.
- (d) Pass 4 – 100% of Target Torque, in circular pattern, until nuts do not turn. 1,2,3,4,5,6,7,8,9,10,11,12,13,14,15,16,17,18,19, 20,21,22,23,24 – 1,2,3,etc.
- (e) Pass 5 (optional) – 100% of Target Torque (performed 4 hours after Pass 4), in circular pattern, until nuts do not turn.

Figure 1.37. Tightening sequence called Legacy Pattern and suggested by ASME [Asm´13(2)]

According to the target load, this usually has a value of between 40% and 70% of bolts yielding load. The preload must be enough to ensure no service leakage but, at the same time, it cannot be excessive so as to avoid gasket damage (overloads in specific areas), flange damage (plastic deformations) or even bolt damage. To this regard, the ASME standard provides two different procedures to calculate the target load of the joint [Asm´13(2)]. On the one hand, there is a simple method that defines the minimum load on the bolts, which uses simple equations based on the minimum stress on the gasket in order to avoid leakage. There is also a method called the "joint component approach", which provides a procedure to calculate the maximum load on the bolts to ensure the integrity of the components of the joint. All of the methods take account of phenomena such as fatigue, creep or possible damages due to adverse environmental conditions. These phenomena must be reviewed later for each particular joint.

Tables are also provided with the values of the tightening torque that correspond to the target preload (see the example in Table 1.1 of NORSOK). However, as explained before, it is noted that there is a large scatter in the relation between the torque and the preload of the bolt due to the friction coefficient phenomenon, in which the material, surface finish, lubrication, nut tightening speed, tolerance between threads, the use of a washer or not, geometrical imperfections in the components of the join, misalignments, skills of the operator, among others have played an influence. It involves factors whose influence it is impossible to foresee. Consequently, for the same tightening torque value different preload values will be obtained on the bolt. Therefore, particular emphasis is placed on developing particular tightening

sequences with the corresponding value of the tightening torque, performing experimental measurements on the particular joint that will be used.

Regarding maintenance, a joint that has been designed and assembled properly does not require special maintenance tasks. Accordingly, mention must be made once again that the assembly process should be performed by qualified staff and using perfectly calibrated tools. These tools could be torque wrenches or bolt tensioners, and the same standards provide calibration procedures.

Stud bolt size in	Target residual preload ^{a c} kN	Applied tension with tension tool ^{b c} kN	Applied torque with torque tool and lubricant $\mu=0,12^d$ Nm
½-UNC	44		98
⅝-UNC	71		192
¾-UNC	106	134	341
⅞-UNC	147	186	544
1-UNC	193	244	816
1 ⅛-8UN	255	323	1194
1 ¼-8UN	325	412	1671
1 ⅜-8UN	405	512	2261
1 ½-8UN	492	623	2989
1 ⅝-8UN	589	745	3840
1 ¾-8UN	693	878	4859
1 ⅞-8UN	807	1022	6020
2-8UN	929	1177	7351
2 ¼-8UN	1199	1519	10610
2 ½-8UN	1503	1904	14665
2 ¾-8UN	1667	2111	17766
3-8UN	2004	2539	23240
3 ¼-8UN	2373	3006	29736
3 ½-8UN	2773	3512	37258
3 ¾-8UN	3204	4058	46046
4-8UN	3666	4643	56008
NOTE	Bolting material: ASTM A193 gr.B7, ASTM A193 gr.B16 and ASTM A320, gr.L7 and gr.L43		
^a	Target minimum pre-stress is 75 % of yield such that a minimum of 70 % is achieved due to uncertainties in the make-up procedure. Bolt root diameter used.		
^b	The applied tension is equivalent to 95 % of yield in bolt in order to ensure that a minimum of 75 % of yield (target residual value) is left when preload is transferred from the tension tool to nut.		
^c	Washers may be necessary for some flanges to achieve sufficient residual bolt load with tension tool.		
^d	Torque tests with a specified lubrication procedure shall be performed to determine the appropriate coefficient of friction. Full filling of threads with lubricant is recommended.		

Table 1.1. Tightening torque to apply on bolts and the corresponding preload according to the tool type used for a preload of 70% [Nor´13]

As can be seen, the tightening sequences provided by the standards are for general purposes and require a significant number of passes, which is expensive. The standards also point out that each assembler should perform particular tightening sequences for each particular joint. To this regards, and so as to reduce assembly costs, different methods have been developed which

result in uniform final load distribution on the bolts using only one or two passes. This process is known as tightening sequence optimization. The most popular methods are the Inverse Sequence Method (ISM) and the Elastic Interaction Coefficients Method (EICM), which have been extensively validated in [Bib'96; Nas'08]. Nevertheless, using these methods, obtaining the optimum tightening sequence is expensive due to the analysis and measurements that must be performed. In this sense, these methods are only recommended when the number of joints to be preloaded is high; thus, the time taken to obtain the optimum tightening sequence is compensated reducing the cost of the successive joint assembly. These methods will be explained in detail in Chapter 3 since they are a direct background of this Doctoral Thesis.

5. TOOLS FOR THE SIMULATION OF TIGHTENING SEQUENCES

As mentioned in the previous section, different methods can be used to obtain optimized tightening sequences which provide uniform final load distributions on the joint in one or two passes. In Oil & Gas pipelines, studying an optimized tightening sequence is particularly useful, especially for two reasons: Firstly, less time is required for the assembly process and therefore the economic cost of the pipeline is less; secondly, obtaining a uniform bolt load avoids leakage and maintenance tasks are also minimized.

However, in order to optimize the tightening sequence the entire sequence must be first studied. Various tools used to study tightening sequences will now be presented in order to characterize joints performance.

5.1. EXPERIMENTAL METHODS

Experimental methods are based on performing measurements on the physical system that will be used later on in situ (in this particular case the pipelines joint). The main advantage of the experimental methods is that the model via which the measurements are performed is very similar to the real model, and therefore the obtained results are very precise. However, this is the most expensive simulation method because, generally, large equipment, a

long time and qualified staff are required. Figure 1.38 shows an experimental analysis performed to study the tightening sequence of a joint [Nas'06].

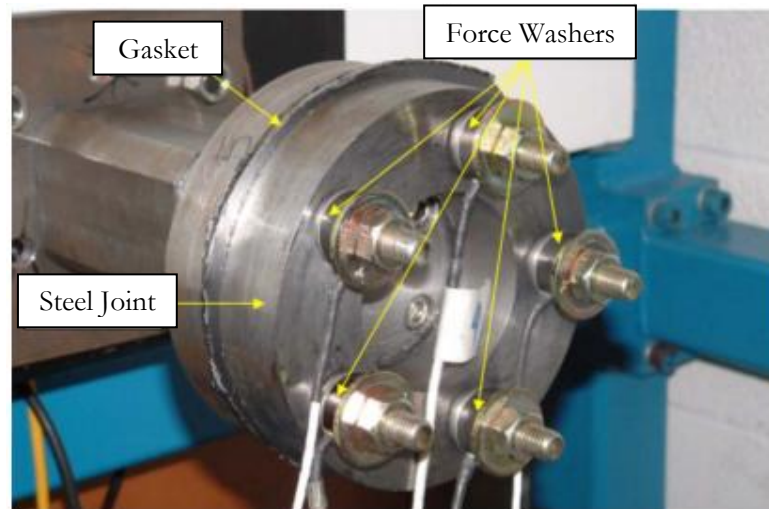


Figure 1.38. Experimental set-up to study tightening sequences [Nas'06]

In the experimental analysis of pipeline bolted joints, the essential factor is to measure the load level of the bolts in real time. To this regard, the methods described in Section 3.1 must be employed, with the most common ones being strain gages and measurements using ultrasound equipment. Accordingly, the bolt final load uncertainty factor explained in Section 3.2 may be reviewed. In this Doctoral Thesis a test bench was used which is explained in Chapter 2.

5.2. FINITE ELEMENT METHOD

Nowadays, the Finite Element Method is particularly popular given its great versatility. The method consists in creating a model which behaves in a similar fashion to the real model, and discretizes volumes on small finite elements. In comparison with experimental methods, the economic cost is much lower and it is also easier to study the response of the model against external loads. However, for pipeline bolted joints, the obtained results are less accurate for three reasons: It is not possible to model most short term relaxation because the surface finish cannot be modelled; the friction coefficient applied on the model is most likely different to the real one; and finally, if the gasket behaves in a particularly non-linear fashion such as the one explained below, the assumed stress strain curve usually includes errors. Figure 1.39 shows the three different parts of a bolted joint Finite Element model.

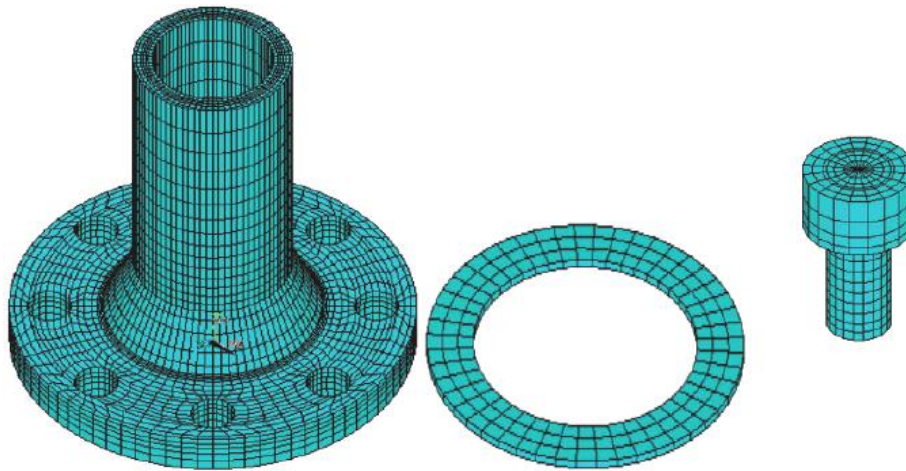


Figure 1.39. Finite Element model of a bolted joint (flange, gasket and bolt)
[Kha '15]

Generally, the Finite Element models of pipeline bolted joints are very similar. In these models only the half of the joint is modelled due to the symmetry of the system, and the load level of the bolts is controlled with a pretension section [Abi'16; Fuk'03; Kon'09; Tak'04]. Nevertheless, more complex models can be found where a highly non-linear gasket is modelled with the behaviour of Figure 1.40. The main problem is that the stress strain behaviour of the gasket has to be obtained experimentally in a compression test machine. Most elastomeric and metal gaskets behave in this manner.

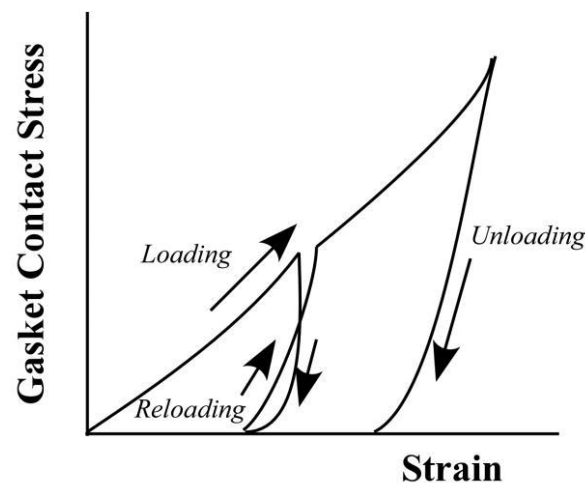


Figure 1.40. Gasket with a highly non-linear behaviour [Fuk '12]

In this Doctoral Thesis, in addition to the experimental set-up developed, a parametric Finite Element model is also developed. The Finite Element model and its validation is explained in detail in Chapter 2.

5.3. METAMODEL

A metamodel is a simplified model that is used to study a particular phenomenon. As its aim is only to obtain a particular result, it is possible to simplify the model considerably and therefore reduce computational cost. Usually, in order to simplify the system, springs and condensed stiffness matrices are used in static analyses.

In [Aba'11; Aba'12; Aba'14] a metamodel is developed to study tightening sequences in the bolted joints of wind turbine towers (see Figure 1.41). With this metamodel, it is possible to simulate tightening sequences in a few seconds and obtain very precise results, so this can be considered a very efficient model.

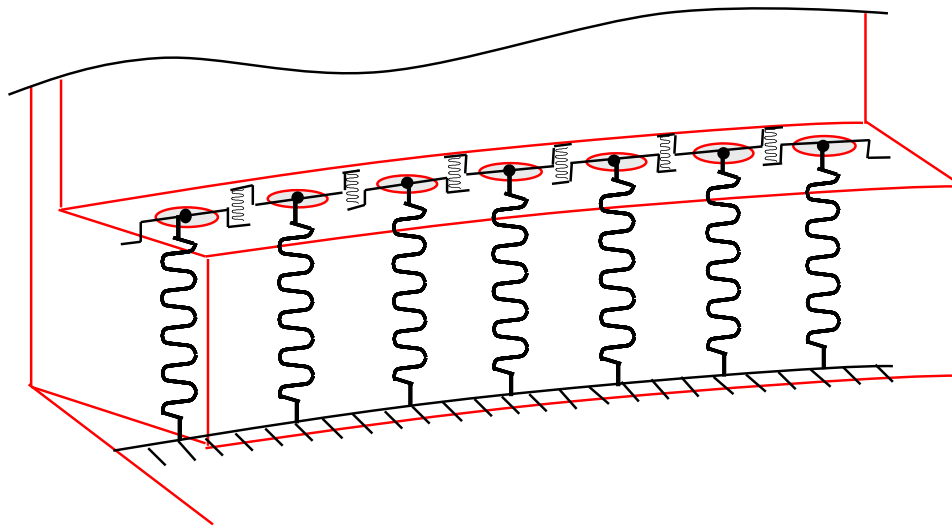


Figure 1.41. Biparametric metamodel of the bolted joint of a wind turbine tower
[Aba'12]

Large effort was made in this Doctoral Thesis to develop a metamodel that would study the tightening sequences in RTJs. However, the contact between the flange and the octagonal gasket behaves in a highly non-linear fashion. Due to this phenomenon, the difficulty of the metamodel increased considerably resulting in a very complex model, so the metamodel was ruled out and a more efficient alternative was finally chosen.

5.4. ANALYTICAL MODELS

The analytical model is the simplest model. It consists in simplifying the real model using mathematical equations, generally relating to the Resistance and

Elasticity of materials. Accordingly, the computational cost is reduced considerably.

In [Zhu'17] an analytical model was developed based on elastic compliances, which provided very accurate results. In [Wan'17] another analytical model is developed for a very simple load case. However, for RTJs, the contact is difficult to model and therefore it is very complicated to create an analytical model.

5.5. MODELS USING SUBSTRUCTURING

Finally, another choice to simulate tightening sequences is with a Finite Element model but modelling the components of the joint with substructures. The substructure technique consists of creating a superelement that only has the degrees of freedom that we wish to study. Accordingly, the stiffness matrix of the model is condensed reducing the degrees of freedom of the model and the computational cost [Aba'17; Avi'02].

Nevertheless, for an RTJ model, most computational costs are a result of the contacts between bolts and flanges, and between gaskets and flanges, whereby, in this bolted joint, this method does not lead to any significant time saving [Pla'15]. Accordingly, this technique was ruled out.

6. MOTIVATION AND OBJECTIVES OF THE DOCTORAL THESIS

As has been mentioned in this Chapter, in order to minimize leakages and reduce maintenance operations in pipelines in the Oil & Gas sector, a uniform bolt load distribution on bolted joints is essential. Thus, uniform pressure distribution is achieved on the contact between the flanges and gasket, and therefore the joint operates optimally. However, whenever a bolt is tightened on a gasketed joint during the tightening sequence, the joint is compressed and the load in previously tightened bolts is consequently reduced, which makes it considerably difficult to obtain a uniform bolt load.

Several standards provide guidelines for the assembly of a bolted joint, with regards to the preparation of the joint (cleaning, detection of possible damages or imperfections, checking the alignment of the joint...) and

regarding the tightening sequence. Nevertheless, general recommendations are provided, most of which are common sense, and it is pointed out that each assembler should develop each particular tightening sequence for each particular joint. In this sense, the ASME standard [Asm'13(2)] suggests that the best way to develop new tightening strategies is by testing them on a test bench and measuring several parameters (bolt load distribution, separation between flanges for all 360 degrees, damages on the gasket, flanges and bolts...) to verify the proper operation of the joint. It should be noted that many companies use their particular assembly procedures, obtaining an improvement for the different gaskets, flanges and particular working conditions. In other words, in order to be reliable and competitive, it is necessary to create particular assembly procedures which are adapted for own products.

In this sense, the tools developed in this Doctoral Thesis have been made in the frame of a collaboration with ULMA (manufacturer of industrial flanges), and MATZ-ERREKA (bolts manufacturer), who contacted the research group showing their interest in the study of efficient tightening sequences. Thus, they have collaborated in constructing the test bench and performing the experimental tests, also providing all the required equipment.

Therefore, the first purpose of this Doctoral Thesis is to study the optimization methods for tightening sequences that have been developed thus far on the RTJs, widely used joints in the Oil & Gas sector. As mentioned above, the aim of these methods is to obtain a uniform final load on the bolts with a tightening sequence that consists of only one or two passes. To this regard, in Chapter 3, ISM and EICM are first explained and subsequently validated.

Secondly, on the basis of the conclusions obtained from studying the optimization methods, a new method is developed which has been called the Tetraparametric Assembly Method (TAM). The main advantage of this method is that, for RTJs, it obtains the optimized tightening sequence with a considerably lower cost than the methods that are currently used in the industry. The development of this method is explained in Chapter 4. The scope of application for the new method is then studied in Chapter 5, as well as its generalization for two-pass tightening sequences.

In Chapter 6, a computer program is explained which obtains the optimal tightening sequence of any ASME RTJ that is within the scope of application

studied with the TAM. This application was programmed in Visual Basic for Applications (VBA) in Microsoft Excel.

Finally, to draw the Doctoral Thesis to a conclusion, Chapter 7 proposes another alternative to study optimal tightening sequences. This method is developed to study different types of joints, and therefore, for use when the TAM is not valid. This method is based on the superelements technique. In this case it is possible to use the superelements technique because the effect of the contact phenomena in these types of joints is not as significant as in RTJs.

To study optimal tightening sequences, a test bench and a Finite Element model were used, both of them explained in Chapter 2. Accordingly, the results obtained during the Doctoral Thesis were widely validated.

CHAPTER 2. TOOLS USED FOR THE SIMULATION OF TIGHTENING SEQUENCES

1. INTRODUCTION

The importance of studying tightening sequences to obtain an efficient assembly was explained in Chapter 1. Furthermore, the different tools used for analyzing tightening sequences were presented with the advantages and the disadvantages indicated of each one. In this Doctoral Thesis, a test bench and a Finite Element model are used for the reasons explained in Chapter 1. These methods will not be explained in detail.

2. TEST BENCH

Figure 2.1 shows the test bench designed and manufactured for this Doctoral Thesis. It consists of a bolted joint welded to two pipe segments. The bolted joint consist of two RTJ flanges of NPS of 24", Class 150 and SCHD 40 [Asm´13(1)], a metal gasket - ring shaped and with an octagonal profile R76 [Asm´12(2)], and 20 bolts (see Figure 2.2) The materials used are ASTM A105 steel for the flanges ($E=201$ GPa, $\nu=0.3$) and soft iron for the gasket ($E=198$ GPa, $\nu=0.3$). Regarding the bolts, they have a metric of $1^{1/4}$ with 8 threads (UN series), class 10.9, with a tensile stress area of 1 in².



Figure 2.1. Test Bench

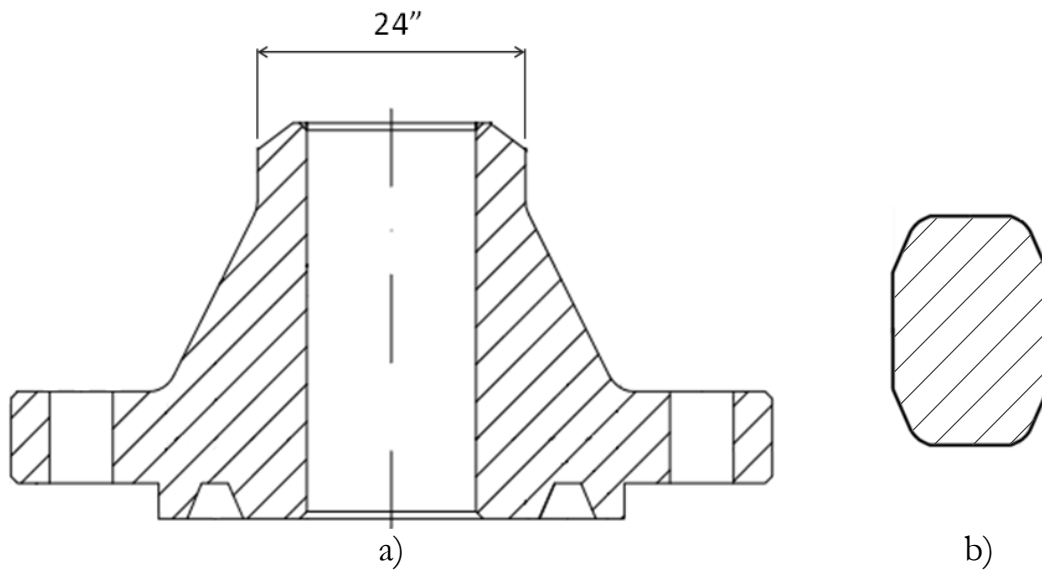


Figure 2.2. Joint type of the test bench: a) RTJ of NPS 24", Class 150 and SCHD 40 [Asm ´ 13(1)] b) metal ring gasket with octagonal profile R76 [Asm ´ 12(2)]

A hydraulic torque wrench was used to apply the bolt initial load, so the axial load in the bolt was generated by means of a torque. Torque wrenches are used to preload bolts via torque, and they can be either manual or hydraulic tools depending on the target load. For this particular test bench, the value of the applied torque is very high, and therefore the hydraulic torque wrench of Figure 2.3 was used. The torque wrench was connected to the portable pump of Figure 2.4 to achieve the necessary pressure. Finally, it should be pointed out that the head of the torque wrench was interchangeable for the purpose of preloading any bolt metric.



Figure 2.3. Torque wrench of the test bench



Figure 2.4. Portable pump of the test bench

On the other hand, as explained in Chapter 1, most failures on bolted joints are due to an inadequate preload on the bolts rather than due to design flaws of the flanges or bolts. Nevertheless, when the value of the torque is controlled rather than the preload of the bolt, a high scatter is obtained in bolt initial load with an approximate error of 30%. Therefore, in order to obtain high test bench precision, the initial load of the bolts was measured with an ultrasound unit [Bic'95].

The underlying concepts regarding the using ultrasound equipment to measure bolt load are relatively simple. Generally, a small acoustic transducer is located at the top of the bolt. An electronic device generates a small impulse voltage on the transducer to create a small ultrasound burst (see Figure 2.5). The sound waves that pass through the bolt rebound on the end of the bolt and return to the transducer. The electronic device that measures time must be extremely precise as the final results obtained with the ultrasound equipment are directly related with the time measurement.

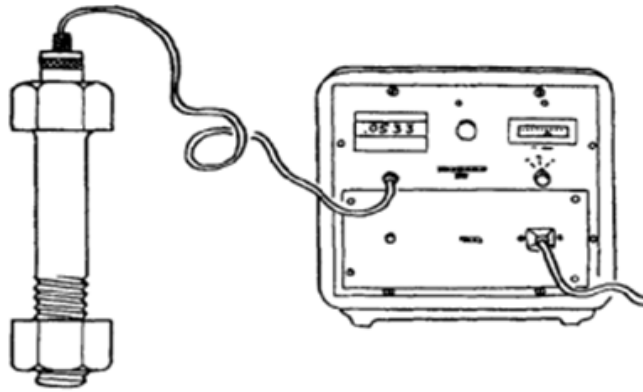


Figure 2.5. Ultrasound measuring device [Bic '95]

When bolt preload increases, the time needed for the signal to go out and return increases due to two different reasons: the bolt length increases and therefore the travel distance is longer, and the sound waves speed decreases when bolt stress increases. The changes in these two parameters is a linear function which depends on preload as shown in Figure 2.6, and therefore the sum of the two is also a linear function dependent on time. Consequently, these devices are designed to measure the time and calculate and represent bolt length variation, bolt stress and bolt preload.

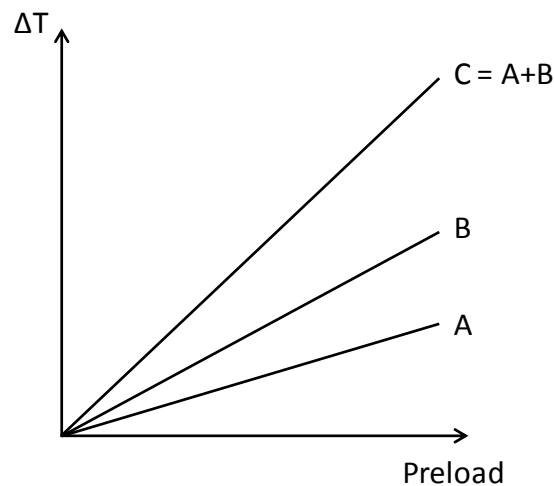


Figure 2.6. Time variation due to: bolt length variation (line A), sound wave speed variation (line B) and a variation of both (line C)

In the experimental set up of this Doctoral Thesis the ultrasound device i-bolt® was used [Err'www]. This technology requires equip each bolt permanently with a transducer on the top, at the bottom or on both sides (see Figure 2.7). Each bolt also includes a bar code that is used to automatically save the results of every bolt on a computer. Finally, the

electronic device is also required to generate the impulse voltage to the transducer. With this technology, a precision of 3σ better than $\pm 3\%$ is obtained, i.e., in 99,7% of measurements, the error is less than 3% whereby, with this device, failures due to an incorrect preload are avoided. Figure 2.8 shows how the level of load of the bolts was monitored when a bolt was being preloaded on the test bench.

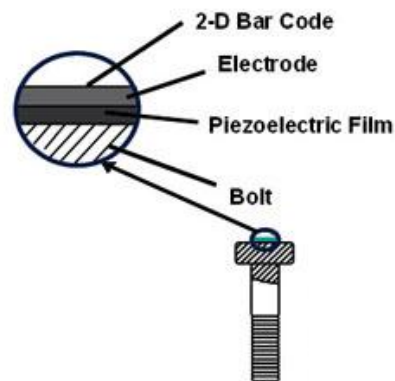


Figure 2.7. Bolt equipped with *i-bolt*® technology [Loa´www]



Figure 2.8. Measurement of bolt preload during the load process

3. PARAMETRIC FINITE ELEMENT MODEL

Currently, the numerical methods are widely used so that the experimental methods are minimized and therefore so too are the associated costs. In this Doctoral Thesis, a parametric Finite Element model was developed with the

Ansys ® Workbench software of an RTJ to study tightening sequences. The model is complex to a certain degree due to its non-linear performance due to the bolts-flange and flange-gasket contacts. Besides, the degrees of freedom are high for the mesh of the model (between 600,000 and 1,500,000 degrees of freedom, depending on the modelled RTJ). These characteristics lead to high computational costs (several hours), and convergence problems may also arise due to loss of contacts. The nature of the model will now be explained.

3.1. MATERIAL

The materials used in this model are the same as those used for the test bench, so the Young modulus of the flange, gasket and bolts are 201, 198 and 210 kN, respectively. Regarding the Poisson coefficient, 0.3 was assumed for the whole joint. The materials were modelled as elastic and linear, after having verified that any possible plastic deformation of the joint had no significant effect on the bolt load results.

3.2. GEOMETRY

As mentioned above, the generated Finite Element model is parametric. This means that the dimensions of the geometry are not defined as a value; they are defined as a variable. Accordingly, with only one parametric model it is possible to generate any RTJ simply applying the dimensions of that joint to the variable. Figure 2.9 shows the variables that were defined to enter the dimension of the joint. The small chamfers and fillet radius were not modelled as they do not have any influence on the behaviour of the joint during the tightening sequence. As will be explained later, in addition to the modelling of the joint, a pipe segment was modelled given the rigidity that it provides the joint, and accordingly, its influence on the tightening sequence.

To generate the model, the symmetry of the joint with regards to the central plane of the joint (central plane of the gasket too) must be taken into account. Accordingly, it is possible to model only the half of the model and later apply boundary conditions which simulate this symmetry. Thus, the degrees of freedom of the model will be half and therefore the computational cost of the analysis will be reduced considerably. The model is also cyclically symmetrical, and therefore generating one sector of the geometry is sufficient; later, to generate the whole model, this sector is repeated as many times as the number of sectors of the joints, with the number of sectors equal to the number of bolts.

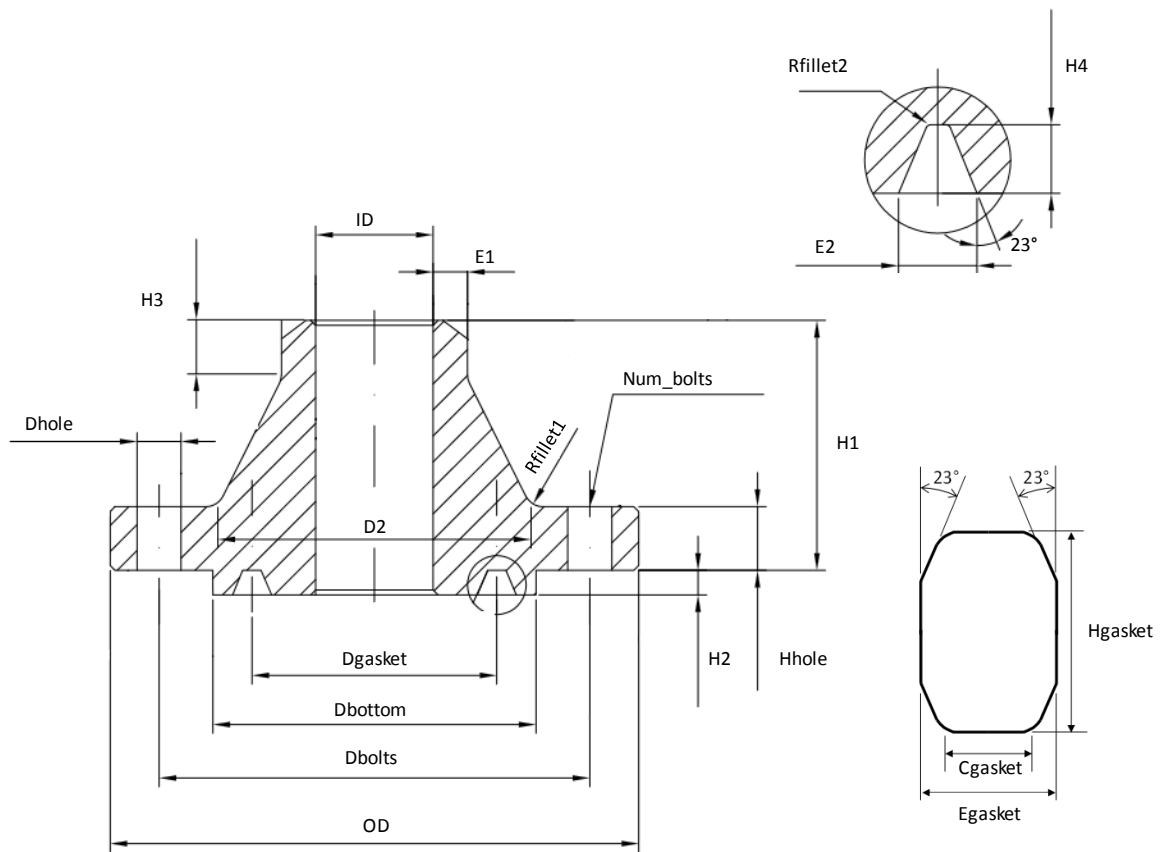


Figure 2.9. Joints geometric characteristics

The first step to model the first sector is to generate a sketch for each component of the joint (flange, gasket, bolts and pipe), dependent on the variables of the model. Secondly, the corresponding degrees of the sector are obtained from the sketches of the flange, gasket and pipe (the degrees are obtained from the number of bolts). Next, with a boolean operation, the bolt hole is created on the flange. Finally, the bolt is generated with a complete revolution of the bolt sketch. Figure 2.10 shows the three components of the sector.

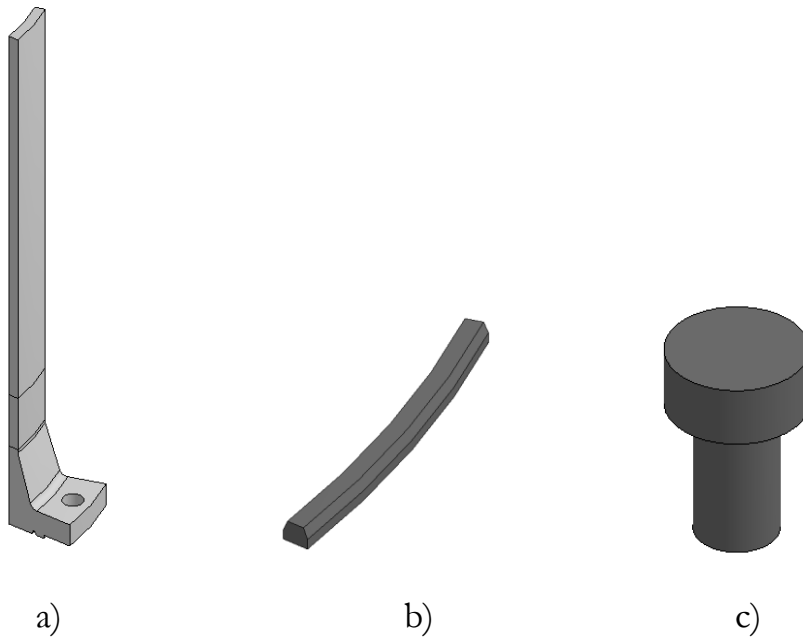


Figure 2.10. Components of the sector a) flange and pipe section b) gasket c) bolt

As can be seen, the flange and pipe sections are defined as a single solid. This is because, in reality, these two solids operate as a continuous system due to the welding bead that is applied. To conclude with this model, a cyclic symmetry is applied to generate the complete model, which can be seen in Figure 2.11.

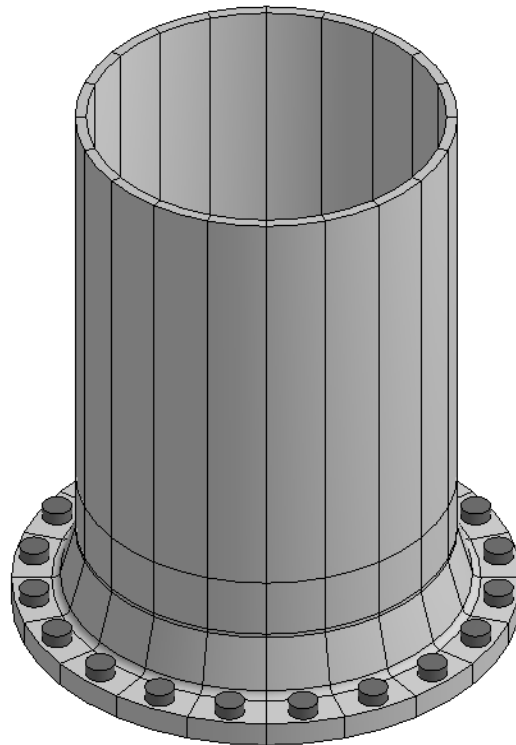


Figure 2.11. Complete model of the joint

3.3. CONTACTS

Two different contacts appear on the model of the joint: On the one hand, the contact between the flange and each bolt, and on the other, the contact between the flange and gasket. Studying the flange-bolt contact, due to the bolt preload, a normal force is generated on the contact surface, and if it is multiplied by the friction coefficient, a friction force is generated. Since no external radial load is applied in the joint, there will not be enough radial load to overcome the friction force, and therefore there will be no relative displacement between the bolt and flange. Consequently, the flange-bolt contact was defined as a “rough” type, i.e. only the relative displacement in an orthogonal direction to the contact plane is permitted; this is as assuming the friction coefficient between the two contact surfaces is infinite. Also, the contact between the flange and gasket was assumed to be frictional because of the possible relative displacements that may take place during the tightening sequence. The friction coefficient was defined as another variable of the model as the friction coefficient on the steel-steel contact is usually approximately 0.2 to 0.3.

3.4. MESH

The bolts, gasket and pipe section were meshed with lower order hexahedrons (Solid185). This element type, which is illustrated in Figure 2.12, is used for three-dimensional models. It is composed of eight nodes with three degrees of freedom: translations in the directions X, Y and Z.

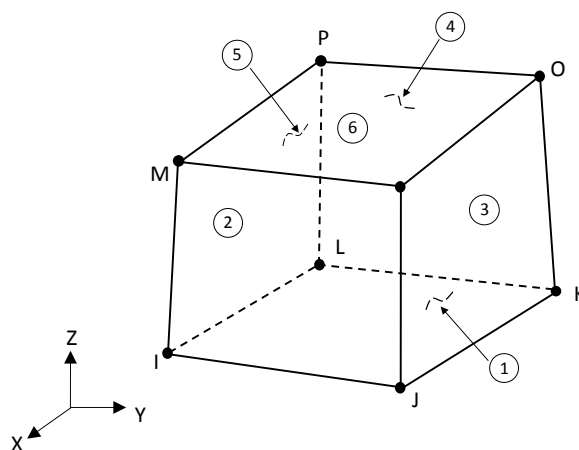


Figure 2.12. Lower order hexahedron (Solid185 in Ansys ®)

In order to obtain an efficient mesh on the flange, a fine mesh was used in the critical areas (particularly on the contact between the flange and gasket), with a coarse mesh on the rest of the volume. Due to the transition between the different sizes of elements, it is not possible to mesh the flange with hexahedrons because elements with a poor aspect ratio are obtained. Lower order tetrahedrons should also be avoided because they are constant stress elements and, as a consequence, they do not provide accurate results. Therefore, the solution was to mesh the flange with high order tetrahedrons. This element type, which is shown in Figure 2.13, is called Solid187 in Ansys® and is composed of 10 nodes with three degrees of freedom of translation. Element displacement behaviour is quadratic and particularly adequate for modelling irregular meshes.

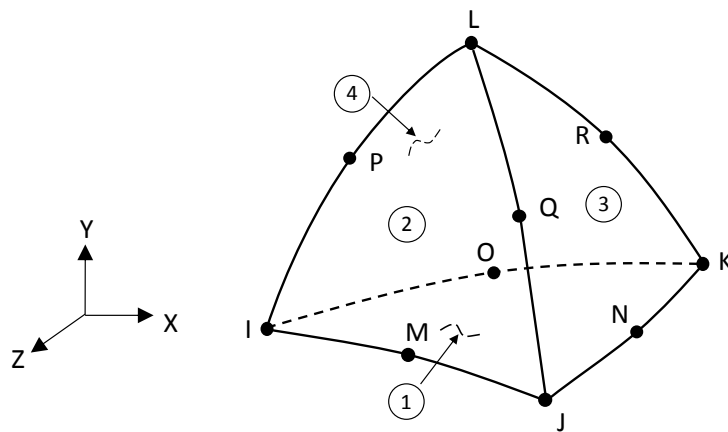


Figure 2.13. Higher order tetrahedron (Solid187 in Ansys ®)

Finally, the two contact element types will also be explained. When a contact surface is defined in Ansys ®, it is necessary to create the “contact” element and the “target” element, called Conta174 and Targe170 respectively, and illustrated in Figure 2.14. These are two-dimensional elements which are attached to the contact surfaces of the three-dimensional elements. To appropriately generate the contact, the contact surface which transmits the force should be meshed with the contact element. On the other hand, the surface which receives the force should be meshed with the target element. To this regard, in this particular model on the bolt-flange contact, the bolt has the contact element and the flange the target element, whilst on the flange-gasket contact, the flange has the contact element and the gasket the target element.

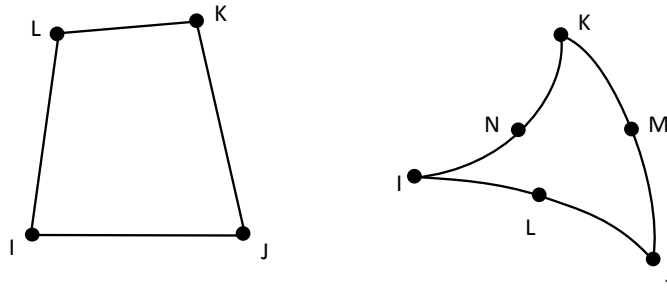


Figure 2.14. Target and contact two-dimensional elements (Conta174 and Targe170 in Ansys ®)

Thus, using the different element types that have been explained, the model was meshed obtaining the resulting model of Figure 2.15.

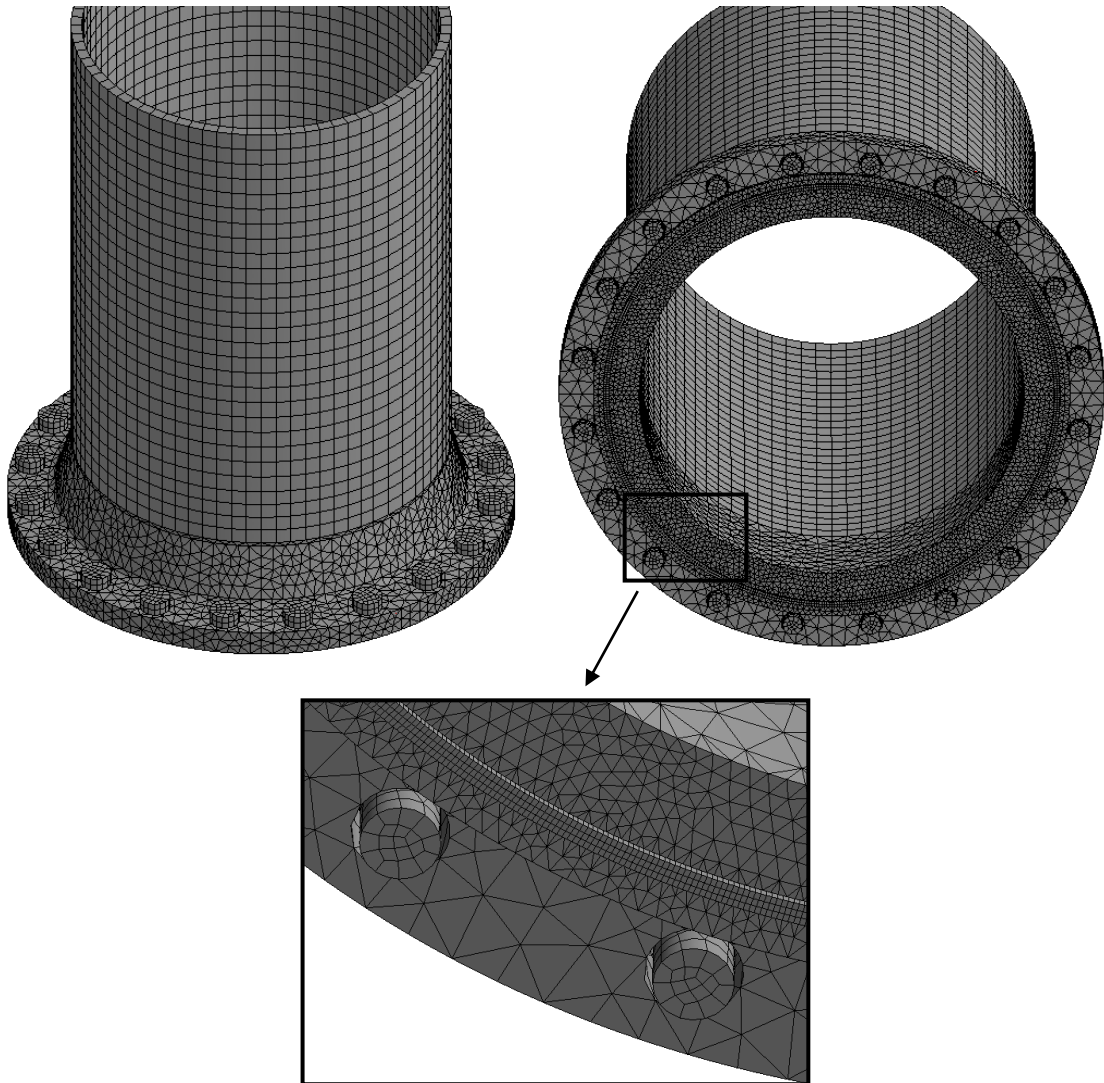


Figure 2.15. Mesh of the Finite Element model

3.5. LOADS AND BOUNDARY CONDITIONS

Once the mesh was finished, the boundary conditions were applied. In this model, it must be taken into account that only half of the joint was modelled given its symmetry. In order to simulate the symmetry of the joint, the vertical displacement has to be constrained (in bolt longitudinal direction) in every node which is located on the symmetry plane of the joint. To be more specific, the vertical displacement is restricted to the base of the bolts and to the base of the gasket, as shown in Figure 2.16. As can be seen, the base of one of the bolts was fixed, and therefore all movement was constrained so as to avoid lateral translation of the model as rigid body motion.

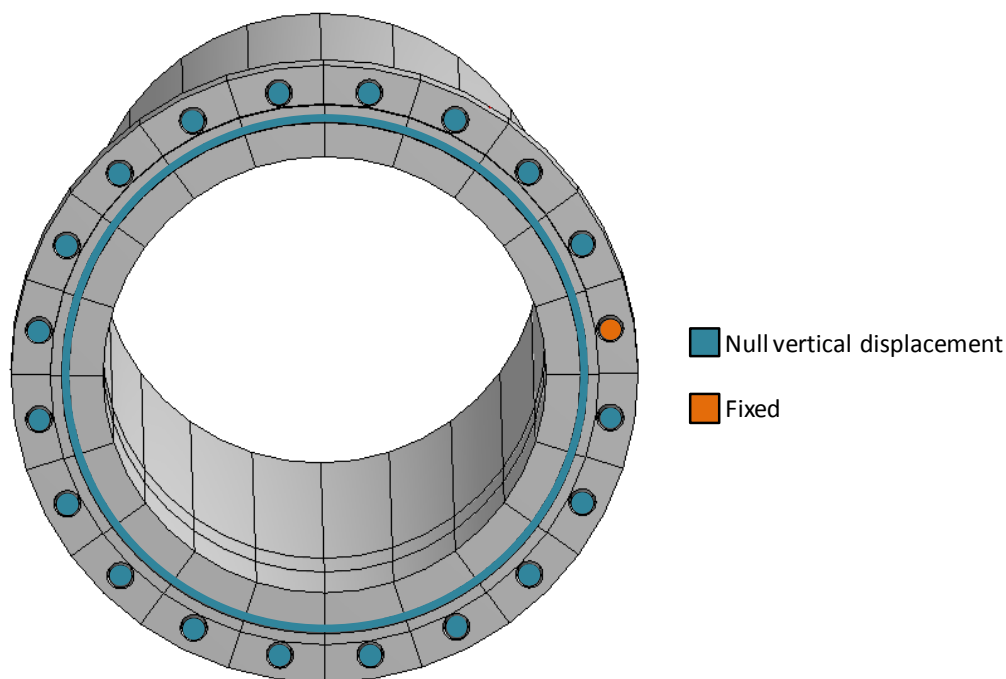


Figure 2.16. Finite Element model's boundary conditions

To simulate the tightening sequence, it is necessary to use the same number of load steps as the number of bolts the joint has. Load steps are used to apply the preload of the bolt at different moments, so the bolts are preloaded one by one and at different moments, simulating a real tightening sequence. Otherwise, if all the bolts are preloaded together, phenomena such as elastic interaction or rigid body motion, explained in Chapter 1, are avoided.

The preload of the bolts was applied through pretension sections, as shown in Figure 2.17, which reduce bolt length until the bolt reaches the target preload.

This tool provides three different choices to simulate the different circumstances of the bolt during the tightening sequence:

- Open: this represents the situation where there is no bolt or the bolt is not tightened yet. In this situation, the pretension section gets larger or shorter without transferring any load.
- Load: this represents the situation where the bolt is being tightened. The pretension section is reduced until the bolt is preloaded to the established load.
- Lock: this represents the situation where the bolt has already been tightened. The length of the pretension section does not change in this situation but the load of the bolt can vary due to joint deformation.

Using the load steps and the three choices of this tool, the tightening sequences can be simulated.

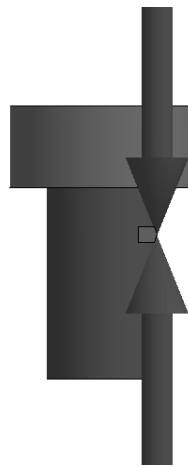


Figure 2.17. Pretension section of one bolt

3.6. RESULTS EXTRACTION

The key results in this Doctoral Thesis are essentially the load level of every bolt in each load step. With these measurements, it is possible to study the behaviour of the joint and thus calculate the influence of elastic interaction and solid rigid motion during the tightening sequence. As will be explained in Chapter 3, this is necessary to define an optimum tightening sequence. In order to simplify post-processing tasks, the results are obtained from Ansys® automatically via APDL macros.

3.7. POSSIBLE SOURCES OF ERROR

As a consequence of the Finite Element model simplifications, the results may contain a slight margin of error. Apart from discretization error, all possible sources of error will now be described:

Small plastifications: Assuming that the material is linear and elastic, the model does not take into account small plastifications on the flange or gasket due to stress concentrations. In order to study this phenomenon, a tightening sequence was simulated using both linear and non-linear material models (with quite large tightening loads); even though local yielded zones exist in the gasket-flange contact surface, bolt load distribution at the end of the tightening sequence was found to be very similar for both analyses. Thus, it was verified that material nonlinearities do not have any significant influence in bolt load variations.

Short term relaxation: Assuming that the material is linear and elastic, the model also does not take into account short term relaxation, explained in Chapter 1. Nevertheless, it is necessary to assume this simplification because even if a material with a yielding stress were defined, it is not possible to model the surface finish of the components. The only way to compensate the short term relaxation is to measure its value experimentally and increase the tightening loads that value.

Friction coefficient: When a Finite Element model is performed, a friction coefficient between the contact surfaces is assumed, and sometimes, it does not match with the real value because it depends on a large number of factors (lubrication, materials, surface finish and humidity, amongst others). To this regard, in this Doctoral Thesis a range of values for the friction coefficient is studied, whereby its influence on the results obtained using the Finite Element model is determined.

Large deformations: The flange or gasket might be subjected to large deformations and therefore the stiffness matrices could be modified, and this has an important effect on the obtained results. Therefore, a further two analyses were performed, one assuming large deformations and the other one not. The obtained results were the same for both models so this option was ruled out.

4. FINITE ELEMENT MODEL VALIDATION

The advantages and disadvantages of the models used in this Doctoral Thesis (experimental and numerical) have been explained in this Chapter. As mentioned previously, the main disadvantage of the Finite Element model compared with the test bench is the accuracy because, as explained in the previous section, the Finite Element model has several sources of error. To this regard, this section attempts to validate the Finite Element model comparing its bolt load results with those of the experimental set up.

Accordingly, firstly, the geometrical dimension of the test bench was applied to the Finite Element model, and, with regards to the friction coefficient, a value of 0.25 was assumed as the mean value of the previously specified range. Secondly, two different tightening sequences were performed on both models in order to compare the obtained results. In the first tightening sequence, every bolt was tightened to 350 kN following assembly pattern 1 of Figure 2.18a. In the second tightening sequence, every bolt was tightened to 200 kN, following assembly pattern 2 of Figure 2.18b. These two assembly patterns were extracted from ASME Standard [Asm'13(2)].

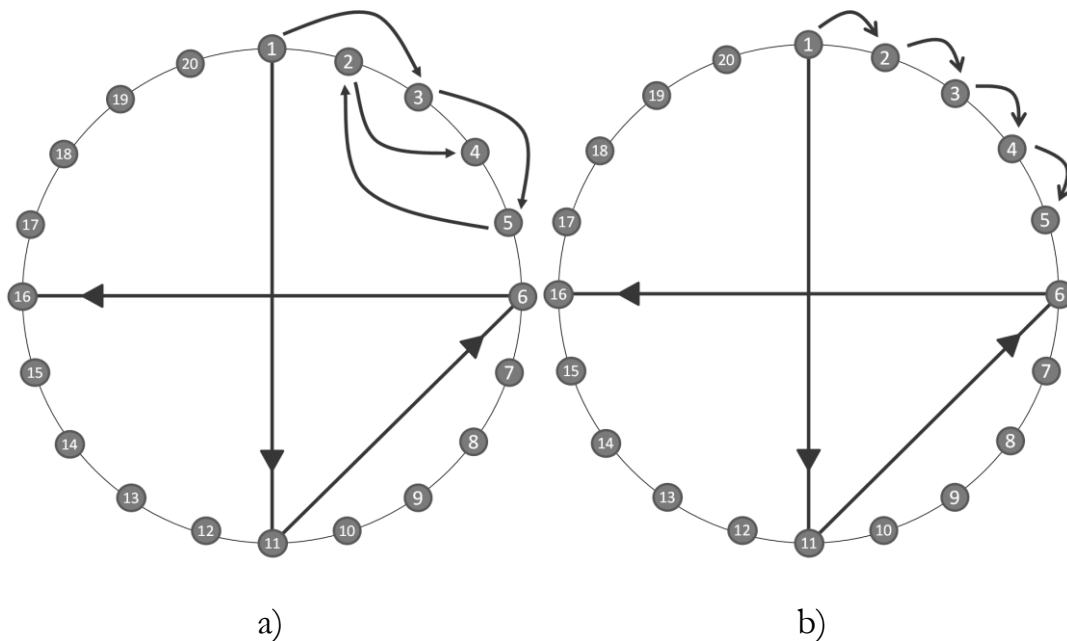
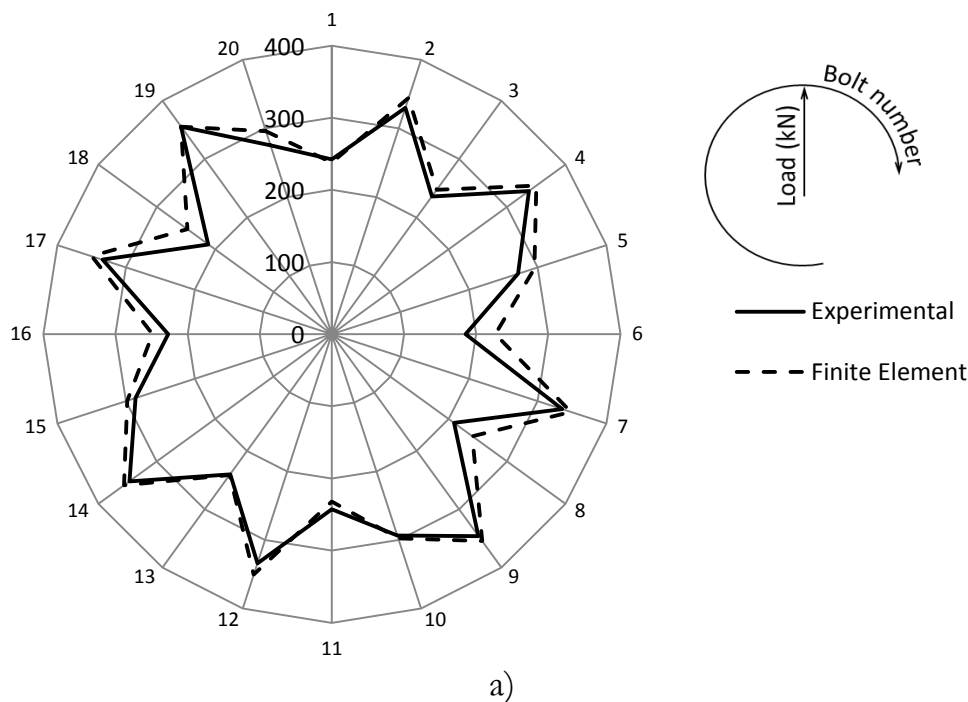


Figure 2.18. Studied assembly patterns a) assembly pattern 1: 1-11-6-16 → 3-13-8-18 → 5-15-10-20 → 2-12-7-17 → 4-14-9-19 b) assembly pattern 2: 1-11-6-16 → 2-12-7-17 → 3-13-8-18 → 4-14-9-19 → 5-15-10-20

Recalling the purpose of these models, they attempt to simulate the loss of loads of the bolts during the tightening sequence. To this regards, the Finite Elements model is validated if the final loads are similar to the final loads obtained in the experimental set up. Figure 2.19 compares the obtained final loads with both models. As can be seen, the Finite Element and experimental results are similar, with an average relative error (using absolute values for the difference) of 6% and 3.5% for the first and second analysis respectively. It is also noted that the final loads trend is very similar in both models.

The slight difference between both models could be the result of three different factors: Firstly, the error associated with the ultrasound measuring unit; Secondly, the possible sources of error previously commented, especially the short term relaxation [Cur'12]; and finally, on the test bench, a previous hand tightening procedure was performed to assemble all the components which was not simulated in the Finite Element model.

Accordingly, these results indicate that the Finite Elements model accurately simulates tightening sequences in RTJ, and therefore, that it can be used to accurately measure bolt load variations, and thus, validate the new methodology. Nevertheless, after performing all the necessary analyses to develop the new method of this Doctoral Thesis, the final results will be also validated experimentally.



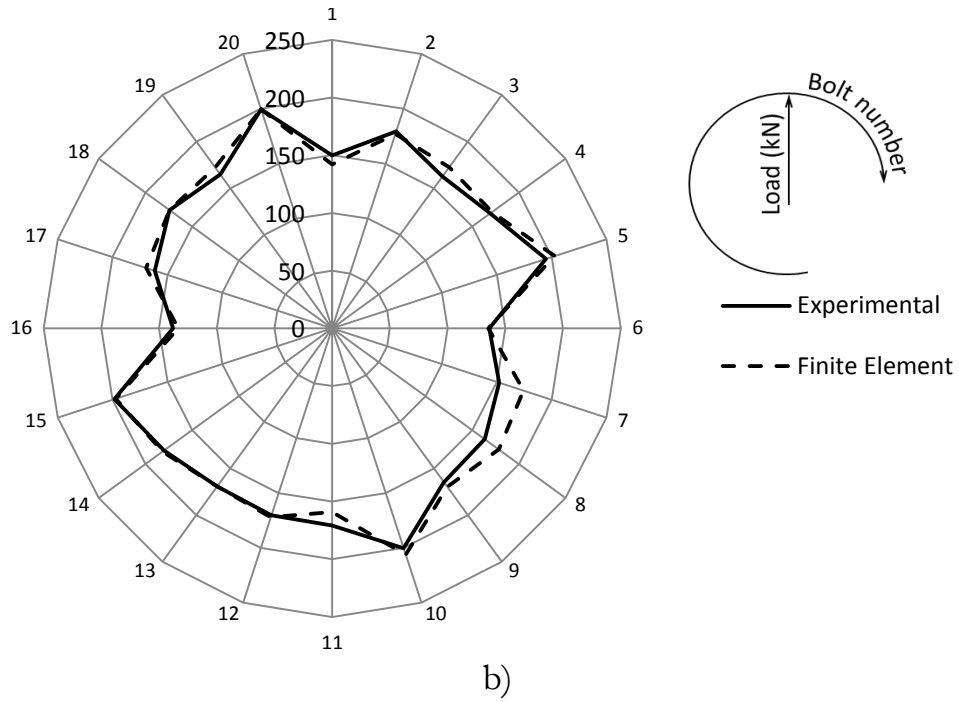


Figure 2.19. Experimental vs Finite Element in the obtained final load of the bolts a) tightening load 350 kN and assembly pattern 1 b) tightening load 200 kN and assembly pattern 2

CHAPTER 3. EXISTING METHODS FOR THE OPTIMIZATION OF BOLT TIGHTENING SEQUENCES

1. INTRODUCTION

The importance of achieving a uniform final load distribution in the assembly of bolted joints was explained in Chapter 1. Thus, a uniform stress distribution is achieved on the gasket, and therefore leakages are avoided during its operating life. Nevertheless, as explained in Chapter 1, due to the uncertainty factors in bolt initial and final loads, obtaining a uniform final load is not straightforward.

Several standards suggest different tightening sequences which showed good behaviour in terms of achieving a uniform final load on the bolts [Asm'13(2); Api'11; Bro'10; Nor'13]. However, the tightening sequence is always performed in several passes, increasing the level of load of the bolts in each pass. Also, it usually follows a star assembly pattern or similar (if circular patterns are used they are always applied in the last passes as shown in Figure 1.35). Obviously, this is extremely expensive. Likewise, standards indicate that these tightening sequences are indicative and generalist, so they strongly recommend that each assembler should develop each particular tightening sequence for each particular product and working conditions.

In order to develop particular tightening sequences for each particular product and also reduce the number of passes, and therefore the assembly cost, more efficient assembly methods were developed. These methods provide uniform bolt load distribution with a tightening sequence of only one or two passes. As mentioned in Chapter 1, this process is known as the optimization of tightening sequences. In the present Chapter, the most popular methods are explained and studied: the Inverse Sequence Method (ISM) and the Elastic Interaction Coefficients Method (EICM).

2. INVERSE SEQUENCE METHOD

The ISM is a very intuitive method which consists in beginning from the final state of the joint and moving backwards to the initial state [Aba'12; Alk'07; Alk'09; Nas'08; Nas'09; Nas'10]. In other words, instead of starting from the initial state, where every bolt is in untightened condition, and preloading the bolts one by one until the tightening sequence is finished, it starts from the final state where every bolt is usually tightened to a uniform bolt load and the

bolts are removed one by one following the inverse direction of the assembly pattern until every bolt is untightened. In the ISM, the tightening load of each bolt is equal to the load that this bolt has in the instant prior to being tightened during the inverse sequence.

to calculate the tightening load of each bolt, the previous moment to be untightened is equal to the tightening load that should be applied to that bolt during the optimized tightening sequence.

As an illustrative example, the joint of Figure 3.1 will be studied. In this joint of five bolts a uniform final load distribution F_f is desired, so it is necessary to start from the final state where every bolt is tightened to the F_f load (load step 1 in Table 3.1). Assuming the desired assembly pattern follows a clockwise pattern (1-2-3-4-5), the first bolt to be untightened should be number 5. As mentioned previously, before removing the bolt the load level of that bolt must be measured (F_5), which in this case is the same value as the target load F_f . Once bolt number 5 has been untightened, the joint is relaxed and, as a consequence, the load level of the other bolts usually increases. In the second load step, the load level of bolt number 4 has to be measured (F_4) and subsequently untightened (see Table 3.1). This process is repeated until the load level of every bolt of the previous moment to be untightened is achieved (and therefore obtaining F_1, F_2, F_3, F_4, F_5). The obtained loads correspond with the optimized tightening sequence, that is to say, preloading bolt number 1 to F_1 , bolt number 2 to F_2 , and so on. Theoretically, the uniform final load distribution F_f is achieved.

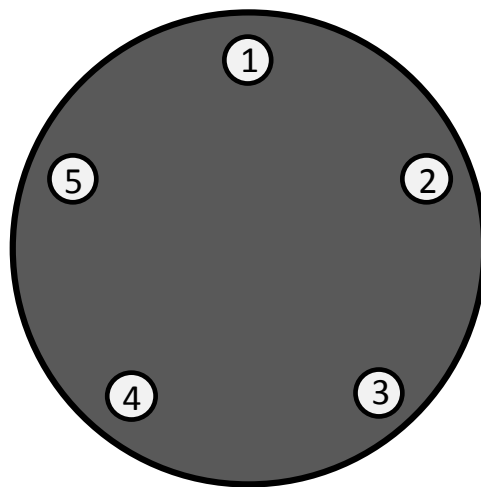


Figure 3.1. An example of a joint with five bolts

		Bolt Number				
		1	2	3	4	5
Load Step	1	F_f	F_f	F_f	F_f	F_f
	2	\vdots	\vdots	\vdots	F_4	0
	3	\vdots	\vdots	F_3	0	0
	4	\vdots	F_2	0	0	0
	5	F_1	0	0	0	0

Table 3.1. Schematic representation of the ISM

This method works on bolted joints with both linear and non-linear behaviour. However, the joint must follow the same path in the strain-stress curve during loading and unloading. In other words, the inverse sequence must behave identically to the optimized tightening sequence but in the opposite direction. It is also necessary for the bolts to get completely untightened during the inverse sequence, which means that this method is only valid when the initial state of the joint has every bolt completely untightened. This is because it is not possible to untighten every bolt to an intermediate load. Assuming that in the previous example bolt number 5 was only untightened until a target intermediate load F_m , at the end of the inverse sequence, the load of bolt number 5 was going to be different due to the elastic interaction phenomenon, and therefore, at the end of the inverse sequence every bolt was not going to be at the target intermediate uniform bolt load F_m . Therefore, the obtained loads would not be valid for the optimized tightening sequence which starts with an initial load F_m on every bolt.

To validate the ISM on RTJs, the Finite Element model explained in Chapter 2 was used with the dimensions of the experimental set up (NPS 24", Class 150 and SCHD 40). Besides, a target load of 250 kN was used, with assembly pattern 1 (see Figure 2.18a) and a friction coefficient of 0.25. The target load of 250 kN represents the 55% of the yielding load of the bolts (the intermediate point between 40% and 70% recommended by the standards, as explained in Chapter 1). Following the explained procedure, first the inverse sequence was performed in order to obtain the tightening loads of the optimized tightening sequence, and the optimized tightening sequence was then tested. The results of the Table 3.2 were obtained from the inverse sequence. This table shows the load level of every bolt in every load step. As mentioned above, the level of load of each bolt prior to being untightened will

be the tightening load of that bolt during the optimized tightening sequence. These loads are indicated in grey in Table 3.2 and are shown reordered in Figure 3.2. Finally, in Table 3.2 it should be noted that in the last load step, four bolts are still tightened. This is because after unloading so many bolts, the Finite Element model starts to move with solid rigid motion and, as a consequence, the analysis commences with convergence problems. Nevertheless, the last four bolts are so far from each other that their load levels will not suffer a big change if any of the other bolts were unloaded. Therefore, the last four bolts were unloaded in the same load step. To this regard, the load of the four bolts of load step 17 was considered their tightening load in the optimized tightening sequence.

	Step1	Step2	Step3	Step4	Step5	Step6	Step7	Step8	Step9	Step10	Step11	Step12	Step13	Step14	Step15	Step16	Step17
Bolt 1	250	251	252	252	253	254	254	254	295	349	349	350	348	348	347	349	360
Bolt 2	250	251	252	252	253	253	254	254	0	0	0	0	0	0	0	0	0
Bolt 3	250	251	251	252	292	293	294	294	337	339	339	340	350	350	349	351	0
Bolt 4	250	251	251	252	0	0	0	0	0	0	0	0	0	0	0	0	0
Bolt 5	250	250	251	252	293	294	296	296	297	298	299	299	0	0	0	0	0
Bolt 6	250	250	252	252	253	253	293	293	294	295	296	296	348	349	358	359	360
Bolt 7	250	251	252	252	253	253	0	0	0	0	0	0	0	0	0	0	0
Bolt 8	250	251	291	291	292	293	335	337	337	338	351	351	350	352	0	0	0
Bolt 9	250	251	0	0	0	0	0	0	0	0	0	0	0	0	0	0	0
Bolt 10	250	251	292	293	293	294	295	297	297	298	0	0	0	0	0	0	0
Bolt 11	250	251	252	253	253	253	254	294	294	295	349	350	348	349	348	359	359
Bolt 12	250	250	252	253	253	253	254	0	0	0	0	0	0	0	0	0	0
Bolt 13	250	250	251	292	292	294	294	336	337	337	339	352	350	351	350	0	0
Bolt 14	250	251	251	0	0	0	0	0	0	0	0	0	0	0	0	0	0
Bolt 15	250	251	251	293	293	295	296	297	297	298	299	0	0	0	0	0	0
Bolt 16	250	251	252	253	253	293	293	294	294	295	296	350	348	358	357	358	359
Bolt 17	250	251	252	253	253	0	0	0	0	0	0	0	0	0	0	0	0
Bolt 18	250	290	291	292	292	335	335	336	337	350	351	353	350	0	0	0	0
Bolt 19	250	0	0	0	0	0	0	0	0	0	0	0	0	0	0	0	0
Bolt 20	250	291	292	292	293	295	295	296	297	0	0	0	0	0	0	0	0

Table 3.2. Load level of every bolt in every load step during the inverse sequence

Figure 3.2 shows the obtained optimized tightening loads (in grey in Table 3.2) and the obtained final loads after applying the optimized tightening loads in the Finite Element model. As can be seen, the obtained final loads are almost uniform with the average load being 245.9 kN and the standard deviation 4.3 kN with regards to the target load of 250 kN. This proves that the ISM provides accurate results in RTJs.

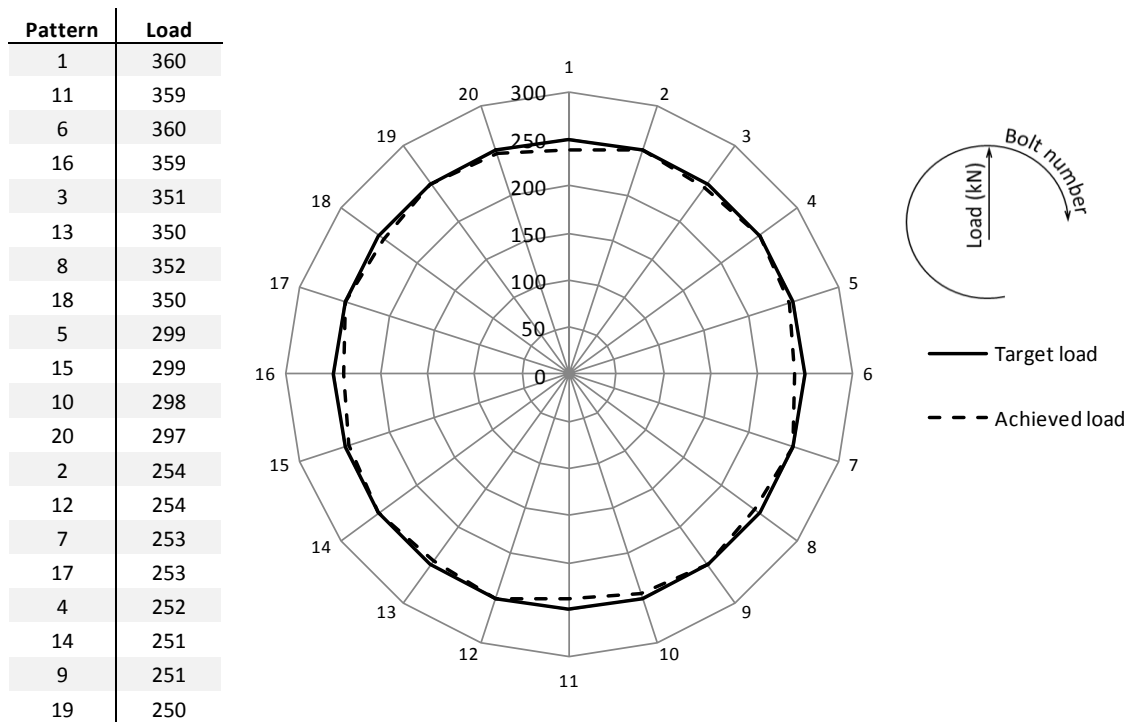


Figure 3.2. Obtained tightening loads (in the table) and final loads (in the polar diagram) with the ISM for assembly pattern 1, target load 250 kN and friction coefficient 0.25

Finally, in order to compare the behaviour of the loads and unloads in RTJs, analysis was performed where every bolt was tightened to the same load level at the same time. Subsequently they were also completely unloaded at the same time. This analysis was performed until different load levels giving the resulting graphic of Figure 3.3. This picture shows the relation between the load and the deformation of the joint, where the load is the preload of the bolts (any of them) and the displacement is the vertical deformation of the center node of the bolt head. As can be seen, loads and unloads have different behaviours, and therefore using the ISM the small error appears in the bolt final load as shown in Figure 3.2.

Regarding the ISM, it should also be mentioned that its main disadvantage is that the bolts must be completely unloaded at the beginning of the tightening sequence. Consequently, this method cannot be used for multiple-pass tightening sequences, which is sometimes unavoidable, as will be explained in section 3.5.

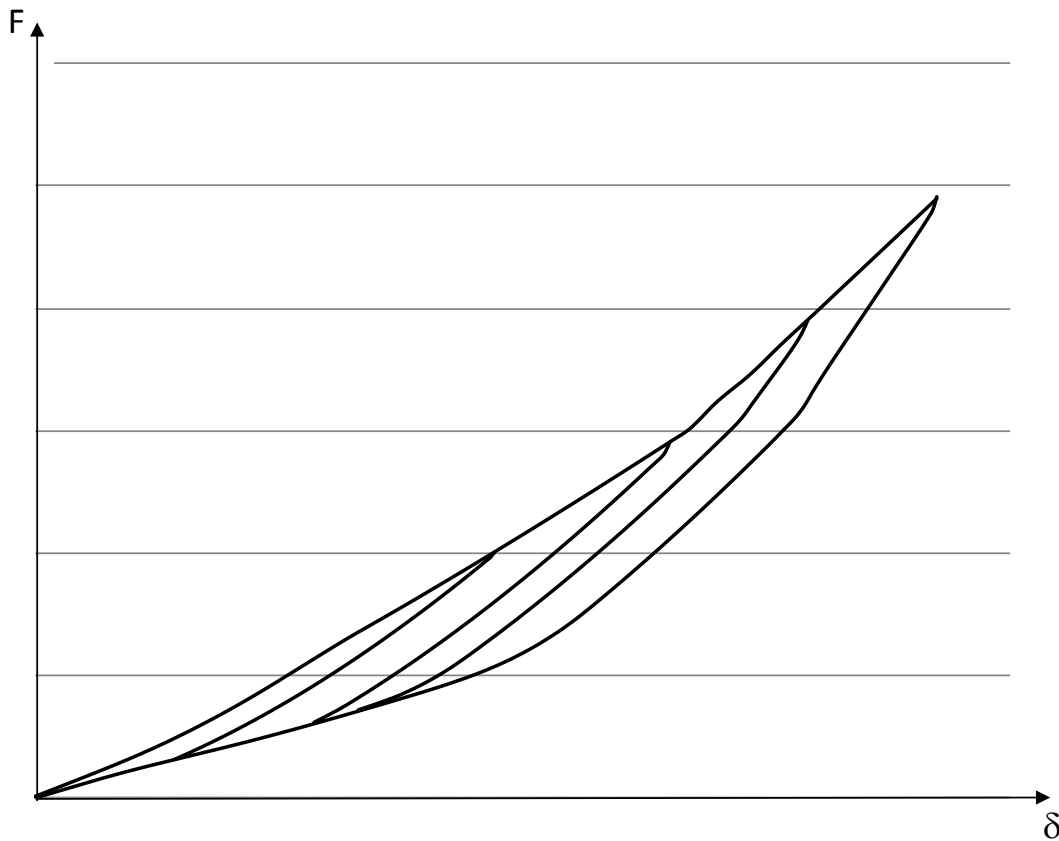


Figure 3.3. Relation between the applied tightening load on the bolts and their vertical displacement during loading and unloading

3. ELASTIC INTERACTION COEFFICIENTS METHOD

The EICM was firstly developed by D. H. Van Campen [Van'69] and later generalized by Bibel et al. [Bib'92; Bib'94; Bib'96; Eze'92; God'94]. This method, just as the ISM, enables the obtaining of the tightening loads of every bolt in order to obtain the target uniform final load distribution.

In this section, the EICM is explained and studied for optimized tightening sequences of one and two passes on RTJs. This method is of particular importance in this Doctoral Thesis because the new methodology (TAM) was developed from the conclusions obtained when the EICM was studied.

3.1. GENERAL DESCRIPTION

The EICM is based on the calculation of a matrix which relates the initial loads (tightening loads) and final loads (at the end of the tightening sequence) of the bolts with the following equation [Bib'92; Bib'94; Bib'96; Fuk'04; God'94]:

$$\{S_f\} = [A] \cdot \{S_i\} \quad (3.1)$$

Where:

$\{S_f\}$ = Vector with bolts final load

$\{S_i\}$ = Vector with bolts initial load

$[A]$ = Elastic interaction coefficients matrix

In other words, the element S_{ik} of vector $\{S_i\}$ is the initial load of bolt k , while the element S_{fk} of the vector $\{S_f\}$ is its final load. Thus, in a joint with n bolts, the equation (3.1) has the following shape:

$$\begin{Bmatrix} S_{f1} \\ S_{f2} \\ S_{f3} \\ \vdots \\ S_{fn-1} \\ S_{fn} \end{Bmatrix} = \begin{bmatrix} 1 & A_{1,2} & A_{1,3} & \cdots & A_{1,n-1} & A_{1,n} \\ 0 & 1 & A_{2,3} & \cdots & A_{2,n-1} & A_{2,n} \\ 0 & 0 & 1 & \cdots & A_{3,n-1} & A_{3,n} \\ \vdots & \vdots & \vdots & \ddots & \vdots & \vdots \\ 0 & 0 & 0 & \vdots & 1 & A_{n-1,n} \\ 0 & 0 & 0 & \vdots & 0 & 1 \end{bmatrix} \begin{Bmatrix} S_{i1} \\ S_{i2} \\ S_{i3} \\ \vdots \\ S_{in-1} \\ S_{in} \end{Bmatrix} \quad (3.2)$$

It is important to note that the bolts are numbered in the order that they are tightened: the first row corresponds to the first bolt being tightened during the tightening sequence; the second row to the second bolt being tightened, and so on. If one of the rows of equation (3.2) is studied, for example the first row (as mentioned it corresponds to the first bolt being tightened), the following equation is obtained:

$$S_{f1} = S_{i1} + A_{1,2} \cdot S_{i2} + A_{1,3} \cdot S_{i3} + \cdots + A_{1,n} \cdot S_{in} \quad (3.3)$$

Equation (3.3) shows that the final load of bolt number 1 (S_{f1}) is equal to its initial load (S_{i1}), plus $A_{1,2}$ times the initial load of bolt number 2 (S_{i2}), plus $A_{1,3}$ times the initial load of bolt number 3 (S_{i3}), etcetera. This means that at the beginning, bolt number 1 has an initial load S_{i1} , when bolt number 2 is

tightened, it undergoes a load variation of $A_{1,2} \cdot S_{i2}$, next bolt number 3 produces a load variation of $A_{1,3} \cdot S_{i3}$, and so on until the whole tightening sequence is completed, obtaining the resulting final load S_{f1} . Therefore, the elements of matrix $[A]$ quantify the elastic interaction, and thus the matrix is called the elastic interaction coefficients matrix.

Usually, elements of matrix $[A]$ have a negative value because the most influential uncertainty factor is the elastic interaction, which entails loss of loads. The elements of this matrix are obtained simulating a whole tightening sequence (in a Finite Element model or in an experimental set-up) and measuring the load level of every bolt after each tightening operation, as explained in detail in the next section. Once matrix $[A]$ has been calculated, the initial loads $\{S_i\}$ can be calculated (tightening loads) in order to obtain a uniform final load on the joint $\{S_f\}$. Tightening loads are obtained by means of the following equation:

$$\{S_i\} = [A]^{-1} \cdot \{S_f\} \quad (3.4)$$

As mentioned above, the EICM is based on the calculation of matrix $[A]$. Next, the procedure to calculate matrix $[A]$ is presented, with an illustrative example similar to the ones presented in [Bib'92; God'94].

3.2. CALCULATION ALGORITHM FOR THE MATRIX $[A]$

Figure 3.4 shows a joint with three bolts with the target load being a uniform final load of 10,000 N, first tightening bolt a , secondly bolt b and finally bolt c . According to the EICM, the tightening load of every bolt is obtained with the equation (3.4). Therefore, it is necessary to first obtain the matrix $[A]$.

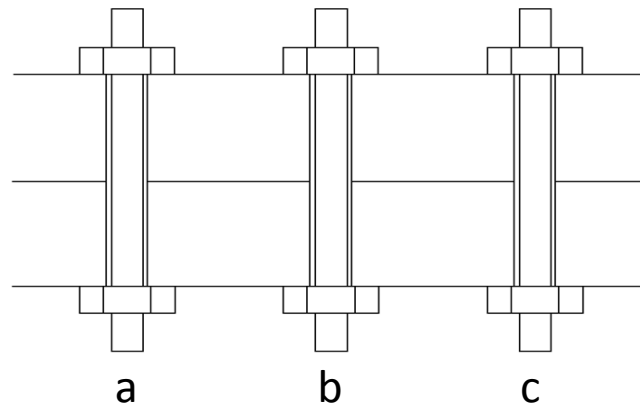


Figure 3.4. Illustrative example of a joint with three bolts

The first step to obtain matrix $[A]$ is to simulate a whole tightening sequence (in a Finite Element model or in an experimental set up), using the target load as the tightening load of every bolt (10,000 N in this example). Besides, the same assembly pattern must be followed and the level of load of every bolt must be measured after each tightening operation. Table 3.3 shows the load level of every bolt after each tightening operation: when bolt b is tightened, the load level of bolt a decreases to 8,250 N due to the elastic interaction phenomenon; likewise, when bolt c is tightened, the load levels of bolts a and b decrease to 7,500 and 9,000 N, respectively.

ASSEMBLY PATTERN	LOAD		
	a	b	c
a	10,000	--	--
b	8,250	10,000	--
c	7,500	9,000	10,000

Table 3.3. Load level on the bolts during the tightening sequence

From these results it is deduced that the vectors with the initial and final loads on the bolts are as follows:

$$\{S_i\} = \begin{pmatrix} 10,000 \\ 10,000 \\ 10,000 \end{pmatrix} \quad \{S_f\} = \begin{pmatrix} 7,500 \\ 9,000 \\ 10,000 \end{pmatrix}$$

Also, with the results of Table 3.3 the auxiliary matrix $[S_h]$ is built, which contains the load level of every bolt in every load step:

$$[S_h] = \begin{bmatrix} 10,000 & 0 & 0 \\ 8,250 & 10,000 & 0 \\ 7,500 & 9,000 & 10,000 \end{bmatrix}$$

Once this matrix has been obtained, the elements $A_{i,j}$ of matrix $[A]$ can be obtained using the following mathematical equation [Bib'92; God'94]:

$$\begin{aligned}
A_{i,j} &= 1 && \text{if } i = j \\
A_{i,j} &= 0 && \text{if } i > j \\
A_{i,j} &= \frac{[S_h]_{j,i} - [S_h]_{j-1,i}}{[S_h]_{j,j}} && \text{if } i < j
\end{aligned} \tag{3.5}$$

Calculating matrix $[A]$ for this example:

$$[A] = \begin{bmatrix} 1 & -0.175 & -0.075 \\ 0 & 1 & -0.1 \\ 0 & 0 & 1 \end{bmatrix}$$

As explained in the previous section, from the first row it is deduced that the final load of bolt a is equal to its initial load, minus 0.175 times the initial load of bolt b , minus 0.075 times the initial load of bolt c . Summarizing, the optimization process comprises the following steps:

- 1) Simulate a tightening sequence in a Finite Element model or on a test bench applying the target load as tightening loads. The load level of every bolt must be measured after each tightening operation. These values are entered in the auxiliary matrix $[S_h]$.
- 2) With the obtained measurements, equation (3.5) is used to obtain the matrix $[A]$.
- 3) Once the matrix $[A]$ has been obtained, equation (3.4) is used to obtain the tightening loads $\{S_i\}$ that provide the target uniform final load $\{S_f\}$.

3.3. DISCUSSION OF THE METHOD

In conclusion, a complete tightening sequence must be simulated, measuring the load levels of every bolt after each tightening operation to obtain the matrix $[A]$, which obviously entails a very high cost. This method also assumes that the initial and final loads on the bolts are linearly related with matrix $[A]$ for a specific assembly pattern, friction coefficient and load level. However, the behaviour of the joint during the tightening sequence is sometimes non-linear due to the non-linear material of the gasket, changes in the contact status between components and/or large deformations.

In [Bib'92; Bib'94; Bib'96; Eze'92] the EICM was adapted to obtain optimal tightening sequences on non-linear joints. For this purpose, matrix $[A]$ is calculated iteratively (simulating sequences over and over) in order to adjust it to the working loads, which increases the cost significantly. Thus, a uniform final load was achieved on a non-linear joint with only a one-pass tightening sequence. The obtained error was less than $\pm 2\%$ (measured as the average load of every bolt divided by the target final load). In this case, the method consisted of the following steps:

- 1) Simulate a tightening sequence in a Finite Element model or on a test bench applying the target load as tightening loads. The load level of every bolt must be measured after each tightening operation. These values are entered in the auxiliary matrix $[S_h]$.
- 2) With the obtained measurements, equation (3.5) is used to obtain the matrix $[A]$.
- 3) Once the matrix $[A]$ has been obtained, equation (3.4) is used to obtain the tightening loads that provide the target uniform final load.
- 4) If the obtained final loads do not tally with the target final uniform load (with an admissible error), matrix $[A]$ is recalculated with the last results obtained.
- 5) The initial loads that provide the target uniform final load are also recalculated with the new matrix $[A]$.
- 6) Steps 4 and 5 are repeated until the obtained error in the uniform final load is smaller than the established criterion.

In the next section the EICM is validated for RTJ with the parametric Finite Element model of the joint using the geometric dimensions of the test bench. Moreover, the need to calculate matrix $[A]$ iteratively in RTJs is studied.

3.4. VALIDATION OF THE EICM FOR ONE-PASS TIGHTENING SEQUENCES ON RTJS

For the validation of the EICM, two different tightening sequences were simulated with different friction coefficients, assembly patterns and target loads in each one. The objective is to validate the method on RTJs and also discover the influence of these parameters in the accuracy of the method.

3.4.1. FIRST VALIDATION ANALYSIS

In the first analysis, the tightening sequence has a target uniform load of 350 kN (maximum preload suggested by the standards in this particular joint [Asm'13(2)]), following assembly pattern 1 of Figure 2.18a and with a friction coefficient of 0.2.

The first step to obtain this matrix is to simulate a tightening sequence using 350 kN as the tightening load for every bolt, the target assembly pattern and the studied friction coefficient. Figure 3.5 shows the load level of every bolt during the tightening sequence. The first conclusion drawn from this picture is that the first loaded bolts lose an extensive load during the tightening sequence, while the last loaded bolts do not lose any load. This is due to the elastic interaction phenomenon. As explained in Chapter 1, when a bolt is tightened, the joint is compressed and, as a consequence, previously tightened bolts lose load. In this sense, the sooner a bolt is tightened, the greater the influence of the elastic interaction phenomenon because the amount of bolts that are tightened afterwards increases. Due to this phenomenon, it can be deduced that, in the optimized tightening sequence, the first bolts tightened must have a higher tightening load than the target load. Thus, this “overload” compensates for the loss of loads that the bolts will suffer during the tightening sequence. On the other hand, it can be seen that the solid rigid motion does not affect this joint because the load of any bolt increases when another bolt is preloaded during the tightening sequence.

From Figure 3.5, the load level of every bolt in every load step can be obtained and therefore the $[S_h]$ matrix can be built. With matrix $[S_h]$, matrix $[A]$ is calculated using the equation (3.5). Following this, the tightening loads are obtained by equation (3.4). Following this procedure the tightening loads of Figure 3.6 were obtained. Also, the polar diagram of Figure 3.6 shows the obtained final load distribution in the simulation of the optimized tightening sequence in the Finite Element model. The final load distribution obtained is completely uniform, with an average load of 347 kN and a standard deviation of 4.7 kN (target load is 350 kN). This means that in the first validation analysis, the EICM provides extremely precise results without any need to iteratively recalculate the matrix $[A]$, in spite of the non-linearity of the joint.

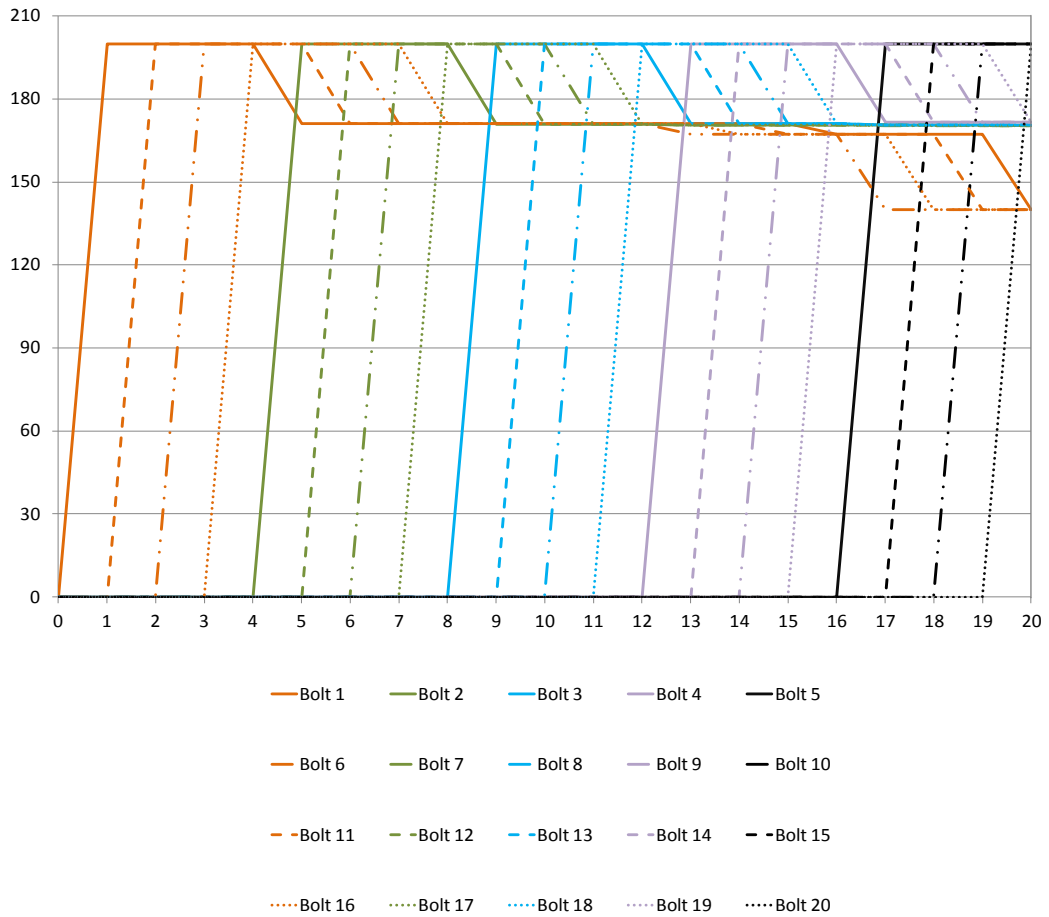


Figure 3.5. Load level of bolts during the tightening sequence of the first validation analysis (horizontal axis load step, vertical axis level of load on the bolts)

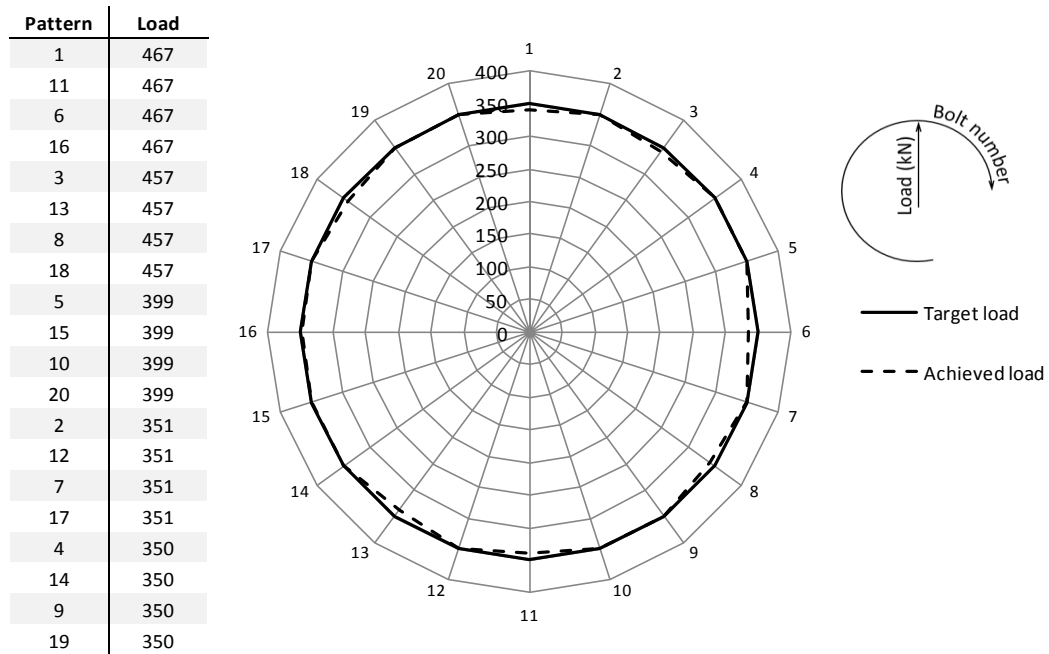


Figure 3.6. Obtained initial loads (in the table) and final loads (in the polar diagram) with the EICM using assembly pattern1, target load 350 kN and friction coefficient 0.2

3.4.2. SECOND VALIDATION ANALYSIS

Another analysis was performed with the opposite parameters to the previous analysis in order to completely validate the EICM, so the target load was 200 kN (minimum preload suggested by the standards in this particular joint [Asm'13(2)]), following assembly pattern 2 of Figure 2.18b and with a friction coefficient of 0.3 (as mentioned in Chapter 2, the friction coefficient on steel-steel contacts is between 0.2 and 0.3). Following the same procedure as the first analysis, the results of Figures 3.7 and 3.8 were obtained.

As can be seen, the final load distribution obtained is completely uniform, with the average load being 200 kN and the standard deviation 0.4 kN (in Figure 3.8 the lines are overlapped). Therefore, it is proven that varying all the parameters of the analysis, the ECIM also provides extremely accurate results.

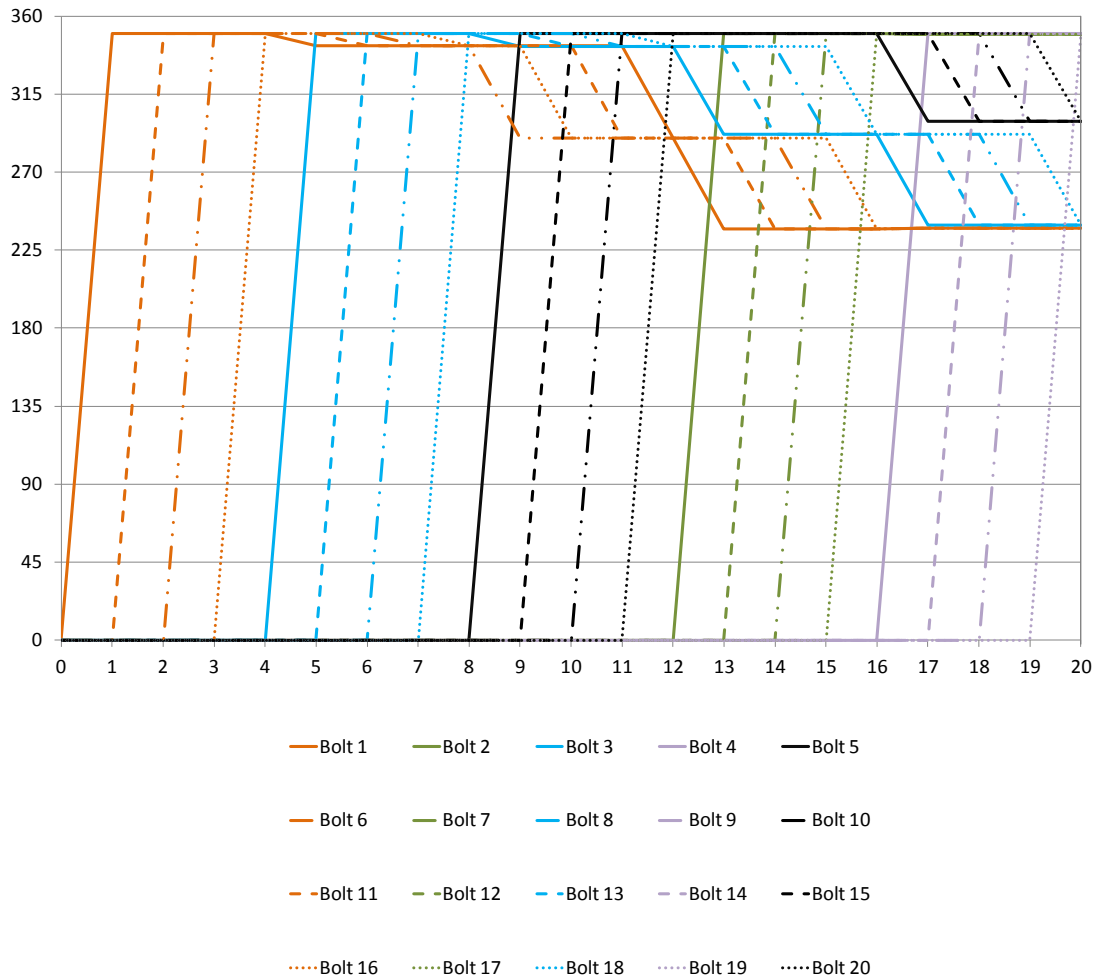


Figure 3.7. Load level of the bolts during the tightening sequence of the second validation analysis (horizontal axis load step, vertical axis level of load on the bolts)

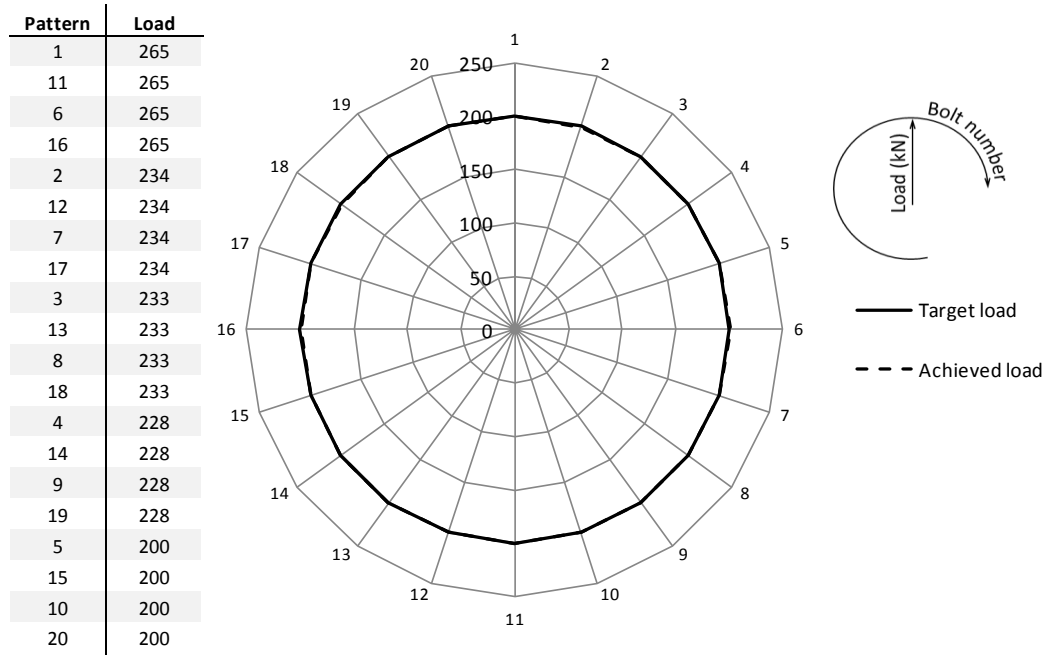


Figure 3.8. Obtained initial loads (in the table) and final loads (in the polar diagram) with the EICM using assembly pattern2, target load 200 kN and friction coefficient 0.3

3.5. GENERALIZATION OF THE EICM FOR TWO-PASS TIGHTENING SEQUENCES ON RTJS

Sometimes, during the tightening sequence, the tightening load of some bolts is extremely high and, as a consequence, a tightening sequence with more than one pass is necessary. In other words, when any of the values of vector $\{S_i\}$ of the equation (3.4) exceeds the bolt yielding load or when the flange or the gasket suffers damages due to an excessive bolt tightening load, a tightening sequence of at least two passes is necessary. This usually happens in two situations: When the target load is extremely close to bolt yielding load, or when elastic interaction has a large influence, and therefore, the tightening load of the bolts is much higher than the target load. For simplicity, the EICM for two-pass tightening sequences will be explained, but the process is the same for tightening sequences with more passes. Nevertheless, a two-pass tightening sequence is usually enough for standard joints [Nas'05; Nas'08].

As described previously, in one-pass tightening sequences, the initial and final loads are related with the equation (3.1). For two-pass tightening sequences, the equation of the EICM is as follows [Aba'14; Bib'96; Eze'92; Fuk'04]:

$$\{S_{f2}\} = [A] \cdot \{S_{i1}\} + [B] \cdot \{\Delta S\} \quad (3.6)$$

And replacing (3.1) in (3.6):

$$\{S_{f2}\} = \{S_{f1}\} + [B] \cdot \{\Delta S\} \quad (3.7)$$

Where:

$\{S_{f1}\}$ = Vector with bolts final load after the first pass

$\{S_{f2}\}$ = Vector with bolts final load after the second pass

$\{S_{i1}\}$ = Vector with bolts initial load in the first pass

$\{\Delta S\}$ = Vector with bolts load increment to apply in the second pass

$[A]$ = Elastic interaction coefficients matrix of the first pass

$[B]$ = Elastic interaction coefficients matrix of the second pass

Expanding the equation (3.7):

$$\begin{Bmatrix} S_{f21} \\ S_{f22} \\ S_{f23} \\ \vdots \\ S_{f2n} \end{Bmatrix} = \begin{Bmatrix} S_{f11} \\ S_{f12} \\ S_{f13} \\ \vdots \\ S_{f1n} \end{Bmatrix} + \begin{bmatrix} 1 & B_{1,2} & B_{1,3} & \dots & B_{1,n} \\ B_{2,1} & 1 & B_{2,3} & \dots & B_{2,n} \\ B_{3,1} & B_{3,2} & 1 & \dots & B_{3,n} \\ \vdots & \vdots & \vdots & \ddots & \vdots \\ B_{n,1} & B_{n,2} & B_{n,3} & \dots & 1 \end{bmatrix} \begin{Bmatrix} \Delta S_1 \\ \Delta S_2 \\ \Delta S_3 \\ \vdots \\ \Delta S_n \end{Bmatrix} \quad (3.8)$$

Therefore, as in one-pass bolt tightening sequences, once matrix $[B]$ is obtained, it is possible to calculate the load increment vector $\{\Delta S\}$ which has to be applied to the bolts in the second pass in order to achieve a uniform final load distribution. Therefore, the aim of the second pass is to go from the bolt final load in the first pass $\{S_{f1}\}$ to the bolt final load at the end of the second pass $\{S_{f2}\}$, and for that purpose, the tightening loads are calculated with the matrix $[B]$.

As can be observed, matrix $[B]$ is very similar to matrix $[A]$. However, there are some minor differences because, at the beginning of the first pass, the bolts are completely unloaded while at the beginning of the second pass, the bolts are already loaded to $\{S_{f1}\}$. As a consequence, the elements under the main diagonal in matrix $[B]$ are not necessarily null. This concept will be better explained with the development of the TAM in Chapters 4 and 5.

3.6. VALIDATION OF THE EICM FOR TWO-PASS TIGHTENING SEQUENCES ON RTJS

In order to validate the EICM for two-pass tightening sequences, one analysis was performed using the Finite Element model, establishing a uniform final load of 200 kN at the end of the first pass and a uniform final load of 350 kN at the end of the second pass. Also, assembly pattern 1 was used for the first pass and assembly pattern 2 for the second pass (see Figure 2.18), together with a friction coefficient of 0.25.

To this regard, first of all, a two-pass tightening sequence was simulated in which the tightening loads of the first pass were 200 kN and the tightening loads of the second pass 350 kN. Thus, the influence of the elastic interaction was studied and matrices $[A]$ and $[B]$ were obtained following the previously explained procedure. Once both matrices were obtained, with equations (3.4) and (3.6) the tightening loads in the first pass and the loads increment in the second pass were obtained, respectively. Once this process was performed, the tightening loads of Table 3.4 were obtained for the optimized two-pass tightening sequence.

First pass		Second pass	
Pattern	Load	Pattern	Load
1	269	1	418
11	269	11	417
6	268	6	417
16	269	16	417
3	264	2	385
13	263	12	385
8	266	7	384
18	264	17	384
5	230	3	385
15	229	13	385
10	229	8	385
20	229	18	384
2	200	4	385
12	200	14	384
7	199	9	384
17	199	19	384
4	200	5	351
14	200	15	350
9	200	10	350
19	200	20	350

Table 3.4. Obtained tightening loads with the EICM for an optimized two-pass tightening sequence

Finally, the optimized tightening sequence was simulated in the Finite Element model applying the tightening loads of Table 3.4, and the results of the polar diagram of Figure 3.9 were obtained. As can be observed, the obtained final load distribution is completely uniform, with the average load being 349 kN and the standard deviation 0.96 kN. Therefore, it has been proven that the EICM provides very accurate results on RTJs for both, one-pass tightening sequences and multiple-pass tightening sequences.

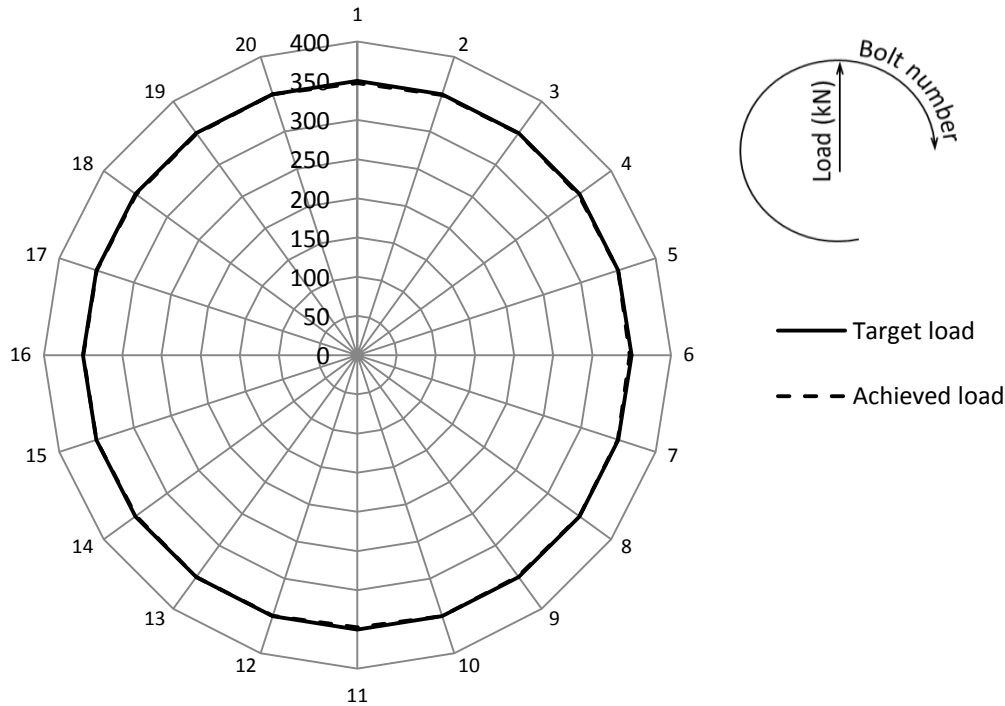


Figure 3.9. Obtained final load distribution with an optimized two-pass tightening sequence of the EICM

4. COMPARISON OF BOTH METHODS: EICM AND ISM

Comparing the EICM and the ISM, it is appreciated that the results of the EICM are slightly more accurate, but in both cases completely successful. On the other hand, and more importantly, in contrast to the ISM the EICM enables optimized multiple-pass tightening sequences, which is very useful when the target load is so close to bolt yielding load or when the elastic interaction phenomenon plays a significant influence, because possible damages on the gasket, flange or bolts are avoided.

However, obtaining the optimized tightening sequence is expensive for both methods because a whole tightening sequence must be carried out and a high number of measurements must be performed to understand the behaviour of the joint. To this end, this Doctoral Thesis studies the influence of the different operational parameters in matrix $[A]$, to subsequently - based on the obtained conclusions - develop a new method called TAM. This method obtains optimized tightening sequences for RTJs in a much more efficient way than the EICM or the ISM.

Chapter 4 reviews the elements of matrix $[A]$ and the new method is developed for optimized one-pass tightening sequences. Following that, the new methodology is generalized in Chapter 5 to optimized two-pass tightening sequences and the range of application is studied among all the standardized ASME RTJs [Asm'12(2); Asm'13(1)].

CHAPTER 4. TETRAPARAMETRIC ASSEMBLY METHOD

1. INTRODUCTION

The most popular methods found in specialist literature to perform optimized tightening sequences were explained in Chapter 3: the EICM and the ISM. Both of them have also been validated for RTJs with the Finite Element model. However, as has been pointed out in Chapter 3, obtaining the optimized tightening sequence is extremely expensive in both methods, because a whole tightening sequence must be performed and the load levels of the bolts must be measured during the tightening sequence.

In this regard, this Chapter develops a new method called the Tetraparametric Assembly Method (TAM) [Cor'16(1); Cor'16(2); Cor'17(1)]. As will be demonstrated throughout this Chapter, this method is much more efficient than the methods explained in Chapter 3, because the optimized tightening sequence of the joint is obtained with a much lower cost and with no loss of accuracy.

The TAM is based on the EICM. Therefore, in this Chapter, first the elements of the matrix $[A]$ are studied in detail, with the TAM then developed based on the conclusions.

2. STUDY OF THE ELEMENTS OF MATRIX $[A]$

For this section, a large number of analyses were carried out in order to determine the influence of the different operational parameters on the elements of matrix $[A]$. As in Chapter 3, the Finite Element model with the geometrical dimensions of the experimental set up were used (NPS 24", Class 150 and SCHD 40), and the studied parameters were: friction coefficient (0.2 and 0.3), target load (200 kN and 350 kN) and assembly pattern (assembly patterns 1 and 2 of Figure 2.18).

First of all, the four different analyses with the assembly pattern 1 were performed, combining the two target loads and the two friction coefficients. Figure 4.1 shows the obtained matrix $[A]$ for each analysis (the numbers of the picture were rounded off but later all the decimals were used). As explained in Chapter 3, the elements that appear in the matrices quantify the influence of the elastic interaction phenomenon during the assembly process.

1	0	0	0	-0.02	0	0	0	0	0	0	-0.14	-0.14	0	0	0	0	0	0	0	-1E-3
0	1	0	0	0	-0.02	0	0	0	0	0	-0.14	0	-0.14	0	0	0	0	0	-1E-3	0
0	0	1	0	0	0	-0.02	0	-0.14	0	0	0	0	-0.14	0	-1E-3	0	0	0	0	0
0	0	0	1	0	0	0	-0.02	0	-0.14	0	0	0	0	-0.14	0	-1E-3	0	0	0	0
0	0	0	0	1	0	0	0	-0.02	0	0	0	0	0	0	-0.14	0	0	0	0	0
0	0	0	0	0	1	0	0	0	-0.02	0	0	0	0	0	0	-0.14	0	0	0	0
0	0	0	0	0	0	1	0	0	0	0	0	0	-1E-3	0	-0.14	0	0	0	0	0
0	0	0	0	0	0	0	1	0	0	0	0	0	0	-1E-3	0	-0.14	0	0	0	0
0	0	0	0	0	0	0	0	1	0	0	0	0	-1E-3	0	0	-0.14	0	0	0	0
0	0	0	0	0	0	0	0	0	1	-1E-3	0	0	0	0	0	0	0	0	-0.14	0
0	0	0	0	0	0	0	0	0	0	1	0	0	0	-2E-3	0	0	0	0	0	0
0	0	0	0	0	0	0	0	0	0	0	1	0	0	0	-2E-3	0	0	0	0	0
0	0	0	0	0	0	0	0	0	0	0	0	1	0	0	0	-2E-3	0	0	0	0
0	0	0	0	0	0	0	0	0	0	0	0	0	1	0	0	0	0	0	-2E-3	0
0	0	0	0	0	0	0	0	0	0	0	0	0	0	1	0	0	0	0	0	0
0	0	0	0	0	0	0	0	0	0	0	0	0	0	0	1	0	0	0	0	0
0	0	0	0	0	0	0	0	0	0	0	0	0	0	0	0	1	0	0	0	0
0	0	0	0	0	0	0	0	0	0	0	0	0	0	0	0	0	1	0	0	0
0	0	0	0	0	0	0	0	0	0	0	0	0	0	0	0	0	0	1	0	0
0	0	0	0	0	0	0	0	0	0	0	0	0	0	0	0	0	0	0	0	1

a)

1	0	0	0	-0.02	0	0	0	0	0	0	-0.15	-0.15	0	0	0	0	0	0	0	2E-3
0	1	0	0	0	-0.02	0	0	0	0	0	-0.15	0	-0.15	0	0	0	0	0	2E-3	0
0	0	1	0	0	0	-0.02	0	-0.15	0	0	0	0	-0.15	0	2E-3	0	0	0	0	0
0	0	0	1	0	0	0	-0.02	0	-0.15	0	0	0	0	-0.15	0	2E-3	0	0	0	0
0	0	0	0	1	0	0	0	-0.02	0	0	0	0	0	0	-0.14	0	0	0	0	0
0	0	0	0	0	1	0	0	0	-0.02	0	0	0	0	-0.14	0	0	-0.15	0	0	0
0	0	0	0	0	0	1	0	0	0	-0.02	0	0	0	-0.14	0	0	0	0	-0.15	0
0	0	0	0	0	0	0	1	0	0	0	0	0	0	0	-0.14	0	0	0	0	0
0	0	0	0	0	0	0	0	1	0	0	0	0	0	0	0	-0.14	0	0	0	0
0	0	0	0	0	0	0	0	0	1	0	0	0	0	0	0	0	-0.14	0	0	0
0	0	0	0	0	0	0	0	0	0	1	0	0	0	0	0	0	0	0	0	0
0	0	0	0	0	0	0	0	0	0	0	1	0	0	0	0	0	0	0	0	0
0	0	0	0	0	0	0	0	0	0	0	0	1	0	0	0	0	0	0	0	0
0	0	0	0	0	0	0	0	0	0	0	0	0	1	0	0	0	0	0	0	0
0	0	0	0	0	0	0	0	0	0	0	0	0	0	1	0	0	0	0	0	0
0	0	0	0	0	0	0	0	0	0	0	0	0	0	0	1	0	0	0	0	0
0	0	0	0	0	0	0	0	0	0	0	0	0	0	0	0	1	0	0	0	0
0	0	0	0	0	0	0	0	0	0	0	0	0	0	0	0	0	1	0	0	0
0	0	0	0	0	0	0	0	0	0	0	0	0	0	0	0	0	0	1	0	0
0	0	0	0	0	0	0	0	0	0	0	0	0	0	0	0	0	0	0	0	1

b)

1	0	0	0	-0.02	0	0	0	0	0	0	-0.14	-0.14	0	0	0	0	0	0	-3E-3
0	1	0	0	0	-0.02	0	0	0	0	-0.14	0	0	-0.14	0	0	0	0	0	-3E-3
0	0	1	0	0	0	-0.02	0	-0.14	0	0	0	0	0	-0.14	0	-3E-3	0	0	0
0	0	0	1	0	0	0	-0.02	0	-0.14	0	0	0	0	0	-0.14	0	-3E-3	0	0
0	0	0	0	1	0	0	0	-0.02	0	0	0	0	0	0	0	0	0	0	0
0	0	0	0	0	1	0	0	0	-0.02	0	0	0	-0.14	0	0	0	-0.14	0	0
0	0	0	0	0	0	1	0	0	0	-0.02	0	0	0	-0.14	0	0	0	-0.14	0
0	0	0	0	0	0	0	1	0	0	0	0	0	-4E-3	0	-0.14	0	0	0	0
0	0	0	0	0	0	0	0	1	0	0	0	0	0	0	-4E-3	0	-0.14	0	0
0	0	0	0	0	0	0	0	0	1	0	0	0	-4E-3	0	0	0	0	-0.14	0
0	0	0	0	0	0	0	0	0	0	1	-4E-3	0	0	0	0	0	0	0	-0.14
0	0	0	0	0	0	0	0	0	0	0	1	0	0	0	-4E-3	0	0	0	0
0	0	0	0	0	0	0	0	0	0	0	0	1	0	0	0	-4E-3	0	0	0
0	0	0	0	0	0	0	0	0	0	0	0	0	1	0	0	0	0	-4E-3	0
0	0	0	0	0	0	0	0	0	0	0	0	0	0	1	0	0	0	0	-4E-3
0	0	0	0	0	0	0	0	0	0	0	0	0	0	0	1	0	0	0	0
0	0	0	0	0	0	0	0	0	0	0	0	0	0	0	0	1	0	0	0
0	0	0	0	0	0	0	0	0	0	0	0	0	0	0	0	0	1	0	0
0	0	0	0	0	0	0	0	0	0	0	0	0	0	0	0	0	0	1	0
0	0	0	0	0	0	0	0	0	0	0	0	0	0	0	0	0	0	0	1

c)

1	0	0	0	-0.02	0	0	0	0	0	0	-0.15	-0.15	0	0	0	0	0	0	5E-4
0	1	0	0	0	-0.02	0	0	0	0	-0.15	0	0	-0.15	0	0	0	0	0	5E-4
0	0	1	0	0	0	-0.02	0	-0.15	0	0	0	0	0	-0.15	0	5E-4	0	0	0
0	0	0	1	0	0	0	-0.02	0	-0.15	0	0	0	0	0	-0.15	0	5E-4	0	0
0	0	0	0	1	0	0	0	-0.02	0	0	0	0	-0.15	0	0	0	0	0	0
0	0	0	0	0	1	0	0	0	-0.02	0	0	0	0	-0.15	0	0	0	-0.15	0
0	0	0	0	0	0	1	0	0	0	-0.02	0	0	0	0	-0.15	0	0	0	-0.15
0	0	0	0	0	0	0	1	0	0	0	0	0	-0	-3E-4	-0.14	0	0	0	0
0	0	0	0	0	0	0	0	1	0	0	0	0	0	-3E-4	-0	0	-0.14	0	0
0	0	0	0	0	0	0	0	0	1	0	0	0	-3E-4	0	0	0	0	-0.14	0
0	0	0	0	0	0	0	0	0	0	1	-3E-4	0	0	0	0	0	0	0	-0.14
0	0	0	0	0	0	0	0	0	0	0	1	0	0	0	-1E-3	0	0	0	0
0	0	0	0	0	0	0	0	0	0	0	0	1	0	0	0	-1E-3	0	0	0
0	0	0	0	0	0	0	0	0	0	0	0	0	1	0	0	0	-1E-3	0	0
0	0	0	0	0	0	0	0	0	0	0	0	0	0	1	0	0	0	0	0
0	0	0	0	0	0	0	0	0	0	0	0	0	0	0	1	0	0	0	0
0	0	0	0	0	0	0	0	0	0	0	0	0	0	0	0	1	0	0	0
0	0	0	0	0	0	0	0	0	0	0	0	0	0	0	0	0	1	0	0
0	0	0	0	0	0	0	0	0	0	0	0	0	0	0	0	0	0	1	0
0	0	0	0	0	0	0	0	0	0	0	0	0	0	0	0	0	0	0	1

d)

Figure 4.1. Obtained matrix [A] with the assembly pattern 1 and with a) $\mu=0.3$ - $F=200\text{kN}$ b) $\mu=0.2$ - $F=200\text{kN}$ c) $\mu=0.3$ - $F=350\text{kN}$ d) $\mu=0.2$ - $F=350\text{kN}$

Regarding the shape of the matrices, it must be pointed out that the non null elements (marked in grey) are located exactly in the same position in the four matrices. This is because the assembly pattern is the same, and therefore, it is obvious that the loss of loads of each bolt occurs at the same moment. It should also be noted that the elements have almost the same value in the four matrices. This means that both the load level and the friction coefficient have very little influence on the level of elastic interaction of the joint, and therefore, on this particular joint it is not necessary to recalculate matrix $[A]$ when the load level or the friction coefficient changes.

Figure 4.2 shows the obtained $[A]$ matrices for assembly pattern 2. As can be observed, comparing the matrices of assembly pattern 1 and the matrices of assembly pattern 2, the location of the elements is different; this is because the bolts are preloaded in a different order. On the other hand, it can be appreciated once again that the value of the elements is almost the same for different load levels (200 kN and 350 kN), and for different friction coefficients (0.2 and 0.3). Therefore, it can be assumed that the studied joint has a unique matrix $[A]$, consisting of some elements which have almost the same value for different load levels and different friction coefficients. For different assembly patterns the elements are located in different positions, but as will be explained in the next section, these locations can be easily deduced. In this sense, once matrix $[A]$ has been obtained, it can be used to perform analyses with any parameters (friction coefficient, level of load and assembly pattern).

Based on the conclusion obtained, the new method is developed which obtains the matrix $[A]$ without performing a whole tightening sequence and without measuring the load level of every bolt after each tightening operation, as was done with the EICM to obtain the matrices of Figures 4.1 and 4.2 (see Chapter 3). Accordingly, the new method reduces the cost of the optimization process considerably in the assembly of bolted joints.

1	0	0	0	-0.14	0	0	0	-4E-4	0	0	0	0	0	0	-0.02	0	0	0	-0.14
0	1	0	0	0	-0.14	0	0	0	-4E-4	0	0	0	0	0	-0.02	0	0	0	-0.14
0	0	1	0	0	0	-0.14	0	0	0	-4E-4	0	-0.02	0	0	0	-0.14	0	0	0
0	0	0	1	0	0	0	-0.14	0	0	0	-4E-4	0	-0.02	0	0	0	-0.14	0	0
0	0	0	0	1	0	0	0	-0.15	0	0	0	-2E-3	0	0	0	0	0	0	-6E-4
0	0	0	0	0	1	0	0	0	-0.15	0	0	0	-2E-3	0	0	0	0	0	-6E-4
0	0	0	0	0	0	1	0	0	0	-0.15	0	0	0	-2E-3	0	-6E-4	0	0	0
0	0	0	0	0	0	0	1	0	0	0	-0.15	0	0	0	-2E-3	0	-6E-4	0	0
0	0	0	0	0	0	0	0	1	0	0	0	-0.14	0	0	0	-2E-3	0	0	0
0	0	0	0	0	0	0	0	0	1	0	0	0	-0.14	0	0	0	-2E-3	0	0
0	0	0	0	0	0	0	0	0	0	1	0	0	0	-0.14	0	0	0	-2E-3	0
0	0	0	0	0	0	0	0	0	0	0	1	0	0	0	-0.14	0	0	0	-2E-3
0	0	0	0	0	0	0	0	0	0	0	0	1	0	0	0	-0.14	0	0	0
0	0	0	0	0	0	0	0	0	0	0	0	0	1	0	0	0	-0.14	0	0
0	0	0	0	0	0	0	0	0	0	0	0	0	0	1	0	0	0	0	-0.14
0	0	0	0	0	0	0	0	0	0	0	0	0	0	0	1	0	0	0	0
0	0	0	0	0	0	0	0	0	0	0	0	0	0	0	0	1	0	0	0
0	0	0	0	0	0	0	0	0	0	0	0	0	0	0	0	0	1	0	0
0	0	0	0	0	0	0	0	0	0	0	0	0	0	0	0	0	0	1	0
0	0	0	0	0	0	0	0	0	0	0	0	0	0	0	0	0	0	0	1

a)

1	0	0	0	-0.15	0	0	0	3E-3	0	0	0	0	0	0	-0.02	0	0	0	-0.14
0	1	0	0	0	-0.15	0	0	0	3E-3	0	0	0	0	0	-0.02	0	0	0	-0.14
0	0	1	0	0	0	-0.15	0	0	0	3E-3	0	-0.02	0	0	0	-0.14	0	0	0
0	0	0	1	0	0	0	-0.15	0	0	0	3E-3	0	-0.02	0	0	0	-0.14	0	0
0	0	0	0	1	0	0	0	-0.16	0	0	0	2E-3	0	0	0	0	0	0	3E-3
0	0	0	0	0	1	0	0	0	-0.16	0	0	0	2E-3	0	0	0	0	0	3E-3
0	0	0	0	0	0	1	0	0	0	-0.16	0	0	0	2E-3	0	3E-3	0	0	0
0	0	0	0	0	0	0	1	0	0	0	-0.16	0	0	0	2E-3	0	3E-3	0	0
0	0	0	0	0	0	0	0	1	0	0	0	-0.15	0	0	0	1E-3	0	0	0
0	0	0	0	0	0	0	0	0	1	0	0	0	-0.15	0	0	0	1E-3	0	0
0	0	0	0	0	0	0	0	0	0	1	0	0	0	-0.15	0	0	0	1E-3	0
0	0	0	0	0	0	0	0	0	0	0	1	0	0	0	-0.15	0	0	0	1E-3
0	0	0	0	0	0	0	0	0	0	0	0	1	0	0	0	-0.15	0	0	0
0	0	0	0	0	0	0	0	0	0	0	0	0	1	0	0	0	-0.15	0	0
0	0	0	0	0	0	0	0	0	0	0	0	0	0	1	0	0	0	0	0
0	0	0	0	0	0	0	0	0	0	0	0	0	0	0	1	0	0	0	0
0	0	0	0	0	0	0	0	0	0	0	0	0	0	0	0	1	0	0	0
0	0	0	0	0	0	0	0	0	0	0	0	0	0	0	0	0	1	0	0
0	0	0	0	0	0	0	0	0	0	0	0	0	0	0	0	0	0	1	0
0	0	0	0	0	0	0	0	0	0	0	0	0	0	0	0	0	0	0	1

b)

1	0	0	0	-0.15	0	0	0	-2E-3	0	0	0	0	0	0	-0.02	0	0	0	-0.14
0	1	0	0	0	-0.15	0	0	0	-2E-3	0	0	0	0	-0.02	0	0	0	-0.14	0
0	0	1	0	0	0	-0.15	0	0	0	-2E-3	0	-0.02	0	0	0	-0.14	0	0	0
0	0	0	1	0	0	0	-0.15	0	0	0	-2E-3	0	-0.02	0	0	0	-0.14	0	0
0	0	0	0	1	0	0	0	-0.15	0	0	0	-4E-3	0	0	0	0	0	0	-2E-3
0	0	0	0	0	1	0	0	0	-0.15	0	0	0	-4E-3	0	0	0	0	0	-2E-3
0	0	0	0	0	0	1	0	0	0	-0.15	0	0	0	-4E-3	0	-2E-3	0	0	0
0	0	0	0	0	0	0	1	0	0	0	-0.15	0	0	0	-4E-3	0	-2E-3	0	0
0	0	0	0	0	0	0	0	1	0	0	0	-0.15	0	0	0	-4E-3	0	0	0
0	0	0	0	0	0	0	0	0	1	0	0	0	-0.15	0	0	0	-4E-3	0	0
0	0	0	0	0	0	0	0	0	0	1	0	0	0	-0.15	0	0	0	-4E-3	0
0	0	0	0	0	0	0	0	0	0	0	1	0	0	0	-0.14	0	0	0	0
0	0	0	0	0	0	0	0	0	0	0	0	1	0	0	0	-0.14	0	0	0
0	0	0	0	0	0	0	0	0	0	0	0	0	1	0	0	0	-0.14	0	0
0	0	0	0	0	0	0	0	0	0	0	0	0	0	1	0	0	0	0	-0.14
0	0	0	0	0	0	0	0	0	0	0	0	0	0	0	1	0	0	0	0
0	0	0	0	0	0	0	0	0	0	0	0	0	0	0	0	1	0	0	0
0	0	0	0	0	0	0	0	0	0	0	0	0	0	0	0	0	1	0	0
0	0	0	0	0	0	0	0	0	0	0	0	0	0	0	0	0	0	1	0
0	0	0	0	0	0	0	0	0	0	0	0	0	0	0	0	0	0	0	1

c)

1	0	0	0	-0.16	0	0	0	7E-4	0	0	0	0	0	0	-0.02	0	0	0	-0.14
0	1	0	0	0	-0.16	0	0	0	7E-4	0	0	0	0	-0.02	0	0	0	-0.14	0
0	0	1	0	0	0	-0.16	0	0	0	7E-4	0	-0.02	0	0	0	-0.14	0	0	0
0	0	0	1	0	0	0	-0.16	0	0	0	7E-4	0	-0.02	0	0	0	-0.14	0	0
0	0	0	0	1	0	0	0	-0.16	0	0	0	2E-4	0	0	0	0	0	0	2E-3
0	0	0	0	0	1	0	0	0	-0.16	0	0	0	2E-4	0	0	0	0	0	2E-3
0	0	0	0	0	0	1	0	0	0	-0.16	0	0	0	2E-4	0	2E-3	0	0	0
0	0	0	0	0	0	0	1	0	0	0	-0.16	0	0	0	2E-4	0	2E-3	0	0
0	0	0	0	0	0	0	0	1	0	0	0	-0.16	0	0	0	-5E-4	0	0	0
0	0	0	0	0	0	0	0	0	1	0	0	0	-0.16	0	0	0	-5E-4	0	0
0	0	0	0	0	0	0	0	0	0	1	0	0	0	-0.16	0	0	0	-5E-4	0
0	0	0	0	0	0	0	0	0	0	0	1	0	0	0	-0.15	0	0	0	0
0	0	0	0	0	0	0	0	0	0	0	0	1	0	0	0	-0.15	0	0	0
0	0	0	0	0	0	0	0	0	0	0	0	0	1	0	0	0	-0.15	0	0
0	0	0	0	0	0	0	0	0	0	0	0	0	0	1	0	0	0	0	0
0	0	0	0	0	0	0	0	0	0	0	0	0	0	0	1	0	0	0	0
0	0	0	0	0	0	0	0	0	0	0	0	0	0	0	0	1	0	0	0
0	0	0	0	0	0	0	0	0	0	0	0	0	0	0	0	0	1	0	0
0	0	0	0	0	0	0	0	0	0	0	0	0	0	0	0	0	0	1	0
0	0	0	0	0	0	0	0	0	0	0	0	0	0	0	0	0	0	0	1

d)

Figure 4.2. Obtained matrix [A] with the assembly pattern 2 and with a) $\mu=0.3 - F=200kN$ b) $\mu=0.2 - F=200kN$ c) $\mu=0.3 - F=350kN$ d) $\mu=0.2 - F=350kN$

3. DEVELOPMENT OF THE TETRAPARAMETRIC ASSEMBLY METHOD

Most of the elements in matrices $[A]$ of Figures 4.1 and 4.2 are null. This means that when a bolt is tightened during the tightening sequence, only a few bolts suffer a loss of load (obviously, the bolts that are close to the bolt being tightened). To further understand this, in the analysis of Figure 4.2d it can be seen that, according to the first row and remembering equation (3.3), the final load of bolt number 1 is equal to its tightening load, minus 0.16 times the tightening load of bolt number 2, plus 0.0007 times the tightening load of bolt number 3, minus 0.02 times the tightening load of bolt number 19, minus 0.14 times the tightening load of bolt number 20. In this sense, the load level of bolt number 1 only varies when bolts 2, 3, 19 or 20 are tightened, so it only varies when a bolt located at one or two distance positions is tightened (see Figure 4.3). In other words, the tightening of one bolt only affects the bolts located at one or two positions of distance, while the remaining bolts do not have any load variation (this is for studied joint NPS 24", Class 150 and SCHD 40). Therefore, a general matrix $[A]$ can be assumed like that presented in Figure 4.3, where Figure 4.3a is related with the assembly pattern 1 and therefore with the matrices of Figure 4.1, and Figure 4.3b with the assembly pattern 2 and matrices of Figure 4.2.

	1	11	6	16	3	13	8	18	5	15	10	20	2	12	7	17	4	14	9	19	
1	1	0	0	0	γ	0	0	0	0	0	0	α	β	0	0	0	0	0	0	0	δ
11	0	1	0	0	0	γ	0	0	0	0	α	0	0	β	0	0	0	0	0	δ	0
6	0	0	1	0	0	0	γ	0	α	0	0	0	0	0	β	0	δ	0	0	0	0
16	0	0	0	1	0	0	0	γ	0	α	0	0	0	0	0	β	0	δ	0	0	0
3	0	0	0	0	1	0	0	0	γ	0	0	0	α	0	0	0	β	0	0	0	0
13	0	0	0	0	0	1	0	0	0	γ	0	0	0	α	0	0	0	β	0	0	0
8	0	0	0	0	0	0	1	0	0	0	γ	0	0	0	α	0	0	0	β	0	0
18	0	0	0	0	0	0	0	1	0	0	0	γ	0	0	0	α	0	0	0	0	β
5	0	0	0	0	0	0	0	0	1	0	0	0	0	0	-0	δ	β	0	0	0	0
15	0	0	0	0	0	0	0	0	0	1	0	0	0	0	δ	-0	0	β	0	0	0
10	0	0	0	0	0	0	0	0	0	0	1	0	0	δ	0	0	0	0	β	0	0
20	0	0	0	0	0	0	0	0	0	0	0	1	δ	0	0	0	0	0	0	0	β
2	0	0	0	0	0	0	0	0	0	0	0	0	1	0	0	0	δ	0	0	0	0
12	0	0	0	0	0	0	0	0	0	0	0	0	0	1	0	0	0	δ	0	0	0
7	0	0	0	0	0	0	0	0	0	0	0	0	0	0	1	0	0	0	δ	0	0
17	0	0	0	0	0	0	0	0	0	0	0	0	0	0	0	1	0	0	0	0	δ
4	0	0	0	0	0	0	0	0	0	0	0	0	0	0	0	0	1	0	0	0	0
14	0	0	0	0	0	0	0	0	0	0	0	0	0	0	0	0	0	1	0	0	0
9	0	0	0	0	0	0	0	0	0	0	0	0	0	0	0	0	0	0	1	0	0
19	0	0	0	0	0	0	0	0	0	0	0	0	0	0	0	0	0	0	0	0	1

a)

	1	11	6	16	2	12	7	17	3	13	8	18	4	14	9	19	5	15	10	20
1	1	0	0	0	α	0	0	0	δ	0	0	0	0	0	0	γ	0	0	0	β
11	0	1	0	0	0	α	0	0	0	δ	0	0	0	0	γ	0	0	0	β	0
6	0	0	1	0	0	0	α	0	0	0	δ	0	γ	0	0	0	β	0	0	0
16	0	0	0	1	0	0	0	α	0	0	0	δ	0	γ	0	0	0	β	0	0
2	0	0	0	0	1	0	0	0	β	0	0	0	δ	0	0	0	0	0	0	δ
12	0	0	0	0	0	1	0	0	0	β	0	0	0	δ	0	0	0	0	0	δ
7	0	0	0	0	0	0	1	0	0	0	β	0	0	0	δ	0	δ	0	0	0
17	0	0	0	0	0	0	0	1	0	0	0	β	0	0	0	δ	0	δ	0	0
3	0	0	0	0	0	0	0	0	1	0	0	0	β	0	0	0	δ	0	0	0
13	0	0	0	0	0	0	0	0	0	1	0	0	0	β	0	0	0	δ	0	0
8	0	0	0	0	0	0	0	0	0	0	1	0	0	0	β	0	0	0	δ	0
18	0	0	0	0	0	0	0	0	0	0	0	1	0	0	0	β	0	0	0	δ
4	0	0	0	0	0	0	0	0	0	0	0	0	1	0	0	0	β	0	0	0
14	0	0	0	0	0	0	0	0	0	0	0	0	0	1	0	0	0	β	0	0
9	0	0	0	0	0	0	0	0	0	0	0	0	0	0	1	0	0	0	β	0
19	0	0	0	0	0	0	0	0	0	0	0	0	0	0	0	1	0	0	0	β
5	0	0	0	0	0	0	0	0	0	0	0	0	0	0	0	0	1	0	0	0
15	0	0	0	0	0	0	0	0	0	0	0	0	0	0	0	0	0	1	0	0
10	0	0	0	0	0	0	0	0	0	0	0	0	0	0	0	0	0	0	1	0
20	0	0	0	0	0	0	0	0	0	0	0	0	0	0	0	0	0	0	0	1

b)

Figure 4.3. Matrix $[A]$ for the reviewed joint and a) assembly pattern 1 b) assembly pattern 2

As it can be appreciated, these matrices only have four different coefficients α , β , γ and δ . These coefficients correspond to the four possible load cases that can take place during the tightening sequences. Table 4.1 provides a schematic explanation of the four different load cases and shows the equations to obtain these coefficients. The equations were deduced from the equation (3.5), which can be noted in the calculation of the matrix $[A]$ when $i < j$, because the calculation of this element is the load level of that bolt in the current load step minus the load level of that bolt in the previous load step, divided by the load level of the bolt being tightened in the current load step. Thus, once the meaning of the elements is understood, the matrices of Figure 4.3 can be studied. For example, the first row of matrix $[A]$ of Figure 4.3a represents the loss of loads of bolt number 1 when assembly pattern 1 is used. To this regard, in accordance with Table 4.1: γ is in the fifth column because when bolt number 3 is tightened, bolt number 2 has still not been tightened; α is in the twelfth column because when bolt number 20 is tightened bolt number 19 has still not been tightened; β is in the thirteenth column because when bolt number 2 is tightened bolt number 3 has already been tightened; δ is in the twentieth column because when bolt number 19 is tightened bolt number 20 has already been tightened. In Figure 4.3b the coefficients have a different position because the assembly pattern is different, but the procedure is the

same and therefore these locations of coefficients α , β , γ and δ can be easily predicted. This proves that for different assembly patterns the matrix $[A]$ is the same but with the coefficients located in different rows and columns, as has been mentioned in the previous section.

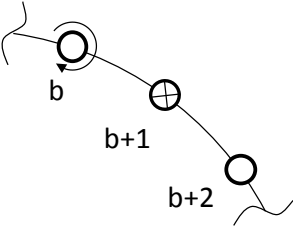
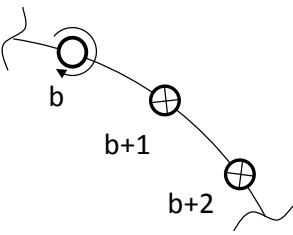
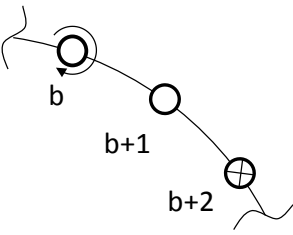
	<p>Bolt b is tightened to load F_b.</p> <p>Bolt $b+1$ was previously tightened to load F_{b+1} and, after tightening bolt b, its load becomes F_{b+1}'.</p> <p>Bolt $b+2$ is not previously tightened.</p>	$\alpha = \frac{F_{b+1}' - F_{b+1}}{F_b}$ <p>α estimates the load loss of bolt $b+1$ when bolt b is tightened, with bolt $b+2$ not previously tightened.</p>
	<p>Bolt b is tightened to load F_b.</p> <p>Bolt $b+1$ was previously tightened to load F_{b+1} and, after tightening bolt b, its load becomes F_{b+1}'.</p> <p>Bolt $b+2$ was previously tightened to load F_{b+2} and, after tightening bolt b, its load becomes F_{b+2}'.</p>	$\beta = \frac{F_{b+1}' - F_{b+1}}{F_b}$ <p>β estimates the load loss of bolt $b+1$ when bolt b is tightened, with bolt $b+2$ previously tightened.</p> $\delta = \frac{F_{b+2}' - F_{b+2}}{F_b}$ <p>δ estimates the load loss of bolt $b+2$ when bolt b is tightened, with bolt $b+1$ previously tightened.</p>
	<p>Bolt b is tightened to load F_b.</p> <p>Bolt $b+1$ is not previously tightened.</p> <p>Bolt $b+2$ was previously tightened to load F_{b+2} and, after tightening bolt b, its load becomes F_{b+2}'.</p>	$\gamma = \frac{F_{b+2}' - F_{b+2}}{F_b}$ <p>γ estimates the load loss of bolt $b+2$ when bolt b is tightened, with bolt $b+1$ not previously tightened.</p>

Table 4.1. The four different load cases of matrix $[A]$ elements. The equations were deduced from equation (3.5)

Thus, assuming that the matrices of Figures 4.1 and 4.2 have the shape of Figure 4.3, the average value of each coefficient can be calculated. Table 4.2 shows the obtained value for each coefficient in each matrix of Figures 4.1 and 4.2. Regarding the load level, it can be appreciated that its influence is minimal and therefore it is completely negligible (δ varies from one case to another but its contribution is minimal because it has a value much smaller than the other coefficients). Regarding the friction coefficient and the assembly pattern, it can be noted that their influence is slightly larger; however they do not have a big influence.

Load	μ	Assembly pattern 1				Assembly pattern 2			
		α	β	γ	δ	α	β	γ	δ
200	0.2	-0.147	-0.147	-0.018	0.002	-0.152	-0.151	-0.019	0.002
	0.3	-0.139	-0.138	-0.019	-0.002	-0.144	-0.142	-0.020	-0.001
350	0.2	-0.148	-0.148	-0.021	0.000	-0.155	-0.153	-0.019	0.001
	0.3	-0.140	-0.139	-0.022	-0.004	-0.147	-0.144	-0.021	-0.003

Table 4.2. Values of matrix $[A]$ coefficients using the EICM

Concepts of Table 4.1 were useful to understand the elements of matrix $[A]$, and they were also useful to establish the basis from where the new TAM method was developed. This method calculates matrix $[A]$ with a simple analysis of two load steps. Figure 4.4 provides a schematic indication of the two load steps that must be carried out in a RTJ with 20 bolts (as an example, the joint of the experimental set up has 20 bolts). As indicated with red circles, in the first load step, several bolts are tightened to a known preload; as mentioned before, in RTJs the load level is not significant, but using a level of load which is similar to the target load is recommended; likewise, if a Finite Element model is used, the friction coefficient should be as realistic as possible, even though it does not have a significant influence as proved before. In the second load step, bolts indicated with a green triangle are preloaded as shown in Figure 4.4, in such a way that all the load cases explained in Table 4.1 take place; thus, measuring the load variation of the bolts that have been preloaded in the first load step and using the equations of Table 4.1, the coefficients α , β , γ and δ of matrix $[A]$ can be calculated,

avoiding the analysis of the whole tightening sequence with the measurements of every bolt in every load step, as in the EICM.

In short, according to Table 4.1:

- α is obtained from the loss of load of bolt number 8 when bolt number 9 is tightened, or from the loss of load of bolt number 15 when bolt number 16 is tightened.
- β is obtained from the loss of load of bolt number 4 when bolt number 3 is tightened, or from the loss of load of bolt number 17 when bolt number 16 is tightened.
- γ is obtained from the loss of load of bolt number 1 when bolt number 3 is tightened, or from the loss of load of bolt number 11 when bolt number 9 is tightened.
- δ is obtained from the loss of load of bolt number 5 when bolt number 3 is tightened, or from the loss of load of bolt number 18 when bolt number 16 is tightened.

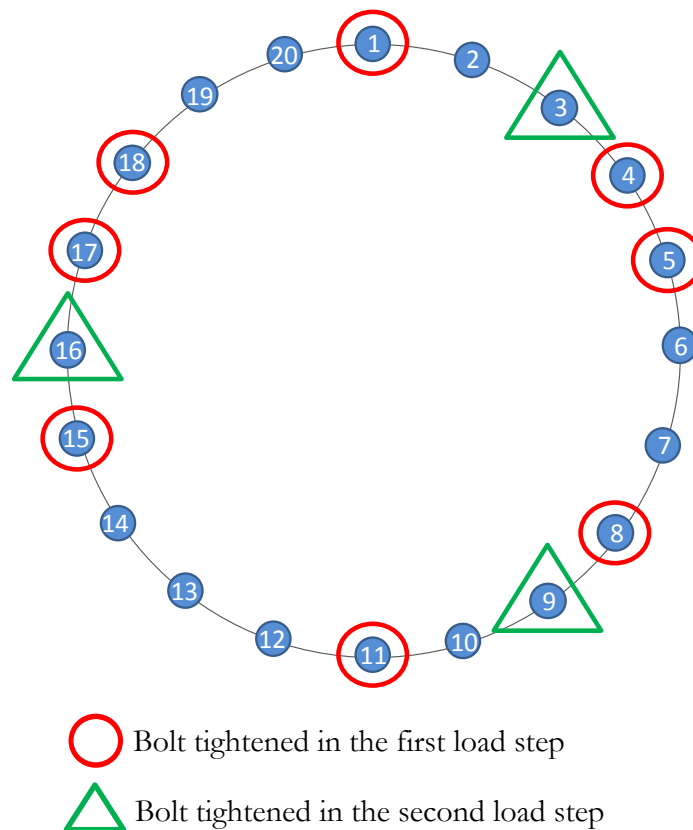


Figure 4.4. Explanation of the two load steps of the TAM to obtain matrix $[A]$ in a joint with 20 bolts

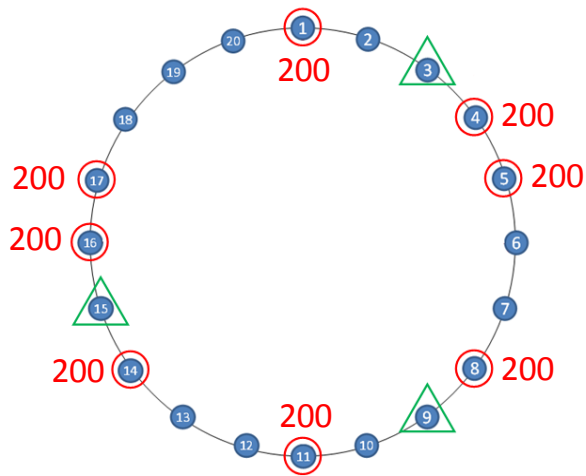
As it can be appreciated, the analysis is redundant because each coefficient can be twice obtained. It can be used to verify the obtained results.

Figure 4.5 provides an illustrative example where a uniform bolt load of 200 kN is desired. Therefore, in the first load step, the bolts with a red circle must be tightened (see Figure 4.5a). In the second load step, the bolts with a green triangle must be tightened, and due to the elastic interaction, the load level of the bolts that have been previously tightened varies (see Figure 4.5b). In the next step, equations of Table 4.1 are used in order to obtain the four different coefficients, resulting in:

$$\begin{aligned}\alpha &= (168 - 200) / 200 = -0.16 & \beta &= (169 - 200) / 200 = -0.155 \\ \gamma &= (196 - 200) / 200 = -0.02 & \delta &= (201 - 200) / 200 = 0.005\end{aligned}$$

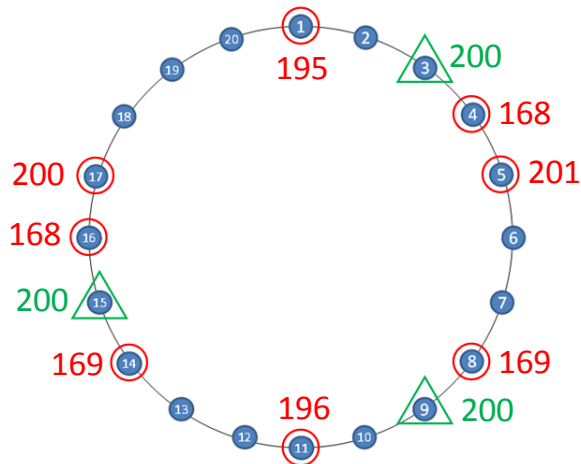
Once these coefficients are obtained, the matrix $[A]$ has to be constructed for the corresponding assembly pattern as shown in Figure 4.3, and finally, using equation (3.4), the tightening load for the target load is calculated obtaining the optimized tightening sequence as a result.

Figure 4.4 has shown the analysis that has to be performed with the TAM on a joint with 20 bolts to obtain the four coefficients of matrix $[A]$. On joints with a different number of bolts, deducing the analysis that has to be performed is simple: All that is required is to select the bolts that have to be tightened in the first load step and in the second load step in such a way that the four different situations of Table 4.1 take place. Thus, the four coefficients α , β , γ and δ can be calculated. Figure 4.6 shows the analysis that has to be carried out with the TAM on a joint with 12, 16 or 24 bolts; joints with fewer bolts have not been analyzed, as it will be explained later.



In the first step the red bolts are tightened to the target load

a)

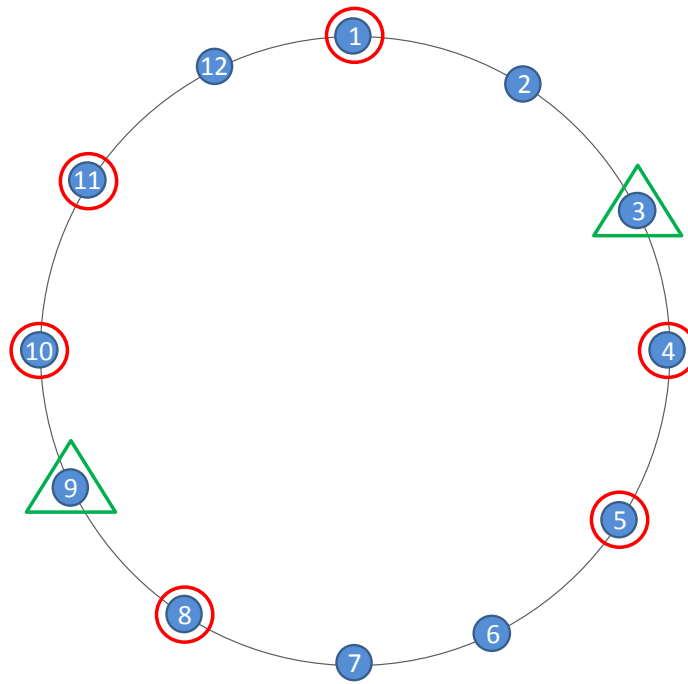


In the second step the green bolts are tightened to the target load

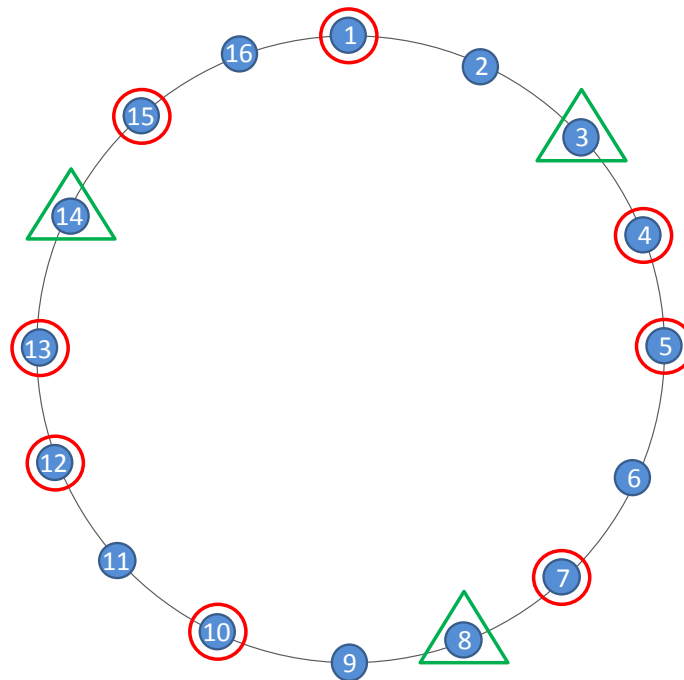
The red bolts lose part of their load due to the elastic interaction

b)

Figure 4.5. Illustrative example of the TAM on a joint with 20 bolts a) first load step
b) second load step



a)



b)

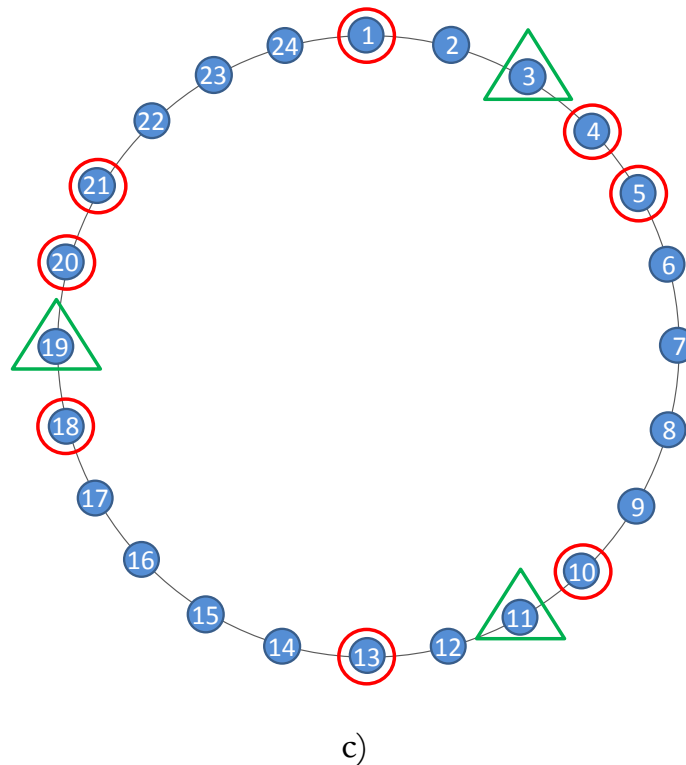


Figure 4.6. Two load step analysis of the TAM on joints with a) 12 bolts b) 16 bolts
c) 24 bolts

Obviously, the TAM costs much less than the EICM. Assuming that the joint under review has 20 bolts, if a Finite Element model is used, the TAM only needs to simulate an analysis of two load steps while the EICM needs to simulate 20 load steps in order to simulate the whole tightening sequence (there are 20 bolts in the joint). Also, in the analysis of the whole tightening sequence (EICM), convergence problems could appear due to the solid rigid motion in the first load steps when only a few bolts are tightened, which increases the cost even further. From Figure 4.4, it can also be deduced that if a test bench is used, the TAM only needs eleven tightening operations (eight bolts in the first load step and three bolts in the second load step) and nineteen measurements (the load level of the bolts tightened in the first load step has to be measured twice in order to obtain the loss of loads of the bolts). Instead, with the EICM a whole tightening sequence must be carried out (load steps = n , being n the number of bolts) and the load level of every bolt must be measured in every load step, which results in twenty tightening operations and 210 measurements (measurements = $n \cdot (n + 1)/2$). Therefore, it can be appreciated that the cost of the TAM is much lower than the EICM, so it is a more efficient method when an RTJ is reviewed.

4. RESULTS AND VALIDATION OF THE TETRAPARAMETRIC ASSEMBLY METHOD

To completely validate the TAM, this section is divided in three parts where the joint of the test bench is studied (NPS 24", Class 150 and SCHD 40). First of all, this method is compared with the EICM to check if both methods provide similar optimized tightening sequences (bolt initial loads are compared). Secondly, the initial loads obtained with the TAM are used as tightening loads in the Finite Element model explained in Chapter 2, to verify that they provide a uniform final load. Finally, in order to validate the new methodology experimentally, two optimized tightening sequences of the TAM are simulated in the experimental set up explained in Chapter 2 in order to compare the final load with the target load.

4.1. COMPARISON BETWEEN TAM AND EICM

Table 4.3 shows the coefficients obtained with the TAM (see Figure 4.4). In these analyses, the different load levels were not taken into account because, as demonstrated in the first section of this Chapter, their influence is completely negligible. The obtained results are very similar to those presented in Table 4.1 and obtained with the EICM, so it can be forecast that both methods will provide very similar results.

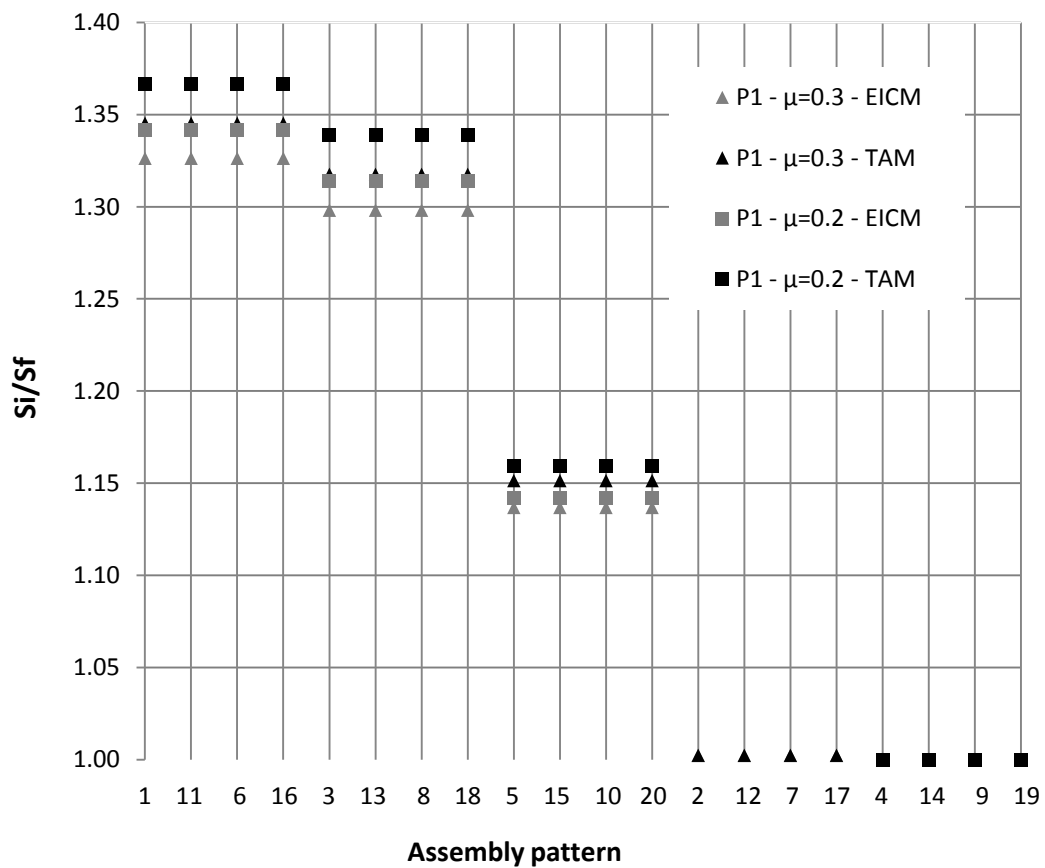
μ	α	β	γ	δ
0.2	-0.154	-0.16	-0.022	0
0.3	-0.144	-0.149	-0.021	-0.002

Table 4.3. Coefficients value of matrix $[A]$ according to the TAM

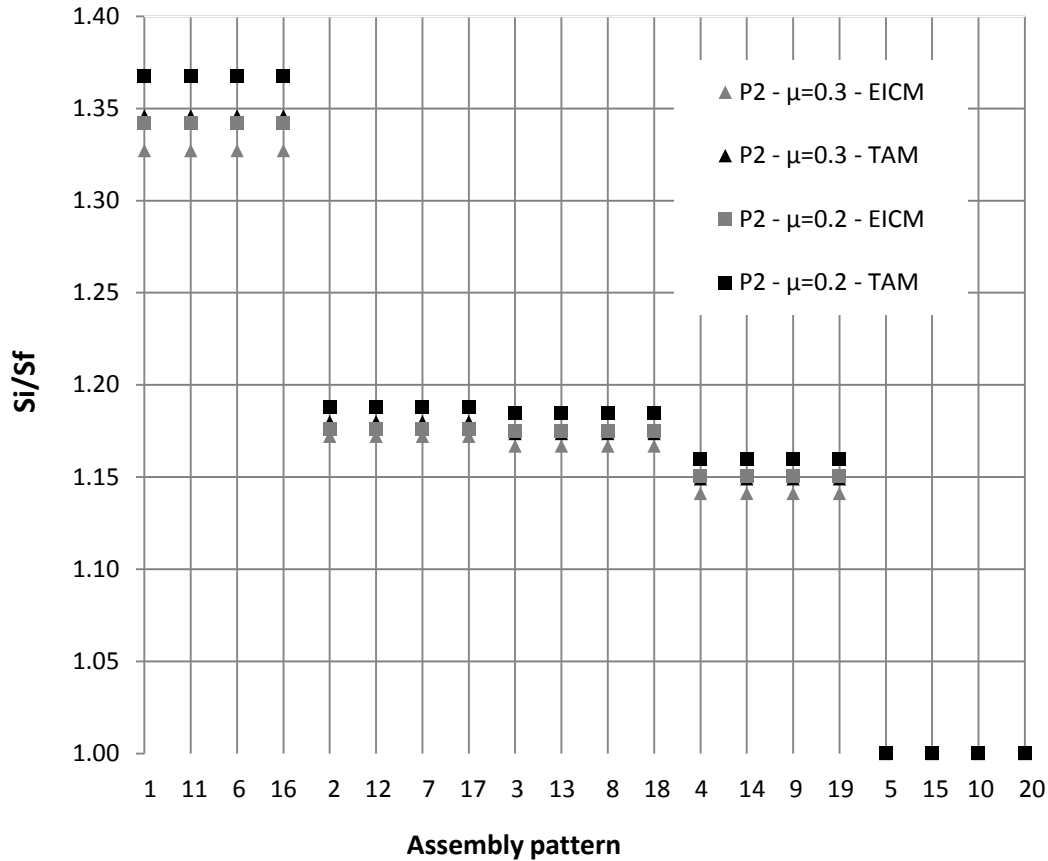
In order to directly compare both methods, the tightening loads obtained with the EICM (coefficients of Table 4.1) and with the TAM (coefficients of Table 4.3) were compared. To that end, first matrix $[A]$ was constructed with the coefficients of each method, and secondly, equation (3.4) was used to obtain the initial loads. Figure 4.7 shows the obtained initial loads as the ratio between the initial and the final load in the bolts (because the level of load does not have influence). It can be seen that the obtained results with the EICM and with the TAM are very similar (in every case the relative error is

less than 2%). This was expected as the coefficients α , β , γ and δ were very similar in both cases.

Figure 4.7 also shows the small difference between the two friction coefficients due to the small difference of coefficients α , β , γ and δ in matrix $[A]$. As the difference is small it can be stated that the friction coefficient does not have a big influence; nevertheless, in order to obtain the most accurate value of coefficients α , β , γ and δ , it is recommended that the two load step analysis of Figure 4.4 is performed by FEM with a friction coefficient as realistic as possible, or by performing the analysis experimentally.



a)



b)

Figure 4.7. Comparison of the ratio between the initial and the final load on the bolts using the EICM and the TAM a) assembly pattern 1 b) assembly pattern 2

4.2. VALIDATION OF THE TETRAPARAMETRIC ASSEMBLY METHOD WITH THE FINITE ELEMENT MODEL

From the ratio between initial and final loads of Figure 4.7, the TAM initial loads were obtained in order to simulate an optimized tightening sequence in the Finite Element model explained in Chapter 2. Two validation analyses were performed: In the first one, a tightening load of 350 kN, a friction coefficient of 0.3 and the first assembly pattern was used, and in the second one, the same target load with the same friction coefficient but with the second assembly pattern. Table 4.4 shows the initial load that has to be applied to each bolt during the tightening sequence of each analysis in order to obtain a uniform bolt final load according to the TAM. A similar accuracy was achieved for a target load of 200 kN and a friction coefficient of 0.2.

Analysis 1		Analysis 2	
Pattern	Load	Pattern	Load
1	471	1	471
11	471	11	471
6	471	6	471
16	471	16	471
3	461	2	413
13	461	12	413
8	461	7	413
18	461	17	413
5	403	3	411
15	403	13	411
10	403	8	411
20	403	18	411
2	351	4	402
12	351	14	402
7	351	9	402
17	351	19	402
4	350	5	350
14	350	15	350
9	350	10	350
19	350	20	350

Table 4.4. Obtained initial loads with the Finite Element validation analyses

Figure 4.8 shows the bolt final load distribution obtained with analysis 1 of Table 4.4. The obtained average load was 351 kN and the standard deviation 1.65 kN, so it can be stated that the obtained final load distribution is virtually uniform. Also, Figure 4.9 shows the obtained results in analysis 2 of Table 4.4. In this case the obtained average load was 348 kN with a standard deviation of 1.51 kN. Thus, it was demonstrated that the new method provides very accurate results for the reviewed joint (and with a much smaller cost than the EICM).

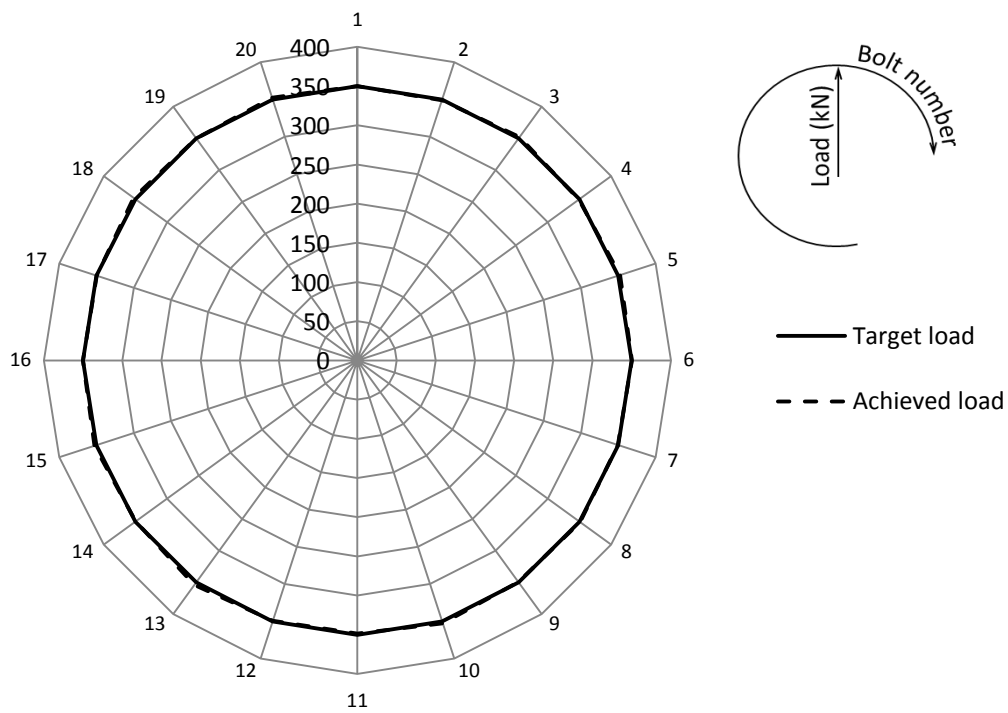


Figure 4.8. Finite Element results obtained with the TAM in analysis 1

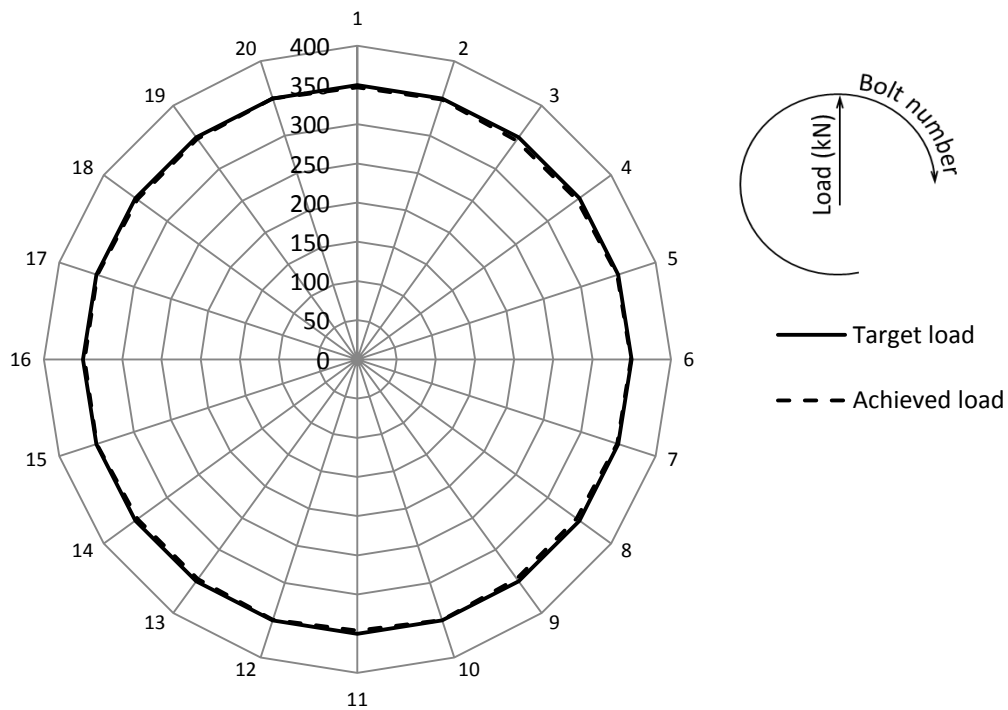


Figure 4.9. Finite Element results obtained with the TAM in analysis 2

4.3. VALIDATION OF THE TETRAPARAMETRIC ASSEMBLY METHOD WITH THE TEST BENCH

Finally, in order to validate the TAM experimentally, a further two analyses were performed on the test bench explained in Chapter 2. For that purpose, the ratio between initial and final loads of Figure 4.7 was used. In the first analysis, assembly pattern 1 with a target load of 200 kN was established. The tightening loads used correspond to a friction coefficient of 0.2 because, after performing several experimental analyses and comparing them with the Finite Element model results, it was found that the friction coefficient between the flange and the gasket was closer to 0.2 than 0.3. In Figure 4.10 the obtained final load distribution after the analysis can be appreciated, and as can be seen, it is completely uniform. The obtained average load was 207 kN with a standard deviation of 6.6 kN. Most of the obtained error is because the i-bolt technology (ultrasonic measurement equipment) and the torque wrench of the experimental set up were not connected to each other, and therefore when the torque wrench reached the target load, it did not stop, automatically increasing its load. As a consequence, the initial loads applied with the torque wrench were slightly different from those indicated in Figure 4.10.

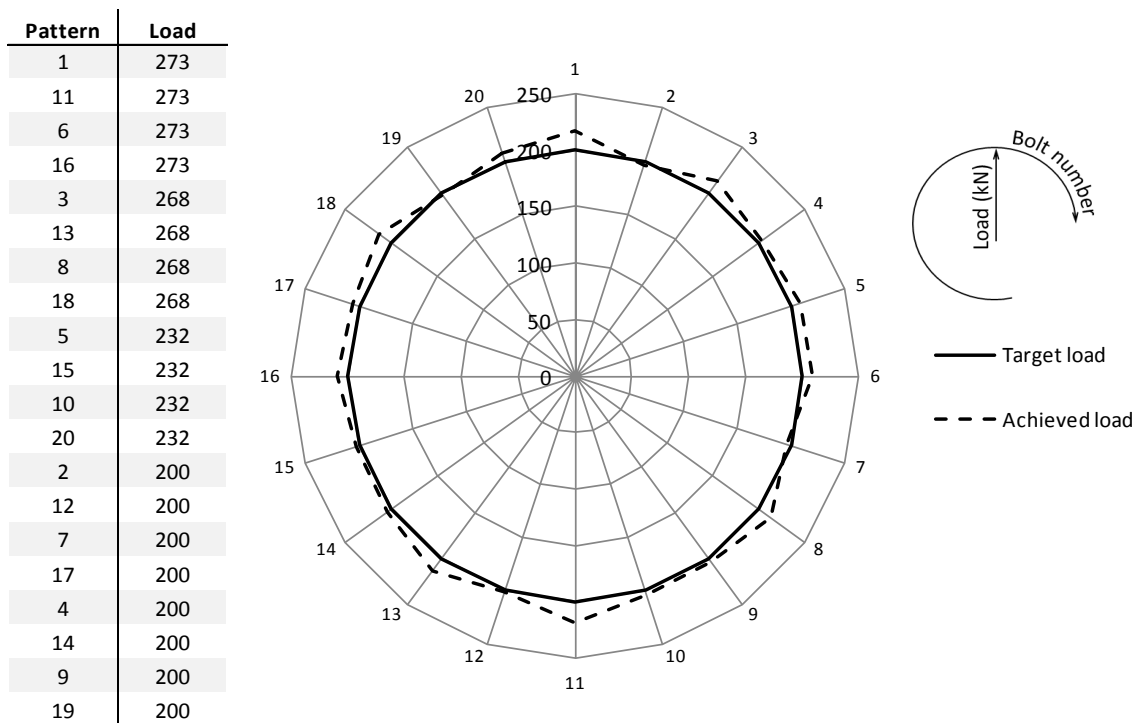


Figure 4.10. Obtained experimental results with the TAM (target load 200 kN and assembly pattern 1)

In the second analysis a new assembly pattern was used, which tightened the first four bolts following the star pattern and the rest of the bolts in a circular pattern (star-circular pattern); from the point of view of the assembler, this is much simpler and faster than the ones proposed in Figure 2.18. Figure 4.11 shows the calculated initial loads for the target uniform final load of 200 kN and the star-circular pattern. It also shows the final load distribution obtained; once more, the obtained results are highly satisfactory with an average load of 198 kN and a standard deviation of 5.1 kN.

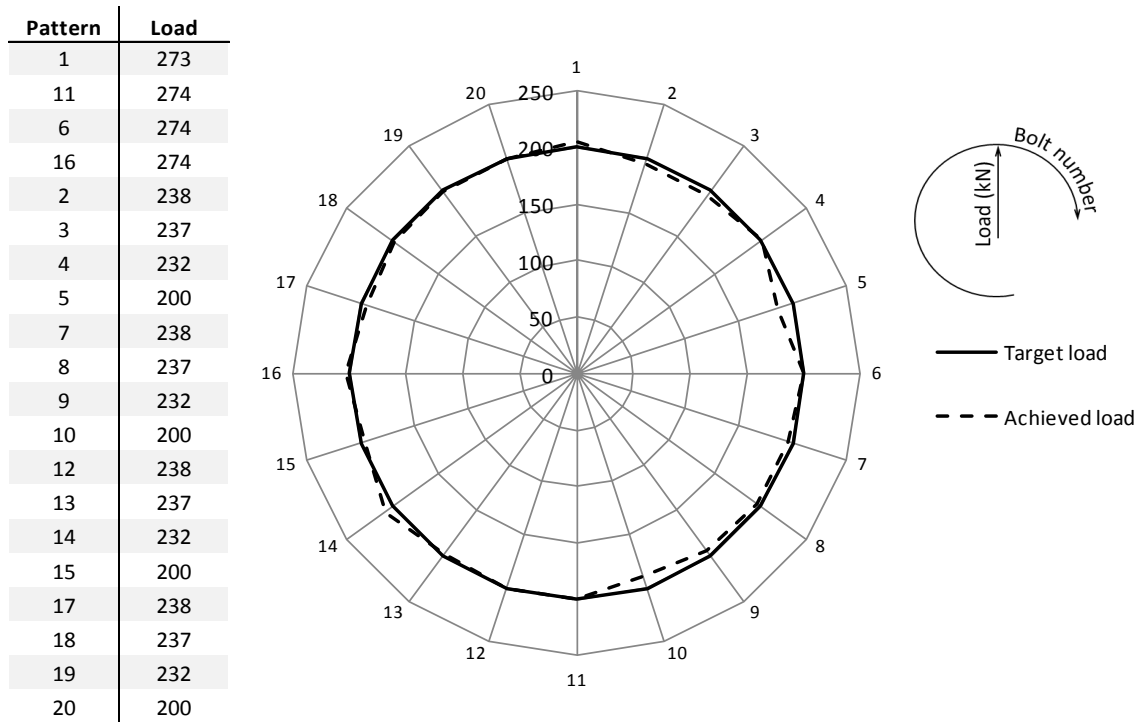


Figure 4.11. Obtained experimental results with the TAM (target load 200 kN and star-circular pattern)

5. CONCLUDING REMARKS

The results obtained in this Chapter have shown the high accuracy of the TAM when an RTJ is studied. In this Chapter, only the geometry of the test bench has been studied (NPS 24", Class 150 and SCHD 40), and therefore the whole range of application where the method can be of use has not been taken into account. The range of application will be studied in Chapter 5.

It should also be pointed out that in this Chapter, the yielding load of the bolts has not been used in the Finite Element model. If a bolt reaches yielding

point, it is necessary to use a two-pass tightening sequence, which means that, besides matrix $[A]$, it is necessary to calculate matrix $[B]$, as has been explained in Chapter 3. The matrix of the first pass can be obtained with the TAM process presented in this Chapter. Chapter 5 develops the generalization of the TAM and explains how matrix $[B]$ has to be obtained for multiple-pass tightening sequences.

Finally, it should also be mentioned that the gasket could exceed the yield stress due to very high initial loads. However, as explained in Chapter 2, it was verified that small plastic deformations that may occur on the gasket do not have a big influence in the elastic interaction phenomenon. Thus, in order to simplify and reduce the computational cost, the coefficients of the TAM of Table 4.3 were obtained assuming linear and elastic materials in the analysis of two load steps of Figure 4.4; the experimental results of Figures 4.10 and 4.11 verify that these simplifications do not have any influence on the accuracy of the TAM.

CHAPTER 5. GENERALIZATION OF THE TETRAPARAMETRIC ASSEMBLY METHOD

1. INTRODUCTION

In Chapter 4 the TAM was developed, which calculates optimized tightening sequences in RTJs. This methodology has proved to be more efficient than the EICM, because it provides very accurate results with a significant cost saving. As explained in Chapter 4, the method is based on four coefficients which can be obtained with a simple analysis of two load steps in a Finite Element model or an experimental test bench. These coefficients represent the influence of the elastic interaction in the reviewed joint, and therefore the behaviour of the joint during the tightening sequence. Thus, the tightening loads of an optimized tightening sequence can be calculated in order to obtain a uniform final load distribution after performing a one-pass tightening sequence.

Obviously, the calculated tightening loads are usually higher than the uniform final target load, in order to overcome the loss of loads produced by the elastic interaction phenomenon during the tightening sequence. If the joint is particularly flexible, the loss of loads can be large and, as a consequence, very high tightening loads would be necessary. High tightening loads on the bolts may result in the failure of the gasket, large deformations on the joint or even the yielding of the bolts. Therefore, in these cases, multiple-pass tightening sequence is more suitable [Bib'96; Nas'05; Nas'08]; in these sequences, the tightening loads are smaller than in one-pass tightening sequences, so the aforementioned problems can be avoided. In this sense, this Chapter generalizes the TAM for multiple-pass tightening sequences.

On the other hand, this Chapter also studies the range of application of the TAM among the RTJs of the ASME standard [Cur'12; Asm'12(2); Asm'13(1)], because in Chapter 4 the methodology has only been validated for a particular joint (RTJ of NPS 24", Class 150 and SCHD 40). Also, at the end of the Chapter, the coefficients of the TAM are obtained for every joint which falls within the studied range of application and thus a library of coefficients is generated which can be used by any assembler to define optimized tightening sequences in ASME RTJs.

2. MULTIPLE-PASS TIGHTENING SEQUENCES WITH THE TETRAPARAMETRIC ASSEMBLY METHOD

This section explains the mathematical development of the TAM for multiple-pass tightening sequences. The generalization is also validated with the experimental set up explained in Chapter 2.

2.1. GENERAL DESCRIPTION

For simplicity, the TAM will be explained for two-pass tightening sequences, as two passes are usually more than enough. Nevertheless, the procedure for tightening sequences with more than two passes is exactly the same.

In the two-pass tightening sequence, the aim is to pass from the bolt final load obtained in the first pass (which can be obtained with the TAM explained in Chapter 4), to the target uniform final load distribution after a second pass. To this end, going back to the equation (3.7) of Chapter 3, it is necessary to obtain the matrix $[B]$, the elastic interaction coefficients matrix of the second pass. Thus, if the final loads of the first pass, the final target load of the second pass and the matrix $[B]$ are known, the bolts load increments of the second pass can be calculated. Figure 5.1 shows the shape of matrix $[B]$ of equation (3.8), for a joint with 20 bolts and assembly pattern 1 (see Figure 2.18). As can be seen in Figure 4.3a, matrix $[B]$ is very similar to matrix $[A]$, however there are some differences. At the beginning of the second pass, the bolts are already tightened and, as a consequence, the elements under the main diagonal in matrix $[B]$ are not always null; also, for the same reason, according to Table 4.1, elements α and γ do not exist in matrix $[B]$ because the bolt is always tightened (only the coefficients β and δ will appear). Finally, it can be observed in Figure 5.1 that the matrix $[B]$ is symmetrical. This is because the loss of load of bolt j when bolt i is tightened is always equal to the loss of load of bolt i when bolt j is tightened (Maxwell reciprocal displacements theorem [Bar'04]).

	1	11	6	16	3	13	8	18	5	15	10	20	2	12	7	17	4	14	9	19
1	1	0	0	0	δ	0	0	0	0	0	0	β	β	0	0	0	0	0	0	δ
11	0	1	0	0	0	δ	0	0	0	0	β	0	0	β	0	0	0	0	δ	0
6	0	0	1	0	0	0	δ	0	β	0	0	0	0	0	β	0	δ	0	0	0
16	0	0	0	1	0	0	0	δ	0	β	0	0	0	0	0	β	0	δ	0	0
3	δ	0	0	0	1	0	0	0	δ	0	0	0	β	0	0	0	β	0	0	0
13	0	δ	0	0	0	1	0	0	0	δ	0	0	0	β	0	0	0	β	0	0
8	0	0	δ	0	0	0	1	0	0	0	δ	0	0	0	β	0	0	0	β	0
18	0	0	0	δ	0	0	0	1	0	0	0	δ	0	0	0	β	0	0	0	β
5	0	0	β	0	δ	0	0	0	1	0	0	0	0	0	δ	0	β	0	0	0
15	0	0	0	β	0	δ	0	0	0	1	0	0	0	0	0	δ	0	β	0	0
10	0	β	0	0	0	0	δ	0	0	0	1	0	0	δ	0	0	0	0	β	0
20	β	0	0	0	0	0	0	δ	0	0	0	1	δ	0	0	0	0	0	0	β
2	β	0	0	0	β	0	0	0	0	0	0	δ	1	0	0	0	δ	0	0	0
12	0	β	0	0	0	β	0	0	0	0	δ	0	0	1	0	0	0	δ	0	0
7	0	0	β	0	0	0	β	0	δ	0	0	0	0	0	1	0	0	0	δ	0
17	0	0	0	β	0	0	0	β	0	δ	0	0	0	0	0	1	0	0	0	δ
4	0	0	δ	0	β	0	0	0	β	0	0	0	δ	0	0	0	1	0	0	0
14	0	0	0	δ	0	β	0	0	0	β	0	0	0	δ	0	0	0	1	0	0
9	0	δ	0	0	0	0	β	0	0	0	β	0	0	0	δ	0	0	0	1	0
19	δ	0	0	0	0	0	0	β	0	0	0	β	0	0	0	δ	0	0	0	1

Figure 5.1. Matrix $[B]$ for a joint with 20 bolts and assembly pattern 1

Once matrix $[B]$ has been explained, the procedure to obtain the initial loads in a two-pass tightening sequence will be explained. For the first pass, matrix $[A]$ and the TAM previously explained in Chapter 4 is used, which results in $\{S_{f1}\}$ uniform bolt load distribution at the end of the first pass. For the second pass, the vector with the bolts load increments $\{\Delta S\}$ has to be calculated with equation (5.1):

$$\{\Delta S\} = [B]^{-1} \cdot (\{S_{f2}\} - \{S_{f1}\}) \quad (5.1)$$

Vector $\{\Delta S\}$ contains the load increment that has to be applied to each bolt during the second pass; in other words, the tightening load in the second pass minus the level of load of that bolt in the previous moment to be tightened in the second pass:

$$\{\Delta S\} = \{S_{i2}\} - \{S_{i2}^*\} \quad (5.2)$$

Where $\{S_{i2}\}$ is the vector with the bolt initial load in the second pass, and $\{S_{i2}^*\}$ is the vector with the bolt load in the previous moment to be tightened in the second pass. To calculate the second vector the following equation can be used:

$$\{S_{i2}^*\} = \{S_{f1}\} + [C] \cdot \{\Delta S\} \quad (5.3)$$

Where the resulting vector of term $[C] \cdot \{\Delta S\}$ corresponds to the loss of load of the bolts between the end of the first pass and the moment prior to the tightening of each bolt during the second pass. Therefore, matrix $[C]$ can be deduced from matrix $[B]$ using the following mathematical expression:

$$C_{i,j} = \begin{cases} B_{i,j} & \text{if } i < j \\ 0 & \text{if } i \geq j \end{cases} \quad (5.4)$$

At this point, the initial loads of the second pass are obtained by combining equations (5.2) and (5.3):

$$\begin{aligned} \{S_{i2}\} &= \{S_{i2}^*\} + \{\Delta S\} = \{S_{f1}\} + [C] \cdot \{\Delta S\} + \{\Delta S\} \\ &= \{S_{f1}\} + ([C] + [I]) \cdot \{\Delta S\} \end{aligned} \quad (5.5)$$

And replacing (5.1) in (5.5):

$$\{S_{i2}\} = \{S_{f1}\} + (([C] + [I]) \cdot [B]^{-1}) \cdot (\{S_{f2}\} - \{S_{f1}\}) \quad (5.6)$$

Calling matrix $[D]$ to $([C] + [I]) \cdot [B]^{-1}$, equation (5.6) has the following shape:

$$\{S_{i2}\} = \{S_{f1}\} + [D] \cdot (\{S_{f2}\} - \{S_{f1}\}) \quad (5.7)$$

In short, the initial loads that have to be applied in the first and second passes are calculated with the equations (3.4) and (5.7), respectively. The last step to complete this process is to select an optimal value for the uniform final load after the first pass $\{S_{f1}\}$. As explained previously, the objective of a two-pass tightening sequence is to decrease the tightening loads of the bolts, so the optimum value of $\{S_{f1}\}$ will be the one that requires the minimum tightening loads in both passes. The highest tightening load always corresponds to the first bolt being tightened during the tightening sequence; therefore, the next equation should be fulfilled in order to minimize the tightening loads in the two-pass sequence:

$$\max(\{S_{i1}\}) = \max(\{S_{i2}\}) \rightarrow S_{i11} = S_{i21} \quad (5.8)$$

Where S_{i11} is the tightening load of bolt 1 in pass 1, and S_{i21} is the tightening load of bolt 1 in pass 2. In other words, the optimal tightening sequence takes place when the maximum initial load in the first and second passes is equal,

because this way the value of the maximum load is minimized and the possible failures in the joint are avoided. Also, to calculate the optimal value of the final load after the first pass $\{S_{f1}\}$, it will be assumed that after the first pass, a uniform bolt load is achieved, so every element of vector $\{S_{f1}\}$ will have the same value S_{f1} , as every bolt of vector $\{S_{f2}\}$ will also have the same value S_{f2} (target assembly uniform load). Replacing the first row of equations (3.4) and (5.7) in the equation (5.8):

$$\sum_{j=1}^n (A_{1,j}^{-1}) \cdot S_{f1} = S_{f1} + \sum_{j=1}^n (D_{1,j}) \cdot (S_{f2} - S_{f1}) \quad (5.9)$$

Thus, the optimum value of the final load after the first pass $S_{f1,optimum}$ is achieved:

$$S_{f1,optimum} = \sum_{j=1}^n (D_{1,j}) \cdot S_{f2} / \left(\sum_{j=1}^n (A_{1,j}^{-1}) + \sum_{j=1}^n (D_{1,j}) - 1 \right) \quad (5.10)$$

Finally, it must be mentioned that when a one-pass tightening sequence is not enough because some bolts exceed the yielding stress, instead of using a tightening sequence of two passes, it is possible to use a tightening sequence of only one pass and several tightening procedures. Thus, the cost would be lower than in a tightening sequence of two passes and the joint would not suffer any damages. These tightening sequences will be studied in section 3.

2.2. VALIDATION

For the validation of the multiple-pass TAM the experimental set up explained in Chapter 2 was used. The two different analyses carried out are explained in Table 5.1 . In analysis 1, a star pattern is used for both passes, while mainly a clockwise pattern is used in analysis 2. Therefore, in the first analysis, the gasket will be compressed more uniformly during the tightening sequence, minimizing local overloads which could cause damages on the flange and/or gasket; on the other hand, with the pattern of analysis 2 faster assembly is achieved and it is also simpler from the point of view of the operator.

Analysis	Target load	Number of passes	Assembly pattern
1	350 kN	2	First pass: 1-11-6-16 → 3-13-8-18 → 5-15-10-20 → 2-12-7-17 → 4-14-9-19
			Second pass: 1-11-6-16 → 3-13-8-18 → 5-15-10-20 → 2-12-7-17 → 4-14-9-19
2	350 kN	2	First pass: 1-11-6-16 → 2-3-4-5 → 7-8-9-10 → 12-13-14-15 → 17-18-19-20
			Second pass: 1-2-3-4 → 5-6-7-8 → 9-10-11-12 → 13-14-15-16 → 17-18-19-20

Table 5.1. Experimental analyses performed for the validation of the multiple-pass TAM

The coefficients used to build matrix $[B]$ were the coefficients obtained and used in Chapter 4 for the validation of the one-pass TAM tightening sequences (see Table 4.3). Table 5.2 shows the initial loads for the first and second pass obtained with the equations (3.4) and (5.7) for a target load of 350 kN; according to equation (5.10) the optimal final load after the first pass is 280 kN, with which the maximum load during the tightening sequence is 383 kN in both passes.

In analysis 1, introducing the initial loads of the Table 5.2 in the experimental set up, the final load distribution of Figure 5.2 was obtained. The obtained average load in this analysis was 341 kN with a standard deviation of 2.7 kN. Regarding to the second analysis, Figure 5.3 shows the final load distribution obtained, with the average load being 338 kN (a relative error smaller than 4%) with a standard deviation of 3.4 kN. As explained in Chapter 4, most of the error is the result of the applied tightening loads on the test bench that were slightly different from those indicated in Table 5.2, because there was no feedback control between the torque wrench and the ultrasound measurement equipment. Also, the coefficients do not take into account short term relaxation because, as explained in Chapter 2, it is not possible to simulate this phenomenon with the Finite Element model. Nevertheless, the obtained results are very satisfactory, being very close to the desired final load. As a

consequence, it can be stated that the TAM also provides accurate results in multiple-pass tightening sequences.

Initial loads of the analysis 1				Initial loads of the analysis 2			
First pass		Second pass		First pass		Second pass	
Bolt 1	383	Bolt 1	383	Bolt 1	383	Bolt 1	383
Bolt 11	383	Bolt 11	383	Bolt 11	383	Bolt 2	367
Bolt 6	383	Bolt 6	383	Bolt 6	383	Bolt 3	367
Bolt 16	383	Bolt 16	383	Bolt 16	383	Bolt 4	367
Bolt 3	375	Bolt 3	383	Bolt 2	333	Bolt 5	367
Bolt 13	375	Bolt 13	383	Bolt 3	332	Bolt 6	367
Bolt 8	375	Bolt 8	383	Bolt 4	325	Bolt 7	367
Bolt 18	375	Bolt 18	383	Bolt 5	280	Bolt 8	367
Bolt 5	325	Bolt 5	366	Bolt 7	333	Bolt 9	367
Bolt 15	325	Bolt 15	366	Bolt 8	332	Bolt 10	367
Bolt 10	325	Bolt 10	366	Bolt 9	325	Bolt 11	367
Bolt 20	325	Bolt 20	366	Bolt 10	280	Bolt 12	367
Bolt 2	280	Bolt 2	350	Bolt 12	333	Bolt 13	367
Bolt 12	280	Bolt 12	350	Bolt 13	332	Bolt 14	367
Bolt 7	280	Bolt 7	350	Bolt 14	325	Bolt 15	367
Bolt 17	280	Bolt 17	350	Bolt 15	280	Bolt 16	367
Bolt 4	280	Bolt 4	350	Bolt 17	333	Bolt 17	367
Bolt 14	280	Bolt 14	350	Bolt 18	332	Bolt 18	367
Bolt 9	280	Bolt 9	350	Bolt 19	325	Bolt 19	367
Bolt 19	280	Bolt 19	350	Bolt 20	280	Bolt 20	350

Table 5.2. Initial loads corresponding to the analyses of the Table 5.1

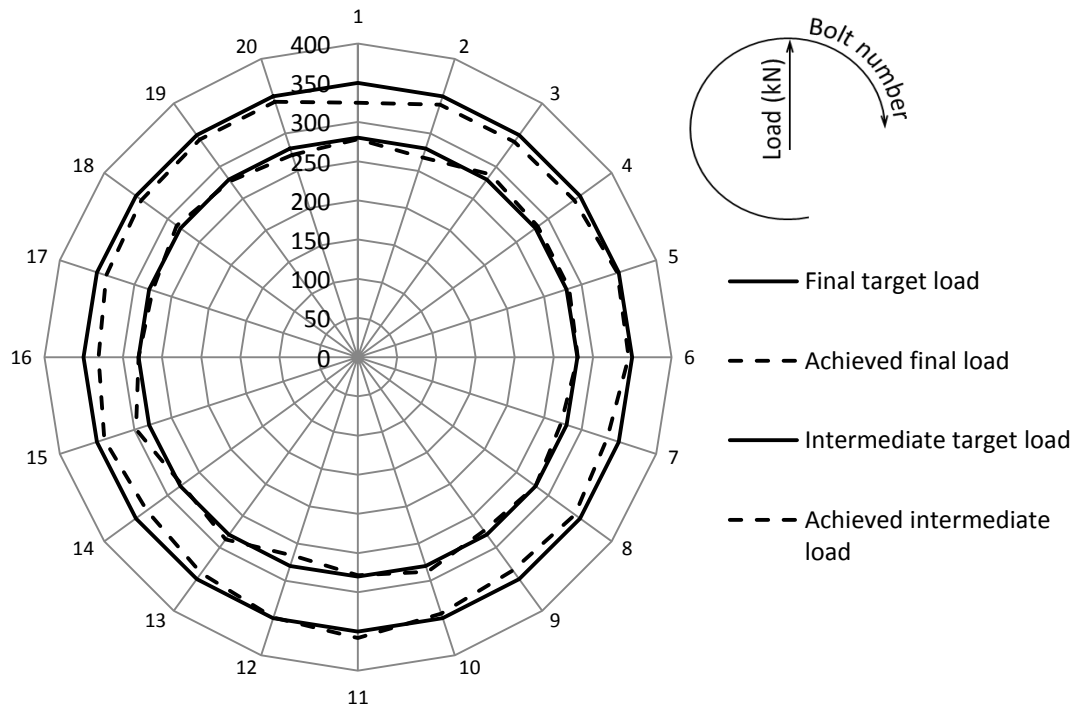


Figure 5.2. Final load distribution obtained experimentally for analysis 1 with the multiple-pass TAM

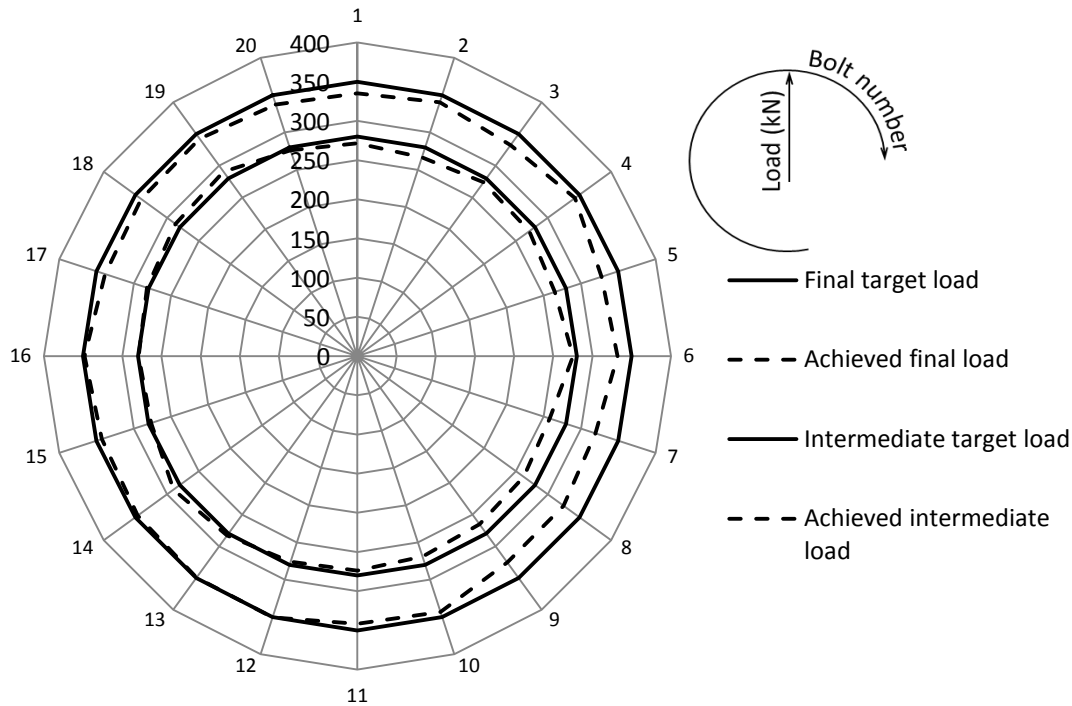


Figure 5.3. Final load distribution obtained experimentally for analysis 2 with the multiple-pass TAM

3. ONE AND A HALF PASS TIGHTENING SEQUENCES

As explained in the previous section, the multiple-pass tightening sequences are very useful when, in a single-pass tightening sequence, the tightening load of a bolt exceeds the yielding load of the bolts. If a two-pass tightening sequence is performed, the tightening loads of the bolts decrease and therefore the yielding of the bolts is avoided. In short, in two-pass tightening sequences the tightening loads are lower and therefore possible damages in the joint are avoided, but in return, the number of tightening operations is double and, as a consequence, the cost is much higher.

To this regard, it could be assumed that there is an intermediate point where no bolt exceeds the yielding load and the cost is less than in an optimized two-pass tightening sequence. This could happen performing a tightening sequence with a whole pass and with a second pass where only a few bolts are tightened; in other words, in the most optimum case, in the second pass, preloading only the bolts that would exceed the yielding point if a one-pass

tightening sequence is performed. Thus, the optimum point is achieved because the tightening loads are smaller than in the one-pass tightening sequence and the cost is also smaller than in the two-pass tightening sequence. Optimization of the one and a half pass tightening sequences is developed and validated in this section.

3.1. GENERAL DESCRIPTION

The procedure of these tightening sequences consists of the following steps:

- Perform the optimization process for a single pass (Chapter 4)
- Take note of the bolts whose tightening load exceeds the yielding load
- Decrease the tightening load of these bolts to avoid the yielding
- Perform a second pass where only these bolts are tightened and therefore avoid a tightening sequence of two passes

To this end, firstly, equation (3.4) has to be solved and we must check which bolts exceed the yielding load. For a general purpose case, it is assumed that the bolts from 1 to j exceed the yielding point and the bolts from $j+1$ to n do not exceed the yielding point (it should be noted that the bolts are ordered following the assembly pattern). To avoid the yielding of every bolt, the tightening loads that exceed the yielding point should be reduced to a load below the yielding point, so the load of the bolts from 1 to j must be reduced. In order to obtain a simple tightening sequence from the point of view of the assembler, the tightening load of the first j bolts will be assumed as the load of the bolt $j+1$, because that way a large number of bolts will be tightened to the same load. Following this process, the tightening loads of the first pass will be:

$$\{S_{i1}\} = \begin{Bmatrix} S_{i11} \\ S_{i12} \\ \vdots \\ S_{i1j} \\ S_{i1j+1} \\ \vdots \\ S_{i1n} \end{Bmatrix} \longrightarrow \begin{Bmatrix} S_{i1j+1} \\ S_{i1j+1} \\ \vdots \\ S_{i1j+1} \\ S_{i1j+1} \\ \vdots \\ S_{i1n} \end{Bmatrix} \quad (5.11)$$

In the second pass, only the first j bolts will be tightened in order to reduce the cost as much as possible. Thus, a tightening sequence of a whole pass and j tightening operations will be achieved. It is clear that the j bolts must also be

preloaded in the second pass because otherwise they would be exceeding the yielding point or the target load would not be achieved. Besides, it must be taken into account that due to the tightening operations in the second pass, the bolts from $j+1$ to n will suffer a loss of load in the second pass which is not taken into account in the equation (5.11). Therefore, a uniform bolt load would not be achieved after the tightening sequence unless an additional load is added to the bolts to overcome the elastic interaction of the second pass.

The additional load of the first pass which has to be applied from bolt j to n has to take two issues into account: Firstly, the loss of loads due to the j tightening operations in the second pass, and secondly, the applied additional load in the first pass, which would cause an additional loss of load that has not been considered in equation (5.11). In order to take account of these two issues, a mixed matrix called $[M]$ has to be developed, which is composed of matrices $[A]$ and $[B]$. As explained in Chapter 3, each column of matrices $[A]$ and $[B]$ represents one load step where one bolt is tightened. In matrix $[M]$ each column also represents one load step where one bolt is tightened, and that column is also equal to the column of matrix $[A]$ if that bolt is not preloaded in the second pass. If that bolt is tightened in the second pass, the column of matrix $[M]$ is equal to the column of matrix $[B]$. As an illustrative example, Figure 5.4 shows matrix $[M]$ for assembly pattern 1 of Figure 2.18a when the first eight bolts exceed the yielding load in a single-pass tightening sequence. As can be seen, the first eight columns are equal to matrix $[B]$ of Figure 5.1 and the other columns are equal to matrix $[A]$ of Figure 4.3a.

	1	11	6	16	3	13	8	18	5	15	10	20	2	12	7	17	4	14	9	19	
1	1	0	0	0	δ	0	0	0	0	0	0	α	β	0	0	0	0	0	0	0	δ
11	0	1	0	0	0	δ	0	0	0	0	α	0	0	β	0	0	0	0	0	δ	0
6	0	0	1	0	0	0	δ	0	α	0	0	0	0	0	β	0	δ	0	0	0	0
16	0	0	0	1	0	0	0	δ	0	α	0	0	0	0	0	β	0	δ	0	0	0
3	δ	0	0	0	1	0	0	0	γ	0	0	0	α	0	0	0	β	0	0	0	0
13	0	δ	0	0	0	1	0	0	0	γ	0	0	0	α	0	0	0	β	0	0	0
8	0	0	δ	0	0	0	1	0	0	0	γ	0	0	0	α	0	0	0	β	0	0
18	0	0	0	δ	0	0	0	1	0	0	0	γ	0	0	0	α	0	0	0	0	β
5	0	0	β	0	δ	0	0	0	1	0	0	0	0	0	δ	0	β	0	0	0	0
15	0	0	0	β	0	δ	0	0	0	1	0	0	0	0	0	δ	0	β	0	0	0
10	0	β	0	0	0	0	δ	0	0	0	1	0	0	δ	0	0	0	0	β	0	0
20	β	0	0	0	0	0	0	δ	0	0	0	1	δ	0	0	0	0	0	0	0	β
2	β	0	0	0	β	0	0	0	0	0	0	0	1	0	0	0	δ	0	0	0	0
12	0	β	0	0	0	β	0	0	0	0	0	0	0	1	0	0	0	δ	0	0	0
7	0	0	β	0	0	0	β	0	0	0	0	0	0	0	1	0	0	0	δ	0	0
17	0	0	0	β	0	0	0	β	0	0	0	0	0	0	0	1	0	0	0	0	δ
4	0	0	δ	0	β	0	0	0	0	0	0	0	0	0	0	0	1	0	0	0	0
14	0	0	0	δ	0	β	0	0	0	0	0	0	0	0	0	0	0	1	0	0	0
9	0	δ	0	0	0	0	β	0	0	0	0	0	0	0	0	0	0	0	1	0	0
19	δ	0	0	0	0	0	0	β	0	0	0	0	0	0	0	0	0	0	0	0	1

Figure 5.4. Matrix $[M]$ when the first 8 bolts exceed the yielding load and when assembly pattern 1 is used

For example, in matrix $[M]$ if bolt 20 is studied (12 rows), this takes into account the loss of loads caused in the second pass by bolts 1 and 18, and also takes into account the loss of loads caused in the first pass by the additional load of bolts 2 and 19. Therefore, to calculate the additional loads, matrix $[M]$ has to be applied in equation (5.1), giving rise to the following equation:

$$\{\Delta S\} = [M]^{-1} \cdot (\{S_{f2}\} - \{S_{f1}\}) \quad (5.12)$$

And adding the additional loads to the bolts that do not exceed the yielding load in the first pass (subscript N refers to New):

$$\{S_{i1N}\} = \begin{cases} S_{i1Nk} = S_{i1k} & \text{if } 1 \leq k \leq j \\ S_{i1Nk} = S_{i1k} + \Delta S_k & \text{if } j + 1 \leq k \leq n \end{cases} \quad (5.13)$$

With vector $\{S_{i1N}\}$ being the obtained new tightening loads for the first pass, which takes into account the additional load, as follows:

$$\{S_{i1N}\} = \begin{pmatrix} S_{i1j+1} \\ S_{i1j+1} \\ \vdots \\ S_{i1j+1} \\ S_{i1Nj+1} \\ \vdots \\ S_{i1Nn} \end{pmatrix} \quad (5.14)$$

At this point, two issues must be considered. On the one hand, in vector $\{S_{i1N}\}$ it is possible that another new bolt exceeds the yielding load (it should be noted that in vector $\{S_{i1N}\}$ the loads from bolt $j+1$ onwards are higher than in vector $\{S_{i1}\}$). In that case a second iteration should be performed where it is considered that this bolt has to also be preloaded in the second pass. On the other hand, in vector $\{S_{i1N}\}$ that appears in the equation (5.14), the tightening load of the first j bolts (S_{i1j+1}) is not equal to the tightening load of bolt $j+1$ (S_{i1Nj+1}). However, in order to obtain a tightening sequence as simple as possible from the point of view of the assembler, the same tightening load is desired for those bolts. Accordingly, the tightening sequence will have less different load levels. To this end, another iteration is performed where the tightening loads of the first pass of equation (5.11) are assumed as the following:

$$\{S_{i1}\}_2 = \begin{Bmatrix} S_{i1Nj+1} \\ S_{i1Nj+1} \\ \vdots \\ S_{i1Nj+1} \\ S_{i1Nj+1} \\ \vdots \\ S_{i1n} \end{Bmatrix} \quad (5.15)$$

Thus, the tightening loads match again. With the tightening loads of the second iteration $\{S_{i1}\}_2$ the same process is carried out using equations (5.12) to (5.15). Once the second iteration is completed, a check must be performed to ensure that the difference between the tightening loads of the first pass of the first j bolts and the tightening load of the first pass of bolt $j+1$ is smaller than an established value. In that case, the iterative process would be finished, or otherwise a new iteration should be performed.

Once the tightening loads of the first pass are iteratively obtained, the tightening load of the j bolts of the second pass must be obtained. To this end, firstly, the obtained final loads $\{S_{f1}\}$ when the tightening loads $\{S_{i1}\}_X$ are applied in the first pass must be calculated:

$$\{S_{f1}\} = [A] \cdot \{S_{i1}\}_X \quad (5.16)$$

And once these loads are obtained, equation (5.17) can be used, which was deduced from equation (5.6)

$$\{S_{i2}\} = \{S_{f1N}\} + (([C] + [I]) \cdot [M]^{-1}) \cdot (\{S_{f2}\} - \{S_{f1}\}) \quad (5.17)$$

From vector $\{S_{i2}\}$ the only factor to be taken into account are the loads from bolt 1 to bolt j . Thus, with the tightening loads of vectors $\{S_{i1}\}_X$ and $\{S_{i2}\}$ a bolt tightening sequence is achieved with a whole pass plus j tightening operations.

3.2. ILLUSTRATIVE EXAMPLE AND VALIDATION

Next, a tightening sequence of one and a half passed is will be used, step by step, in an example for clearer understanding. Aside from this, with the obtained results the developed algorithm is also validated. For that purpose, the Finite Element model is going to be used with the geometry of the

experimental set up (NPS 24", Class 150 and SCHD 40), assembly pattern 1 of Figure 2.18a and a friction coefficient of 0.2. The target load is 350 kN while the yielding load of the bolts is assumed to be 450 kN.

As explained in the previous section, in the first step, the equation (3.4) has to be solved in order to find out which bolts exceed the yielding load of the bolts in a single-pass tightening sequence. Accordingly, the tightening loads of the Table 5.3 are obtained, and as can be seen in this example, the first eight bolts being tightened exceed the yielding load. Therefore, the tightening load of these bolts must be replaced by the tightening load of the ninth bolt being tightened.

Bolt No.	{S _{i1} }	Bolt No.	{S _{i1} }
1	479	1	406
11	479	11	406
6	479	6	406
16	479	16	406
3	469	3	406
13	469	13	406
8	469	8	406
18	469	18	406
5	406	5	406
15	406	15	406
10	406	10	406
20	406	20	406
2	350	2	350
12	350	12	350
7	350	7	350
17	350	17	350
4	350	4	350
14	350	14	350
9	350	9	350
19	350	19	350

Table 5.3. Obtained tightening loads with equation (3.4) for the illustrative example, and modification to avoid yielding load

In the second load step, the additional load of the bolts that do not exceed the yielding load is calculated, because, as mentioned before, the bolts of the first pass need an additional load to overcome the elastic interaction phenomenon of the second pass. For that purpose, first the matrix [M] has to be created, secondly, equation (5.12) has to be used, and finally, the equation (5.13) (see Table 5.4). Here the additional loads of the first eight bolts must be avoided because the loads correspond to the second pass of the tightening sequence.

Bolt No.	{ ΔS }	Bolt No.	{ S_{i1N} }
1	77	1	406
11	77	11	406
6	77	6	406
16	77	16	406
3	68	3	406
13	68	13	406
8	68	8	406
18	68	18	406
5	14	5	420
15	14	15	420
10	14	10	420
20	14	20	420
2	23	2	373
12	23	12	373
7	23	7	373
17	23	17	373
4	11	4	361
14	11	14	361
9	11	9	361
19	11	19	361

Table 5.4. Additional loads and the new tightening loads obtained for the illustrative example

Next, the same process is repeated iteratively until the initial load of the first eight bolts being tightened is almost equal to the initial load of the ninth bolt being tightened. In this example, the iterative process is repeated until the difference between the loads is less than 0.1%. The initial loads of the Table 5.5 are obtained in only three iterations.

Subsequently, the equation (5.16) is used with the initial loads of the last iteration (see Table 5.5) to obtain the final loads of the first pass. Once these final loads are obtained, the initial loads of the second pass are calculated from the equation (5.17), as shown in the Table 5.6.

Bolt No.	$\{S_{i1}\}_3$
1	418
11	418
6	418
16	418
3	418
13	418
8	418
18	418
5	418
15	418
10	418
20	418
2	369
12	369
7	369
17	369
4	359
14	359
9	359
19	359

Table 5.5. Obtained initial loads for the first pass with three iterations

Bolt No.	$\{S_{i2}\}$
1	350
11	350
6	350
16	350
3	350
13	350
8	350
18	350
5	0
15	0
10	0
20	0
2	0
12	0
7	0
17	0
4	0
14	0
9	0
19	0

Table 5.6. Obtained initial loads for the second pass using the initial loads of the Table 5.5

In conclusion, the initial loads of Tables 5.5 and 5.6 were applied in the Finite Element model in order to verify the validity of the developed algorithm. Accordingly, the final loads of Figure 5.5 were obtained, where the average load is 351.9 kN and the standard deviation 0.546 kN. Therefore, it has been proven that the one and a half pass tightening sequences provide extremely accurate results.

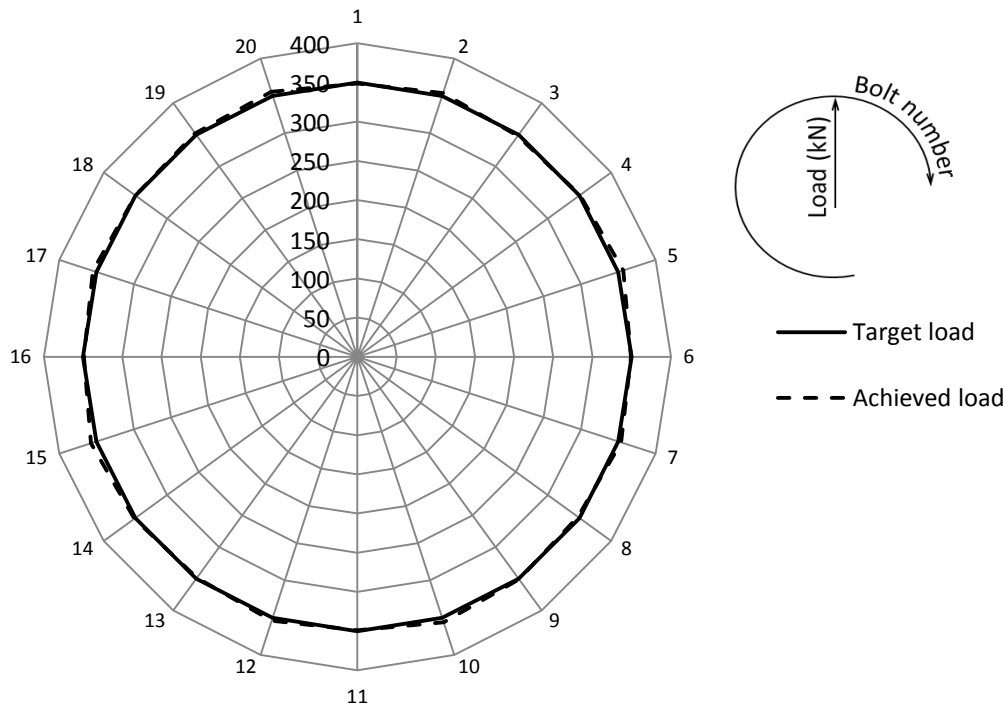


Figure 5.5. Final results in the illustrative example

4. RANGE OF APPLICATION OF THE TETRAPARAMETRIC ASSEMBLY METHOD

Up to this point of the Doctoral Thesis, the TAM has only been validated for the ASME RTJ of NPS 24", Class 150 and SCHD 40. To this regard, this section studies the range of application of the method for the various ASME RTJs [Asm'13(1)]. Firstly, it must be noted that among all the joints, those with a nominal pipe size of less than 10" and those of class 2500 were ruled out due to high rigidity. In these joints, the local deformation is small compared to the solid rigid motion. Accordingly, the TAM does not provide accurate results because, as explained in Chapter 4, this method is not suitable for extremely rigid joints as it does not simulate the solid rigid motion. Also, there are few bolts on these joints (usually 8 or less), so the assembly time is

low and therefore an optimized tightening sequence is not particularly necessary. Thus, the study of the range of application of the TAM was limited to the joints of the dashed square of Figure 5.6.

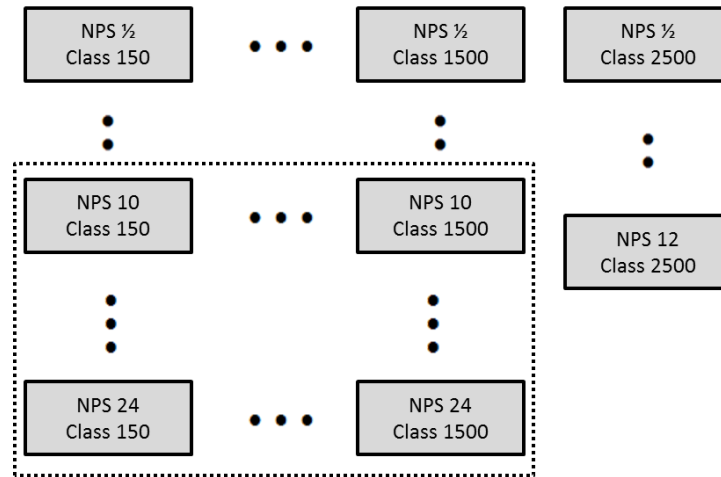


Figure 5.6. Studied range of application

On the other hand, instead of studying every joint inside the dashed square, only the four corners were studied since they are the most critical joints. The SCHD was selected based on the following criteria:

- The NPS 24” and Class 150 joint is the most flexible joint, and therefore SCHD 10 was selected (the most flexible option).
- The higher the class, the higher the stiffness of the joint. So, for NPS 24” and Class 1500 joint and for the NPS 10” and Class 1500 joint, the SCHD 160 was selected (the most rigid option).
- The NPS 10” and Class 150 joint only has one SCHD in the standard, so that one was selected

Analysing Figure 4.4, and based on Chapter 4, the four coefficients of the TAM were obtained for each joint (see Table 5.7). In the Finite Element analysis, a friction coefficient of 0.25 and a target load of 55% of bolt yielding load was assumed (we must recall that the influence of both parameters is very small). For each joint, with the obtained coefficients, two different assembly patterns (see Table 5.8), two different friction coefficients (0.2 and 0.3) and two final loads (40% and 70% of bolt yielding load) were studied. Therefore, combining the two assembly patterns, two friction coefficients and two load levels, eight analyses were performed for each joint. As can be seen, different assembly patterns, friction coefficients and target loads were studied and

unique coefficients were obtained for each joint, proving that in these joints these parameters also have a small influence on the value of the coefficients. Accordingly, it is proven that in every joint inside the dashed square of Figure 5.6, it is possible to obtain unique coefficients because the influence of the friction coefficient, target load and assembly pattern can be avoided.

	α	β	γ	δ
Class 150 NPS 10	-0.095	-0.103	0.009	0.017
Class 150 NPS 24	-0.186	-0.195	-0.044	-0.007
Class 1500 NPS 10	-0.176	-0.209	-0.028	0.022
Class 1500 NPS 24	-0.21	-0.191	-0.087	-0.032

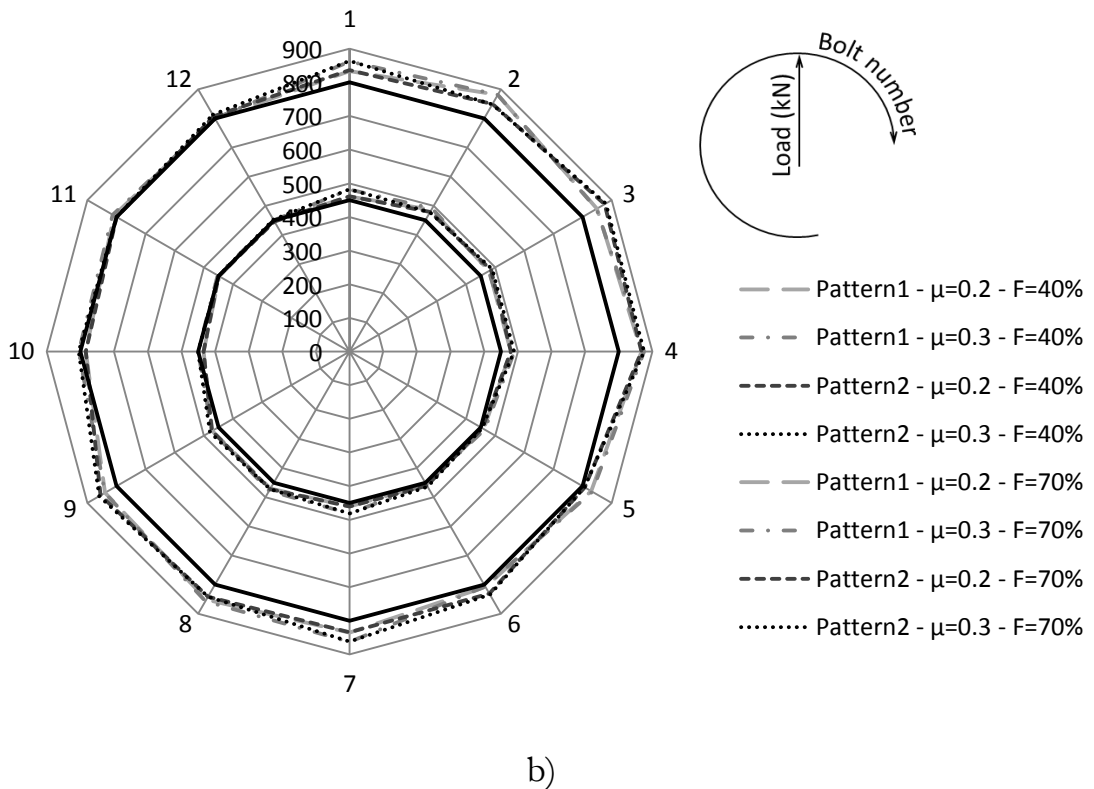
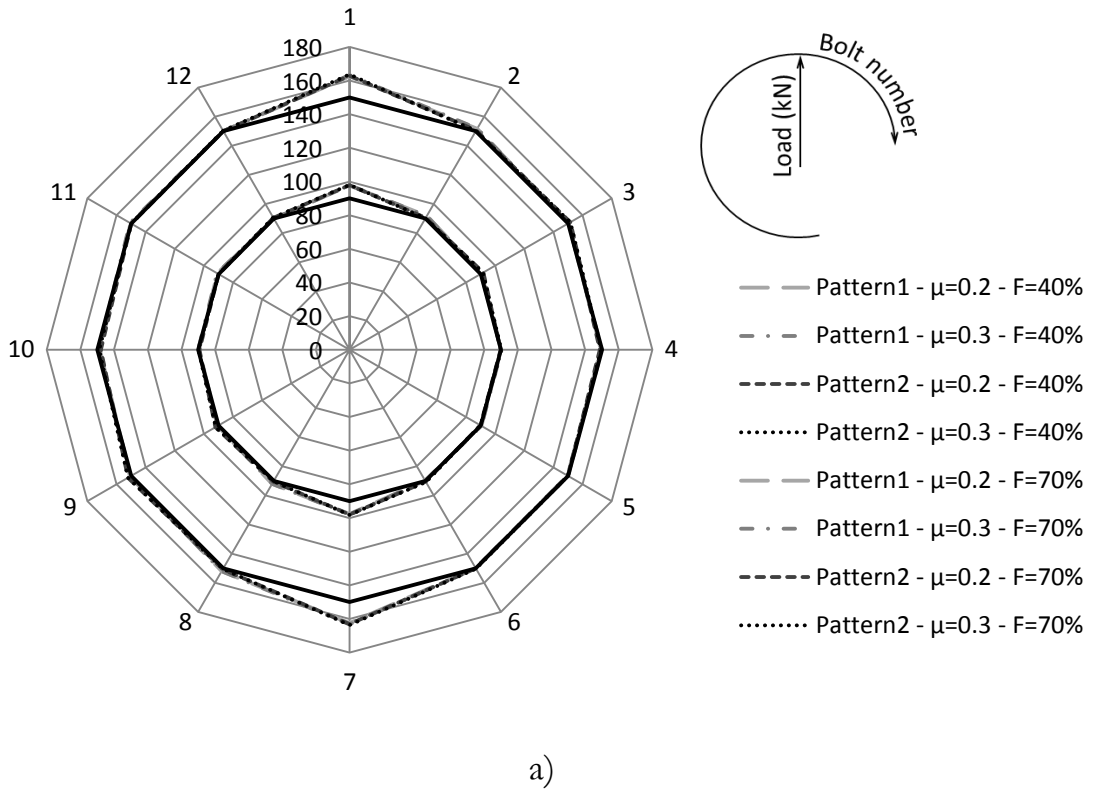
Table 5.7. Coefficients obtained with the TAM

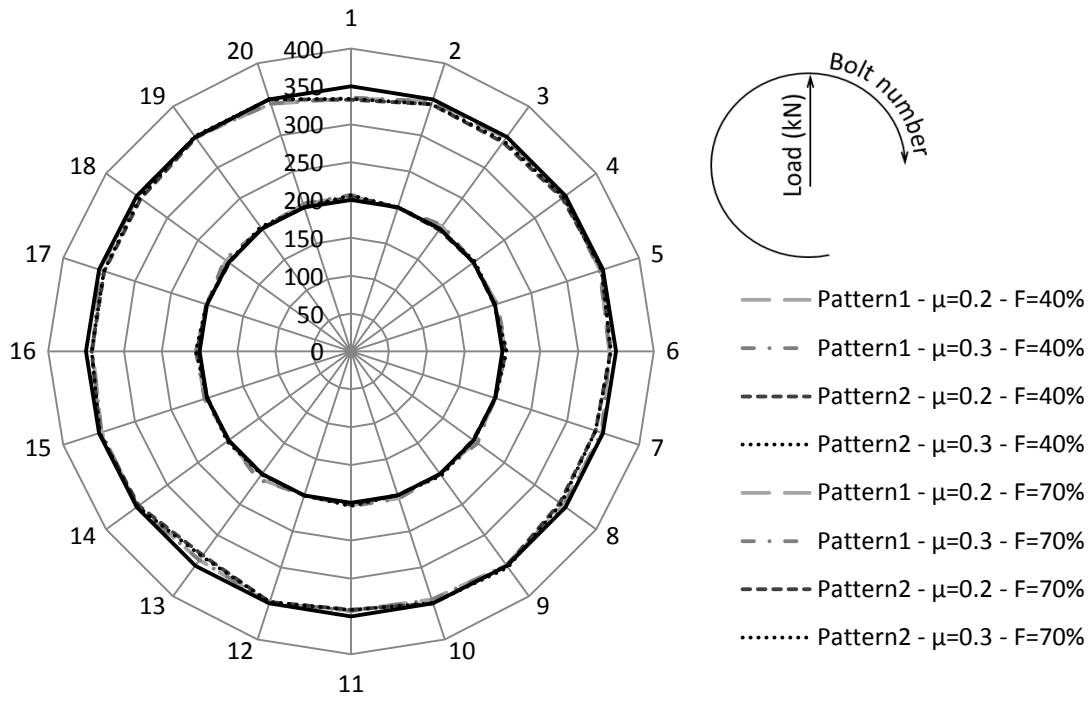
Pattern 1	
NPS10 Class150 NPS10 Class1500	1-7-4-10 → 2-8-5-11 → 3-9-6-12
NPS24 Class1500	1-9-5-13 → 3-11-7-15 → 2-10-6-14 → 4-12-8-16
NPS24 Class150	1-11-6-16 → 3-13-8-18 → 5-15-10-20 → 2-12-7-17 → 4-14-9-19
Pattern 2	
NPS10 Class150 NPS10 Class1500	1-7-4-10 → 3-9-6-12 → 2-8-5-11
NPS24 Class1500	1-9-5-13 → 2-10-6-14 → 3-11-7-15 → 4-12-8-16
NPS24 Class150	1-11-6-16 → 2-12-7-17 → 3-13-8-18 → 4-14-9-19 → 5-15-10-20

Table 5.8. Assembly patterns for the different joints

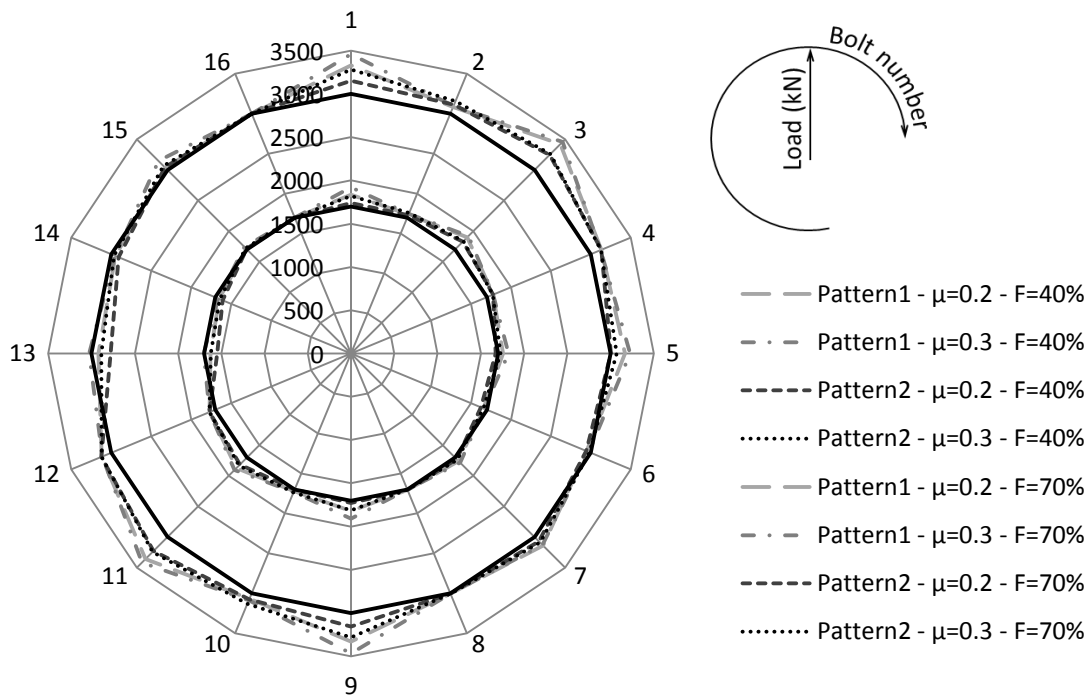
To study of the range of application of the TAM, one-pass tightening sequences were used in order to minimize computational costs. Obviously, the accuracy of the two-pass tightening sequence will be similar because the same coefficients value is used in these sequences. Therefore, applying the calculated tightening loads with the equation (3.4) in the parametric Finite Element model explained in Chapter 2, the final load distributions of Figure 5.7 were obtained. As can be seen, the higher the class of the RTJ, the lower

the accuracy of the TAM. This is a result of the rigidity of the joint (when the class increases, the rigidity also increases), because the solid rigid motion becomes predominant and therefore the accuracy of the results decreases. Nevertheless, all the obtained results appear to be completely admissible.





c)



d)

Figure 5.7. Results obtained with the TAM for different joints a) NPS10 Class150 b) NPS10 Class1500 SCHD160 c) NPS24 Class150 SCHD10 d) NPS24 Class1500 SCHD160

In order to study the obtained results in detail, for each analysis, the relative error was calculated between the obtained average load and the target final load (see Table 5.9). In this table it is also appreciated how, in the small classes, the error is much smaller than in the larger classes, due to the solid rigid motion. Finally, to synthesize Table 5.9 and obtain clearer results, Table 5.10 was obtained. This table shows the maximum error obtained on each joint, and therefore, the maximum errors that can be obtained using the TAM. Thus, it is proven that using this method, the error is always less than 5.6%.

Order	Load	μ	10" class	24" class	10" class	24" class
			150	150	1500	1500
1	40%	0.2	1.92	1.24	2.86	2.92
		0.3	1.99	1.55	4.49	4.66
	70%	0.2	1.53	1.23	4.03	4.18
		0.3	1.69	1.21	5.04	5.59
2	40%	0.2	1.91	0.33	2.87	0.68
		0.3	2	0.8	4.5	2.45
	70%	0.2	1.52	1.73	4.04	2.03
		0.3	1.68	1.47	5.07	3.46

Table 5.9. Relative errors obtained in each analysis

Flange	Maximum error percentage (%)
NPS 10" Class 150	2
NPS 24" Class 150	1.73
NPS 10" Class 1500	5.07
NPS 24" Class 1500	5.59

Table 5.10. Obtained maximum errors in the four RTJs

5. RTJ COEFFICIENTS LIBRARY

In the previous section, the range of application of the TAM has been defined and it was also proven how the error from this method within the range of application is always less than 5.6%.

Here, the four coefficients of the TAM were obtained for every ASME RTJ inside the range of application of Figure 5.6. Thus, a coefficients library was generated in order to considerably simplify the cost of obtaining the optimized tightening sequence. In other words, in Chapter 4, it has been explained that in the TAM, an analysis of two load steps must be performed to obtain the four coefficients of the matrices $[A]$ and $[B]$ and thus the tightening loads of the optimized tightening sequence. However, if a library with the four coefficients of every joint is provided, the previous analyses can be avoided because the matrices $[A]$ and $[B]$ will already be defined and available for the assembler. Thus, previous analyses are avoided and a much higher efficiency of the TAM is achieved.

To obtain the four coefficients of every joint, the analysis in Figure 4.4 was carried out on every joint. Just as in the study of the range of application in the previous section, a friction coefficient of 0.25 and a preload of 55% of the bolt yielding load was assumed. Thus, the coefficients library was obtained in full. Tables 5.11 to 5.16 show the coefficients of the classes from 150 to 1500, respectively. In the tables, SCHED 0 means that the joint does not have different SCHEDs defined in the standard. On the other hand, if a box is filled out with a dash, this means that the joint is not defined in the standard. Finally, mention must be made that in the tables, the coefficients have been rounded to three decimal places due to lack of space; however, all the coefficients have been used throughout the Doctoral Thesis.

Class 150

		SCHD											
		0	10	20	30	40	60	80	100	120	140	160	
NPS	Coef. α	10	-0,095	-	-	-	-	-	-	-	-	-	-
	12	-0,046	-	-	-	-	-	-	-	-	-	-	
	14	-	-0,116	-0,109	-0,102	-0,097	-0,084	-0,074	-0,065	-0,059	-0,055	-0,051	
	16	-	-0,188	-0,178	-0,169	-0,153	-0,139	-0,125	-0,115	-0,108	-0,101	-0,097	
	18	-	-0,129	-0,122	-0,111	-0,101	-0,090	-0,081	-0,074	-0,068	-0,065	-0,062	
	20	-	-0,201	-0,186	-0,173	-0,163	-0,143	-0,132	-0,122	-0,113	-0,107	-0,103	
	24	-	-0,186	-0,166	-0,151	-0,146	-0,127	-0,113	-0,101	-0,094	-0,090	-0,086	

a)

		SCHD										
		0	10	20	30	40	60	80	100	120	140	160
NPS	Coef. β	10	-0,103	-	-	-	-	-	-	-	-	-
	12	-0,048	-	-	-	-	-	-	-	-	-	
	14	-	-0,127	-0,119	-0,112	-0,105	-0,091	-0,080	-0,070	-0,063	-0,058	-0,054
	16	-	-0,192	-0,184	-0,176	-0,159	-0,143	-0,130	-0,118	-0,111	-0,103	-0,099
	18	-	-0,132	-0,126	-0,115	-0,105	-0,093	-0,084	-0,076	-0,070	-0,067	-0,063
	20	-	-0,207	-0,192	-0,176	-0,168	-0,149	-0,134	-0,124	-0,116	-0,110	-0,104
	24	-	-0,195	-0,179	-0,159	-0,155	-0,131	-0,119	-0,107	-0,098	-0,091	-0,089

b)

Coef. γ		SCHD										
		0	10	20	30	40	60	80	100	120	140	160
NPS	10	0,009	-	-	-	-	-	-	-	-	-	-
	12	0,005	-	-	-	-	-	-	-	-	-	-
	14	-	0,009	0,009	0,008	0,008	0,007	0,007	0,006	0,006	0,006	0,006
	16	-	-0,023	-0,020	-0,017	-0,013	-0,009	-0,005	-0,003	-0,001	0,001	0,002
	18	-	-0,009	-0,007	-0,003	-0,001	0,002	0,003	0,004	0,004	0,004	0,004
	20	-	-0,044	-0,037	-0,030	-0,026	-0,020	-0,015	-0,011	-0,009	-0,007	-0,005
	24	-	-0,044	-0,033	-0,025	-0,021	-0,014	-0,010	-0,006	-0,004	-0,003	-0,002

c)

Coef. δ		SCHD										
		0	10	20	30	40	60	80	100	120	140	160
NPS	10	0,017	-	-	-	-	-	-	-	-	-	-
	12	0,003	-	-	-	-	-	-	-	-	-	-
	14	-	0,019	0,018	0,017	0,016	0,014	0,012	0,011	0,011	0,010	0,010
	16	-	0,014	0,014	0,014	0,013	0,012	0,012	0,012	0,012	0,012	0,012
	18	-	0,008	0,009	0,011	0,011	0,011	0,011	0,011	0,010	0,010	0,009
	20	-	-0,003	-0,002	-0,001	0,000	0,001	0,003	0,004	0,004	0,005	0,005
	24	-	-0,007	-0,003	-0,001	0,000	0,001	0,003	0,004	0,005	0,005	0,005

d)

Table 5.11. Coefficients obtained with the TAM for the RTJs of class 150 a) coefficient α b) coefficient β c) coefficient γ d) coefficient δ

Class 300

		SCHD											
		0	10	20	30	40	60	80	100	120	140	160	
NPS	Coef. α	10	-0,156	-	-	-	-	-	-	-	-	-	-
	12	-0,176	-	-	-	-	-	-	-	-	-	-	
	14	-	-0,237	-0,228	-0,222	-0,219	-0,206	-0,195	-0,187	-0,177	-0,171	-0,166	
	16	-	-0,264	-0,258	-0,252	-0,239	-0,227	-0,213	-0,203	-0,195	-0,186	-0,180	
	18	-	-0,265	-0,260	-0,250	-0,240	-0,228	-0,217	-0,207	-0,198	-0,192	-0,187	
	20	-	-0,219	-0,210	-0,199	-0,194	-0,177	-0,168	-0,158	-0,149	-0,144	-0,139	
	24	-	-0,278	-0,264	-0,249	-0,240	-0,223	-0,207	-0,193	-0,186	-0,179	-0,172	

a)

		SCHD										
		0	10	20	30	40	60	80	100	120	140	160
NPS	Coef. β	10	-0,162	-	-	-	-	-	-	-	-	-
	12	-0,185	-	-	-	-	-	-	-	-	-	
	14	-	-0,240	-0,227	-0,223	-0,215	-0,204	-0,194	-0,185	-0,177	-0,170	-0,166
	16	-	-0,265	-0,262	-0,253	-0,241	-0,228	-0,215	-0,204	-0,193	-0,186	-0,182
	18	-	-0,264	-0,258	-0,247	-0,236	-0,224	-0,213	-0,203	-0,197	-0,189	-0,184
	20	-	-0,216	-0,201	-0,192	-0,187	-0,173	-0,161	-0,152	-0,144	-0,138	-0,134
	24	-	-0,282	-0,269	-0,252	-0,240	-0,223	-0,207	-0,192	-0,184	-0,177	-0,172

b)

Coef. γ		SCHD										
		0	10	20	30	40	60	80	100	120	140	160
NPS	10	-0,015	-	-	-	-	-	-	-	-	-	-
	12	-0,017	-	-	-	-	-	-	-	-	-	-
	14	-	-0,070	-0,068	-0,064	-0,061	-0,055	-0,049	-0,045	-0,042	-0,039	-0,037
	16	-	-0,079	-0,076	-0,073	-0,066	-0,059	-0,053	-0,048	-0,043	-0,039	-0,037
	18	-	-0,101	-0,097	-0,091	-0,085	-0,077	-0,072	-0,066	-0,060	-0,057	-0,054
	20	-	-0,083	-0,074	-0,069	-0,065	-0,056	-0,050	-0,044	-0,039	-0,036	-0,034
	24	-	-0,109	-0,100	-0,089	-0,082	-0,071	-0,062	-0,055	-0,049	-0,045	-0,041

c)

Coef. δ		SCHD										
		0	10	20	30	40	60	80	100	120	140	160
NPS	10	0,013	-	-	-	-	-	-	-	-	-	-
	12	0,017	-	-	-	-	-	-	-	-	-	-
	14	-	-0,012	-0,013	-0,012	-0,012	-0,011	-0,010	-0,009	-0,009	-0,008	-0,008
	16	-	-0,005	-0,003	-0,003	-0,003	-0,002	-0,002	-0,003	-0,003	-0,002	-0,002
	18	-	-0,034	-0,032	-0,030	-0,029	-0,027	-0,025	-0,023	-0,021	-0,021	-0,020
	20	-	-0,035	-0,031	-0,027	-0,025	-0,022	-0,019	-0,015	-0,012	-0,010	-0,009
	24	-	-0,037	-0,034	-0,030	-0,028	-0,023	-0,020	-0,018	-0,015	-0,013	-0,011

d)

Table 5.12. Coefficients obtained with the TAM for the RTJs of class 300 a) coefficient α b) coefficient β c) coefficient γ d) coefficient δ

Class 400

		SCHD											
		0	10	20	30	40	60	80	100	120	140	160	
NPS	Coef. α	10	-	-	-0,187	-0,181	-0,179	-0,169	-0,162	-0,156	-0,150	-0,144	-0,140
	12	-	-	-0,201	-0,192	-0,186	-0,174	-0,167	-0,158	-0,152	-0,147	-0,142	
	14	-	-0,244	-0,238	-0,231	-0,225	-0,215	-0,205	-0,193	-0,184	-0,180	-0,175	
	16	-	-0,266	-0,257	-0,254	-0,240	-0,229	-0,217	-0,207	-0,196	-0,188	-0,183	
	18	-	-0,267	-0,263	-0,253	-0,243	-0,233	-0,221	-0,211	-0,202	-0,197	-0,192	
	20	-	-0,200	-0,191	-0,181	-0,174	-0,162	-0,152	-0,143	-0,137	-0,131	-0,127	
	24	-	-0,286	-0,275	-0,264	-0,259	-0,243	-0,233	-0,218	-0,210	-0,205	-0,199	

a)

		SCHD											
		0	10	20	30	40	60	80	100	120	140	160	
NPS	Coef. β	10	-	-	-0,195	-0,189	-0,182	-0,171	-0,163	-0,155	-0,150	-0,144	-0,140
	12	-	-	-0,211	-0,202	-0,194	-0,180	-0,171	-0,162	-0,155	-0,150	-0,145	
	14	-	-0,242	-0,236	-0,230	-0,226	-0,211	-0,202	-0,192	-0,185	-0,181	-0,175	
	16	-	-0,265	-0,258	-0,252	-0,240	-0,229	-0,216	-0,207	-0,195	-0,188	-0,182	
	18	-	-0,260	-0,255	-0,245	-0,237	-0,226	-0,214	-0,205	-0,198	-0,192	-0,187	
	20	-	-0,196	-0,186	-0,176	-0,170	-0,158	-0,148	-0,140	-0,134	-0,128	-0,124	
	24	-	-0,287	-0,271	-0,257	-0,252	-0,237	-0,226	-0,216	-0,208	-0,204	-0,196	

b)

Coef. γ		SCHD										
		0	10	20	30	40	60	80	100	120	140	160
NPS	10	-	-	-0,029	-0,027	-0,026	-0,024	-0,024	-0,023	-0,023	-0,022	-0,022
	12	-	-	-0,026	-0,023	-0,021	-0,019	-0,017	-0,016	-0,015	-0,014	-0,014
	14	-	-0,078	-0,075	-0,072	-0,069	-0,064	-0,057	-0,053	-0,049	-0,046	-0,044
	16	-	-0,084	-0,080	-0,077	-0,071	-0,065	-0,059	-0,054	-0,050	-0,046	-0,043
	18	-	-0,106	-0,103	-0,097	-0,092	-0,085	-0,079	-0,073	-0,069	-0,065	-0,063
	20	-	-0,079	-0,073	-0,067	-0,063	-0,057	-0,051	-0,047	-0,044	-0,041	-0,039
	24	-	-0,113	-0,104	-0,094	-0,092	-0,082	-0,075	-0,069	-0,064	-0,061	-0,057

c)

Coef. δ		SCHD										
		0	10	20	30	40	60	80	100	120	140	160
NPS	10	-	-	0,016	0,015	0,014	0,011	0,010	0,008	0,006	0,004	0,002
	12	-	-	0,023	0,022	0,020	0,018	0,016	0,014	0,012	0,011	0,009
	14	-	-0,013	-0,012	-0,012	-0,012	-0,012	-0,012	-0,011	-0,011	-0,011	-0,011
	16	-	-0,008	-0,008	-0,008	-0,007	-0,007	-0,007	-0,007	-0,008	-0,008	-0,008
	18	-	-0,038	-0,037	-0,035	-0,033	-0,032	-0,030	-0,029	-0,028	-0,027	-0,026
	20	-	-0,045	-0,042	-0,039	-0,037	-0,033	-0,030	-0,028	-0,026	-0,024	-0,023
	24	-	-0,027	-0,024	-0,020	-0,022	-0,021	-0,019	-0,017	-0,018	-0,017	-0,016

d)

Table 5.13. Coefficients obtained with the TAM for the RTJs of class 400 a) coefficient α b) coefficient β c) coefficient γ d) coefficient δ

Class 600

Coef. α		SCHD										
		0	10	20	30	40	60	80	100	120	140	160
NPS	10	-	-	-0,244	-0,239	-0,235	-0,224	-0,219	-0,213	-0,207	-0,201	-0,198
	12	-	-	-0,252	-0,245	-0,237	-0,225	-0,217	-0,207	-0,205	-0,198	-0,193
	14	-	-0,257	-0,252	-0,247	-0,243	-0,231	-0,221	-0,210	-0,205	-0,198	-0,192
	16	-	-0,294	-0,289	-0,283	-0,271	-0,259	-0,251	-0,235	-0,226	-0,217	-0,213
	18	-	-0,263	-0,257	-0,249	-0,241	-0,227	-0,219	-0,208	-0,199	-0,194	-0,189
	20	-	-0,287	-0,276	-0,266	-0,262	-0,247	-0,235	-0,224	-0,214	-0,206	-0,201
	24	-	-0,289	-0,280	-0,268	-0,258	-0,244	-0,229	-0,215	-0,206	-0,198	-0,193

a)

Coef. β		SCHD										
		0	10	20	30	40	60	80	100	120	140	160
NPS	10	-	-	-0,244	-0,236	-0,232	-0,221	-0,214	-0,207	-0,200	-0,195	-0,191
	12	-	-	-0,241	-0,235	-0,229	-0,216	-0,209	-0,201	-0,198	-0,193	-0,188
	14	-	-0,256	-0,250	-0,245	-0,240	-0,229	-0,220	-0,209	-0,203	-0,196	-0,191
	16	-	-0,293	-0,291	-0,284	-0,273	-0,262	-0,245	-0,239	-0,224	-0,221	-0,215
	18	-	-0,257	-0,254	-0,244	-0,235	-0,224	-0,213	-0,203	-0,197	-0,190	-0,185
	20	-	-0,270	-0,261	-0,251	-0,246	-0,232	-0,224	-0,212	-0,204	-0,198	-0,192
	24	-	-0,274	-0,264	-0,253	-0,245	-0,229	-0,219	-0,206	-0,197	-0,190	-0,185

b)

Coef. γ		SCHD										
		0	10	20	30	40	60	80	100	120	140	160
NPS	10	-	-	-0,072	-0,069	-0,067	-0,064	-0,061	-0,058	-0,055	-0,053	-0,051
	12	-	-	-0,096	-0,092	-0,088	-0,081	-0,077	-0,072	-0,070	-0,067	-0,065
	14	-	-0,095	-0,091	-0,089	-0,086	-0,080	-0,074	-0,068	-0,065	-0,062	-0,060
	16	-	-0,117	-0,114	-0,110	-0,098	-0,095	-0,086	-0,082	-0,077	-0,073	-0,068
	18	-	-0,095	-0,092	-0,086	-0,082	-0,075	-0,071	-0,066	-0,062	-0,059	-0,056
	20	-	-0,133	-0,127	-0,121	-0,117	-0,108	-0,100	-0,094	-0,088	-0,083	-0,080
	24	-	-0,132	-0,127	-0,118	-0,113	-0,104	-0,094	-0,087	-0,081	-0,077	-0,073

c)

Coef. δ		SCHD										
		0	10	20	30	40	60	80	100	120	140	160
NPS	10	-	-	0,015	0,013	0,012	0,009	0,007	0,004	0,002	0,000	-0,001
	12	-	-	-0,019	-0,019	-0,017	-0,016	-0,016	-0,015	-0,020	-0,019	-0,020
	14	-	-0,019	-0,019	-0,019	-0,019	-0,019	-0,020	-0,020	-0,020	-0,020	-0,021
	16	-	-0,015	-0,014	-0,015	-0,016	-0,016	-0,019	-0,018	-0,020	-0,020	-0,019
	18	-	-0,019	-0,019	-0,018	-0,018	-0,018	-0,018	-0,018	-0,018	-0,019	-0,019
	20	-	-0,054	-0,052	-0,050	-0,050	-0,047	-0,045	-0,043	-0,041	-0,040	-0,039
	24	-	-0,056	-0,054	-0,050	-0,048	-0,045	-0,042	-0,040	-0,038	-0,037	-0,035

d)

Table 5.14. Coefficients obtained with the TAM for the RTJs of class 600 a) coefficient α b) coefficient β c) coefficient γ d) coefficient δ

Class 900

		SCHD											
		0	10	20	30	40	60	80	100	120	140	160	
NPS	Coef. α	10	-	-	-0,258	-0,254	-0,252	-0,243	-0,239	-0,235	-0,231	-0,225	-0,222
	12	-	-	-0,253	-0,249	-0,244	-0,236	-0,230	-0,224	-0,219	-0,215	-0,210	
	14	-	-0,244	-0,240	-0,237	-0,234	-0,222	-0,214	-0,206	-0,201	-0,194	-0,190	
	16	-	-0,252	-0,245	-0,242	-0,233	-0,222	-0,211	-0,205	-0,197	-0,189	-0,185	
	18	-	-0,260	-0,257	-0,250	-0,240	-0,231	-0,221	-0,210	-0,205	-0,199	-0,193	
	20	-	-0,271	-0,264	-0,257	-0,250	-0,238	-0,227	-0,217	-0,208	-0,201	-0,198	
	24	-	-0,262	-0,258	-0,247	-0,241	-0,225	-0,218	-0,210	-0,202	-0,197	-0,194	

a)

		SCHD											
		0	10	20	30	40	60	80	100	120	140	160	
NPS	Coef. β	10	-	-	-0,247	-0,242	-0,238	-0,231	-0,226	-0,222	-0,218	-0,215	-0,211
	12	-	-	-0,243	-0,236	-0,234	-0,227	-0,220	-0,214	-0,210	-0,206	-0,202	
	14	-	-0,233	-0,229	-0,224	-0,220	-0,212	-0,203	-0,195	-0,191	-0,184	-0,180	
	16	-	-0,240	-0,235	-0,230	-0,222	-0,212	-0,203	-0,195	-0,190	-0,181	-0,178	
	18	-	-0,252	-0,250	-0,240	-0,233	-0,223	-0,213	-0,206	-0,198	-0,193	-0,189	
	20	-	-0,260	-0,254	-0,248	-0,241	-0,229	-0,219	-0,209	-0,202	-0,194	-0,189	
	24	-	-0,259	-0,257	-0,246	-0,234	-0,217	-0,215	-0,209	-0,197	-0,199	-0,191	

b)

Coef. γ		SCHD										
		0	10	20	30	40	60	80	100	120	140	160
NPS	10	-	-	-0,088	-0,085	-0,083	-0,079	-0,078	-0,074	-0,073	-0,069	-0,067
	12	-	-	-0,113	-0,109	-0,106	-0,101	-0,098	-0,095	-0,092	-0,090	-0,086
	14	-	-0,100	-0,096	-0,095	-0,092	-0,086	-0,081	-0,078	-0,074	-0,071	-0,068
	16	-	-0,100	-0,096	-0,094	-0,090	-0,083	-0,078	-0,074	-0,070	-0,066	-0,063
	18	-	-0,101	-0,099	-0,095	-0,090	-0,084	-0,079	-0,074	-0,069	-0,067	-0,064
	20	-	-0,107	-0,103	-0,099	-0,095	-0,088	-0,083	-0,077	-0,073	-0,069	-0,067
	24	-	-0,116	-0,108	-0,101	-0,098	-0,092	-0,089	-0,083	-0,076	-0,080	-0,073

c)

Coef. δ		SCHD										
		0	10	20	30	40	60	80	100	120	140	160
NPS	10	-	-	0,018	0,017	0,015	0,011	0,007	0,004	0,000	-0,002	-0,002
	12	-	-	-0,039	-0,039	-0,040	-0,040	-0,041	-0,043	-0,042	-0,044	-0,043
	14	-	-0,034	-0,035	-0,035	-0,035	-0,035	-0,036	-0,036	-0,035	-0,036	-0,035
	16	-	-0,030	-0,030	-0,031	-0,031	-0,031	-0,032	-0,031	-0,031	-0,031	-0,031
	18	-	-0,025	-0,026	-0,026	-0,026	-0,027	-0,027	-0,027	-0,027	-0,027	-0,027
	20	-	-0,025	-0,025	-0,025	-0,026	-0,026	-0,027	-0,027	-0,027	-0,028	-0,028
	24	-	-0,029	-0,027	-0,027	-0,027	-0,027	-0,030	-0,029	-0,033	-0,031	-0,033

d)

Table 5.15. Coefficients obtained with the TAM for the RTJs of class 900 a) coefficient α b) coefficient β c) coefficient γ d) coefficient δ

Class 1500

		SCHD											
		0	10	20	30	40	60	80	100	120	140	160	
NPS	Coef. α	10	-	-	-0,231	-0,226	-0,222	-0,212	-0,204	-0,196	-0,189	-0,183	-0,176
	12	-	-	-0,224	-0,218	-0,215	-0,208	-0,202	-0,198	-0,193	-0,192	-0,188	
	14	-	-0,242	-0,239	-0,236	-0,235	-0,233	-0,228	-0,224	-0,219	-0,214	-0,211	
	16	-	-0,265	-0,262	-0,257	-0,252	-0,245	-0,237	-0,231	-0,226	-0,219	-0,215	
	18	-	-0,262	-0,260	-0,255	-0,250	-0,242	-0,236	-0,228	-0,222	-0,217	-0,214	
	20	-	-0,250	-0,248	-0,238	-0,234	-0,226	-0,220	-0,213	-0,208	-0,202	-0,200	
	24	-	-0,263	-0,261	-0,251	-0,246	-0,237	-0,226	-0,220	-0,220	-0,214	-0,210	

a)

		SCHD											
		0	10	20	30	40	60	80	100	120	140	160	
NPS	Coef. β	10	-	-	-0,273	-0,267	-0,263	-0,250	-0,242	-0,233	-0,225	-0,217	-0,209
	12	-	-	-0,197	-0,194	-0,185	-0,179	-0,175	-0,173	-0,173	-0,170	-0,169	
	14	-	-0,208	-0,205	-0,203	-0,203	-0,202	-0,199	-0,197	-0,195	-0,190	-0,189	
	16	-	-0,230	-0,229	-0,224	-0,220	-0,214	-0,208	-0,203	-0,201	-0,197	-0,194	
	18	-	-0,232	-0,229	-0,224	-0,221	-0,214	-0,210	-0,204	-0,199	-0,196	-0,193	
	20	-	-0,219	-0,218	-0,209	-0,206	-0,199	-0,194	-0,189	-0,185	-0,179	-0,180	
	24	-	-0,232	-0,229	-0,221	-0,217	-0,209	-0,201	-0,196	-0,198	-0,192	-0,191	

b)

Coef. γ		SCHD										
		0	10	20	30	40	60	80	100	120	140	160
NPS	10	-	-	-0,023	-0,024	-0,026	-0,026	-0,024	-0,024	-0,027	-0,029	-0,028
	12	-	-	-0,102	-0,101	-0,096	-0,092	-0,088	-0,087	-0,085	-0,083	-0,081
	14	-	-0,109	-0,106	-0,104	-0,104	-0,104	-0,101	-0,099	-0,096	-0,093	-0,091
	16	-	-0,120	-0,119	-0,116	-0,112	-0,107	-0,102	-0,098	-0,095	-0,091	-0,088
	18	-	-0,118	-0,116	-0,112	-0,109	-0,104	-0,100	-0,096	-0,093	-0,090	-0,088
	20	-	-0,110	-0,110	-0,103	-0,100	-0,095	-0,091	-0,087	-0,084	-0,080	-0,081
	24	-	-0,120	-0,117	-0,111	-0,108	-0,101	-0,095	-0,090	-0,092	-0,089	-0,087

c)

Coef. δ		SCHD										
		0	10	20	30	40	60	80	100	120	140	160
NPS	10	-	-	0,056	0,053	0,049	0,043	0,041	0,034	0,030	0,024	0,022
	12	-	-	-0,028	-0,027	-0,028	-0,031	-0,030	-0,034	-0,034	-0,039	-0,041
	14	-	-0,025	-0,025	-0,025	-0,027	-0,032	-0,034	-0,037	-0,037	-0,038	-0,038
	16	-	-0,023	-0,024	-0,024	-0,025	-0,027	-0,028	-0,030	-0,030	-0,031	-0,032
	18	-	-0,020	-0,021	-0,022	-0,023	-0,025	-0,026	-0,028	-0,029	-0,031	-0,031
	20	-	-0,019	-0,018	-0,020	-0,020	-0,021	-0,023	-0,025	-0,025	-0,026	-0,030
	24	-	-0,020	-0,021	-0,020	-0,022	-0,020	-0,019	-0,022	-0,030	-0,032	-0,032

d)

Table 5.16. Coefficients obtained with the TAM for the RTJs of class 1500 a) coefficient α b) coefficient β c) coefficient γ d) coefficient δ

CHAPTER 6. APPLICATION IN EXCEL VBA OF THE TETRAPARAMETRIC ASSEMBLY METHOD

1. INTRODUCTION

Chapter 4 explored the TAM for single-pass tightening sequences. Later, in Chapter 5, the method was generalised for multiple-pass tightening sequences; its range of application was also studied; and finally, a library with the four coefficients of the TAM was generated for every RTJ which is inside the range of application. Therefore, at this point, the method is completely developed.

A computer application programmed in “Visual Basic for Applications” of Microsoft Excel is explained in this Chapter, implementing the methodology explained in Chapters 4 and 5 [Cor’17(2)]. The application is divided in two sections: The optimization section and the simulation section. The aim of the optimization section is to enter, as input data, the parameters of the joint to be studied and the target load, and to obtain the resulting tightening load of every bolt which provides the target load; that is to say, the optimized tightening sequence. On the other hand, in the simulation section, the tightening loads are the input data, and therefore, the final load distribution of the bolts is obtained as a result, which sometimes can be particularly useful, as will be later explained.

To this regard, this Chapter first studies the optimization section of the computer application, followed by the simulation section, and finally an illustrative example which indicates the significant advantages this application provides.

2. OPTIMIZATION SECTION OF THE APPLICATION

In the optimization section, equations (3.4) and (5.7) are used in order to obtain the tightening loads of every bolt. For that purpose, the input data of Figure 6.1 is used. As can be seen, the joint type, number of passes, target load, bolt yielding load, and assembly pattern must be introduced as input data.

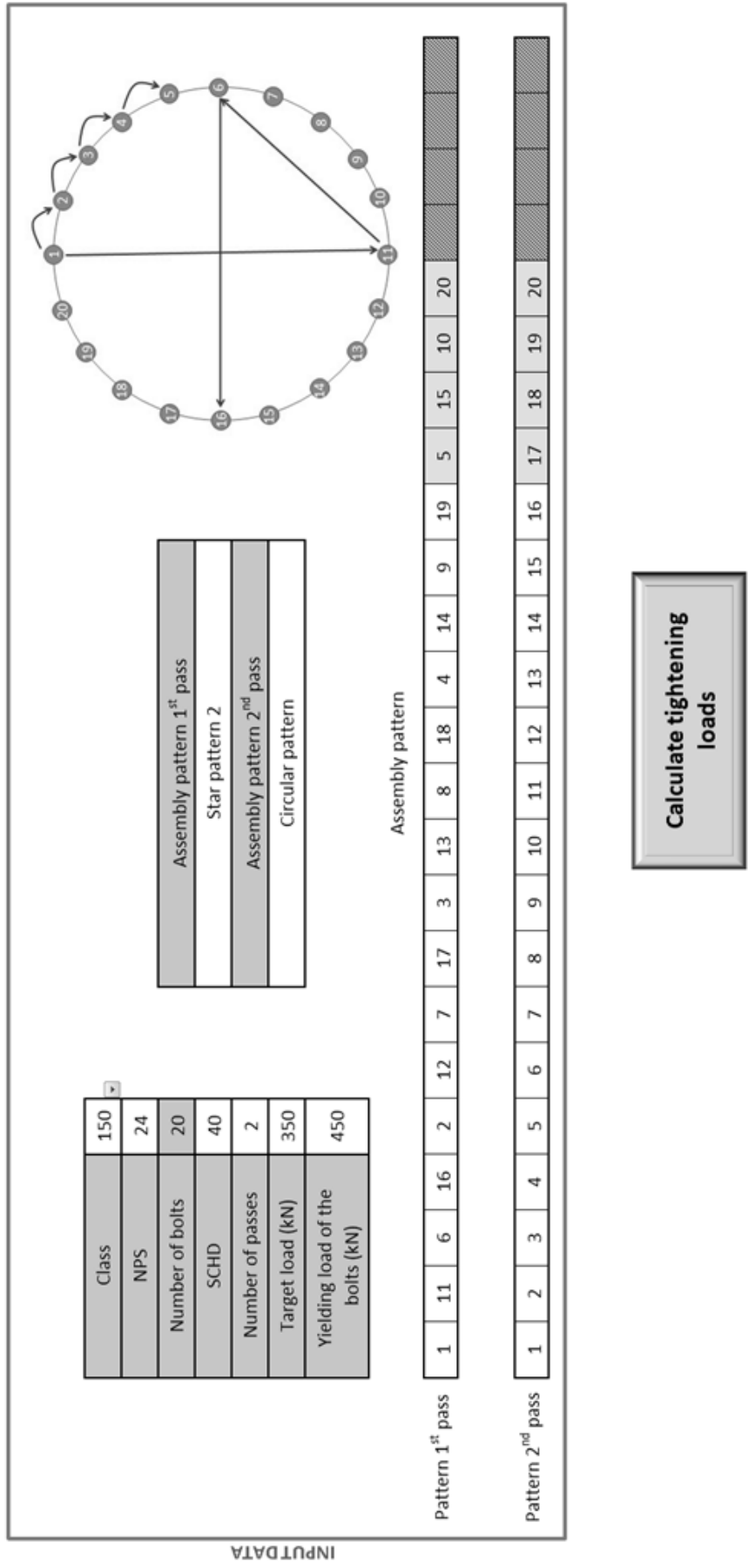


Figure 6.1. Input data of the optimization section

As illustrated in Figure 6.2, the class of the desired joint, the nominal pipe size (NPS), the SCHD and the number of passes is selected via pop-up windows (the number of bolts appears automatically). Thus, entering the input data is easier. The target load and the yield load of the bolts must be entered manually.

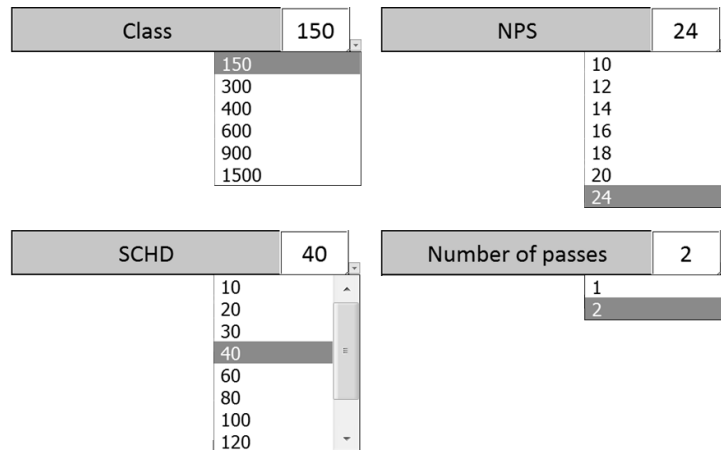


Figure 6.2. Pop-up Windows for the type of joint and number of passes

Regarding the assembly pattern, the five different choices of Figure 6.3 are offered for both, the first and the second pass. Star assembly patterns 1 and 2 correspond with the assembly patterns of the ASME standard [Asm'13(2)] (see Figure 2.18 for a joint with 20 bolts), the circular assembly pattern follows a clockwise pattern and the star-circular pattern tightens the first four bolts following the star pattern and the other bolts following the circular pattern. When a tightening sequence is selected, this is written automatically in the rows of the lower part of Figure 6.1. Finally, an assembly pattern can also be entered manually.

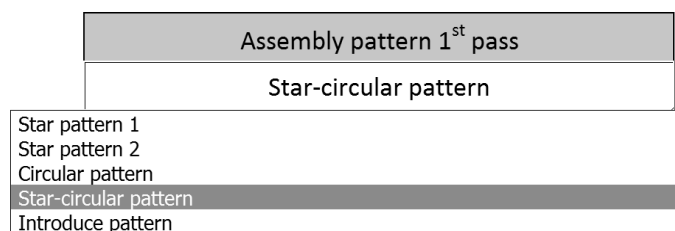
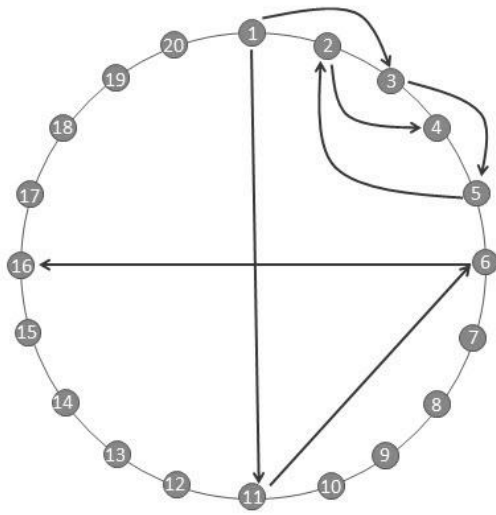
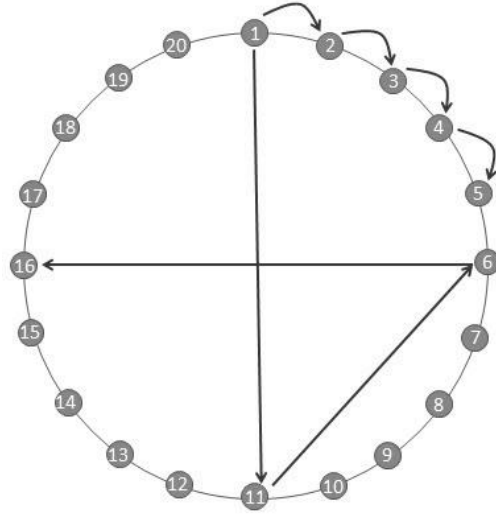


Figure 6.3. Pop-up window of the assembly patterns

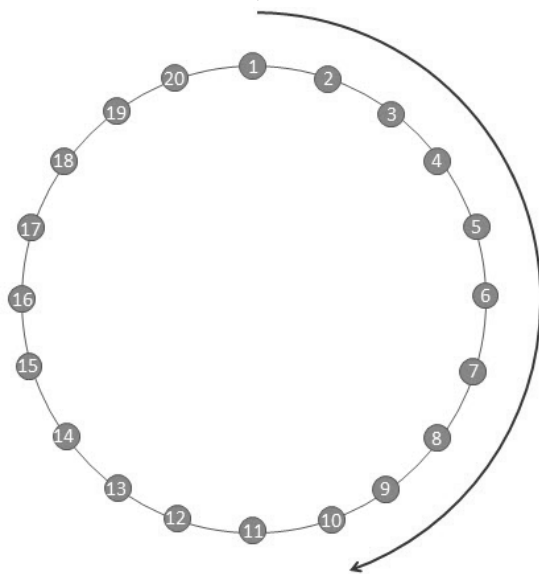
The picture of the assembly pattern (upper right hand side of Figure 6.1) also changes automatically when the number of bolts or the assembly pattern varies. Figure 6.4 shows the pictures of the different assembly patterns on a joint with 20 bolts.



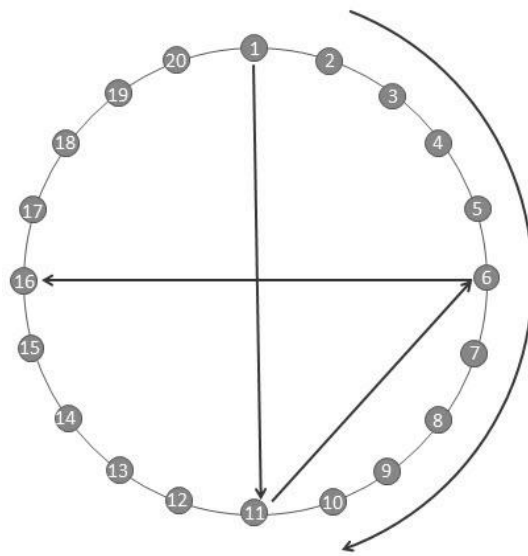
a)



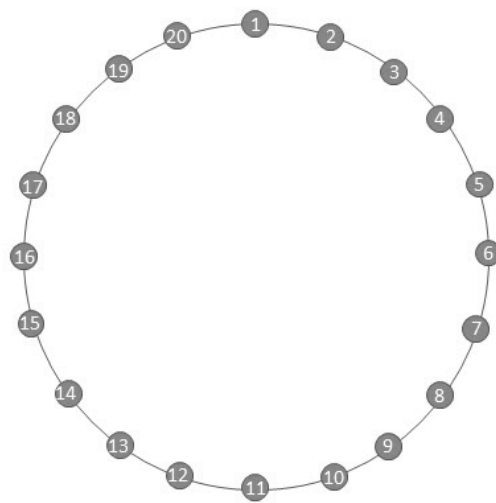
b)



c)



d)



e)

Figure 6.4. Assembly patterns on a joint with 20 bolts a) star assembly pattern 1: 1-11-6-16→3-13-8-18→5-15-10-20→2-12-7-17→4-14-9-19 b) star assembly pattern 2: 1-11-6-16→2-12-7-17→3-13-8-18→4-14-9-19→5-15-10-20 c) circular pattern: 1-2-3-4-5-6-7-8-9-10-11-12-13-14-15-16-17-18-19-20 d) star-circular pattern: 1-11-6-16→2-3-4-5-7-8-9-10-12-13-14-15-17-18-19-20 e) enter assembly pattern

Finally, it should also be pointed out that, apart from the pictures, every cell is updated automatically when any parameter is modified. For instance, starting from the status of Figure 6.1, the NPS, the number of passes and the assembly pattern will be varied. As a result, the status of Figure 6.5 is obtained and, as can be seen, changing the NPS, the number of bolts has been updated automatically and the SCHD cell has become blank (this is because this particular NPS-class combination does not have different SCHDs). On the other hand, there are only 12 bolts and the assembly pattern has only one pass, so the cells of the lower part that correspond to the assembly pattern and are of no use, have been marked with black lines also, as they have been disabled in order to avoid user data entry. It can be also seen how the picture of the assembly pattern has also been updated automatically.

Once the input data is established, the “calculate tightening loads” button must be pressed to obtain the bolt tightening loads. Assuming that the input data of Figure 6.1 are used, the results of Figure 6.6 are obtained. As can be seen, one table indicates the tightening loads that should be applied in the first pass and in the second pass in order to obtain a uniform final load of 350 kN at the end of the tightening sequence. The tightening loads are also shown in a graph.

Next, the application automatically generates two reports which can be printed or saved by the user when the obtained results are relevant. Both reports have the same information but with a different format, so the user can choose between them according to their wishes or requirements. The first report, called “Report_O1”, is shown in Figure 6.7. As can be seen, this is a very visual report which shows the input data of Figure 6.1, the results of Figure 6.6 and an explanatory text box which explains the obtained results. On the other hand, Figure 6.8 shows the second report called “Report_O2”. This report provides the same information, but it does not show the graph of results.

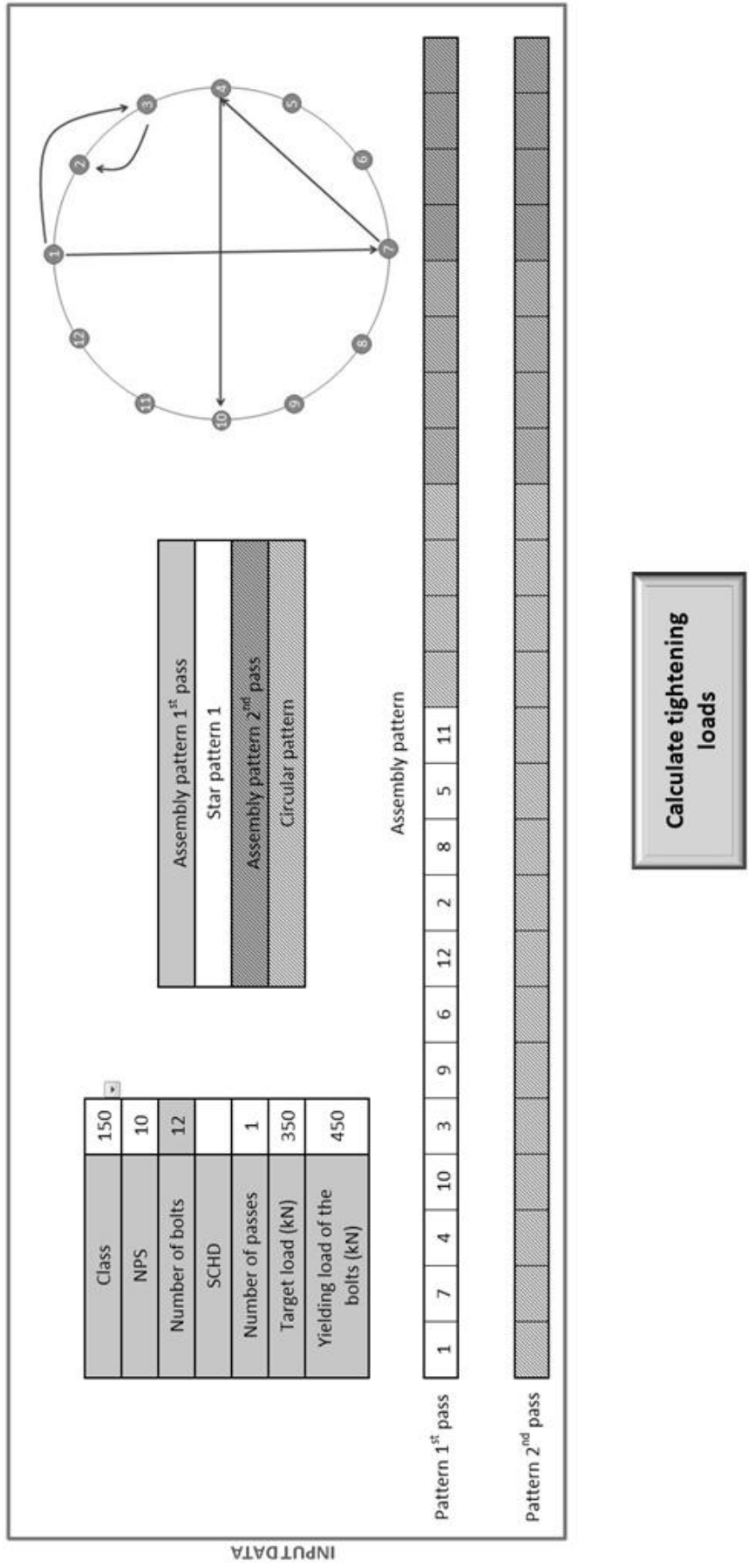


Figure 6.5. Update of the input data when several parameters are altered

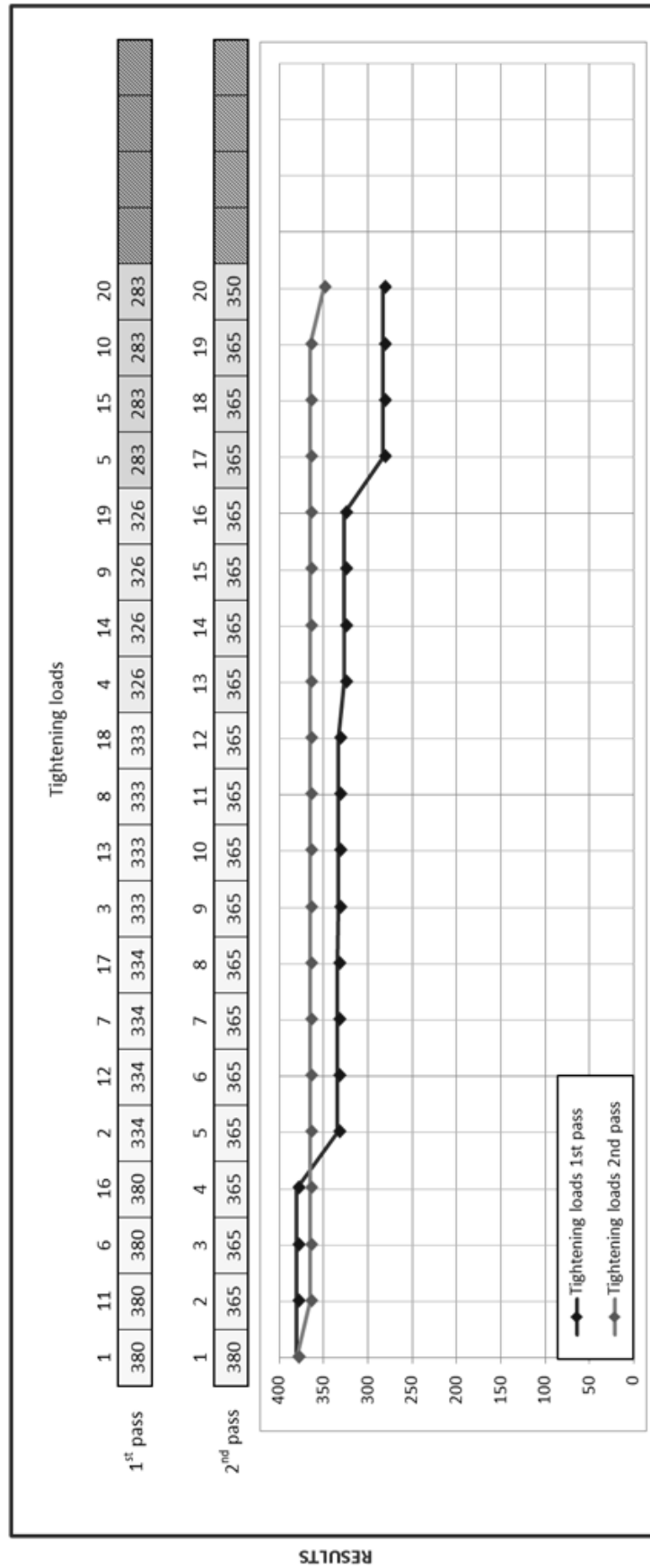


Figure 6.6. Results obtained in the optimization section introducing the input data of Figure 6.1

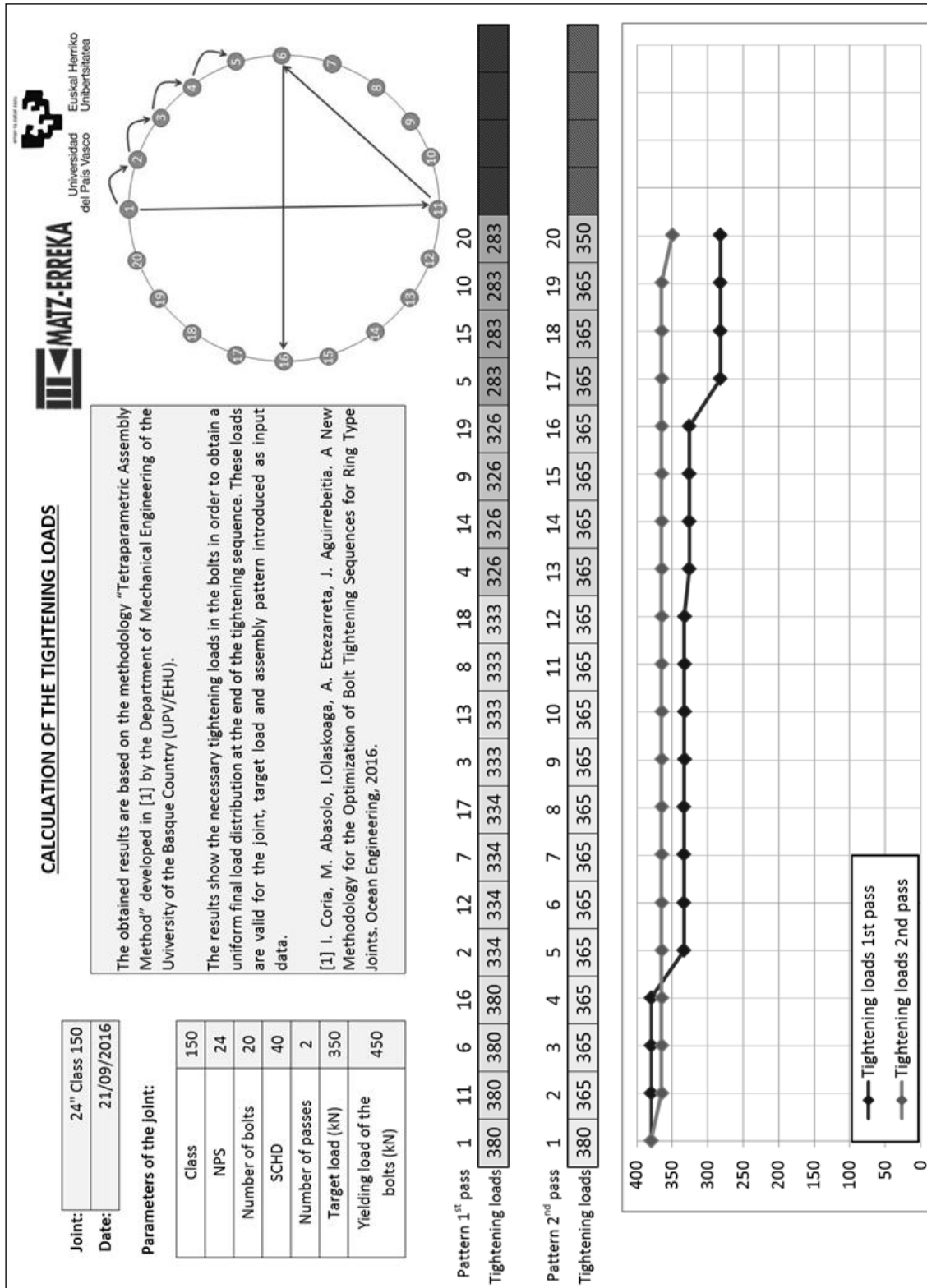


Figure 6.7. Report_O1 of the application

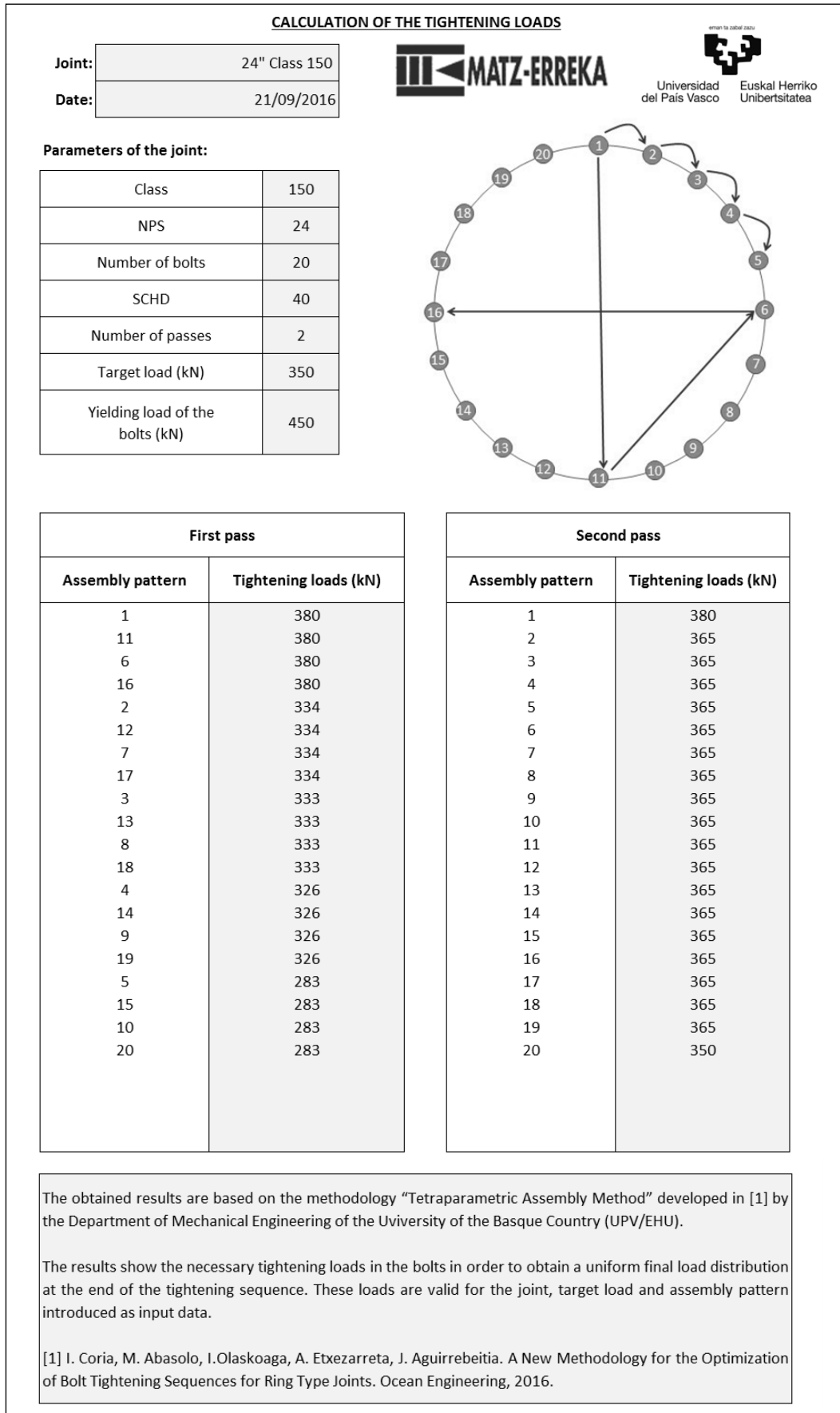


Figure 6.8. Report_O2 of the application

3. SIMULATION SECTION OF THE APPLICATION

As mentioned above, the simulation section is exactly the opposite of the optimization section, so in this section, the input data will be the tightening loads and the obtained results will be the final load distribution on the bolts. Accordingly, equations (3.1) and (3.7) explained in Chapter 3 must be used. Figure 6.9 shows the input data of the simulation section. As can be seen, it is very similar to the optimization section of Figure 6.1, but with the difference being that this one does not include the box to enter the target load. Instead there are two tables to enter bolt tightening loads.

The “Import results from optimization” button can also be seen. This button is used to enter the obtained results as input data in the optimization section. As will be later explained, this can be extremely useful in some situations. In this example, it can be seen that the results of Figure 6.6 are the input data of Figure 6.9, because the data was imported from the previous optimization.

Once the input data has been introduced, the “Calculate final loads” button is pressed and the bolt final load distribution is obtained. Figure 6.10 shows the results for this example, and, as expected, the final load is completely uniform. This is because the tightening loads obtained in the previous section correspond with a uniform final load so, if the results from optimization are imported and any data is modified, the final load that is obtained in the simulation section is obviously uniform. When the results are obtained, the application generates two reports called “Report_S1” and “Report_S2”. The first report is shown in Figure 6.11, and, as can be appreciated, it is very similar to “Report_O1”, which is shown in Figure 6.7. The second report is shown in Figure 6.12 and it is very similar to the report of Figure 6.8. The selection between both reports is left again in the hands of the user.

The simulation section was generated for when the tightening loads obtained in the optimization process are very variable, in other words, when the tightening load of most bolts is different. In this situation, it may be of interest to tighten bolts with a similar tightening load to the same load level in order to group the tightening load of every bolt in only three or four different load levels. Thus, the assembly process is considerably simplified. This concept will be explained in detail in the illustrative example of the next section.

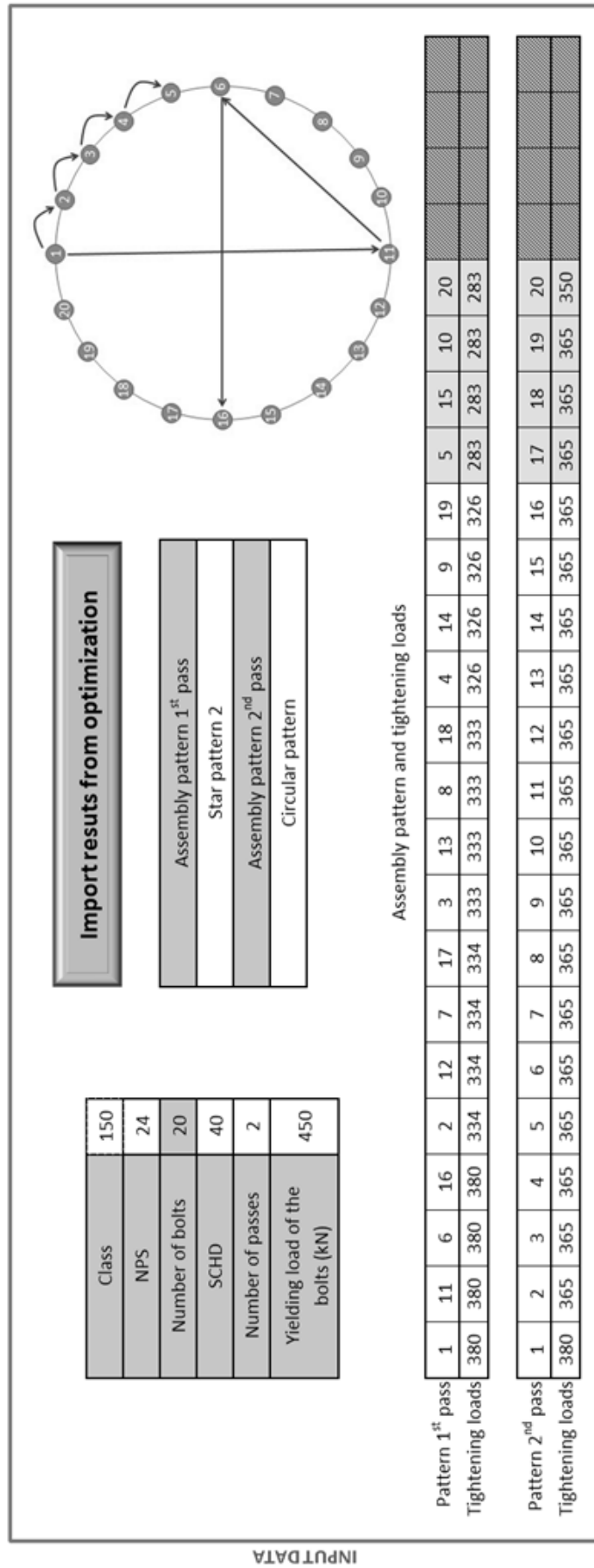


Figure 6.9. Input data of the simulation section

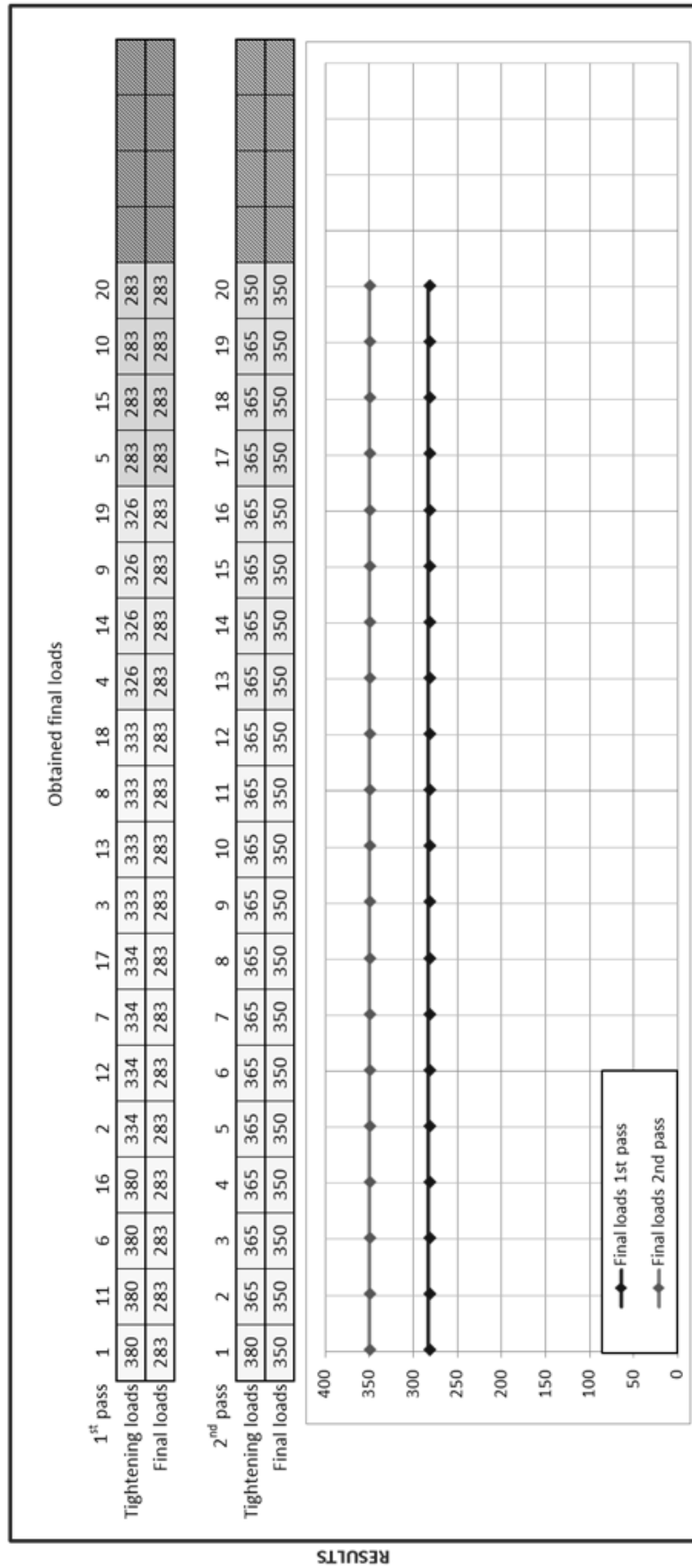


Figure 6.10. Results obtained in the simulation section with the input data of Figure 6.9

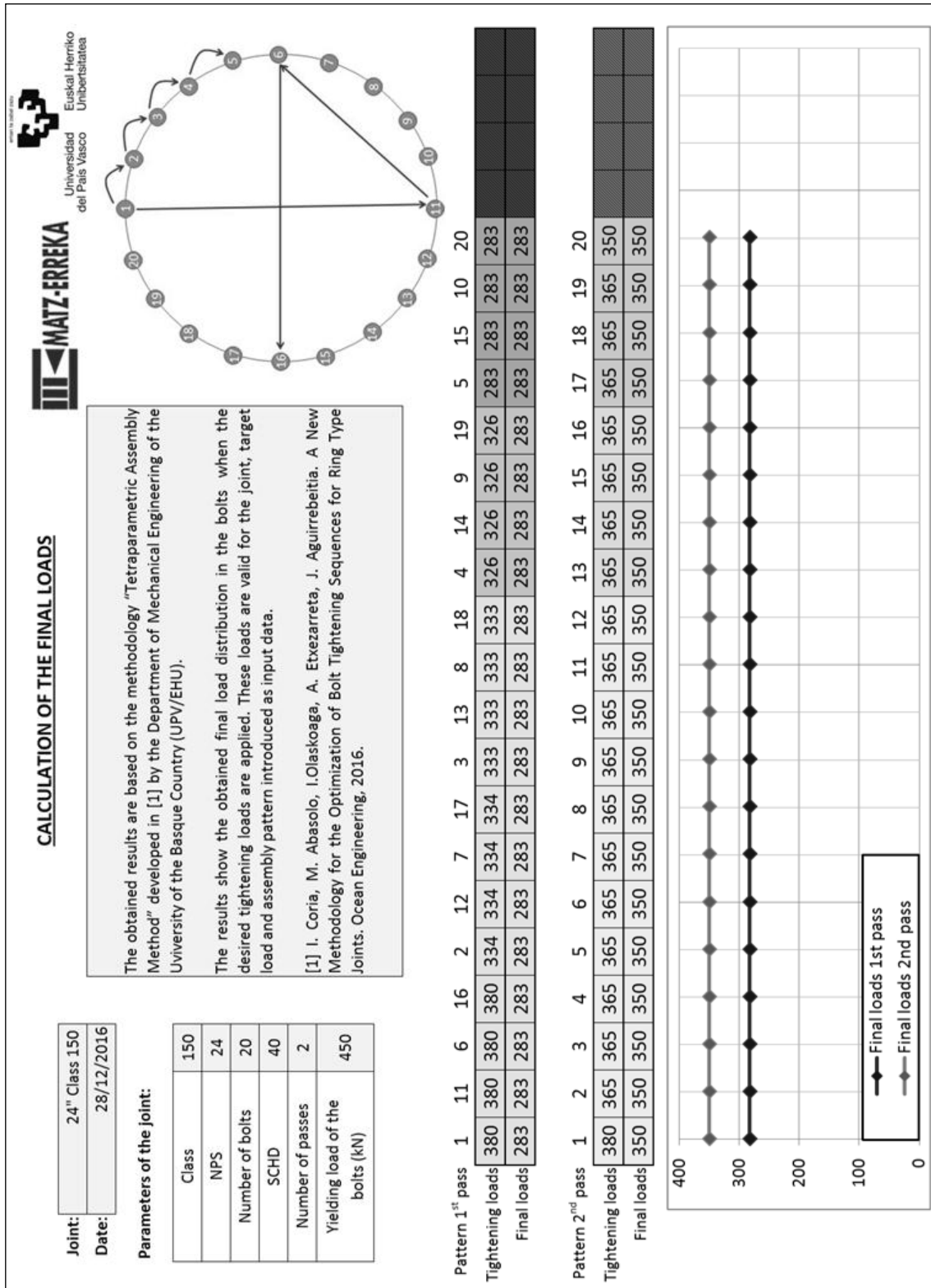


Figure 6.11. Report_S1 of the application

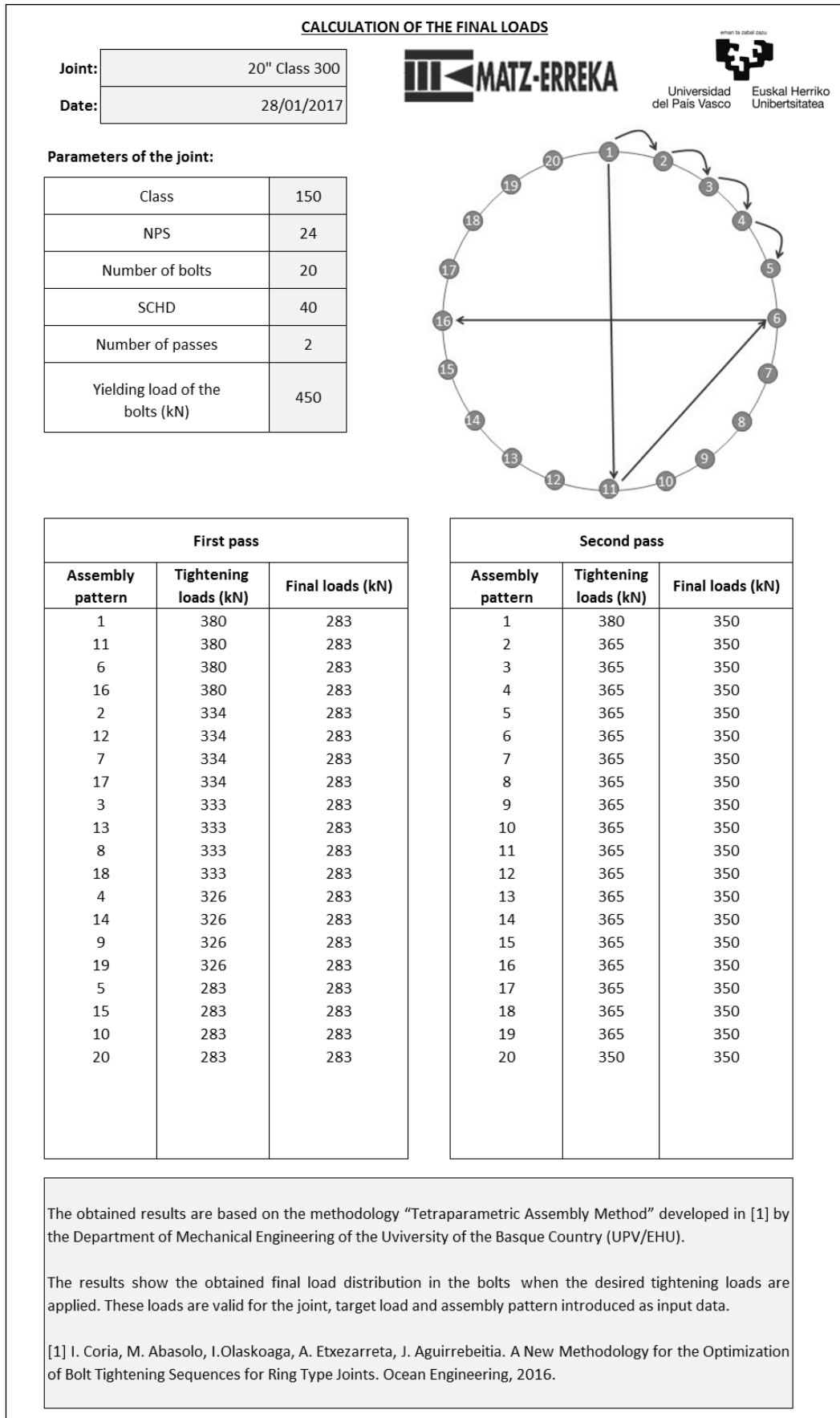


Figure 6.12. Report_S2 of the application

4. ILLUSTRATIVE EXAMPLE

Assume that a pipeline of several kilometers is going to be built joining the pipe sections with RTJs of NPS 20", Class 300 and SCHD 60. Due to the high number of bolted joints, it is of interest to obtain an optimized tightening sequence which decreases the assembly time of each joint as much as possible. To this end, the application explained in this Chapter will be used. As initial data, it is known that the bolts have a yielding load of 450 kN and that the target load is 350 kN.

First of all, the input data is entered in the application. Regarding to the number of passes, a single-pass tightening sequence is going to be selected because the assembly time required is obviously less than the two-pass tightening sequence. Also, the star-circular assembly pattern will be used due to its simplicity. Thus, the first four bolts are preloaded following a star pattern in order to appropriately fix the joint and the remaining bolts are later preloaded following a circular pattern (as in Figure 6.4d but a joint with 24 bolts). When bolts are tightened following a circular pattern, the gasket could have local high loads during the tightening sequence. Therefore, once the tightening sequence is defined, in order to avoid leakages, a Finite Element model or an experimental set up should be employed to check that applying the obtained tightening sequence, the gasket shows no signs of excessive plastic deformations.

Once every input data has been entered, the "Calculate tightening loads" button is pressed. Then, the Figure 6.13 warning is displayed on the application, which points out that, with the entered input data, the tightening load of several bolts exceeds bolt yielding load (see the load of the first four bolts in Figure 6.14, higher than the 450 kN of the yielding load), and therefore a two-pass tightening sequence should be performed.

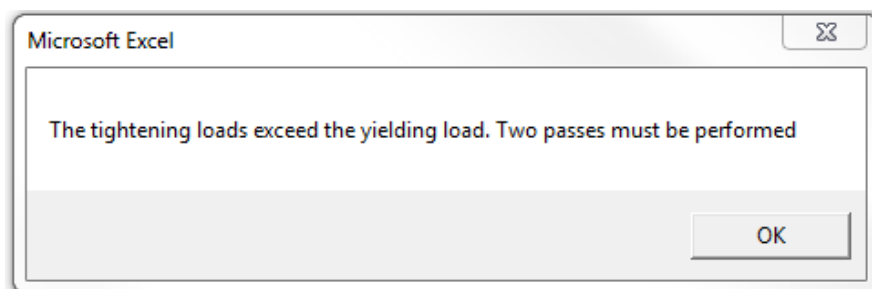


Figure 6.13. Warning message when the tightening loads exceed bolt yielding load

In order to obtain a simple tightening sequence, in the second pass, the circular assembly pattern is selected (the other parameters were not modified). Accordingly, the results of Figure 6.15 are obtained, and, as can be seen, any of the tightening loads exceed bolt yielding load. Nevertheless, as mentioned previously, a check should later be performed to ensure that when applying the obtained optimized tightening sequence the gasket does not have very high plastic deformations.

Observing the tightening loads that must be applied in the first pass, it can be appreciated that the values are almost all different between them. This complicates the assembly process significantly, and increases the probabilities of mistakes being made due to an oversight. In this sense, it is of interest to slightly modify the tightening loads in order to obtain an easier tightening sequence from the point of view of the assembler. For that purpose the simulation section is used.

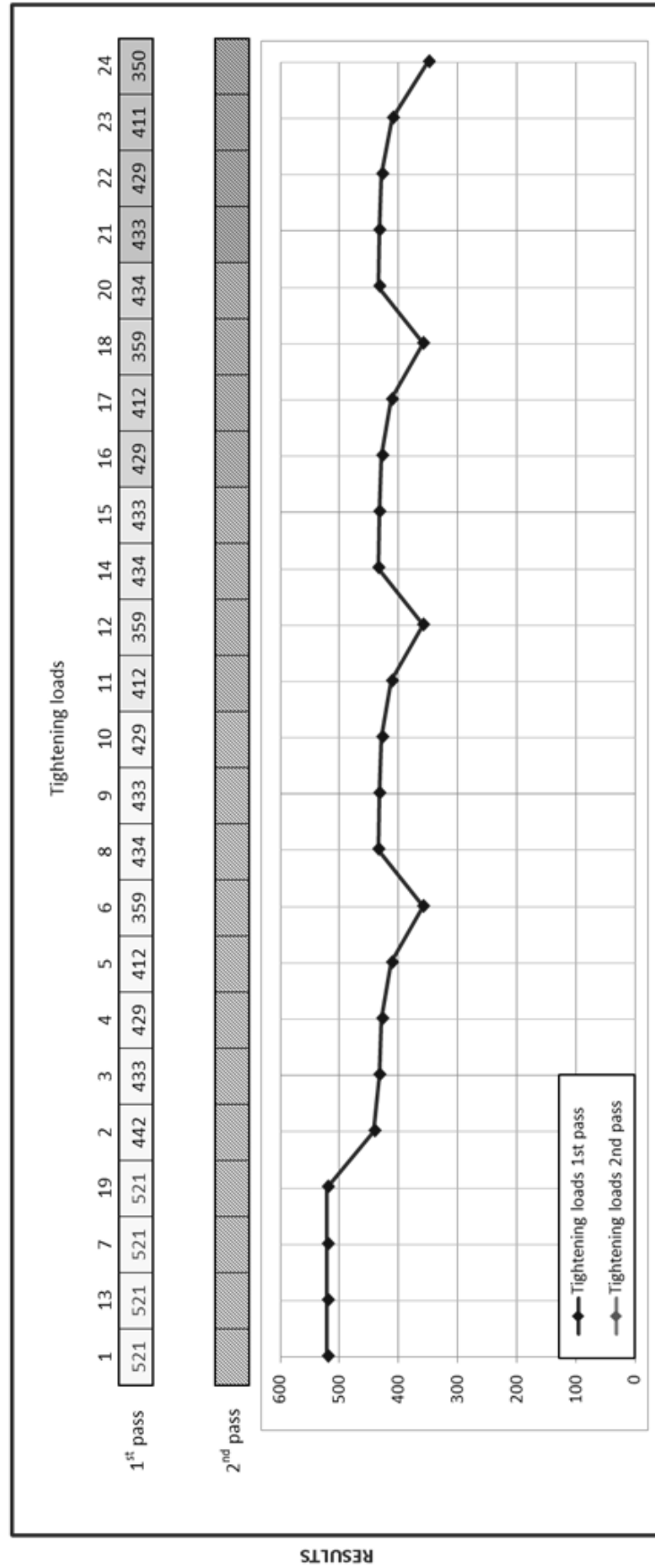


Figure 6.14. The results obtained in the illustrative example for the one-pass tightening sequence in the optimization section

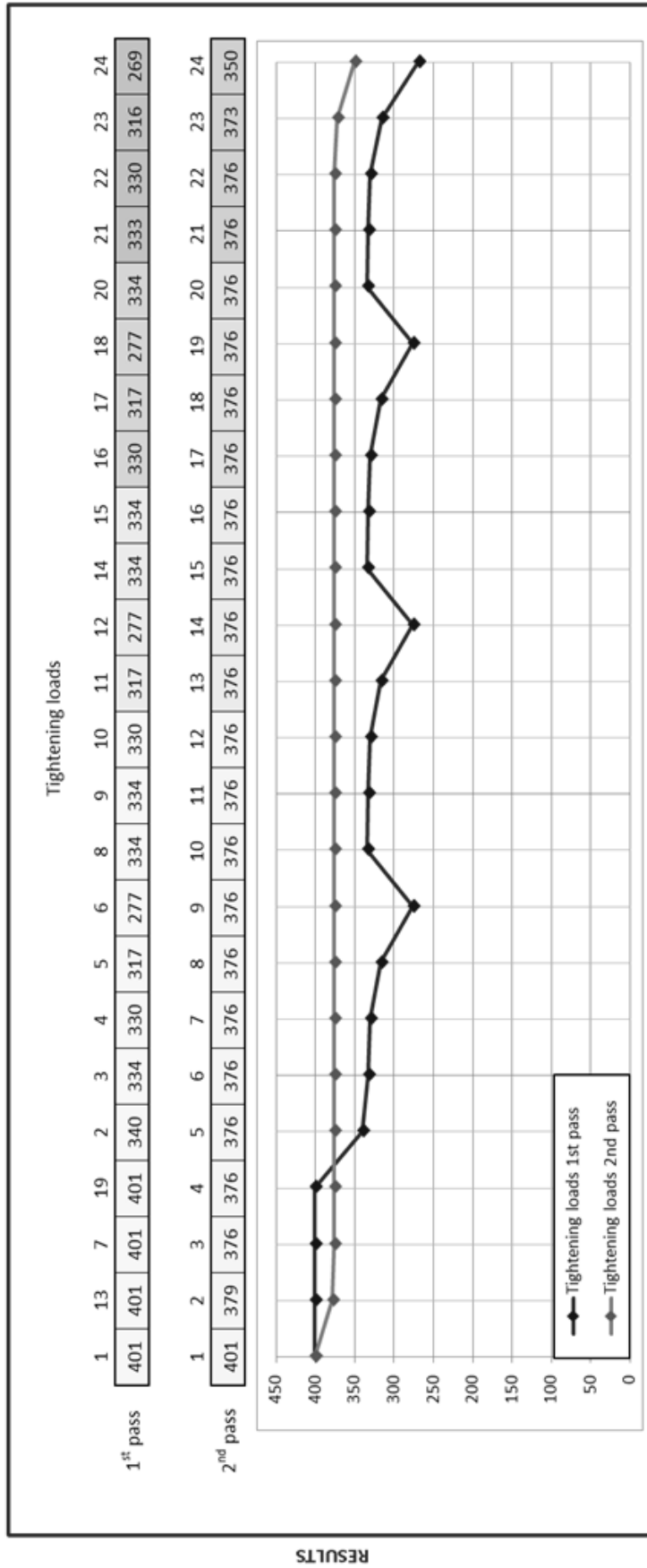


Figure 6.15. The results obtained in the illustrative example for the two-pass tightening sequence in the optimization section

The results obtained in the optimization section have been imported to the simulation section using the “Import results from optimization” button (see Figure 6.9). Thus, the manual entering of data is avoided. Finally, the tightening loads should be modified in order to simplify the tightening sequence as much as possible.

Starting with the first pass (Figure 6.15), it can be appreciated that the first four bolts have the same initial load and it is so far from the initial load of the other bolts, so the initial load of this bolts is not going to be modified. The load level of bolts 2, 3, 4 and 5 is very similar, so it is possible that tightening these bolts to an intermediate load of 330 kN will result in the final load still being fairly uniform and therefore the results are still acceptable. The same occurs with the bolts from 8 to 11, from 14 to 17 and from 20 to 23, so these bolts could be also tightened to 330 kN. Finally, to conclude with the first pass, bolts 6, 12, 18 and 24 could be tightened to 277 kN. Thus, the first pass has been considerably simplified, having only three different levels of load, as shown in Figure 6.16: 401 kN, 330 kN and 277 kN.

Regarding the second pass, the simplification is much easier because the load level of almost every bolt is the same before any modifications. Nevertheless, it can be simplified slightly more assuming that the level of load from bolt 2 to bolt 23 is 376 kN. Thus, in the second pass there are also three different levels of load: 401 kN for the first bolt, 376 kN for the bolts from 2 to 23, and 350 kN for bolt 24. Once the data has been entered in the application, the window with the input data is as follows: Figure 6.16.

Thus, after pressing the “Calculate final loads” button, the final load distribution of Figure 6.17 is obtained, where it can be appreciated how, at the end of the second pass, the load distribution is almost uniform; the average load is 350 kN and the standard deviation 1.56 kN. Therefore, it can be stated that an optimum tightening sequence has been achieved in which the assembly process has been simplified as much as possible, and which also provides a very uniform final load distribution. Given the satisfactory results, “Report_S2” has been generated to save and/or print the results when required (see Figure 6.18).

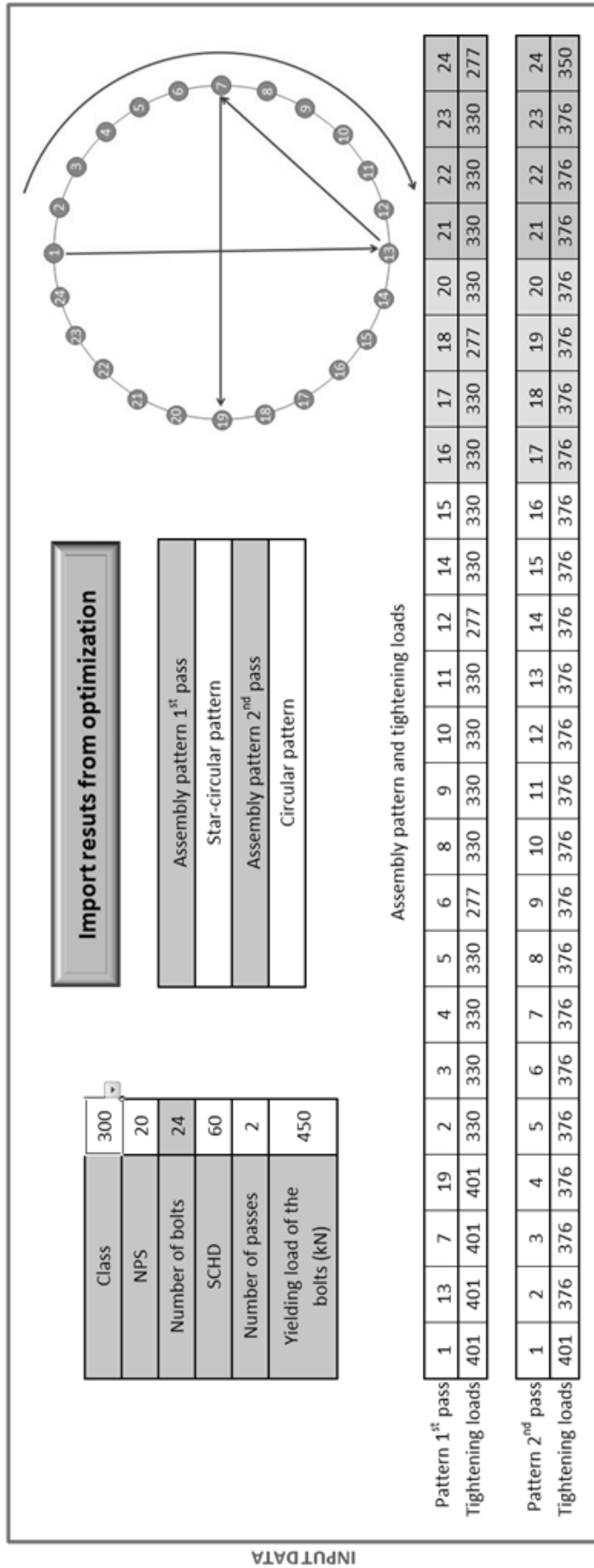


Figure 6.16. Input data in the simulation section of the illustrative example

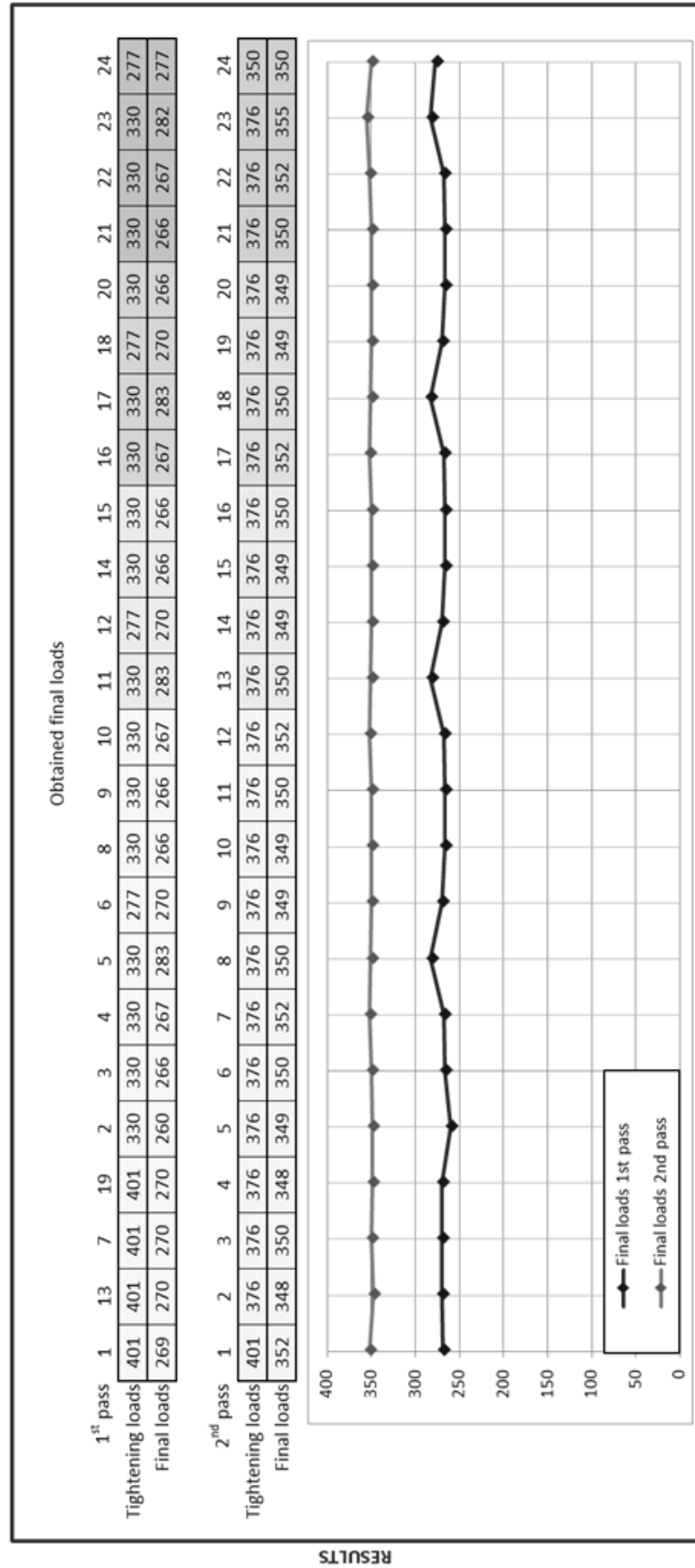


Figure 6.17. The results obtained in the simulation section of the illustrative example

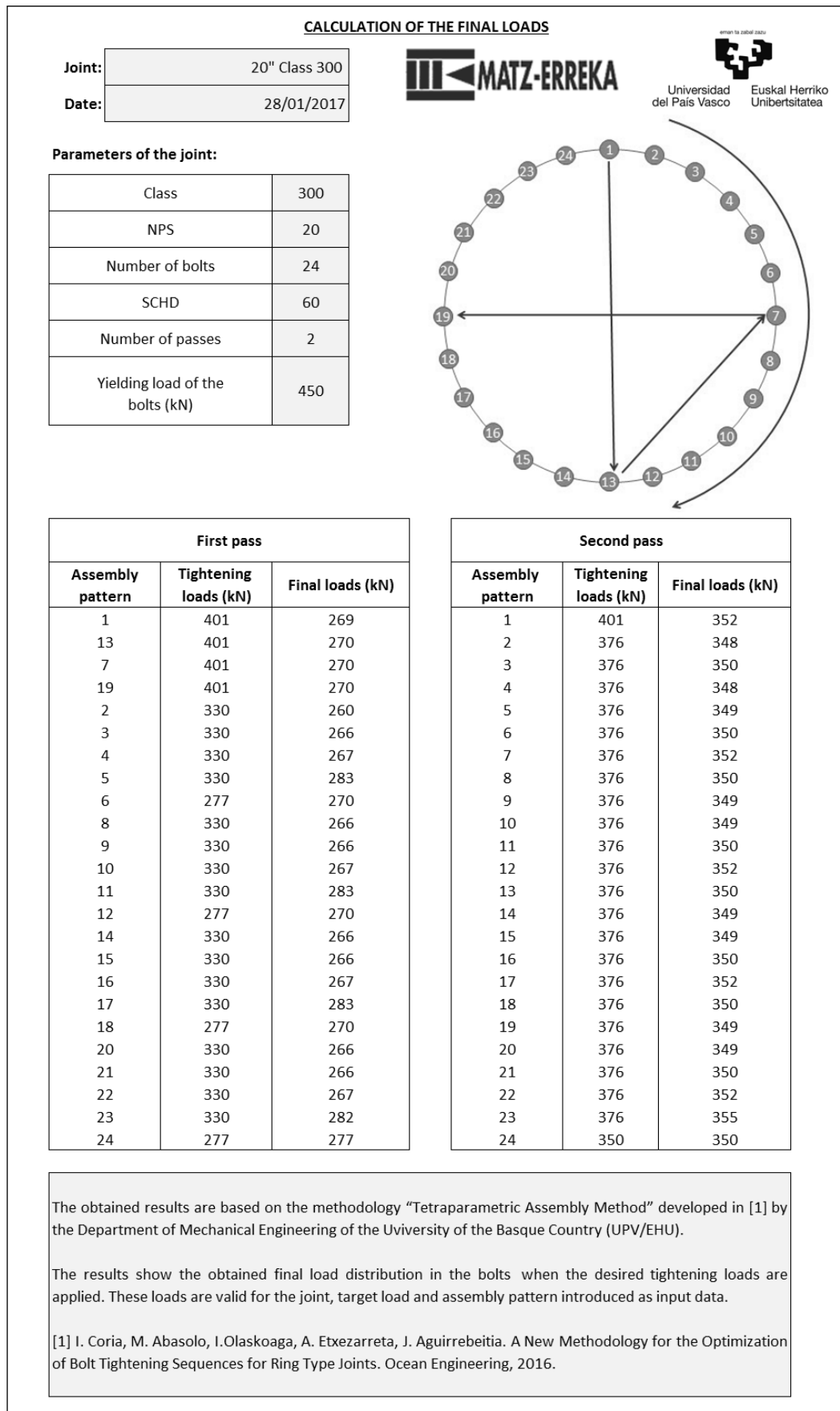


Figure 6.18. Report_S2 with the obtained final results in the illustrative example

**CHAPTER 7. ALTERNATIVE OPTIMIZATION
METHODOLOGY FOR OTHER TYPES OF
JOINTS**

1. INTRODUCTION

Up to this point in the Doctoral Thesis, a new method has been developed to study optimal tightening sequences in ASME RTJs. However, this method is not valid for other types of joints. In this sense, a new method is presented in this Chapter to study optimal tightening sequences in other joints.

A FE model based on the superelements technique is presented. Thus, the degrees of freedom of the model are considerably reduced and therefore so are the computational cost. Once the model is defined, the EICM is programmed, which is solved in a few seconds due to the low cost of the new model. The new optimization process has also been experimentally validated with a new test bench. It must be remarked that this technique proved not to be as efficient as the TAM for RTJs because contact nonlinearity of this type of joint has a great influence in its behaviour during the tightening sequence.

To this regard, this Chapter first explains the superelements technique, followed by an explanation of the new superelement-based model. Then, two different test benches used for validation purposes are described, and finally the validation results are presented. The experimental tests were carried out in the university “École de technologie supérieure” of Montreal, Canada.

2. BASICS OF THE SUPERELEMENTS TECHNIQUE

As is well known, the superelements technique consists of condensing a group of Finite Elements into a unique element called a superelement [Aba'17; Kom'09; Pla'15]. This technique is particularly useful when a large structural system is studied that is made up of different modules, usually with one of them being the main module to be studied. As will be later explained, the main advantage of this method is that it is possible to considerably reduce the cost of the analysis.

As an illustrative example, Figure 7.1 shows the simplified Finite Element model of an aircraft (the same concepts will be later used for the bolted joint). The plane is the large structural system which is composed of four modules: the airframe, the two wings and the tail. It is assumed that only the results of the airframe will be studied. Therefore, as explained above, in the

superelements technique, the airframe will be the main module, while the tail and the wings will be secondary modules that will be replaced by a superelement, as shown in Figure 7.2.

When a superelement is generated, the nodes which are to remain must be selected, as well as which ones will be eliminated; the nodes that remain on the model are known as master nodes. The master nodes must be the nodes that connect the superelement with the rest of the model, and the nodes that have an external load or boundary condition applied. Comparing Figures 7.1 and 7.2, if the original model of the wing has 84 nodes, the superelement that replaces it only has 18 nodes (the master nodes); the same occurs with the tail of the plane.

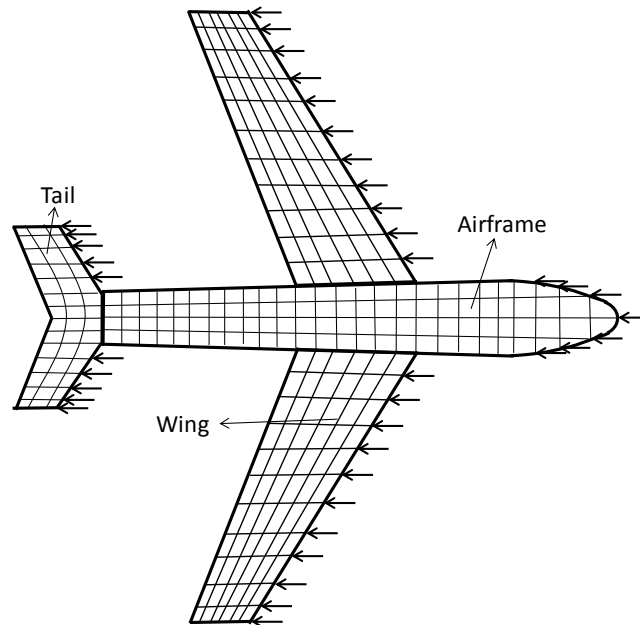


Figure 7.1. Conventional Finite Element model of the plane

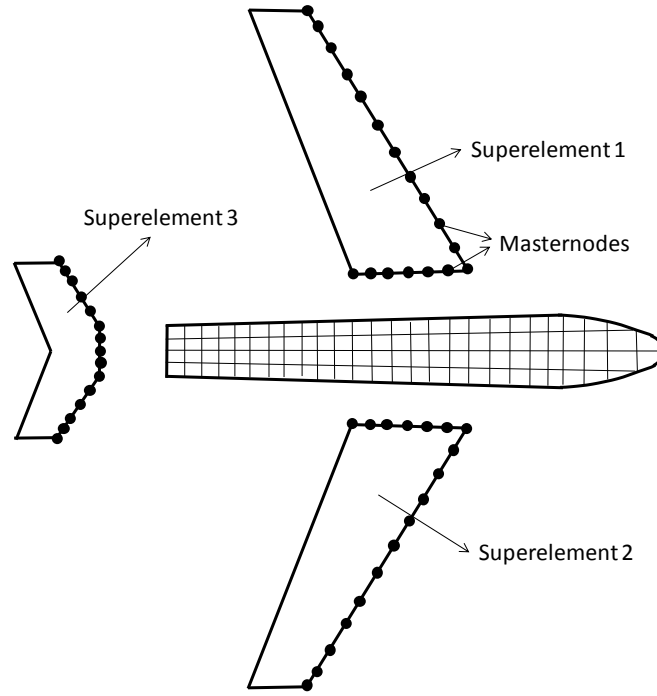


Figure 7.2. Finite Element model of the plane based on the superelements technique

The stiffness matrix of the superelement is calculated from the static equilibrium equation of the module that it is replacing. For example, where $[K]^{wing}$ is the stiffness matrix of the Finite Element model of the wing of Figure 7.1, and $\{\delta\}^{wing}$ and $\{F\}^{wing}$ nodes displacements and loads of the model, the equation is:

$$\{F\}^{wing} = [K]^{wing} \cdot \{\delta\}^{wing} \quad (7.1)$$

The matrix and the vectors of equation (7.1) can be reordered to locate the degrees of freedom of the master nodes in the first rows and columns:

$$\begin{Bmatrix} \{F_m\}^{wing} \\ \{F_o\}^{wing} \end{Bmatrix} = \begin{bmatrix} [K_{mm}]^{wing} & [K_{mo}]^{wing} \\ [K_{om}]^{wing} & [K_{oo}]^{wing} \end{bmatrix} \cdot \begin{Bmatrix} \{\delta_m\}^{wing} \\ \{\delta_o\}^{wing} \end{Bmatrix} \quad (7.2)$$

In the equation, the subscript m refers to the master nodes degrees of freedom of the superelement, while the subscript o refers to the other nodes of the original model. The elements of vector $\{F_o\}^{wing}$, refers to the nodes that are not a master node, and therefore, their value is null because, as explained before, the external loads and the boundary conditions are always applied in a master node. Thus, performing equation (7.2):

$$\begin{cases} \{F_m\}^{wing} = [K_{mm}]^{wing} \cdot \{\delta_m\}^{wing} + [K_{mo}]^{wing} \cdot \{\delta_o\}^{wing} \\ 0 = [K_{om}]^{wing} \cdot \{\delta_m\}^{wing} + [K_{oo}]^{wing} \cdot \{\delta_o\}^{wing} \end{cases} \quad (7.3)$$

From the second equation of (7.3):

$$\{\delta_o\}^{wing} = -([K_{oo}]^{wing})^{-1} \cdot [K_{om}]^{wing} \cdot \{\delta_m\}^{wing} \quad (7.4)$$

Replacing equation (7.4) in the first equation of (7.3):

$$\begin{aligned} \{F_m\}^{wing} = & \left([K_{mm}]^{wing} - [K_{mo}]^{wing} \cdot ([K_{oo}]^{wing})^{-1} \right. \\ & \left. \cdot [K_{om}]^{wing} \right) \cdot \{\delta_m\}^{wing} \end{aligned} \quad (7.5)$$

Equation (7.5) relates to the loads applied in the master nodes with the displacement of those nodes. Therefore, equation (7.5) is the static equilibrium equation of the wing superelement of Figure 7.2. The stiffness matrix of the wing superelement $[K]_{SE}^{wing}$, is therefore:

$$\begin{aligned} [K]_{SE}^{wing} = & [K_{mm}]^{wing} - [K_{mo}]^{wing} \cdot ([K_{oo}]^{wing})^{-1} \\ & \cdot [K_{om}]^{wing} \end{aligned} \quad (7.6)$$

The same procedure has to be applied to obtain the superelement of the aircraft tail. Thus, when the Finite Element model of Figure 7.2 is solved, the stiffness matrix will be smaller because the degrees of freedom that do not belong to a master node have been deleted. Therefore, the computational cost is minimized considerably.

3. MODEL DEVELOPED BASED ON THE SUPERELEMENT TECHNIQUE

To generate the FE model based on the superelement technique, firstly, a conventional FE model was performed and subsequently simplified. Thus, a NPS 4" and Class 900 raised face joint was modelled with a non-linear solid metal gasket covered with graphite. Figure 7.3 shows the conventional FE

model. In this model the gasket was modelled with the INTER195 element, because it is able to model linear and non-linear materials (the curve is defined via points). The contact defined between the flange and bolts in order to provide continuity to the model should also be noted. A pretension section was applied on the bolts to control bolt load level, as explained in Chapter 2.

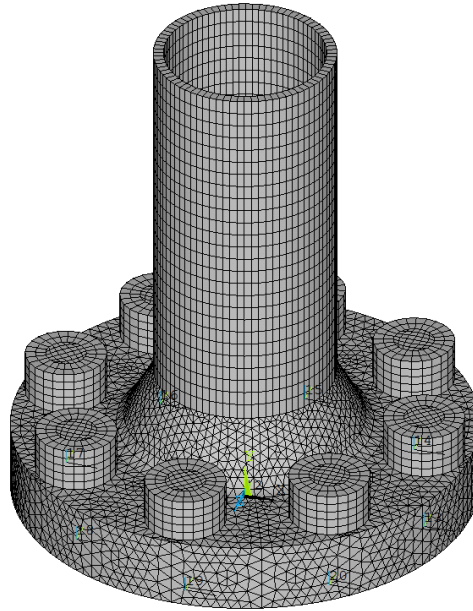


Figure 7.3. Conventional Finite Element model

To simplify this model, firstly, the bolt bodies were modelled by beam elements (with the same stiffness as the bolts) attached to the flange via rigid beams simulating bolts heads, as shown in Figure 7.4. This simplification can be extensively found in specialist literature [Aba'12; Aba'14; Agu'12].

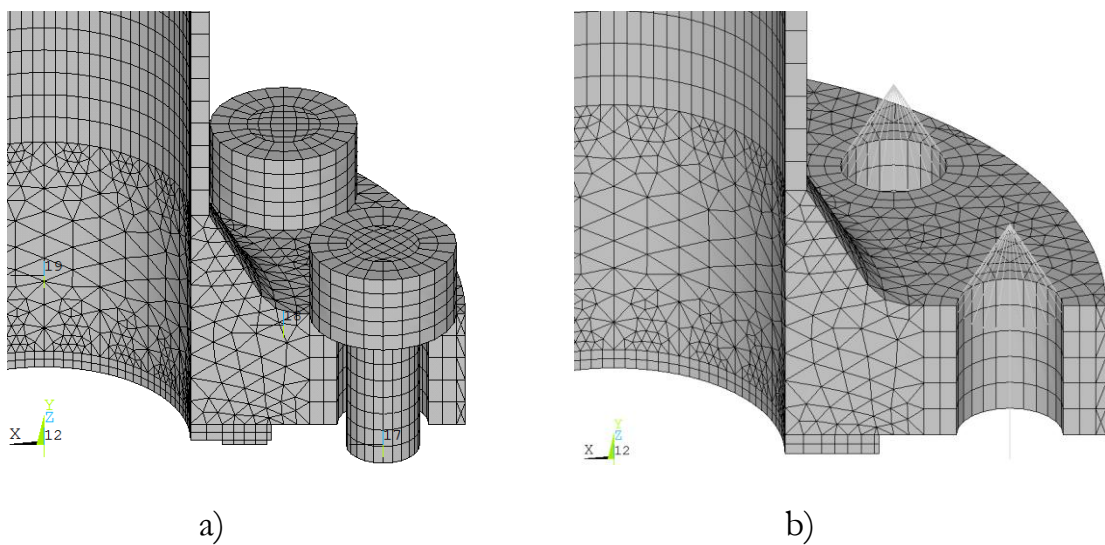


Figure 7.4. Modelled bolts in the a) conventional model b) simplified model

Once the bolts were simplified, the superelement was generated which was made up of the flange and the rigid beams of the bolts, so the gasket and the beam of the bolts were not included inside the element. The superelement can be only modelled with linear elements, so it is not possible to model the gasket as a superelement. On the other hand, in order to control the pretension section of the bolts, these cannot be superelements either. Thus, the superelement of Figure 7.5 was obtained. As master nodes, the nodes that are connected to the bolt beams were selected (which have six degrees of freedom, three of rotation and three of translation), and the nodes that are connected to the gasket (which have only one degree of freedom, the vertical translation). Figure 7.6 shows the master nodes of the superelement. As a result, a model with 1,400 degrees of freedom was obtained; much less than the 300,000 degrees of freedom of the original model. Accordingly, the analysis cost was reduced more than 30 times.

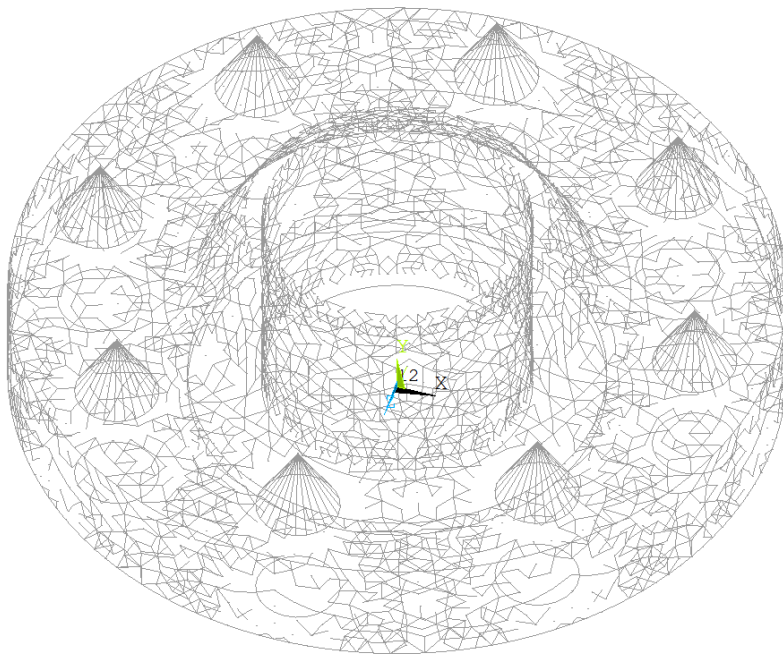


Figure 7.5. Superelement of the flange

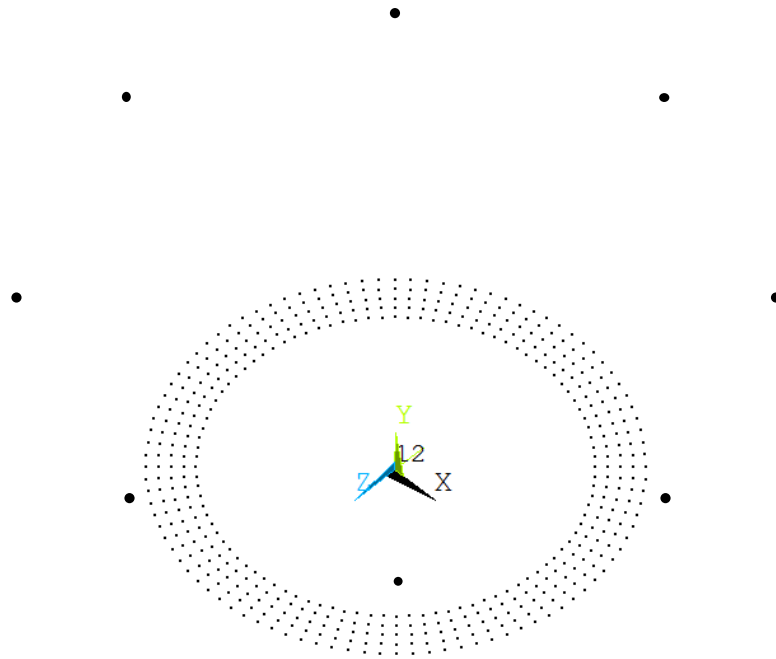


Figure 7.6. Superelement master nodes (thicker nodes 6 DOF, thinner nodes 1 DOF)

As a result of these simplifications, the efficient model of Figure 7.7 was obtained, which can simulate tightening sequences with a significantly lower cost.

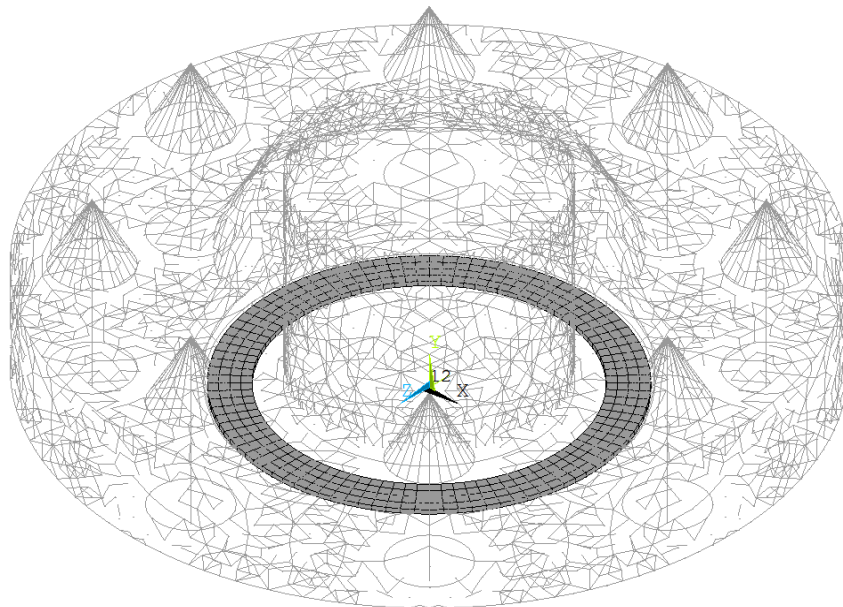


Figure 7.7. Finite Element model based on the superelement technique

4. TEST BENCHES

To validate the Finite Element model developed in the previous section, two different test benches were necessary. On the one hand, the ROTT (Room Temperature Tightness) machine was necessary in order to obtain the stress-deformation curve of the gasket and thus apply that behaviour in the Finite Element model. On the other hand, the experimental set up of the joint was necessary in order to validate the results obtained from the tightening sequences. Both test benches are now explained in detail.

4.1 ROTT MACHINE

Figure 7.8 shows the ROTT machine used in [Gri'13 ; Zhu'17]. This machine is able to measure the gasket stress (with the strain gages that are installed on the bolts), the deformation of the gasket (with the LVDT's that can be seen in Figure 7.8), the internal pressure (with a pressure gage) and the leakages of the internal gas which is usually helium (different instruments depending on the flow rate). For this study, a gas does not need to be inserted because only the compression curve of the gasket is needed.

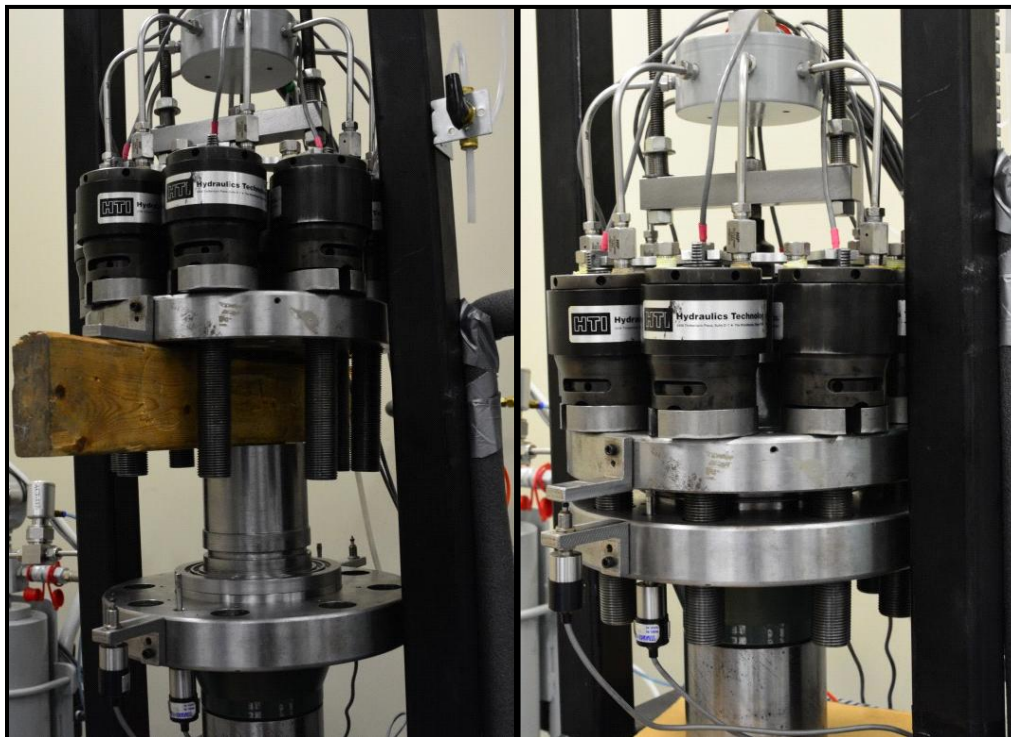


Figure 7.8. ROTT machine

4.2 EXPERIMENTAL SET UP OF THE JOINT

The validation of the model based on the superelements technique was performed monitoring bolts tension in the experimental set up of Figure 7.9. It consists of two NPS 4" and class 900 flanges, with the face and welding neck also raised. The bottom flange is welded to a pipe which is welded to the floor [Zhu'17].

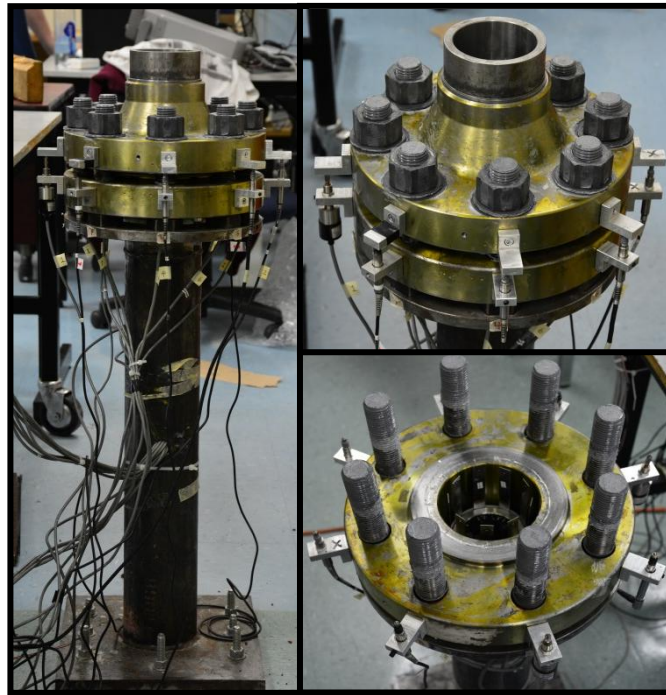


Figure 7.9. Experimental set up of the joint

Several measuring devices are installed in the experimental set up in order to record every result. On the one hand, every bolt is fitted with a strain gage calibrated on an MTS servo-hydraulic tensile machine which measures and saves the load level of the bolt continuously. On the other hand, as can be seen in Figure 7.9, eight LVDTs are installed in order to measure the deformation of the joint during the tightening sequence. A micrometer is used to calibrate the eight LVDT sensors prior to testing. All instruments were connected to a data acquisition system which was connected to a computer. Finally, it must be mentioned that the bolts were tightened with the torque multiplier of Figure 7.10, which is capable of transmitting up to 1600 N.m. As mentioned previously, a solid metal with facing gasket was selected to carry out the validation (see Figure 7.11)



Figure 7.10. Torque multiplier



Figure 7.11. Solid metal with facing gasket

5. VALIDATION OF THE MODEL

In order to validate the simplified Finite Element model, firstly, the gasket was studied on the ROTT machine and its mechanical properties were obtained. Next, linear and non-linear analyses were performed on the test bench and in the simplified Finite Element model in order to obtain the error related to this model. The whole process is explained in detail in this section.

5.1. MECHANICAL PROPERTIES OF THE GASKET

Prior to performing de compression test, the geometrical dimensions of the gasket were measured with a calliper gauge and a micrometer. Accordingly, the dimensions of the Table 7.1 were obtained.

Geometrical dimensions in millimetres

Inner diameter	123.5
Outer diameter	154.5
Thickness	4.01

Table 7.1. Geometrical dimensions of the gasket prior to the compression test

To perform the compression test, the gasket was placed inside the ROTT machine shown in Figure 7.8, and it was loaded and unloaded to different stress values. During this process, stress and the deformation were measured continuously obtaining the behaviour of Figure 7.12. Thus, the non-linear behaviour of the gasket was obtained. It must be pointed out that the deformations correspond to half of the gasket because, in the Finite Element model, only half of the gasket is modelled (the whole gasket would have double the deformation for the same stress value).

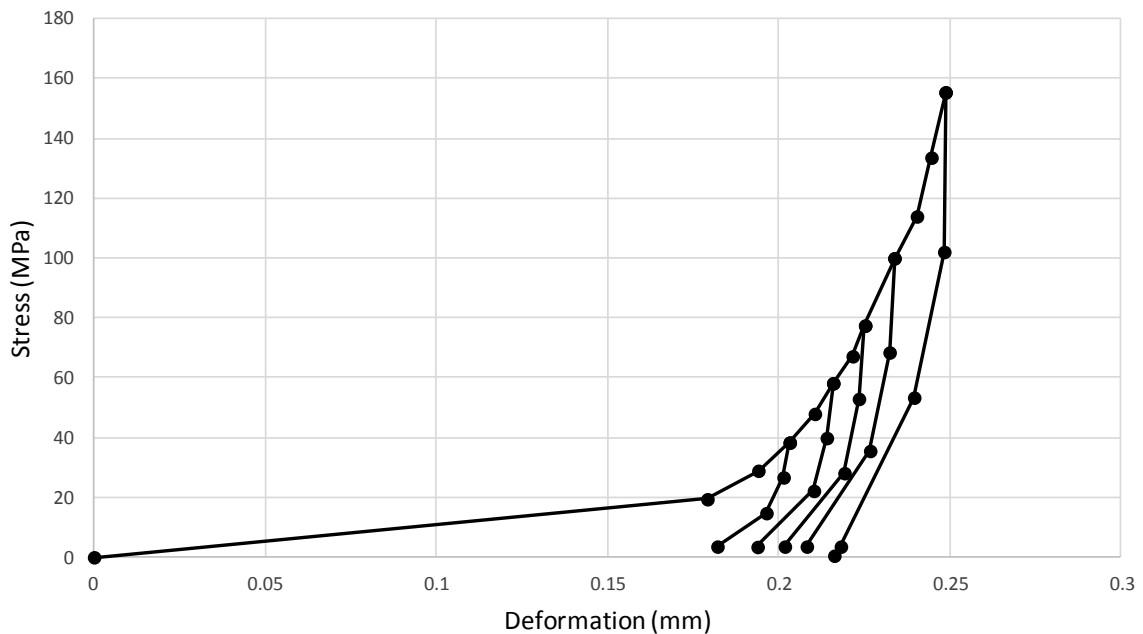


Figure 7.12. Behaviour of the half of the gasket under a compression load

Finally, a linear gasket was required in order to make a first simple validation of the simplified Finite Element model. For that purpose, the gasket was previously compressed because, after all, the non-linear gaskets used to have behaved similar to the one of Figure 7.13. Therefore, if the gasket is compressed to stress “x”, that gasket will have a linear behaviour as long as stress “x” is not exceeded.

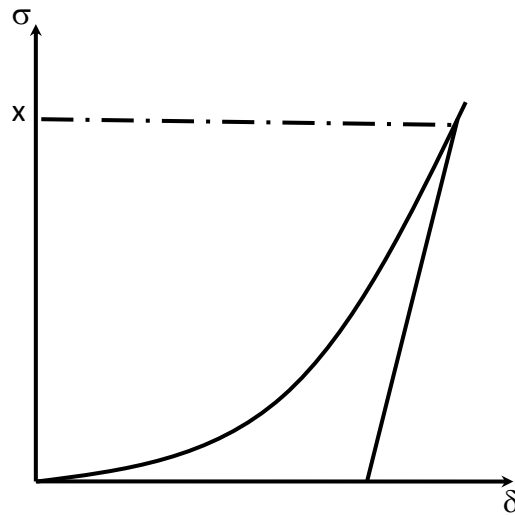


Figure 7.13. Common behaviour of a gasket under a compression load

To this regard, one gasket was compressed several times until the same level of load obtaining the behaviour of Figure 7.14 (black line), where the horizontal axis is the strain of the gasket. As can be seen, the behaviour can be linearly approximated, so, in order to simplify the analysis, it is possible to use the behaviour of the grey line which has a Young modulus of 12,304 MPa. However, it must be taken into account that the previously compressed gasket has suffered plastic deformations, and therefore, the measurements of Table 7.1 are incorrect if the behaviour of Figure 7.14 is used. To this regard, after the compression test, the geometrical dimensions of the gasket were measured again. Table 7.2 shows the obtained results.

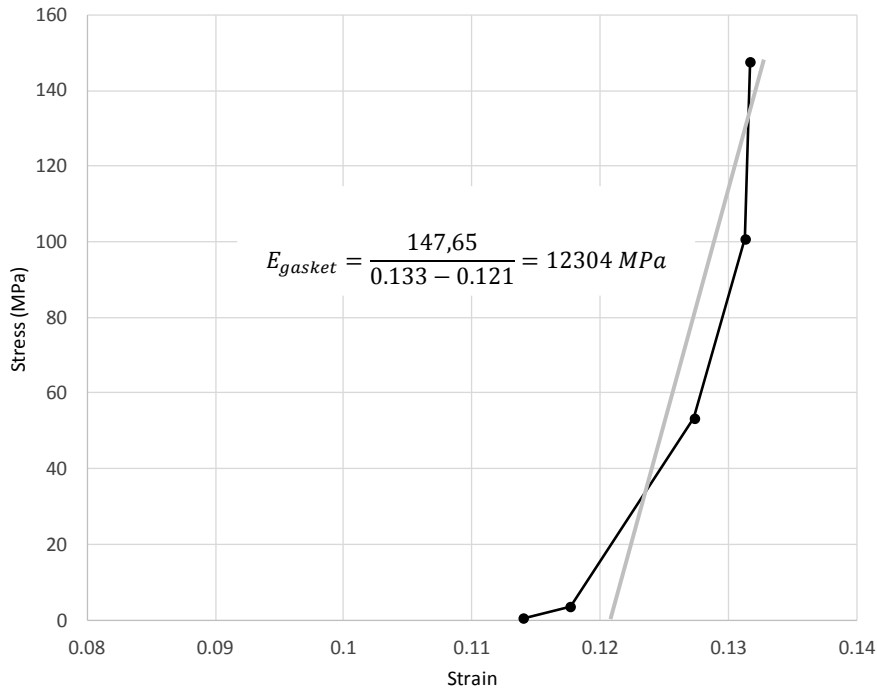


Figure 7.14. Behaviour of a previously compressed gasket (black line) and linear simplification (grey line)

Geometrical dimensions in millimetres

Inner diameter	123.5
Outer diameter	154.7
Thickness	3.59

Table 7.2. Geometrical dimensions of the gasket after the compression test

5.2. VALIDATION WITH LINEAR GASKET

For the linear validation of the model based on superelement technique, the geometrical dimensions of Table 7.2 were used for the gasket, and the Young modulus of 12,304 Mpa. Next, using the EICM and the superelement based model, the initial loads of Figure 7.15 were obtained for a target load of 120 kN and an assembly pattern of 1-5-3-7-2-6-4-8. Finally, in order to validate the model, the initial loads were applied on the test bench of Figure 7.9, obtaining an average load of 120 kN and a standard deviation of 1.67 kN. Figure 7.15 shows the uniform bolt load distribution. As can be seen, the obtained results were very satisfactory, so it can be stated that the superelement-based model provides very accurate results.

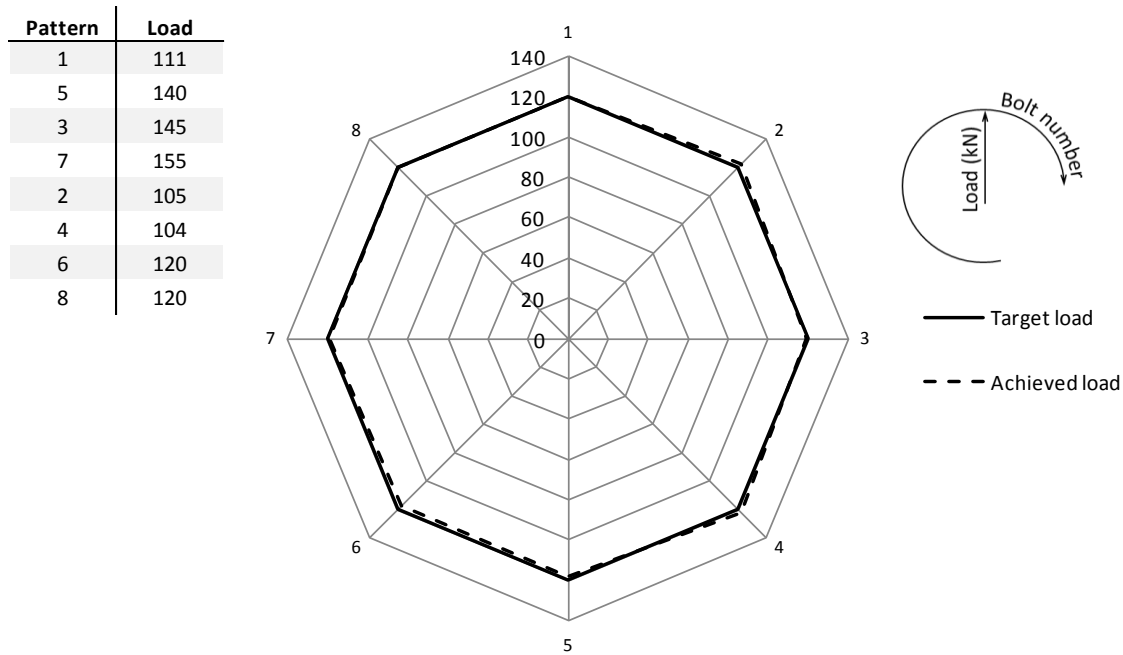


Figure 7.15. Tightening loads obtained with the superelement-based model, and the final load distribution obtained in the test bench using the linear gasket

5.3. VALIDATION WITH NON-LINEAR GASKET

After the linear analysis, the non-linear analysis must be performed in order to fully validate the model. In this case, the geometrical dimensions of Table 7.1 and the behaviour of Figure 7.12 was used for the gasket. Next, following the same procedure, the initial loads of Figure 7.16 were obtained for a target load of 120 kN and an assembly pattern of 1-5-3-7-2-6-4-8. In order to validate the model, the initial loads were applied once again in the test, obtaining an average load of 121 kN and a standard deviation of 3.66 kN. Figure 7.16 shows the uniform bolt load distribution. As can be seen, with the non-linear gasket, the obtained results were also satisfactory. Therefore, the superelement-based model is a particularly good alternative when the joint under review is not an RTJ, given its accurate results.

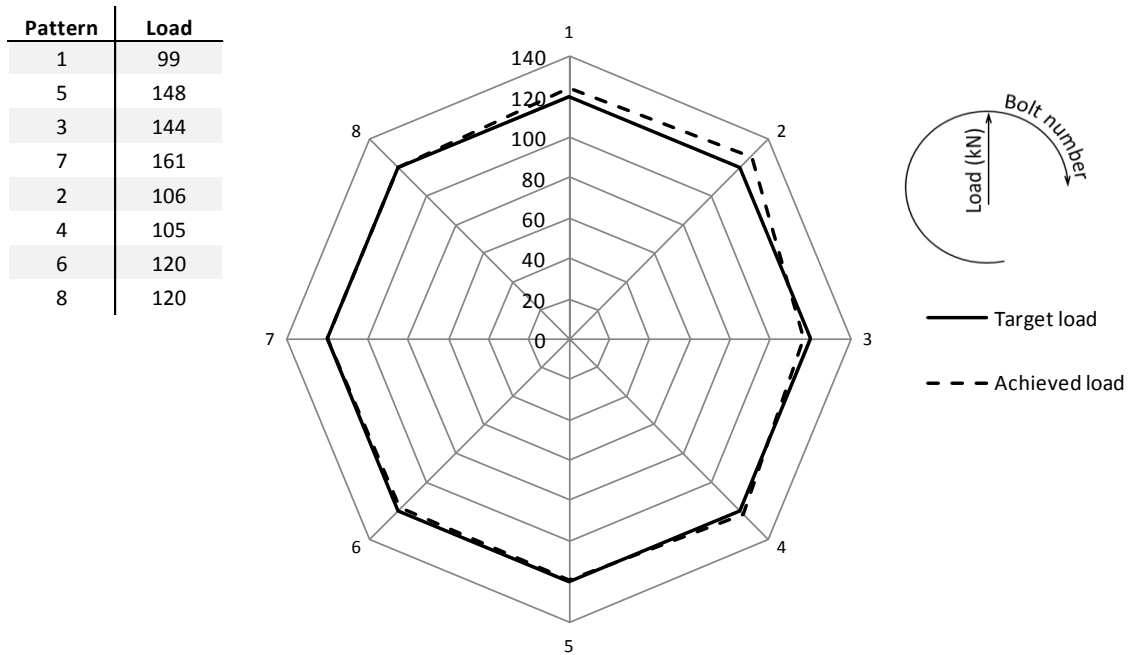


Figure 7.16. Tightening loads obtained with the superelement-based model, and the obtained final load distribution applying those loads on the test bench using the non-linear gasket

6. CONCLUDING REMARKS

The TAM presented in the Doctoral Thesis was specifically developed to study RTJs due to their high applicability. However, several other types of joints are also used in the industry. To this regard, another alternative is presented in this Chapter based on the superelement technique in order to study other types of joints. This technique builds a condensed stiffness matrix based on the appropriate selection of master nodes, thus significantly reducing the dimension and the cost of the problem.

As explained in this Chapter, this method is much more efficient than a conventional FE model because it reduces the computational cost considerably (more than 30 times) without no loss of precision. It was also validated experimentally for both linear and non-linear gaskets.

CHAPTER 8. CONCLUSIONS AND FURTHER RESEARCH

1. CONCLUSIONS

This section summarizes the main conclusions and contributions drawn from the Doctoral Thesis:

- The ISM and the EICM methodologies for the optimization of tightening sequences were validated for RTJs. Although they are widely known in specialist literature, they had not been previously validated for these types of joints.
- A new optimization method was developed for RTJs, called the Tetraparametric Assembly Method (TAM). It is based on four coefficients which represent the influence of the elastic interaction during the tightening sequence. To obtain their values, a simple analysis must be performed with a Finite Element model or with a test bench. Even though the four coefficients do not take into account the loss of load due to phenomena such as short term relaxation, the influence of these factors is much smaller than the influence of elastic interaction.
- The TAM proved to be more efficient than the ISM and the EICM, providing a similar level of accuracy with a much lower cost.
- The values of the coefficients of the TAM only depend on the joint geometry, regardless of the friction coefficient, load level and assembly pattern. Thus, each particular joint is represented by only four different coefficients.
- Likewise, the TAM was generalized for multiple-pass tightening sequences. Even though a single-pass tightening sequence is desirable, the tightening loads could exceed the yielding load; in such case, two-pass tightening sequences must be performed in order to decrease bolt tightening loads.
- In two-pass tightening sequences, the method defines the optimum final load after the first pass in order to minimize tightening loads and thus avoids possible joint damages.
- The generalization of the methodology for more than two passes is straightforward. However, this situation is unlikely in ASME RTJs.
- The range of application of the TAM inside the ASME RTJs was also studied and found to be significantly wide. The error of the optimized tightening sequence was always less than 5.6% for any analyzed RTJ.

- The four coefficients of the TAM were obtained for every RTJ within the range of application. Thus, there is no need to perform any previous analysis in order to obtain the coefficients. Therefore, the efficiency of the TAM increases in comparison with the EICM and ISM.
- The TAM was programmed in Visual Basic for Applications of Microsoft Excel, including the coefficient values for all the ASME RTJs within the range of application. The program was developed to be used by assemblers to calculate easily optimal tightening sequences.
- The TAM was very successfully validated with a multiparametric Finite Element model and with a test bench provided by ULMA and MATZ-ERREKA (flange and bolt manufacturers, respectively).
- Finally, an innovative model was developed for other types of joint. This model, which is based on the superelements technique, was also successfully validated in an experimental setup in the university “École de technologie supérieure” of Montreal, Canada.

2. FURTHER RESEARCH

As a consequence of the research work presented in this Doctoral Thesis, several future research lines have been identified:

- Modification of the TAM in order to consider other bolt load variation factors, such as short term relaxation.
- Study of the range of application of the superelement-based model.
- Development of a new method to define optimal tightening sequences under misalignment loads or external loads.

3. PUBLICATIONS DERIVED FROM THE DOCTORAL THESIS

The research work performed for this Doctoral Thesis has given rise to the following manuscripts in “Journal Citation Report (JCR)” journals and congress presentations:

JCR PUBLICATIONS:

- I. Coria, M. Abasolo, J. Aguirrebeitia, I. Fernández de Bustos. Generalization of the Tetraparametric Assembly Method for the Optimization of Bolt Tightening Sequences in Ring Type Joints. Proceedings of the Institution of Mechanical Engineers, Part E: Journal of Process Mechanical Engineering. JCR Impact Factor: 1,448 (Q2). Under review.
- I. Coria, M. Abasolo, I. Olaskoaga, A. Etxezarreta, J. Aguirrebeitia. A New Method for the Optimization of Bolt Tightening Sequences for Ring Type Joints. Ocean Engineering, 129: 441-450, 2017. JCR Impact Factor: 1,894 (Q1).

CONGRESS PRESENTATIONS:

- I. Coria, I. Martín, A.H. Bouzid, I. Heras, J. Aguirrebeitia. Optimized Bolt Tightening Sequences in bolted joints using a Superelement FE model. Ocean, Offshore & Arctic Engineering, Madrid, Spain, 2018. Under review.
- I. Coria, I. Martín, A.H. Bouzid, I. Heras, M. Abasolo. FEM Superelement Technique Applied to Oil and Gas Bolted Flange Connections. 24th International Conference on Fluid Sealing, Manchester, England, 2018. Under review.
- I. Coria, M. Abasolo, J. Aguirrebeitia, I. Heras. VBA APP for the Calculation of Optimal Tightening Sequences for Ring Type Joints. Pressure Vessels & Piping Conference, Hawaii, USA, 2017.
- I. Coria, M. Abasolo, I. Olaskoaga, A. Etxezarreta, J. Aguirrebeitia. Nueva Metodología para el Desarrollo de Secuencias de Atornillado Óptimas en Uniones RTJ. XXI Congreso Nacional de Ingeniería Mecánica, Elche, 2016.
- I. Coria, M. Abasolo, J. Aguirrebeitia. Efficient Method for the Assembly of Ring Type Joints. Pressure Vessels & Piping Conference, Vancouver, Canada, 2016.

REFERENCES

- [Aba'11] Abasolo M, Aguirrebeitia J, Avilés R, Fernández de Bustos I. A tetraparametric metamodel for the analysis and design of bolting sequences for wind generator flanges. *Journal of pressure vessel technology-ASME*, 2011; 133: 041202.
- [Aba'12] Abasolo M. Metamodelo para la simulación y optimización de secuencias de atornillado en uniones de torres de aerogenerador. Tesis Doctoral, 2012.
- [Aba'14] Abasolo M, Aguirrebeitia J, Avilés R, Fernández de Bustos I. Methodology for the optimization of bolting sequences for wind generator flanges. *Journal of pressure vessel technology-ASME*, 2014; 136: 061202.
- [Aba'17] Abasolo M, Aguirrebeitia J, Coria I, Heras I. Guía práctica de elementos finitos en estática. Paraninfo, 2017. ISBN: 9788428340335.
- [Abi'16] Abid M, Khan A, Nash DH, Hussain M, Wajid HA. Optimized bolt tightening strategies for gasketed flanged pipe joints of different sizes. *International journal of pressure vessels and piping*, 2016; 139–140: 22-27.
- [Agu'12] Aguirrebeitia J, Abasolo M, Avilés R, Fernández de Bustos I. General static load-carrying capacity for the design and selection of four contact point slewing bearings: Finite element calculations and theoretical model validation. *Finite elements in analysis and design*, 2012; 55: 23–30.
- [Alk'07] Alkelani AA, Nassar SA, Housari BA. A novel formulation of elastic interaction in gasketed bolted joints. ASME pressure vessels and piping conference. San Antonio, Texas, 2007.
- [Alk'08] Alkazraji A. A quick guide to pipeline engineering. Woodhead publishing limited and Matthews engineering training Ltd, 2008.
- [Alk'09] Alkelani AA, Nassar SA, Housari BA. Formulation of elastic interaction between bolts during the tightening of flat-face gasketed joints. *Journal of mechanical design*, 2009; 131.

- [Api'11] API specification 17D: Design and operation of subsea production systems—Part 4: Subsea wellhead and tree equipment. American petroleum institute, 2011.
- [Asm'11] ASME BPVC Section VIII Division 1: Rules for construction of pressure vessels. American society of mechanical engineers, 2011.
- [Asm'12(1)] ASME B 31.3: Process piping. American society of mechanical engineers, 2012.
- [Asm'12(2)] ASME B16.20: Metallic gaskets for pipe flanges: ring-joint, spiral-wound and jacketed. American society of mechanical engineers, 2012.
- [Asm'13(1)] ASME B 16.5: Pipe flanges and flanged fittings: NPS 1/2 through NPS 24 metric/inch standard. American society of mechanical engineers, 2013.
- [Asm'13(2)] ASME PCC-1: Guidelines for pressure boundary bolted flange joint assembly. American society of mechanical engineers, 2013.
- [Avi'02] Avilés R. Métodos de análisis para diseño mecánico. Volumen II: elementos finitos en estática. Escuela superior de ingenieros, 2003. ISBN: 8495809079.
- [Bar'04] Barber JR. Elasticity. Solid mechanics and its applications, vol 107. Kluwer academic publishers, 2004. ISBN: 9781402009662.
- [Bau'66] Baubles RC, McCormick GJ, Faroni CC. Loosening of fasteners by vibration. Document ER272-2177, Eng. No. 30 the Elastic Stop Nut Corp. of America, Union, NJ, 1966.
- [Bib'92] Bibel GD, Ezell RM. An improved flange bolt-up procedure using experimentally determined elastic interaction coefficients. Journal of pressure vessel technology, 1992; 114: 439–443.
- [Bib'94] Bibel GD. Method of tightening threaded fasteners. U.S. Patent No. 5,278,775. 1994.

- [Bib´96] Bibel GD, Ezell RM. Bolted flange assembly: Preliminary elastic interaction data and improved bolt-up procedures. WRC Bulletin, 1996; 408.
- [Bic´95] Bickford JH, Nassar S. An introduction to the design and behavior of bolted joints. CRC Press, 1995.
- [Bic´98] Bickford JH, Nassar AS. Handbook of bolts and bolted joints. Marcel Dekker Inc., 1998: 451-453.
- [Bon´80] Bonenberg PR. A basic approach to joint design. Using threaded fasteners seminar. University of Wisconsin-Extensio, 1980
- [Bro´10] Brown W, Waterland J, Lay D. Background on the new ASME PCC-1:2010 appendix F “Alternatives to legacy tightening sequence/pattern. ASME pressure vessels and piping conference. Bellevue, Washington, USA, 2010; PVP2010-25772: 99-105.
- [Cha´91] Chambers C. Spring rate of helical spring lock washers. Lawrence Technological University. Southfield, MI, 1991.
- [Cle´89] Clement B, Bazergui A. A study of the preload relationship in bolting technology: experimental design and analysis. Prepared for the Bolting Technology Council. New York, 1989.
- [Cor´16(1)] Coria I, Abasolo M, Olaskoaga I, Etxezarreta A, Aguirrebeitia J. Nueva metodología para el desarrollo de secuencias de atornillado óptimas en uniones RTJ. XXI congreso nacional de ingeniería mecánica. Elche, 2016.
- [Cor´16(2)] Coria I, Abasolo M, Aguirrebeitia J. Efficient methodology for the assembly of ring type joints. ASME pressure vessels & piping conference. Vancouver, Canada, 2016; PVP2016-63037.
- [Cor´17(1)] Coria I, Abasolo M, Olaskoaga I, Etxezarreta A, Aguirrebeitia J. A new methodology for the optimization of bolt tightening sequences for ring type joints. Ocean Engineering, 2017; 129: 441-450.

- [Cor'17(2)] Coria I, Abasolo M, Aguirrebeitia J, Heras I. VBA APP for the calculation of optimal tightening sequences for ring type joints. ASME pressure vessels & piping conference. Hawaii, USA, 2017.
- [Cur'12] Currie R. Metallic Ring Type Joints (RTJ): overview and recent developments. ASME pressure vessels & piping conference. Toronto, Ontario, Canada, 2012; PVP2012-78175: 91-99.
- [Daa'90] Daadbin A, Chow YM. A theoretical model to study thread loosening. Department of mechanical engineering, University of Newcastle on Tyne. United Kindom, 1990.
- [Deu'75] Deutschman AD. Machine design: theory and practice. Prentice Hall, 1975.
- [Dur'80] Through-hardened Durlock 180® screws lock tight without gouging. Advertisement of SPS Technologies, Jenkintown, PC. Published in Machine Design, 1980.
- [Err'www] <http://www.errekafasteningssolutions.com/en/ibolt/> (accessed May 2016).
- [Esn'79] ESNA Visual Index, ESNA Division, Amerace Corporation, Union, NJ, 1979.
- [Eze'92] Ezell RM. The analytical and experimental study of the elastic interaction in a bolted, flanged, gasketed joint. Doctoral Thesis, University of Akron, 1992.
- [Fer'81] Fernández ML. Tow techniques for marine pipeline installation. Department of civil engineering, Delft university of technology, 1981.
- [Fri'77] Friesth ER. Performance characteristics of bolted joints in design and assembly. SME Technical Paper AD-77-715, 1977.
- [Fuk'03] Fukuoka T, Takaki T. Finite element simulation of bolt up process of pipe flange connections with spiral wound gasket. Journal of Pressure Vessel Technology, 2003; 125: 371-378.
- [Fuk'04] Fukuoka T, Takaki T. Effective bolting up procedure using finite element analysis and elastic interaction coefficient method.

- ASME pressure vessels & piping conference. San Diego, USA, 2004; PVP2004-2634: 155-162.
- [Fuk'12] Fukuoka T, Nomura M, Nishikawa N. Analysis of thermal and mechanical behavior of pipe flange connections by taking account of gasket compression characteristics at elevated temperature. *Journal of pressure vessel technology*, 2012; 134(2): 021202.
- [Ger'07] Gerwick BC. *Construction of marine and offshore structures*, third edition. CRC Press, 2007. ISBN: 9780849330520.
- [God'94] Goddard DL, Bibel GD. Achieving a selected load distribution in the bolted joint of a cylinder head of highly variable stiffness and contact geometry. IMECE. Detroit, Michigan, 1994; SAE Technical Paper 940693.
- [Gri'13] Grine L, Bouzid AH. Analytical and experimental studies of liquid and gas leaks through micro and nano-porous gaskets. *Materials sciences and applications*, 2013; 4, 35817.
- [Guo'94] Guo B, Song S, Chacko J, Ghalambor A. *Offshore pipelines*. Elsevier, 2005. ISBN: 075067847X.
- [Ifi'82] IFI 524: Test procedure for the locking ability performance of metric nonmetallic locking element type prevailing-torque lock screws. 1982.
- [Ifi'87] IFI 124: Test procedure for the locking ability performance of nonmetallic element type prevailing-torque lock screws. 1987.
- [Ifi'93] IFI 100/107: Prevailing-torque type steel hex and hex flange nuts, regular and light hex series. Revised version published in, 1993.
- [Ith'www] <http://www.ith.de/upload/files/Windkraftanlagen.pdf>.
- [Jha'06] Jhang KY, Quan HH, Ha J, Kim NY. Estimation of clamping force in high-tension bolts through ultrasonic velocity measurement. *Ultrasonics*, 2006; 44: 1339–1342.

- [Jun´69] Junker GH. New criteria for self-loosening of fasteners under vibration. *Trans. SAE*, 1969; 78.
- [Jun´74] Junker G. Principles of the calculation of high duty bolted connections – Interpretation of guideline VDI 2230. VDI Berichte, No. 220. Published as an Unbrako technical thesis by SPS, Jenkintown, PA, 1974.
- [Juv´00] Juvinall RC. Marshek KM. Fundamentals of machine component design. Wiley, 2000.
- [Kha´15] Khan NB, Abid M, Jameel M, Wajid HA. Joint strength of gasketed bolted pipe flange joint under combined internal pressure plus axial load with different (industrial and ASME) bolt-up strategy. *Proceedings of the institution of mechanical engineers part E journal of process mechanical engineering*, 2015.
- [Kom´09] Komzsik L. What every engineer should know about computational techniques of finite element analysis, 2nd edn. CRC Press (Taylor & Francis Group), 2009. ISBN-10: 1439802947, ISBN-13: 978-1439802946.
- [Kon´09] Konnaj T, Tsuji H. Finite element simulation for bolted flanged joints assembly with misalignment. ASME pressure vessels and piping conference. Check Republic, Praga, 2009; PVP2009-77471: 125-130.
- [Kum´03] Kumakura S, Saito K. Tightening sequence for bolted flange joint assembly. ASME pressure vessels and piping conference. Cleveland, Ohio, USA, 2003; PVP2003-1867: 9-16.
- [Lej´11] Lejeune H, Birembaut Y, Riedl A, Schunemann A. Investigation on different tightening sequences on several bolted flange types, dimensions and their associated gasket types. ASME pressure vessels and piping conference. Baltimore, Maryland, USA, 2011; PVP2011-57525: 43-49.
- [Loa´www] <http://loadct.com/tech.php>
- [Loc´79] Loctite® Technology, Loctite Corp., Newington, CT, 1979.

- [Mck'80] McKewan J. The effects of plating on torque-tension relationships and vibration resistance. Congress and Exposition of the SAE. Detroit, USA, 1980; Paper no. 800452.
- [Mey'72] Meyer G, Strelow D. Simple diagrams aid in analyzing forces in bolted joints. *Assembly Eng.*, 1972.
- [Mot'76] Motosh N. Determination of joint stiffness in bolted connections. *Trans. ASME*, 1976.
- [Nas'05] Nassar SA, Alkelani, AA. Elastic interaction between fasteners in gasketed bolted joints. ASME pressure vessels and piping conference. Denver, Colorado, USA, 2005; PVP2005-71576: 155-168.
- [Nas'06] Nassar SA, Alkelani AA. Clamp load loss due to elastic interaction and gasket creep relaxation in bolted joints. *Journal of pressure vessel technology*, 2006; 128: 394-401.
- [Nas'08] Nassar SA, Wu Z, Yang X. A new tightening methodology for gasketed joints based on nonlinear finite element analysis. ASME pressure vessels and piping conference. Chicago, Illinois, USA, 2008; PVP2008-61115: 127-137.
- [Nas'09] Nassar SA, Yang X. Novel formulation of bolt elastic interaction in gasketed joints. *Journal of pressure vessel technology*, 2009; 131.
- [Nas'10] Nassar SA, Wu Z, Yang X. Achieving uniform clamp load in gasketed bolted joints using a nonlinear finite element model. *Journal of pressure vessel technology*, 2010; 132.
- [Nor'06] Norton RL. *Machine design: an integrated approach*. Prentice Hall, 2006.
- [Nor'13] NOROK L-005 Edition 3: Compact flanged connections. Norwegian petroleum industry, 2013.
- [Osg'72] Osgood CC. How elasticity influences bolted joint design. *Machine Design*, 1972: 92.

- [Pal'04] Palmer AC. Subsea pipeline engineering. PennWell, Tulsa, Oklahoma, 2004.
- [Pla'15] Plaza J, Abasolo M, Coria I, Aguirrebeitia J, Fernandez de Bustos I. A new finite element approach for the analysis of slewing bearings in wind turbine generators using superelement techniques. *Meccanica*, 2015; 50: 1623–1633.
- [Sak'78] Sakai T. Investigations of bolt loosening mechanism. *Bulletin of the JSME*, 1978; 21: Paper no. 159-9.
- [Sch'99] Schröder G. New European standard for the selection of a suitable method for leak detection and leak tightness testing. European standard EN 1779, 1999.
- [Shi'77] Shigley JE. *Mechanical engineering design*. McGraw-Hill, 1977.
- [Spi'80] Spiralock® Nuts, Greer/Central, a division of the Microdot Corp. Troy, Mi, 1980.
- [Ste'73] Steward R. Torque/tension variables list. Prepared at Wright-Patterson Air force Base, 1973.
- [Tak'02] Takaki T, Fukuoka T. Systematical FE analysis of bolt assembly process of pipe flange connections. ASME pressure vessels and piping conference. Vancouver, BC, Canada, 2002; PVP2002-1092: 147-152.
- [Tak'04] Takaki T, Fukuoka T. Effective bolting up procedure using finite element analysis and elastic interaction coefficient method. ASME pressure vessels and piping conference. San Diego, California, USA, 2004; PVP2004-2634: 155-162.
- [Tir'13] Tirenti J. *Diseño y cálculo de tuberías*. Arveng Consulting, 2013.
- [Van'69] Van Campen DH. *A systematic bolt-tightening procedure for reactor vessel flanges*. University of Technology. Delft, The Netherlands, 1969.
- [Vei'03] Veiga JC. *Juntas Industriales*. Teadit Industria e Comércio, 2003.

-
- [Wan'17] Wang YQ, Wu JK, Liu HB, Kuang K, Cui XW, Han LS. Analysis of elastic interaction stiffness and its effect on bolt preloading. *International Journal of Mechanical Sciences*, 2017; 130: 307-314.
- [Zhi'16] Zhiltsov SS, Zonn IS, Kostianoy AG. *Oil and Gas pipelines in the Black-Caspian seas region*. Springer, 2016.
- [Zhu'17] Zhu L, Bouzid AH, Hong J. Analytical modeling of elastic interaction in bolted flange gasketed joints. *ASME pressure vessels and piping conference*. Hawaii, USA, 2017; PVP2017-66275.

